frontiers | Research Topics

Prevalence and control measures of food-borne pathogens

Edited by
Peng Fei, Stephen Forsythe and Chao Shi

Published in
Frontiers in Microbiology

ISSN 1664-8714
ISBN 978-2-8325-3468-7
DOI 10.3389/978-2-8325-3468-7

About Frontiers

Frontiers is more than just an open access publisher of scholarly articles: it is a pioneering approach to the world of academia, radically improving the way scholarly research is managed. The grand vision of Frontiers is a world where all people have an equal opportunity to seek, share and generate knowledge. Frontiers provides immediate and permanent online open access to all its publications, but this alone is not enough to realize our grand goals.

Frontiers journal series

The Frontiers journal series is a multi-tier and interdisciplinary set of open-access, online journals, promising a paradigm shift from the current review, selection and dissemination processes in academic publishing. All Frontiers journals are driven by researchers for researchers; therefore, they constitute a service to the scholarly community. At the same time, the *Frontiers journal series* operates on a revolutionary invention, the tiered publishing system, initially addressing specific communities of scholars, and gradually climbing up to broader public understanding, thus serving the interests of the lay society, too.

Dedication to quality

Each Frontiers article is a landmark of the highest quality, thanks to genuinely collaborative interactions between authors and review editors, who include some of the world's best academicians. Research must be certified by peers before entering a stream of knowledge that may eventually reach the public - and shape society; therefore, Frontiers only applies the most rigorous and unbiased reviews. Frontiers revolutionizes research publishing by freely delivering the most outstanding research, evaluated with no bias from both the academic and social point of view. By applying the most advanced information technologies, Frontiers is catapulting scholarly publishing into a new generation.

What are Frontiers Research Topics?

Frontiers Research Topics are very popular trademarks of the *Frontiers journals series*: they are collections of at least ten articles, all centered on a particular subject. With their unique mix of varied contributions from Original Research to Review Articles, Frontiers Research Topics unify the most influential researchers, the latest key findings and historical advances in a hot research area.

Find out more on how to host your own Frontiers Research Topic or contribute to one as an author by contacting the Frontiers editorial office: frontiersin.org/about/contact

Prevalence and control measures of food-borne pathogens

Topic editors

Peng Fei — Nanyang Institute of Technology, China

Stephen Forsythe — Foodmicrobe.com, United Kingdom

Chao Shi — Northwest A&F University, China

Citation

Fei, P., Forsythe, S., Shi, C., eds. (2023). *Prevalence and control measures of food-borne pathogens*. Lausanne: Frontiers Media SA.

doi: 10.3389/978-2-8325-3468-7

Table of contents

frontiers | Frontiers in Microbiology

TYPE Original Research
PUBLISHED 10 January 2023
DOI 10.3389/fmicb.2022.1068144

OPEN ACCESS

EDITED BY
Peng Fei,
Nanyang Institute of Technology, China

REVIEWED BY
Liang Gong,
Chinese Academy of Sciences, China
Thayza C. M. Stamford,
Federal University of Pernambuco, Brazil

*CORRESPONDENCE
Lijun Ling
✉ 13919343210@163.com

SPECIALTY SECTION
This article was submitted to Food Microbiology, a section of the journal Frontiers in Microbiology

RECEIVED 12 October 2022
ACCEPTED 20 December 2022
PUBLISHED 10 January 2023

CITATION
Ling L, Luo H, Zhao Y, Yang C, Cheng W and Pang M (2023) Fungal pathogens causing postharvest fruit rot of wolfberry and inhibitory effect of 2,3-butanedione.
Front. Microbiol. 13:1068144.
doi: 10.3389/fmicb.2022.1068144

Fungal pathogens causing postharvest fruit rot of wolfberry and inhibitory effect of 2,3-butanedione

Lijun Ling[1,2,3]*, Hong Luo[1,2], Yunhua Zhao[1,2], Caiyun Yang[1,2], Wenting Cheng[1,2] and Mingmei Pang[1,2]

[1]College of Life Science, Northwest Normal University, Lanzhou, China, [2]Bioactive Products Engineering Research Center for Gansu Distinctive Plants, Northwest Normal University, Lanzhou, China, [3]New Rural Development Research Institute, Northwest Normal University, Lanzhou, China

Fungal pathogen contamination is one of the most important factors affecting the postharvest quality and shelf life of wolfberry fruits. Therefore, the prevention and control of fungal pathogens that cause fruit rot has become particularly important. Volatile antifungal agents of biological origin have broad application prospects. They may be safer and more efficient than traditional physical and chemical methods. Four pathogenic fungi were isolated and purified from rotting wolfberry. These pathogenic fungi were determined to be *Mucor circinelloides* LB1, *Fusarium arcuatisporum* LB5, *Alternaria iridiaustralis* LB7, and *Colletotrichum fioriniae* LB8. In vitro fumigation experiments showed that 2,3-butanedione can effectively inhibit the mycelial growth, spore germination, and sporulation ability of pathogenic fungi. The scanning electron microscope (SEM) showed morphological changes in hyphae. Propidium iodide (PI) Staining and leakage of 260 and 280 nm-absorbing increased, suggesting damage to cell membranes. Furthermore, 2,3-butanedione was found to significantly improve fruit firmness, soluble solid, total phenol, flavonoid, and soluble sugar content, as well as higher SOD enzyme activity and lower PPO and POD enzyme activity in the treated fruit, indicating that 2,3-butanedione can effectively reduce the adverse effects of pathogenic fungi in wolfberry. Based on these results, we conclude that 2,3-butanedione is effective against infection by pathogenic fungi in post-harvest wolfberry. 2,3-butanedione should be considered a viable substitute for conventional fungicides that are currently used to control rot in wolfberry.

KEYWORDS

wolfberry, fungal pathogen, 2.3-butanedione, antifungal activity, postharvest fruit rot

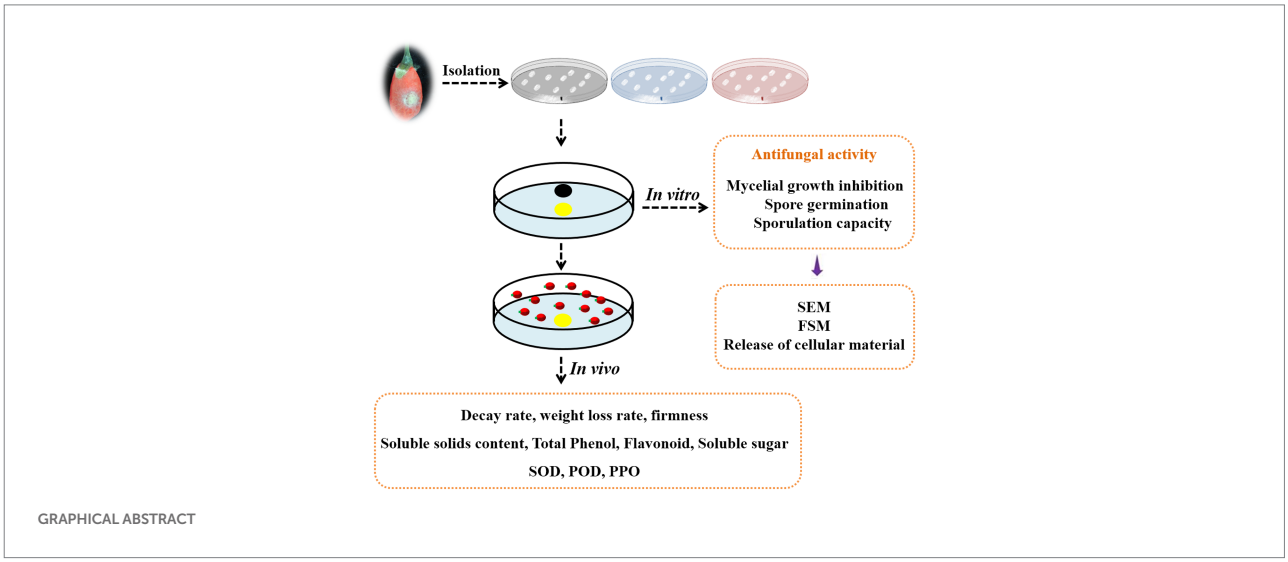

1. Introduction

Wolfberry (*Lycium barbarum* L.), often known as Goji Berry, is one of the most important plants belonging to the Solanaceae family (Liu et al., 2017a). For almost 2000 years, it has been an important Chinese traditional medicine, and it is widely grown in north-western China (Sun et al., 2008). Wolfberry is often used as a nourishing traditional Chinese medicine that has the function of nourishing the liver and kidney, tonifying blood, and relieving cough (Wang et al., 2014). At the same time, wolfberry can also be consumed as a functional food. Wolfberry fruit contains wolfberry polysaccharides, carotenoids, betaine, vitamins and other substances. Wolfberry polysaccharides have the ability of anti-oxidation to provide neuroprotection to the eyes (Chan et al., 2019). Because of its dual use as medicine and functional food, the development of the wolfberry industry has been promoted in recent years.

Postharvest loss refers to the decay and deterioration of agricultural products caused by pathogen infection, respiration and senescence in the process of storage, treatment and transportation after harvest (Zhang et al., 2019). Postharvest decay of harvested fruits and vegetables will cause food safety problems and considerable economic losses (Ambler et al., 2017). The postharvest infection of Chinese wolfberry is mainly caused by fungi. Several fungi have been reported to be associated with postharvest rot of wolfberry including *Alternaria*, *Aspergillus niger*, *Penicillium*, *Trichoderma*, *Aspergillus flavus* (Lan et al., 2014), *Cladosporium* and *Fusarium* (Xiao et al., 2018). However, there are still few reports on the main pathogenic fungi of wolfberry, and more research on it is necessary.

Keeping fruit fresh and disease-free throughout harvest and processing has long been a challenge. Currently, many strategies have been used to manage postharvest diseases of the wolfberry, such as low-temperature refrigeration, modified atmosphere refrigeration, physical treatments and chemical control (using synthetic fungicides), etc. (Yang et al., 2016). However, the most common and effective strategy for controlling postharvest diseases is the application of chemical agents in large quantities (Mari et al., 2016). Considering the negative side effects of fungicides, it is necessary to find a method that can replace fungicides to control postharvest pathogens of wolfberry fruit (Nunes, 2012).

In recent years, biological control has received extensive attention due to its safety, efficiency and environmental protection (Brilli et al., 2019). Numerous studies have shown that some antagonistic microorganisms exhibit strong inhibitory activity against postharvest pathogens in fruits and vegetables (Lemos Junior et al., 2020; Moore et al., 2021). Among them, some microorganisms capable of producing volatile organic compounds (VOCs) have great application prospects. Wonglom et al. (2020) report that VOCs released by *Trichoderma asperellum* T1 mediate antifungal activity and promote growth in lettuce. Zhong et al. (2021) reported that *Pseudomonas fluorescens* ZX produced VOCs against gray mold, effectively reducing the disease of grapes. Volatile organic compounds are not easy to remain, safe and efficient, which has a natural advantage in postharvest disease control (Wallace et al., 2017).

In the antifungal activity of VOCs, some constituent substances showed a strong effect. 2,3-butanedione is a naturally occurring and volatile α-diketone. Due to the aroma and flavor of butter, it is often used as a food additive and an important component of food flavors (Farsalinos et al., 2014). No adverse health effects have been reported at the level of 2,3-butanedione added to foods (Morgan et al., 2016). Our latest study found that endophytic *Bacillus subtilis* CL_2 could significantly inhibit postharvest pathogens of wolfberry by producing VOCs, and the composition and function test of VOCs showed that 2,3-butanedione is the main active ingredient (Ling et al., 2021). 2,3-butanedione has always been used as an edible additive, and it is safe and harmless (Hallagan, 2017). But its powerful antifungal

effect is not well understood. Therefore, it is very necessary to evaluate the postharvest disease control and preservation effect of this substance.

The goal of this research is to isolate and identify the pathogens that cause wolfberry fruit post-harvest rot, as well as to investigate the *in vitro* and *in vivo* antifungal activity of 2,3-butanedione against a fungal pathogen, in order to provide a theoretical foundation for the development of safe and healthy antisepsis technology for fresh wolfberry fruits.

2. Materials and methods

2.1. Postharvest rot-infected wolfberry

In August 2019, fresh wolfberry fruits were picked in Jingyuan County, Gansu Province, packed in foam boxes and brought back to the laboratory. After being stored in a 4°C refrigerator for 2 weeks, the rotten fruits were selected for the isolation of the pathogen.

2,3-butanedione was purchased from Niuniu Biochemical Co., Ltd. (Lanzhou, China). 2,3-butanedione ($C_4H_6O_2$), C431038, Source: Macklin, molecular weight: 86.09, density: 0.985 g/ml, purity: ≥99.0%.

2.2. Pathogens isolation

The fruits of wolfberry with obvious rotting symptoms were disinfected with 75% ethanol for 1 min, and then rinsed with sterile distilled water (SDW) for 3 times; disinfected with 1% sodium sulfite for 5 min and rinsed with SDW 3 times. In an ultra-clean workbench, the rotting tissues were isolated with aseptic tweezers and transferred to Luria-Bertani medium (LB), yeast extract peptone glucose medium (YPD), and potato glucose agar (PDA) (Li et al., 2017). Colonies were transferred to media after 1 and 3 days of cultivation, and the process was repeated until a pure culture of strains was achieved.

2.3. Pathogenicity testing

The pathogenicity of the isolated strains was tested according to Koch's rule. Sterilize the fresh wolfberry fruits with 75% ethanol for 1 min in a sterile environment, and rinse them with SDW 3 times. A sterile inoculating needle is used to pierce the surface of the fruit and inoculate the spore suspension of the isolated strain. Observe the pathogenicity of the isolated strains after incubating at 26°C for 3 d. The strains were inoculated on fresh and healthy wolfberry fruits again, and these pathogenic strains were isolated from the diseased wolfberry fruit tissues after inoculation. After purification and culture of these isolated strains, these pathogenic strains with the same morphological characteristics as the previously isolated strains were obtained, and the strain was identified as the pathogen of wolfberry fruits (María et al., 2018).

2.4. Pathogen identification

The DNA of pathogenic fungi was extracted by CTAB method (Ling et al., 2019). Use fungal ITS1 and ITS4 sequence primers for PCR amplification of strain DNA sequence (Cenobio-Galindo et al., 2019). The cycle parameters were as follows: an initial denaturation step at 95°C for 4 min, followed by 35 cycles of a denaturation step at 94°C for 30 s, an annealing step at 50°C for 60 s and an elongation step at 72°C for 80 s, followed by a final elongation step of 72°C for 8 min. PCR products were sent to Tianqi Gene Biotechnology Co., Ltd. for sequencing. Homologous sequences were analyzed against GenBank sequences using the NCBI nucleotide BLAST tool.[1] Finally, these sequences were used to construct a phylogenetic tree using mega-7.0, and the obtained strains were analyzed and identified.

2.5. Minimum inhibitory concentration and minimum fungicidal concentration

For the minimum inhibitory concentration (MIC) and minimum fungicidal concentration (MFC) experiment, this was determined by the method of Zhou et al. (2017) with minor modifications. The PDA plates were inoculated in the centre with a 6 mm diameter disc of pathogen and then 0, 0.5, 0.75, 1, 1.25, 1.5, 1.75, 2, 2.5, 3, 3.5, 4, 4.5, 5 µl of the corresponding 2,3-butanedione were poured into the sterile filter paper on the lid of the Petri dish, followed by sealing with parafilm to prevent the loss of 2,3-butanedione. The Petri dishes were incubated at 28°C for 5 days, and after 48 h, the lowest 2,3-butanedione concentration that totally inhibited fungal growth was measured as the MIC, and after 96 h, the lowest concentration that entirely prevented fungal growth was calculated as the MFC.

2.6. Antifungal activity of 2,3-butanedione on spore germination and sporulation capacity

2,3-butanedione inhibition of fungal pathogens spore germination was measured using the method of Zhong et al. (2021) with minor modifications. PDA plates were coated with a pathogenic fungal spore suspension (1×10^4 spores/ml). Add 2,3-butanedione (0, 1/4 MIC, 1/2 MIC, MIC) on sterile filter paper in the middle of the plate covering. The plates were sealed and incubated for 12 h at 28 degrees Celsius. A microscope was used to examine the spores. The proportion of sprouted spores out of the total number of examined spores was used to calculate germination rates.

Previous approaches were used to determine the sporulation capacity (Wang et al., 2020). A PDA plate was inoculated with a 6-mm-diameter plug of pathogenic fungus, then 2,3-butanedione

1 http://www.ncbi.nlm.nih.gov/blast

was added on sterile filter paper in the middle of the plate covering. A 6 mm fungal plug was sliced and immersed in SDW after 5 days of incubation. A hemocytometer was used to count the spores on the plug.

2.7. Exploration of the influences of 2,3-butanedione on the mycelial morphology of pathogenic fungi by SSE of SEM technique

Fungal morphology was assayed by SEM, using our previously described method (Ling et al., 2021). At MIC, fungi that had been treated with 2,3-butanedione were cultivated and obtained. The fungal hypha was placed in a glass vial with a rubber stopper containing 2.5% glutaraldehyde fixation solution for 24 h at 4°C. The fixed hyphae were then washed with phosphate-buffered saline (PBS) three times for 15 min each time and dehydrated in an ethanol series (30, 50, 70, 85, and 90% and twice with 100% concentration) for 15 min at each stage. After natural drying, the mycelium block was pasted on a conductive adhesive, gilded, and then detected by SEM.

2.8. Plasma membrane integrity in treated and untreated

For plasma membrane integrity, the method of Tian et al. (2012) was applied with Propidium iodide (PI) staining. After the LB1 mycelia incubated in PDB were collected and washed, the mycelia were resuspended in sterile saline solution containing 5% Tween-20. Place sterile filter paper in the center of the cap, add 2,3-butanedione, and fumigate for 2 d. The mycelia were incubated with PI at a concentration of 100 μl/ml after incubation at 37°C for 30 min in the dark. The fungi were collected, and then washed three times with phosphate-buffered saline. Observe the samples with a fluorescence microscope.

2.9. Release of cellular material

The release of cellular material was tested with a slightly modified method by Kong et al. (2019). The corresponding fungal mycelia were collected and centrifuged from the PDB medium. Then, mycelia were washed twice with SDW and finally fumigated with different concentrations of 2,3-butanedione. Samples were collected and centrifuged with 8,000 g for 5 min. Measure the absorbance of the supernatant at 260 nm and 280 nm using a spectrophotometer. All tests were performed in triplicate.

2.10. Decay rate, weight loss rate and firmness determination

Taking 30 wolfberry fruits in a sterile culture dish and inoculating pathogenic fungus LB1 on wolfberry fruits (without any treatment as a control). The fruit was fumigated with 2,3-butanedione in a closed environment. Any fruit with visible mycelium growing on the surface or rotted area exceeding 12.5% of the surface area was considered as rotted fruit. The decay weight and mass loss of wolfberry fruits were calculated by the following formula.

The firmness of wolfberry fruits treated with 2,3-butanedione for different times were measured using a GY-3 fruit firmness tester (Wei et al., 2018). Determination when taking two wolfberry fruits overlap together, with fruit firmness tester vertical squeeze wolfberry fruit, uniform force will probe into the wolfberry fruits, when the fruit firmness tester probe just through the two fruits stop squeezing, record fruits firmness tester pointer pointed to the reading, repeat three times.

$$\text{Decay rate}(\%) = (\text{number of rotten fruits} / \text{total fruits}) \times 100$$

$$\text{Weight loss}(\%) = \left[\begin{matrix}(\text{initial weight} - \text{final weight}) \\ /\text{initial weight}\end{matrix}\right] \times 100$$

2.11. Soluble solids content and soluble sugar content determination

The effect of 2,3-butanedione treatment on the content of soluble solids in wolfberry fruits were determined by a handheld refractometer. 5 g of wolfberry fruits were weighed into a 2 ml centrifuge tube, ground with a grinding rod until homogenized, centrifuged at 2000 × g for 5 min and then 5 μl of wolfberry fruits homogenate was aspirated and added dropwise to the detection mirror of the handheld refractometer, and the scale was read to determine the amount of soluble solids in the sample solution, expressed as mass fraction (%), with three replicates for each group of treatments (Chen et al., 2015).

The content of soluble sugars in wolfberry fruits was determined by anthrone-sulfuric acid method. In a test tube, 0.5 g of wolfberry fruits were weighed and ground into a homogenate with SDW and boiled for 30 min, then filtered, the residue was recovered and boiled again for 10 min and repeated three times. Pour the filtered boiling extract into a 50 ml volumetric flask and fix the volume with SDW. Pipette 50 μl of the sample extract of wolfberry soluble sugar into a test tube, and then add 0.5 ml of anthranilone-ethyl acetate and 5.0 ml of concentrated sulfuric acid to the test tube in turn. After shaking thoroughly, the tubes were immediately removed from the boiling water bath for 1 min and cooled naturally to room temperature. The absorbance value was measured at the wavelength 630 nm and the soluble sugar content in the fruit of wolfberry fruits was expressed as OD_{630}.

2.12. Total phenol and flavonoid determination

Weigh 1 g wolfberry fruits in a 10 ml centrifuge tube, add 1% hydrochloric acid-methanol solution under the condition of ice bath, grind and mix well. After placing in the dark at 4°C for 30 min, shake three times during the period and collect the filtrate was for later use. Then the filtrate was diluted 5 times with 1% hydrochloric acid-methanol solution, the absorbance at 325 nm was measured by an ultraviolet spectrophotometer, and OD_{325} was used to represent the flavonoids content in wolfberry fruits. The filtrate was diluted 10 times with 1% hydrochloric acid-methanol solution was taken to determine the absorbance at 280 nm, and OD_{280} was used to represent the total phenol content in wolfberry fruits (Habibi et al., 2019).

2.13. SOD, POD, and PPO determination

Weigh 5 g wolfberry fruits in a centrifuge tube, added with 5 ml of extraction buffer and then ground and homogenized under ice bath conditions. Centrifuge at 9614 g for 30 min at 4°C, collect supernatant, and store it at low temperature for later use.

Place each solution in the test tube as listed (Supplementary Table 1). Two test tubes were taken as control tubes. After uniform mixing, one control tube was placed in the dark, and the other test tubes were placed under a 4,000-lx fluorescent lamp for reaction for 15 min, and then immediately placed in the dark to terminate the reaction. Determine the absorbance at 560 nm with an unlit tube as the blank reference zero. Three replicates. SOD activity was calculated (Wu et al., 2020).

Add 3 ml of 25 mmol/l guaiacol solution and 0.5 ml of enzyme extract to the test tube, then 200 ml of 0.5 mol/l H_2O_2 solution to quickly initiate the reaction and start the timer. The initial value was recorded as the absorbance at 470 nm for 15 s, followed by 1 min of recording and 6 continuous measurements. To calculate the POD activity, the process was done three times.

Place 4.0 ml of 50 mmol/l acetic acid–sodium acetate buffer, pH 5.5, and 1.0 ml of 50 mmol/l catechol in the test tube, and add 100 µl of the enzyme extract, beginning immediately. Absorbance at 420 nm for 15 s is the initial value and is recorded at regular intervals for at least six times. And repeat for three times to calculate that PPO activity (Fan et al., 2019).

2.14. Statistical analyses

The SPSS 20.0 software was used to conduct statistical analyses. Duncan's test was applied to compare the mean values. All data were expressed as the mean ± SE by measuring three independent replicates.

3. Results and discussion

3.1. Isolation of pathogens and pathogenicity testing

Wolfberry is a traditional Chinese medicinal herb recognized as the latest "super-fruit" in the world. Due to the tender peel and high-water content, the fresh wolfberry fruits are easy to rot (Jatoi et al., 2017; Liu et al., 2017b). Most pathogenic microbes that cause post-harvest deterioration of wolfberry are fungi. Some pathogenic fungi also yield mycotoxins that convey a risk to human health (Liu et al., 2018). In order to better preserve and store wolfberry after harvest, more pathogenic fungi of wolfberry fruit were isolated, and a safe 2,3-butanedione was used for postharvest control of wolfberry in vapor phase.

After morphological observation and pathogenicity detection, 4 strains of postharvest pathogenic fungi were isolated. They were numbered LB1, LB5, LB7 and LB8. The morphology of 4 pathogenic fungi isolated from wolfberry fruits was shown in Figure 1. The pathogenic fungal LB1 mycelium grows quickly, and the colony color was light yellow (Figure 1A), after about 3 d of growth, a black floating layer appeared on the surface of the mycelium and the colonies could be removed directly from the PDA medium by forceps. A lot of oval spores with cystspores were observed under optical microscopes, and mycelia were seen separable (Figure 1A1). The colony of LB5 looked like white cotton bats (Figure 1B). The hyphae were long and separated, and the spores were scattered (Figure 1B1). Colonies of LB7 on PDA medium were black or dark green and fluffy (Figure 1C), under the light microscope, oval-shaped dark brown conidia could be seen, and many spores were connected (Figure 1C1). The mycelia of the pathogen LB8 were short and felt-like, and the middle color was pink (Figure 1D), as the growth time increased, the surface of the colony became rough, and black particles appeared. Oval spores of LB8 could be seen under a light microscope (Figure 1D1).

After inoculating pathogens for some time (LB1 treatment for 2 d, LB5, LB7 and LB8 treatment for 3 d), Fruits of wolfberry inoculated with pathogens showed different degrees of decay, as shown in Figure 1. As shown in Figure 1A2, the fruit of wolfberry began to rot 1 d after inoculation with pathogen LB1, and on the next day, nearly half of the surface of the fruit was seriously rotted, and a large amount of juice began to precipitate out of the fruit, but there was no mycelium visible to the naked eye. As shown in Figure 1B2, 3 d after inoculation with pathogen LB5, the surface of wolfberry fruit was covered by a large number of hyphae, and the fruit tissue around the hyphae began to soften. In figure (Figure 1C2) and (Figure 1D2), mycelia appeared on the fruit surface of wolfberry 3 d after inoculation with pathogens LB7 and LB8, and the fruit tissue around the pathogen became black and began to soften.

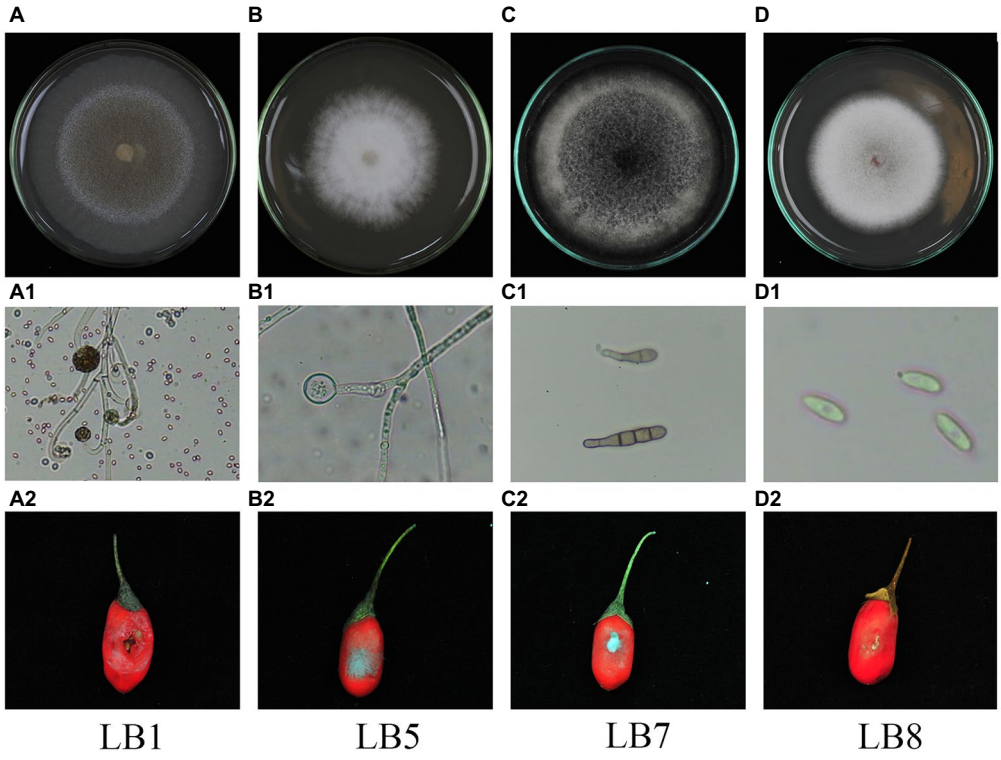

FIGURE 1
Morphological characteristics and pathogenicity detection of pathogenic strains of wolfberry after harvest (**A–D**: surface morphology of pathogenic strains, **A1–D1**: hyphae and spore morphology of pathogenic strains in microscopic morphology, **A2–D2**: observation of pathogenicity of pathogenic strains on fruits).

3.2. Identification of the postharvest fungal pathogens

In order to further characterize the isolates, phylogenetic trees were constructed from species using closely related relatives (Figure 2). The isolated strains show high genetic homology with the known strain sequences in the phylogenetic tree. According to the identification studies, of the 4 pathogenic fungi isolates, LB1 was identified as *Mucor circinelloides,* LB5 was identified as *Fusarium arcuatisporum,* LB7 was identified as *Alternaria iridiaustralis,* and LB8 was identified as *Colletotrichum fioriniae.*

The ITS nucleotide sequences of the isolates have the following accession numbers and GenBank database accession codes: LB1 and MN736542, LB5 and MN944920, LB7 and MN944921, and LB8 and MN944922.

Chinese wolfberry pathogenic fungi were isolated and identified in this study. *M. circinelloides*, *F. arcuatisporum*, *A. iridiaustralis*, and *C. fioriniae* were identified as the main pathogens causing postharvest wolfberry rot. Previous research has shown that *P.*, *Alternaria*, *A. niger*, *Trichoderma* and *Aspergillus* were the main post-harvest pathogenic fungi in Chinese wolfberry (Lan et al., 2014). *Fusarium*, *Alternaria*, *Penicillium*, *Gibberella*, *Fusarium oxysporum*, *Penicillium oxalicum*, *Cladosporium*, *Alternaria pallidus* and *Alternaria alternata* were isolated from post-harvest wolfberry (Liu et al., 2018; Xiao et al., 2018). Compared with previous studies, this was the first report of isolation and identification of *Mucor circinelloides* and *Colletotrichum fioriniae* from postharvest wolfberry. It is worth noting that the identified pathogenic fungi LB1 showed a strong fungal infection to cause the decay of the wolfberry fruit harvested. Therefore, this study chose to explore the inhibition of strain LB1 *in vitro* and *in vivo*.

3.3. Inhibition of 2, 3-butanedione on pathogenic fungi

Table 1 shows the results of 2,3-butanedione in the vapor phase that showed inhibitory efficacy against pathogenic fungus. For the MIC and MFC experiments, 2,3-butanedione was observed to significantly inhibit the growth of strains LB5, LB7 and LB8, while strain LB1 required more 2,3-butanedione to achieve the same inhibitory effect. After 48 h of incubation at 28°C, the lowest concentration of 2,3-butanedione conferring complete inhibition of LB1 was 4.5 μl per plate (MIC). After 96 h of incubation, 2,3-butanedione at 5 μl per plate completely

controlled the growth of LB1, yielding a minimum fungicidal concentration (MFC) of 5 μl per plate.

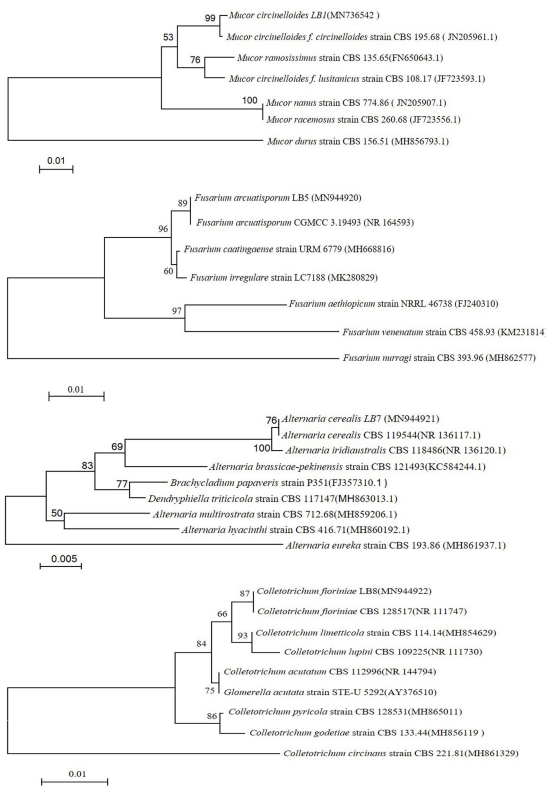

FIGURE 2
Phylogenetic tree of pathogenic fungi in wolfberry postharvest.

3.4. Effects of 2, 3-butanedione on spore germination and sporulation capacity of pathogenic fungi

As shown in Tables 2, 3, the effect of 2,3-butanedione on spore germination and sporulation capacity of pathogenic fungi was determined. Treatment with 2,3-butanedione at all concentrations (0, 1/4 MIC, 1/2 MIC, MIC) tested resulted in significantly lower spore germination rates and sporulation compared to untreated. The inhibitory effect was positively correlated with the concentration of 2,3-butanedione. When the concentration reached MIC value, spore germination and sporulation of LB1 were 14.21% and 39.35 spores/cm^2, respectively, and both values were significantly lower ($p < 0.05$) than those of control (96.8% and 270.83 spores/cm^2, respectively).

3.5. Effects of 2, 3-butanedione on mycelial morphology of pathogenic fungi

Figure 3 depicts the morphological changes seen in pathogenic fungi treated with 2,3-butanedione MIC values. The hyphal morphology of the four pathogenic fungi changed considerably when compared to the control fungi. In comparison to the control group, 2,3-butanedione forced the mycelium of pathogenic fungi LB1 to lose linearity, the surface of the mycelium to become frizzy, and the hyphae wall to become sabotaged (Figures 3A, A1); the mycelium of LB5 to swell and the surface of the hyphae to become sunken (Figures 3B, B1); The hyphae of LB7 were wrinkled and concomitantly sunken (Figures 3C, C1), The mycelia of the

TABLE 1 Minimum inhibitory concentration and minimum fungicidal concentration of 2,3-butanedione against pathogenic fungus.

Concentration (μl per plate)	Mycelial growth inhibition (%)*							
	LB-1		LB-5		LB-7		LB-8	
	48h	96h	48h	96h	48h	96h	48h	96h
0.5	0^a	0^a	33.33 ± 0.18^a	27.78 ± 0.16^a	28.61 ± 0.19^a	20.41 ± 0.25^a	33.41 ± 0.17^a	36.67 ± 0.2^a
0.75	9.25 ± 0.02^b	0^a	60.00 ± 0.24^b	48.27 ± 0.16^b	42.86 ± 0.18^b	32.65 ± 0.12^b	70.62 ± 0.26^b	56.67 ± 0.18^b
1	11.11 ± 0.19^c	2.33 ± 0.19^b	93.33 ± 0.13^c	86.62 ± 0.21^c	50.22 ± 0.26^c	40.82 ± 0.13^c	90.78 ± 0.2^c	83.53 ± 0.18^c
1.25	24.07 ± 0.13^d	10.67 ± 0.19^c	100^d	97.22 ± 0.18^d	64.38 ± 0.25^d	46.67 ± 0.18^d	100^e	96.54 ± 0.19^e
1.5	37.04 ± 0.24^e	24.37 ± 0.14^d	100^d	100^e	85.71 ± 0.16^e	66.67 ± 0.24^e	100^e	100^f
1.75	40.74 ± 0.21^f	31.59 ± 0.21^e	100^d	100^e	100^f	71.37 ± 0.20^f	100^e	100^f
2	48.15 ± 0.23^g	39.69 ± 0.18^f	100^d	100^e	100^f	86.57 ± 0.18^g	100^e	100^f
2.5	62.96 ± 0.15^h	46.22 ± 0.18^g	100^d	100^e	100^f	98.34 ± 0.19^h	100^e	100^f
3	70.37 ± 0.14^i	61.34 ± 0.19^h	100^d	100^e	100^f	100^i	100^e	100^f
3.5	88.89 ± 0.23^j	74.79 ± 0.23^i	100^d	100^e	100^f	100^i	100^e	100^f
4	98.15 ± 0.23^k	88.46 ± 0.18^j	100^d	100^e	100^f	100^i	100^e	100^f
4.5	100^l	98.16 ± 0.20^k	100^d	100^e	100^f	100^i	100^e	100^f
5	100^l	100^l	100^d	100^e	100^f	100^i	100^e	100^f

Data are expressed as means of three replicates ± SD. $^{a-l}$ Values within a column followed by different letters are significantly different ($p < 0.05$).

TABLE 2 Effects of 2,3-butanedione on the spore germination.

Concentration of 2,3-butanedione (μl per plate)	Spore germination (%) incubated for 12h			
	LB-1	LB-5	LB-7	LB-8
0	96.80 ± 2.88^{a}	91.71 ± 3.70^{a}	97.50 ± 2.43^{a}	94.11 ± 4.15^{a}
1/4 MIC	82.40 ± 4.19^{b}	40.80 ± 2.32^{b}	73.40 ± 4.57^{b}	81.75 ± 3.20^{b}
1/2 MIC	48.80 ± 2.64^{c}	10.93 ± 3.23^{c}	21.33 ± 3.45^{c}	35.33 ± 4.88^{c}
MIC	14.21 ± 1.94^{d}	0.00 ± 0.00^{d}	6.45 ± 2.15^{d}	4.80 ± 1.88^{d}

Data are expressed as means of three replicates ± SD. $^{a-d}$ Values within a column followed by different letters are significantly different ($p < 0.05$).

TABLE 3 Effects of 2,3-butanedione on the sporulation capacity.

Concentration of 2,3-butanedione (μl per plate)	Sporulation capacity (x10^4 spores/cm^2) incubated for 4 d			
	LB-1	LB-5	LB-7	LB-8
0	270.83 ± 4.01^{a}	7.87 ± 1.67^{a}	55.44 ± 4.88^{a}	100.92 ± 2.45^{a}
1/4 MIC	167.02 ± 3.71^{b}	3.42 ± 0.40^{b}	32.41 ± 2.45^{b}	50.75 ± 3.21^{b}
1/2 MIC	111.46 ± 6.01^{c}	2.13 ± 0.24^{bc}	10.85 ± 0.42^{c}	20.96 ± 1.26^{c}
MIC	39.35 ± 2.32^{d}	0.32 ± 0.12^{c}	3.24 ± 1.23^{c}	2.32 ± 0.46^{d}

Data are expressed as means of three replicates ± SD. $^{a-d}$ Values within a column followed by different letters are significantly different ($p < 0.05$).

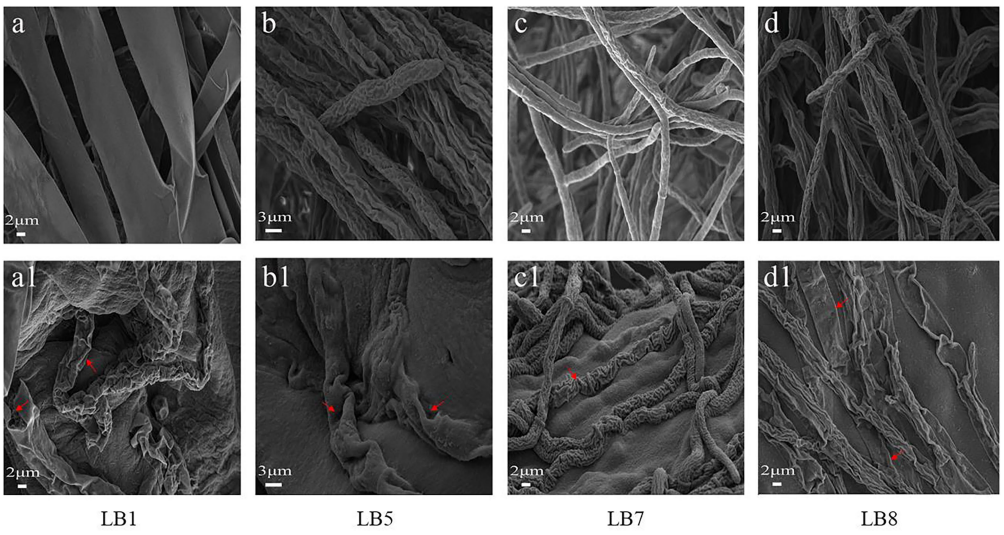

FIGURE 3
Scanning electron microscopy observation of mycelial morphology (**A–D**: control group, **A1–D1**: treatment group with 2,3-butanedione).

pathogenic fungus LB8 were severely distorted and appeared to be severely collapsed and squashed (Figures 3D, D1).

3.6. Effects of 2,3-butanedione on plasmalemma integrity of LB1

Propidium iodide (PI) staining was used to assess the integrity of the plasma membrane by 2.3-butanedione treatment. As shown in Figure 4A, the hyphae of the control group were solely a small portion of red fluorescence while the red fluorescence in the 2,3-butanedione treatment group was remarkably higher. The results indicated that 2,3-butanedione could compromise the integrity of the plasma membrane.

3.7. Release of cell constituents

The internal components of the cell are released when the cell membrane is ruptured by 2,3-butanedione (Figure 4B). In

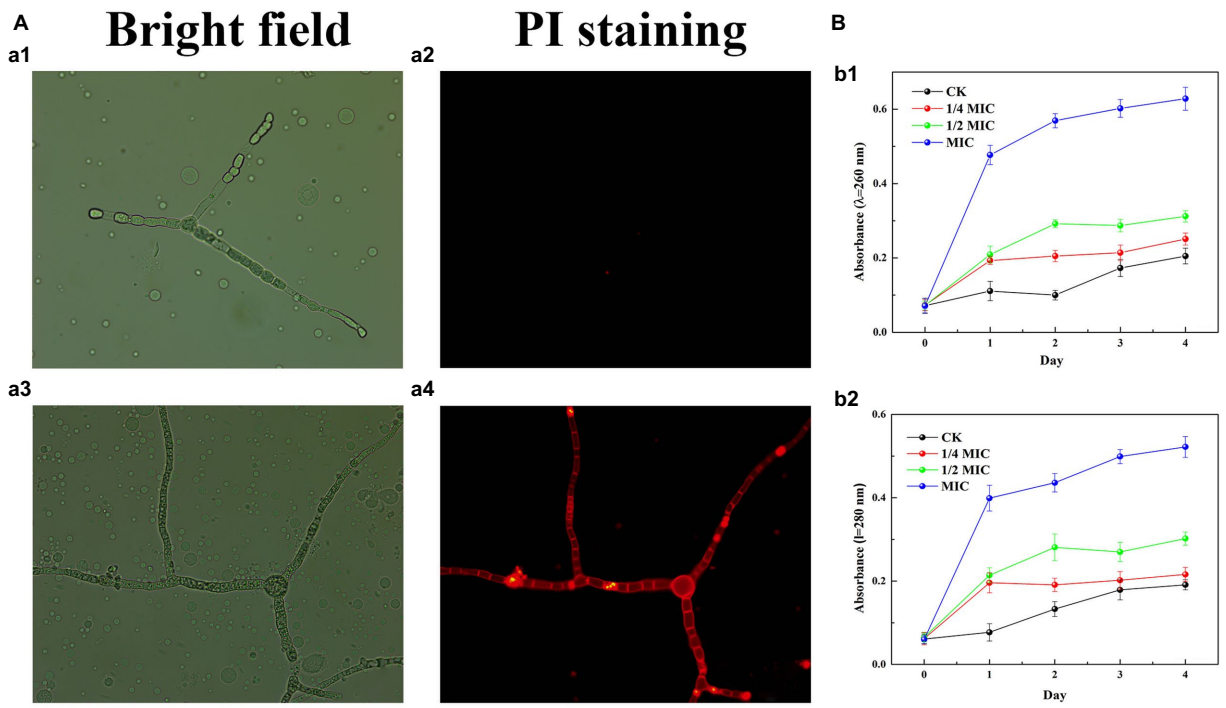

FIGURE 4
(A) Effects of 2,3-butanedione on plasma membrane integrity (**A1**, **A2**: control group, a3-a4: treatment group with 2,3-butanedione, First row: bright field. Second row: propidium iodide). **(B)** Determination of absorbance value at 260nm **(B1)** and 280nm **(B2)** by 2,3-butanedione treatment.

comparison to the control group, the OD_{260} and OD_{280} values rise considerably with treatment time and 2,3-butanedione concentration. This shows that strain LB1 has lost proteins and nucleic acids.

Chaouachi et al. (2021) reported that the *Enterobacter* strain TR1 with 3-methylbutan-1-ol as the main volatile compound has the strongest protective effect on the growth and infection of tomato *Botrytis cinerea*. Zhao et al. (2019) reported that 2, 4-di-tert-butylphenol can significantly inhibit the germination of fungal spores, and change the hyphal morphology and membrane permeability. Essential oils of plants have also been reported to maintain the same antifungal properties (Xu et al., 2021). 2, 3-Butanedione has a strong inhibitory effect on the pathogenic fungi of wolfberry. With the increase of the concentration, it can seriously hinder hyphal growth, spore pullulation and sporulation. SEM results showed that 2,3-butanedione could result the hyphae to shrink, depression, severely collapse and flatten. This result is consistent with other reports on the effects of fungistatic substances. The plasma membrane plays an important role in maintaining the normal life activities of cells. Fluorescence microscopy (FSM) showed that 2,3-butanedione can damage plasma membrane. In addition, the OD_{260} and OD_{280} absorbance values increased, indicating that the increase in cell membrane permeability resulted in the release of internal components. 2,3-Butanedione acts on the cell membrane of pathogenic fungi to produce an inhibitory effect. This is not only consistent with our results, but also consistent with other reports on the effects of antifungal substances (Cui et al., 2021; Li et al., 2021).

3.8. Decay rate, weight loss rate and firmness

Decay rate as shown in Figure 5A, on the 3rd day of treatment, the wolfberry fruits in the group inoculated with the pathogenic fungus LB1 had completely rotted, while the 2,3-butanedione treated group had completely rotted on the 5th day.

The mass loss rate of the fruits induced by strain LB1 was 29.3% on the 3rd day of treatment, while the 2,3-butanedione treated groups was 15.7%. On the 7th day of treatment, the weight loss rate of 2,3-butanedione treated wolfberry fruit was 25.7% lower than that of the wolfberry fruit inoculated with strain LB1 (Figure 5B).

The firmness of wolfberry fruits in the group inoculated with pathogenic fungi LB1 decreased from 2.03×10^5 Pa to 1.16×10^5 Pa after 3 days of treatment, and the firmness was almost undetectable on the 7th day. In contrast, the firmness of the fruit in the 2,3-butanedione treated group was 0.75×10^5 on the 7th day, which was significantly higher than that in the former (Figure 5C). Strain LB1 considerably enhanced the decay rate and weight loss rate, as well as reducing the hardness of wolfberry fruits, as seen in Figure 5. 2,3-butanedione slowed the deterioration of wolfberries induced by strain LB1, decreased the rate of water analysis, kept the firmness of the fruits, and extended the wolfberry's storage time.

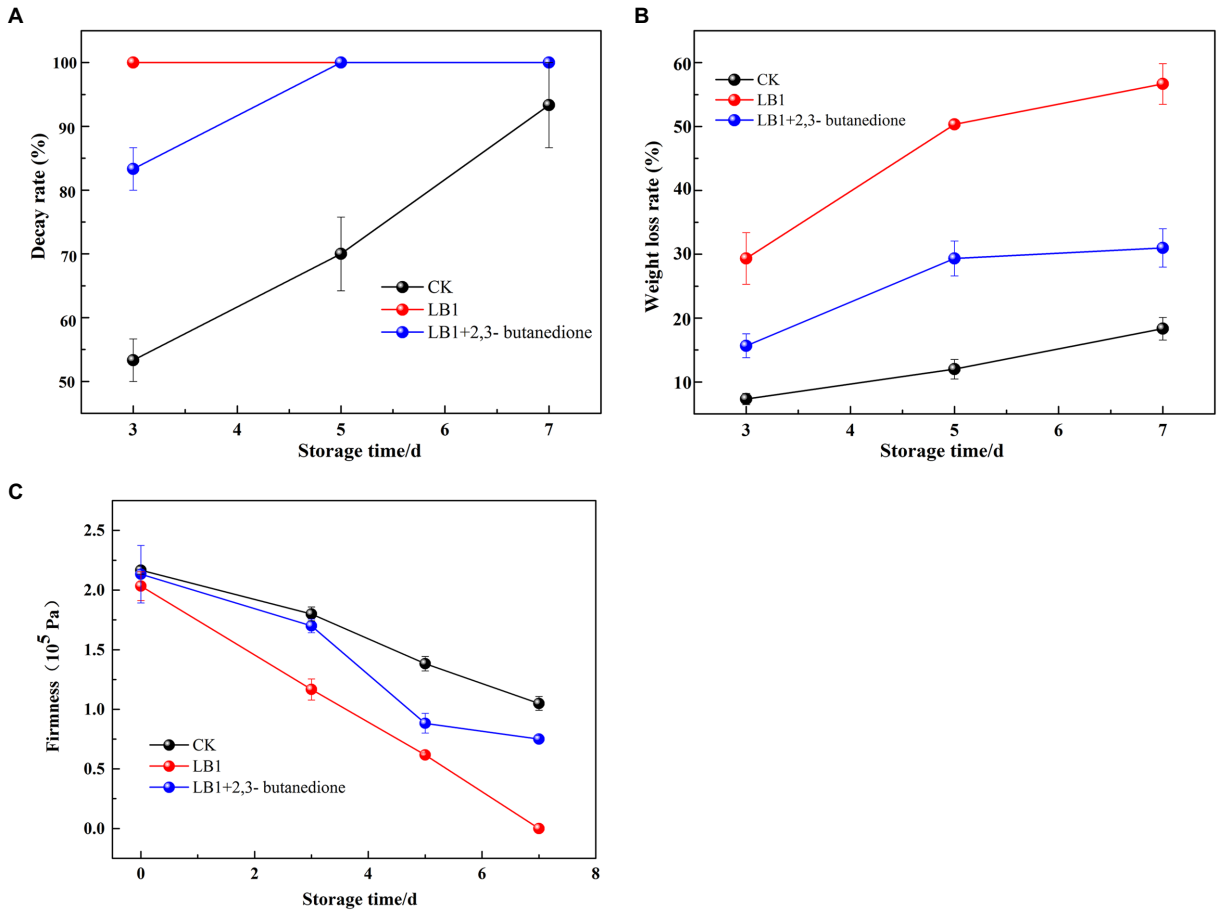

FIGURE 5
Determination of Decay weight, weight loss and firmness of wolfberry fruit after harvest (**A**: Decay weight, **B**: weight loss, **C**: firmness).

3.9. Soluble solids content, total phenol, flavonoid and soluble sugar content

As can be seen from Figure 6, the soluble solids content, soluble sugar content, total phenol and flavonoid in wolfberry fruits showed an overall decreasing trend during the storage process. The soluble solids content, soluble sugar content, total phenol and flavonoid in the 2,3-butanedione treated group were significantly higher than the pathogenic fungi LB1 treated group. However, they were all lower than the control group that had been left blank. This implies that 2,3-butanedione can reduce the rate of nutrient loss caused by the pathogenic LB1 strain.

The disintegration rate, mass loss rate, firmness and soluble solids content of wolfberry fruits directly expressed the quality of wolfberry fruits and affected the storage time of wolfberry fruits. Soluble sugars are the basic substance of the respiration of wolfberry fruits, while the secondary metabolites such as total phenol and flavonoid are closely related to the color development, ripening and aging, flavor formation and stress resistance of wolfberry (Liu et al., 2021). Wang et al. (2012) found 1-methylcyclopropene (1-MCP) could delay the decay time of fresh wolfberry fruits, but it was not a natural product and had low toxicity. Xiao et al. (2018) found that salicylic acid (SA) had an inhibitory effect on pathogenic fungi of wolfberry fruits and could reduce the occurrence of postharvest diseases. However, SA had no meaningful impact on the content of soluble solids in wolfberry fruits, and had a certain irritant to human skin. 2,3-butanedione can virtually stymie the growth and reproduction of pathogenic strain LB1 in wolfberry fruits, delay the utilization and consumption of nutrients in fruits and prolong the storage time of wolfberry fruits. 2,3-butanedione has a small molecular weight, is easy to volatilize, avoids the residue on the surface of the fruit, and is a commonly used food flavor ingredient. Therefore, it is expected to be used as a preservative and biocontrol agent for wolfberry fruit.

3.10. SOD, POD and PPO

The SOD, PPO, and POD activity in wolfberry fruits increased and then decreased after storage, as seen in (Figure 7). The SOD activity of the 2, 3-butanedione treated postharvest fruits were higher in the first 5 days of storage than the control and inoculation strain LB1 treated groups, but decreased on the 7th day. At the beginning of storage, the 2,3-butanedione treatments retained higher SOD activity (Figure 7A). During the evaluation of POD and PPO activities, the POD and PPO activities were higher in the

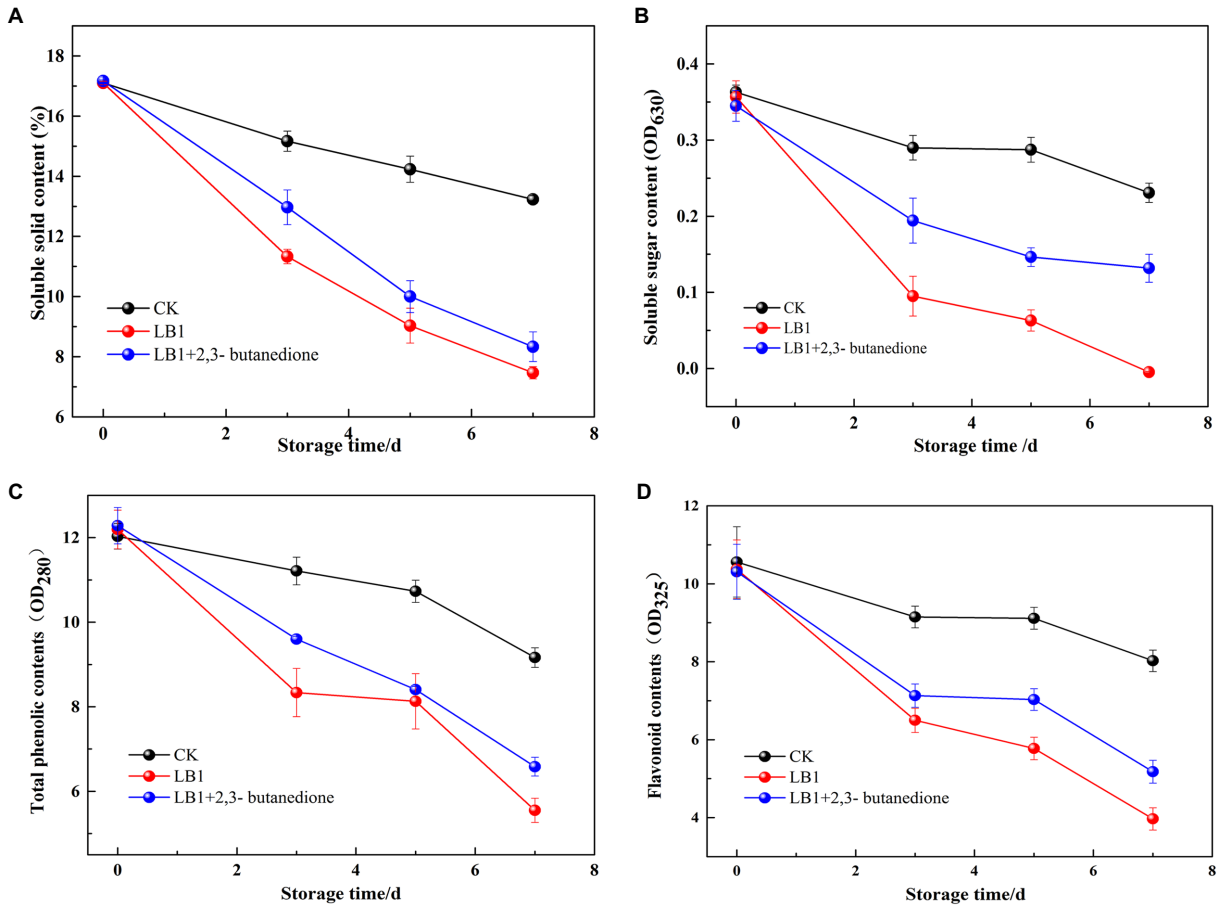

FIGURE 6
Determination of the soluble solids content, total phenols, flavonoids and soluble sugar content of wolfberry fruits after harvest (**A**: soluble solids content, **B**: total phenols, **C**: flavonoids, **D**: soluble sugar content).

butanedione-treated group than in the blank control group, but lower in the treatment group inoculated with pathogenic fungus LB1. This means that PPO and POD activity in wolfberry fruit was kept to a minimum by 2,3-butanedione.

Through the preservation of fruits and vegetables, the activities of SOD, POD, and PPO are closely linked to physiological and biochemical processes (Xu et al., 2016). They are essential for fruit and vegetable stress resistance, postharvest color, and fineness preservation (Wang et al., 2004). The impacts of SOD enzyme activity revealed that the 2,3-butanedione remedy group had significantly higher SOD activity than the LB1 inoculation group. This is agreeing with the research outcomes of Chen (2018). 2,3-butanedione can delay senescence by inducing stress resistance in wolfberry fruits. POD and PPO play a vital function in oxidative metabolism in plants. PPO can oxidize phenolic compounds into quinone compounds that can stymie outgrowth of pathogenic microorganisms (Chen et al., 2019). 2,3-butanedione treatment group POD and PPO enzyme activities were lower than the pathogenic fungus LB1 group, but higher than the control group. 2,3-butanedione can effectively resist fungal attack, inhibit the growth and reproduction of the pathogenic strain LB1 in fruits and prolong the storage period of wolfberry.

4. Conclusion

Four strains of wolfberry pathogenic fungus were isolated, and 2,3-butanedione was confirmed to have antifungal activity and can suppress pathogenic fungi growth and reproduction in fresh wolfberry fruits after harvest, thus extending the storage time of fresh wolfberry fruit. The development of 2,3-butanedione as a post-harvest preservation method for wolfberry fruits has the potential to be significant.

Data availability statement

The original contributions presented in the study are included in the article/Supplementary material, further inquiries can be directed to the corresponding author.

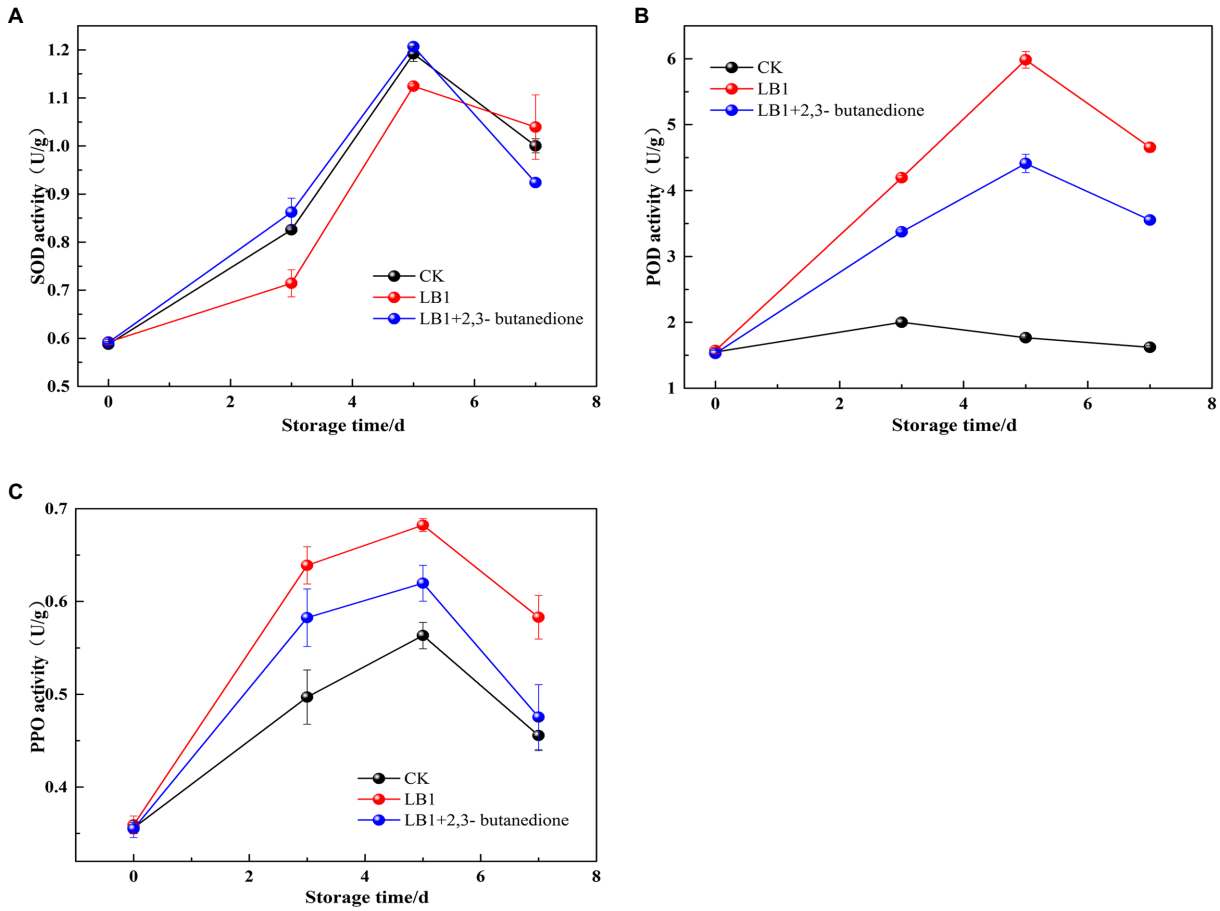

FIGURE 7
Determination of Peroxidase (POD), polyphenoloxidase enzymes (PPO) and superoxide dismutase (SOD) of postharvest wolfberry fruits (**A**: SOD, **B**: POD, **C**: PPO).

Author contributions

All authors contributed to the study conception and design. HL, YZ, CY, and LL performed the material preparation, data collection, and analysis. The first draft of the manuscript was written by HL. All authors commented on previous versions of the manuscript. All authors contributed to the article and approved the submitted version.

Funding

This work was supported by Lanzhou Science and Technology Plan Project 2018–1-104; Special Fund Project for Guiding Science and Technology Innovation and Development in Gansu Province 2019ZX-05; and Gansu Province's Higher Education Industry Support Plan 2020C-21.

Conflict of interest

The authors declare that the research was conducted in the absence of any commercial or financial relationships that could be construed as a potential conflict of interest.

Publisher's note

All claims expressed in this article are solely those of the authors and do not necessarily represent those of their affiliated organizations, or those of the publisher, the editors and the reviewers. Any product that may be evaluated in this article, or claim that may be made by its manufacturer, is not guaranteed or endorsed by the publisher.

Supplementary material

The Supplementary material for this article can be found online at: https://www.frontiersin.org/articles/10.3389/fmicb.2022.1068144/full#supplementary-material

References

Ambler, K., Brauw, A. D., and Godlonton, S. (2017). Measuring postharvest losses at the farm level in Malawi. *Australian J. Agricultural & Resource Econ.* 62, 139–160. doi: 10.1111/1467-8489.12237

Brilli, F., Loreto, F., and Baccelli, I. (2019). Exploiting plant volatile organic compounds (VOCs) in agriculture to improve sustainable defense strategies and productivity of crops. *Front. Plant Sci.* 10:264. doi: 10.3389/fpls.2019.00264

Cenobio-Galindo, A. D. J., Ocampo-López, J., Reyes-Munguía, A., Carrillo-Inungaray, M. L., Cawood, M., Medina-Pérez, G., et al. (2019). Influence of bioactive compounds incorporated in a Nanoemulsion as coating on avocado fruits (Persea americana) during postharvest storage: antioxidant activity, physicochemical changes and structural evaluation. *Antioxidants* 8:500. doi: 10.3390/antiox8100500

Chan, H. H. L., Lam, H. I., Choi, K. Y., Li, S. Z. C., Lakshmanan, Y., Yu, W. Y., et al. (2019). Delay of cone degeneration in retinitis pigmentosa using a 12-month treatment with Lycium barbarum supplement. *J. Ethnopharmacol.* 236, 336–344. doi: 10.1016/j.jep.2019.03.023

Chaouachi, M., Marzouk, T., Jallouli, S., Elkahoui, S., Gentzbittel, L., Ben, C., et al. (2021). Activity assessment of tomato endophytic bacteria bioactive compounds for the postharvest biocontrol of Botrytis cinerea. *Postharvest Biol. Technol.* 172:111389. doi: 10.1016/j.postharvbio.2020.11138

Chen, W. (2018). *Effect of potato glycoside alkaloid on induced disease resistance and fresh-keeping of fresh wolfberry fruits*. China: Gansu agricultural university.

Chen, C., Cai, N., and Chen, J. (2019). Clove essential oil as an alternative approach to control postharvest blue mold caused by Penicillium italicum in citrus fruit. *Biomol. Ther.* 9, 1–13. doi: 10.3390/biom9050197

Chen, M., Lin, H., Zhang, S., Lin, Y., Chen, Y., and Lin, Y. (2015). Effects of adenosine triphosphate (ATP) treatment on postharvest physiology, quality and storage behavior of Longan fruit. *Food Bioprocess Technol.* 8, 971–982. doi: 10.1007/s11947-014-1462-z

Cui, X., Ma, D., Liu, X., Zhang, Z., Li, B., Xu, Y., et al. (2021). Magnolol inhibits gray mold on postharvest fruit by inducing autophagic activity of Botrytis cinerea. *Postharvest Biol. Technol.* 180:111596. doi: 10.1016/j.postharvbio.2021.111596

Fan, X. J., Zhang, B., Yan, H., Feng, J. T., Ma, Z. Q., and Zhang, X. (2019). Effect of lotus leaf extract incorporated composite coating on the postharvest quality of fresh goji (Lycium barbarum L.) fruit. *Postharvest Biol. Technol.* 148, 132–140. doi: 10.1016/j.postharvbio.2018.10.020

Farsalinos, K. E., Kistler, K. A., Gillman, G., and Voudris, V. (2014). Evaluation of electronic cigarette liquids and aerosol for the presence of selected inhalation toxins. *Nicotine Tob. Res.* 17, 168–174. doi: 10.1093/ntr/ntu176

Habibi, F., Ramezanian, A., Rahemi, M., Eshghi, S., Guillen, F., Serrano, M., et al. (2019). Postharvest treatments with gamma-aminobutyric acid, methyl jasmonate, or methyl salicylate enhance chilling tolerance of blood orange fruit at prolonged cold storage. *J. Sci. Food Agric.* 99, 6408–6417. doi: 10.1002/jsfa.9920

Hallagan, J. B. (2017). The use of diacetyl (2,3-butanedione) and related flavoring substances as flavorings added to foods-workplace safety issues. *Toxicology* 388, 1–6. doi: 10.1016/j.tox.2017.05.010

Jatoi, M. A., Jurić, S., Vidrih, R., Vinceković, M., Vuković, M., and Jemrić, T. (2017). The effects of postharvest application of lecithin to improve storage potential and quality of fresh goji (Lycium barbarum L.) berries. *Food Chem.* 230, 241–249. doi: 10.1016/j.foodchem.2017.03.039

Kong, J., Zhang, Y., Ju, J., Xie, Y., Guo, Y., Cheng, Y., et al. (2019). Antifungal effects of thymol and salicylic acid on cell membrane and mitochondria of Rhizopus stolonifer and their application in postharvest preservation of tomatoes. *Food Chem.* 285, 380–388. doi: 10.1016/j.foodchem.2019.01.099

Lan, P., Gao, F. R., Chen, C. K., Wang, W. S., Han, J., Hai-Peng, J. I., et al. (2014). Separation and identification of pathogenic fungi from the postharvest Lycium Barbarmu. *China Fruit & Vegetable* 34, 9–12.

Lemos Junior, W. J. F., Binati, R. L., Felis, G. E., Slaghenaufi, D., Ugliano, M., and Torriani, S. (2020). Volatile organic compounds from Starmerella bacillaris to control gray mold on apples and modulate cider aroma profile. *Food Microbiol.* 89:103446. doi: 10.1016/j.fm.2020.103446

Li, L., Hui, P., Chen, M., Zhang, S., and Zhong, C. (2017). Isolation and identification of pathogenic fungi causing postharvest fruit rot of kiwifruit (Actinidia chinensis) in China. *J. Phytopathol.* 165, 782–790. doi: 10.1111/jph.12618

Li, Z., Wei, Y., Xu, Y., Han, P., Jiang, S., Xu, F., et al. (2021). Terpinen-4-ol treatment maintains quality of strawberry fruit during storage by regulating sucrose-induced anthocyanin accumulation. *Postharvest Biol. Technol.* 174:111461. doi: 10.1016/j.postharvbio.2020.111461

Ling, L. J., Li, Z. B., Jiao, Z. L., Zhang, X., Ma, W. X., Feng, J. J., et al. (2019). Identification of novel endophytic yeast strains from tangerine Peel. *Curr. Microbiol.* 76, 1066–1072. doi: 10.1007/s00284-019-01721-9

Ling, L., Zhao, Y., Tu, Y., Yang, C., Ma, W., Feng, S., et al. (2021). The inhibitory effect of volatile organic compounds produced by Bacillus subtilis CL2 on pathogenic fungi of wolfberry. *J. Basic Microbiol.* 61, 110–121. doi: 10.1002/jobm.202000522

Liu, W. J., Jiang, H. F., Rehman, F. U., Zhang, J. W., Chang, Y., Jing, L., et al. (2017a). Lycium Barbarum polysaccharides decrease hyperglycemia-aggravated ischemic brain injury through maintaining mitochondrial fission and fusion balance. *Int. J. Biol. Sci.* 13, 901–910. doi: 10.7150/ijbs.18404

Liu, J., Sui, Y., Wisniewski, M., Xie, Z. G., Liu, Y. Q., You, Y. M., et al. (2018). The impact of the postharvest environment on the viability and virulence of decay fungi. *Crit. Rev. Food Sci. Nutr.* 58, 1681–1687. doi: 10.1080/10408398.2017.1279122

Liu, Y., Wang, H., Wang, Y. D., Sun, W. Y., Guo, X. X., Ran, G. W., et al. (2017b). Isolation, identification and biological characteristics of pathogenic fungus from Chinese wolfberry fruit. *T. Chinese Society of Agricultural Engineering* 33, 374–380.

Liu, J., Zhao, Y., Xu, H., Zhao, X., Tan, Y., Li, P., et al. (2021). Fruit softening correlates with enzymatic activities and compositional changes in fruit cell wall during growing in Lycium barbarum L. *Int. J. Food Sci. Technol.* 56, 3044–3054. doi: 10.1111/ijfs.14948

Mari, M., Bautista-Baños, S., and Sivakumar, D. (2016). Decay control in the postharvest system: role of microbial and plant volatile organic compounds. *Postharvest Biol. Technol.* 122, 70–81. doi: 10.1016/j.postharvbio.2016.04.014

María, G. S. D., Gilda, Y. A. M., Hugo, C. A. B., and Adrien, G. (2018). Two efficient methods for isolation of high-quality genomic DNA from entomopathogenic fungi. *J. Microbiol. Methods* 148, 55–63. doi: 10.1016/j.mimet.2018.03.012

Moore, G. G., Lebar, M. D., Carter-Wientjes, C. H., and Gilbert, M. K. (2021). The potential role of fungal volatile organic compounds in aspergillus flavus biocontrol efficacy. *Biol. Control* 160:104686. doi: 10.1016/j.biocontrol.2021.104686

Morgan, D. L., Jokinen, M. P., Johnson, C. L., Price, H. C., Gwinn, W. M., Bousquet, R. W., et al. (2016). Chemical reactivity and respiratory toxicity of the alpha-Diketone flavoring agents: 2,3-Butanedione, 2,3-Pentanedione, and 2,3-Hexanedione. *Toxicol. Pathol.* 44, 763–783. doi: 10.1177/0192623316638962

Nunes, C. A. (2012). Biological control of postharvest diseases of fruit. *Eur. J. Plant Pathol.* 133, 181–196. doi: 10.1007/s10658-011-9919-7

Sun, G. Y., Cui, J. Q., Wang, S. F., Zhang, R., and Gleason, M. L. (2008). First report of anthracnose of Lycium barbarum caused by Colletotrichum acutatum in China. *Plant Dis.* 92:1471. doi: 10.1094/PDIS-92-10-1471A

Tian, J., Ban, X., Zeng, H., He, J., Chen, Y., and Wang, Y. (2012). The mechanism of antifungal action of essential oil from dill (Anethum graveolens L.) on Aspergillusflavus. *PLoS One* 7:e30147. doi: 10.1371/journal.pone.0030147

Wallace, R. L., Hirkala, D. L., and Nelson, L. M. (2017). Postharvest biological control of blue mold of apple by Pseudomonas fluorescens during commercial storage and potential modes of action. *Postharvest Biol. Technol.* 133, 1–11. doi: 10.1016/j.postharvbio.2017.07.003

Wang, R. Q., Feng, J. H., Wei, W. W., Xu, X. M., and Qing, Y. W. (2012). Effect of 1-methylcyclopropene and modified atmosphere packaging on quality retention during cold-tempereture storage of Lycium barbarum fruit. *Transactions of the Chinese Society of Agricultural Engineering* 28, 287–292.

Wang, Y. S., Tian, S. P., Xu, Y., Qin, G. Z., and Yao, H. (2004). Changes in the activities of pro-and anti-oxidant enzymes in peach fruit inoculated with Cryptococcus laurentii or Penicillium expansum at 0 or 20 °C. *Postharvest Biol. Technol.* 34, 21–28. doi: 10.1016/j.postharvbio.2004.04.003

Wang, Y. M., Zhang, K., Fei-Hua, X. U., Wang, Y., Ren, X. W., and Zhang, B. L. (2014). Chemical analysis and nutritional evaluation of different varieties of goji berries (Lycium barbarum L.). *Food Sci.* 35, 34–38.

Wang, Z., Zhong, T., Chen, K., Du, M., Chen, G., Chen, X., et al. (2020). Antifungal activity of volatile organic compounds produced by Pseudomonas fluorescens ZX and potential biocontrol of blue mold decay on postharvest citrus. *Food Control* 107499:310. doi: 10.1016/j.foodcont.2020.107499

Wei, L., Mao, W., Jia, M., Xing, S., Ali, U., Zhao, Y., et al. (2018). FaMYB44.2, a transcriptional repressor, negatively regulates sucrose accumulation in strawberry receptacles through interplay with FaMYB10. *J. Exp. Bot.* 69, 4805–4820. doi: 10.1093/jxb/ery249

Wonglom, P., Ito, S., and Sunpapao, A. (2020). Volatile organic compounds emitted from endophytic fungus Trichoderma asperellum T1 mediate antifungal activity, defense response and promote plant growth in lettuce (Lactuca sativa). *Fungal Ecol.* 43:100867. doi: 10.1016/j.funeco.2019.100867

Wu, Q., Gao, H., Zhang, Z., Li, T., Qu, H., Jiang, Y., et al. (2020). Deciphering the metabolic pathways of pitaya Peel after postharvest red light irradiation. *Meta* 10:108. doi: 10.3390/metabo10030108

Xiao, W., Di, X. X., Yong, C., Ling, Z. R., Ping, T. S., and Qiang, L. B. (2018). Isolation and identification of postharvest pathengens in fresh wolfberry from Ningxia and inhibitory effect of salicylic acid. *J. Food Safety and Quaity* 9, 5837–5842.

Xu, F., Wang, S., Xu, J., Liu, S., and Li, G. (2016). Effects of combined aqueous chlorine dioxide and UV-C on shelf-life quality of blueberries. *Postharvest Biol. Technol.* 117, 125–131. doi: 10.1016/j.postharvbio.2016.01.012

Xu, Y., Wei, J., Wei, Y., Han, P., Dai, K., Zou, X., et al. (2021). Tea tree oil controls brown rot in peaches by damaging the cell membrane of Monilinia fructicola. *Postharvest Biol. Technol.* 175:111474. doi: 10.1016/j.postharvbio.2021.111474

Yang, S., Hong, W. C., Jie, C. Z., and Ting, H. Y. (2016). Research Progress on postharvest physiology and storage Technology of Fresh Fruit of Lycium barbarum L. *Storage and Process* 16, 102–106.

Zhang, S. W., Zheng, Q., Xu, B. L., and Liu, J. (2019). Identification of the fungal pathogens of postharvest disease on peach fruits and the control mechanisms of Bacillus subtilis JK-14. *Toxins* 11:322. doi: 10.3390/toxins11060322

Zhao, P. Y., Li, P. Z., Wu, S. Y., Zhou, M. S., and Gao, H. Y. (2019). Volatile organic compounds (VOCs) from Bacillus subtilis CF-3 reduce anthracnose and elicit active defense responses in harvested litchi fruits. *AMB Express* 9:119. doi: 10.1186/s13568-019-0841-2

Zhong, T., Wang, Z., Zhang, M., Wei, X., Kan, J., Zalán, Z., et al. (2021). Volatile organic compounds produced by Pseudomonas fluorescens ZX as potential biological fumigants against gray mold on postharvest grapes. *Biol. Control* 163:104754. doi: 10.1016/j.biocontrol.2021.104754

Zhou, D., Wang, Z., Li, M., Xing, M., Xian, T., and Tu, K. (2017). Carvacrol and eugenol effectively inhibit Rhizopus stolonifer and control postharvest soft rot decay in peaches. *J. Appl. Microbiol.* 124, 166–178. doi: 10.1111/jam.13612

frontiers | Frontiers in Microbiology

TYPE Original Research
PUBLISHED 07 February 2023
DOI 10.3389/fmicb.2022.1115592

OPEN ACCESS

EDITED BY
Chao Shi,
Northwest A&F University, China

REVIEWED BY
Shi-Wu Li,
Shihezi University,
China
Li Nan,
Northwestern Polytechnical University,
China

*CORRESPONDENCE
Na Wei
✉ weina@taaas.org

†These authors have contributed equally to this work and share first authorship

SPECIALTY SECTION
This article was submitted to Food Microbiology, a section of the journal Frontiers in Microbiology

RECEIVED 04 December 2022
ACCEPTED 30 December 2022
PUBLISHED 07 February 2023

CITATION
Wang J, Zhang F, Yao T, Li Y and Wei N (2023) Risk assessment of mycotoxins, the identification and environmental influence on toxin-producing ability of *Alternaria alternate* in the main Tibetan Plateau *Triticeae* crops. *Front. Microbiol.* 13:1115592. doi: 10.3389/fmicb.2022.1115592

Risk assessment of mycotoxins, the identification and environmental influence on toxin-producing ability of *Alternaria alternate* in the main Tibetan Plateau *Triticeae* crops

Jun Wang[1†], Feilong Zhang[2†], Ting Yao[1], Ying Li[2] and Na Wei[2*]

[1]Zhang Zhong-jing School of Chinese Medicine, Nanyang Institute of Technology, Nanyang, China, [2]Institute of Agricultural Product Quality Standard and Testing Research, Tibet Academy of Agricultural and Animal Husbandry Sciences, Lhasa, China

In order to find out the contamination of mycotoxins in *Triticeae* crops of Qinghai-Tibet Plateau, a total of 153 *Triticeae* crop fruits were collected as target samples, and 22 mycotoxins were tested. High detection rate was found in the *Alternaria* mycotoxins, including tentoxin (TEN), tenuazonic acid (TEA) and alternariol (AOH) toxins. To further clarify the production rules of *Alternaria* mycotoxins. A number of 9 high yield toxic strains were selected from 65 bacterial strains and the gene sequences of each were determined. The nine selected *Alternaria* alternate were cultured under specific pH of the culture medium, temperature and ultraviolet (UV) irradiation, and their growth and toxicity were analyzed. The results showed that the toxic capacity of most *A. alternate* increased with the increase of culture environment temperature and decreased with the increase of UV irradiation. However, the production of some toxins did not meet this principle, or even met the principle of relativity. In the culture experiments, a total of five *Alternaria* toxins were detected as positive, which were TEN, AOH, alternariol monomethyl ether (AME), TEA, and *Alternaria* (ALT). The altenusin (ALS) toxin was not detected in the metabolites of the nine *Alternaria* strains. It indicated that the TEN, AOH, AME, TEA, and ALT toxins should be particularly valued in the future risk assessments. This finding provided comprehensive information of mycotoxins contamination in the Tibetan Plateau *Triticeae* crops, it pointed out a direction to the Tibetan Plateau food crops' quality control.

KEYWORDS

mycotoxin, *Alternaria alternate*, toxigenic capacity, hull-less barley, *Triticeae*

Introduction

Triticeae crops, including hull-less barley (*Hordeum vulgare Linn.* var. nudum Hook. F.) and wheat (*Triticum aestivum* L.), were the most important food crops on the Tibetan Plateau for thousands of years (Shun et al., 2011; Galli et al., 2020) The quality and safety of *Triticeae* crops determined the Tibetan economy, people's lives and health (Bryan et al., 2018). Both of hull-less barley and wheat had a long history of planting on the Qinghai-Tibet Plateau, with a large sown area and a wide adaptation range, from the valley slope below 2,500 m to the lakeside plain at around 4,200 m. Among the both, hull-less barley was the dominant characteristic crop of Tibet, and it was the basic ration crop on which the Tibetan people live survival and reproduction (Zeng et al., 2015). The planting area of hull-less barley accounted for about 70% of the total. Wheat was second only to hull-less barley in grain production in Tibet. It was planted in vast agricultural areas from humid and semi-humid areas to

semi-arid and arid areas in western China (Cui et al., 2018). Therefore, the quality and safety of hull-less barley and wheat was directly related to the development of Tibetan agriculture and people's lives (Chen et al., 2021).

The mycotoxins are a class of secondary metabolites with carcinogenic, teratogenic and mutational characteristics produced by fungi such as aspergillus and fusarium, which seriously threaten the health of human and animals (Pereira et al., 2014). At present, more than 400 kinds of mycotoxins had been found, among which the aflatoxin, ochratotoxin, and fumonisin et al. were the main mycotoxins that polluted the alimentarn crops, which could produce in the crop field growth stage to post-harvest storage stage (Piacentini et al., 2017; Hassan and Zhou, 2018). The pollution of food crops by mycotoxins was a widespread problem, and all countries in the world suffered from mycotoxin pollution to varying degrees. Statistical studies have found that the average annual economic loss of corn due to aflatoxin pollution in the United States was 1.68 billion dollars, and in Europe, the toxin pollution of deoxynivalenol was found in more than 44.6% of the tested grains (Qu et al., 2008; Ji et al., 2014; Mitchell et al., 2016). In China, the Ministry of Agriculture has carried out continuous monitoring of wheat mycotoxin pollution for many years and found that the mycotoxin in main wheat producing area was mainly contaminated by deoxynivalenol and zearalenone toxins (Qiu and Shi, 2014; Qiu et al., 2014). However, since the main *Triticeae* crops on the Qinghai-Tibet Plateau were hull-less barley, and the wheat planting area was limited, it did not belong to the main wheat producing areas in China, so the mycotoxin pollution of *Triticeae* crops on the Qinghai-Tibet Plateau was rarely reported.

Tibet had a special geographical location, diverse habitats and rich characteristic fungal resources, which was important value in scientific research. Differences in geographical environment and climatic conditions led to differences in microbial community composition in ecological zones. Natural environment had an important influence on the formation and evolution of biological species, and it was one of the hotspots of global biodiversity research (Fillinger et al., 2020). In China, systematic investigations and studies had been carried out on large fungal resources and characteristic resources in Tibet, and more than 2,000 fungal species have been found, among which endemic species to Tibet account for a high proportion. The altitude span of the agricultural production area in Tibet was 2,000 ~ 4,200 m (Li et al., 2015; Jiang et al., 2016). The geographical environment and climate factors such as temperature, rainfall and ultraviolet radiation changed with the altitude, thus forming complex environmental changes on the height gradient and affecting the species composition of microbial communities. Zhang et al. (2016) studied the impact of environmental conditions on soil microorganisms in Tibet and found that fertile and humid environment contributes to the growth of soil bacteria, and barren drought was conducive to the growth of soil fungi. Ren et al. (2018) studied microbial quantity, bacterial and fungal diversity and community composition with altitude gradient and found that high alpha diversity and the changes along the altitude ladder were greater than the fungal community, and soil temperature and humidity were the main causes of changes in bacterial community composition. However, few studies had been reported on the diversity, phylogeny and evolution of fungal fungi in the Tibetan Plateau.

In this work, in order to find out the contamination of mycotoxins in *Triticeae* crops of Qinghai-Tibet Plateau, 153 *Triticeae* crop fruits were collected as target samples, and 22 mycotoxins including aflatoxin B_1 (AFB_1), aflatoxin B_2 (AFB_2), aflatoxin G_1 (AFG_1), aflatoxin G_2 (AFG_2), ochratoxin A (OTA), ochratoxin B (OTB), ochratoxin C (OTC), sterigmatocystin (ST), zearalenone (ZEN), deoxynivalenol (DON), 3-Acetyl Deoxynivalenol (3-AcDON), 15-Acetyl Deoxynivalenol (15-AcDON), HT-2 toxin (HT-2), trichothecenes (T-2), fumonisin B_1 (FB_1), fumonisin B_2 (FB_2), alternariol monomethyl ether (AME), tenuazonic acid (TEA), alternariol (AOH), tentoxin (TEN), altenusin (ALS), and *Alternaria* (ALT) were tested in these samples. The 22 mycotoxins included *Aspergillus*, *Fusarium*, and *Alternaria* mycotoxins. These three classes of mycotoxins were widely detected in agricultural production (Agriopoulou et al., 2020; Li et al., 2021). The detection rates of TEN and TEA were the two highest targets, and all the two mycotoxins belong to *Alternaria* toxins (López et al., 2016; Mukesh et al., 2017; Gotthardt et al., 2019), produced by *Alternaria alternata* (Estiarte et al., 2016; Yang et al., 2017; Huang et al., 2020). In order to explore the mycotoxin production of *A. alternata*, a total of 65 bacterial strains were collected from different coordinate positions on the Qinghai-Tibet Plateau, then nine high yield toxic strains were selected and the gene sequences of each were determined. Tibet has a special geographical location, high altitude, strong ultraviolet light, and large temperature difference between day and night, which is bound to affect the toxic production of parasitic fungi in *Triticeae* crops on the Qinghai-Tibet Plateau (Liu et al., 2021; Yao et al., 2021). To clarify these rules, the nine selected bacterial strains were cultured under different experimental conditions, and their growth and toxicity were analyzed. The conclusion in this work was benefit for mycotoxin pollution reduction in *Triticeae* crops, scientific supervision and the Tibetan people's consumption safety.

Materials and methods

Main reagents

A total of 153 crop fruits were obtained from Lhasa, Nyingchi, Qamdo, Shannan and Xigaze, and stored at 4°C. The standard solutions of 22 mycotoxins each containing 100 μg/mL were acquired from Pribolab Co. (Shandong, PR China), stored at-20°C. A total of 65 *A. alternata* were isolated from hull-less barley and wheat from different regions and stored at −80°C. The potato dextrose agar (PDA) medium was purchased from Qingdao Hope Bio-Technology Co., Ltd. (Shandong, PR China). Chromatographic grade of methanol, ammonium acetate, formic acid and acetonitrile were purchased from Merck Chemical (Shanghai, PR China).

Detection of the mycotoxins in *Triticeae* crops samples

The 22 mycotoxins in the *Triticeae* crop fruits were analyzed by the standardized method with some modifications (Zhao et al., 2017).

Sample pretreatment

The samples (5.0 g ± 0.01 g) were accurately weighed and placed into 50 mL centrifuge tube. The acetonitrile of 20 mL was added and a homogenization process was sustained for 30 min with a homogenizer to fully dissolve the mycotoxins into acetonitrile. Then the system was separated by a centrifuge at 6,000 rpm for 10 min. The supernatant of 1.5 mL was absorbed into a 5 mL plastic vial, and 0.5 mL of ultrapure water was added. After the system has been mixed evenly and filtered through a 0.22 μm PTEE, the solution was taken as sample solution for high-performance liquid chromatography - mass spectrometer (HPLC–MS/MS).

HPLC–MS/MS analysis

An AB SCIEX Triple Quad™ 5,500 HPLC–MS/MS, with a CAPCELL PAK C_{18} MGIIfilled column (2.1 mm × 100 mm, 5 μm) was employed for separation and detection. The temperature of column for chromatographic separation was set at 35°C and the injection volume was set as 2.0 μl. The gradient elution program was set with mobile phase A of 0.1% formic acid (v/v) in 2 mol/l ammonium acetate and mobile phase B of methanol and a flow rate of 0.30 mL/min was set up. The modes of electrospray ionization (ESI) ion and multiple reaction monitoring (MRM) were used to determine the mycotoxins quantitatively. The ion spray voltage was set at 5500 V, the ion source temperature at 550°C and the curtain gas was 60 psi.

Measurements of the growth parameters

The evaluation of *A. alternata* growth rate was performed by measuring the bacterial colony diameter of PDA medium. The medium was inoculated with 8 mm of *A. alternata* cake with the mycelial were faced downwards and cultivated in a special environment. The bacterial colony diameter was determined by cross method, and the diameter of bacterial colony was the diameter of the colony minus the diameter of the cake.

Isolation of high toxin-producing ability of *Alternaria alternata*

In a sterile room, the toxin-producing ability of each *A. alternata* was determined by spread plated on the PDA medium and incubated at 25°C for 7 days. The PDA medium was scraped off the hyphae and dried at 60°C. The dried medium was blended with acetonitrile and placed for 12 h at room temperature. The mixture was filtered through a 0.22 μm PTEE to LC-MS/MS assay. According to the analytic results, a total of nine strains were selected from the 65 *A. alternata*, and the information of nine *A. alternata* was as shown in Table 1.

Strain identification

The genomic DNA of the nine strains *A. alternata* was extracted using a GenEluteTM kit (Tiangen Biotech Co., Ltd., Beijing, China) in accordance with the manufacturer's protocol. The PCR amplification was performed as follows: initial denaturation at 95°C for 3 min, 27 cycles of denaturing at 95°C for 30 s, annealing at 55°C for 30 s and extension at 72°C for 45 s. The 16S rDNA genes were amplified using the primers of 7F (5′-CAGAGTTTGAT CCTGGCT-3′) and 1540R (5′-AGGAGGTGATCCAGCCGCA-3′). PCR products were purified and sequenced by the Beijing Liuhe Huada Gene Technology Co., Ltd. After the alignment of the sequencing results on the NCBI website, the sequences with high homology were downloaded to construct the phylogenetic trees on the neighbour-joining method in MEGA 6.0 software.

The effect of the *Alternaria alternata* growth conditions

The culture of nine toxigenic strains

In order to examine the toxin-production capacity of the nine toxigenic strains in different environments, the simulated environment of the Qinghai-Tibetan Plateau was constructed in the laboratory at an altitude of 3,650 m, and the activities of them were monitored in medium in relation to two different factors: the incubation temperature and the UV irradiation. Hyphal growth rate method was used to determine the effects of different conditions on fungi. The 15 mL culture medium was poured into 90 mm diameter dish. After cooling and solidification, a piece of 8 mm fungus cake was added in the center of each dish, with hyphae face down and placed in specific environmental species for culture, and each treatment was repeated three times.

The detection

After 7 days of culture, the colony diameter was measured by the cross-crossing method, and the average value of the three measurements was used as the measurement result, minus the bacterial cake diameter as the colony diameter. The growing mycelia were carefully collected and dried at 60°C for 12 h. The toxin-production ability was measured by HPLC-MS/MS according to the proposed method. The targets were six common *Alternaria* toxins, including TEN, AOH, AME, TEA, ALS and ALT.

The PH of the culture medium

The PDA culture medium was selected to verify the effect of pH conditions. The pH of PDA culture medium was adjusted with 0.2 mol/L disodium hydrogen orthophosphate to 5.8.

Temperature

The nine strains *A. alternata* were individually inoculated on the PDA medium and incubated for at different temperature (15°C, 25°C, and 28°C) for 12 h, and then incubated at 10°C for 12 h, kept for 7 days. The diameter of colony was measured every other day since the third day. And toxin-production ability was evaluated according to the toxin-production after 7 days of culture.

UV irradiation

The PDA medium was used to culture the nine strains *A. alternata* and exposed to with UV irradiation. After the inoculation of different strains, the medium was incubated at 25°C for 12 h, and then incubated at 10°C for 12 h, alternate ran kept for 7 days. From the third day on, the systems were irradiated for 0, 3, 5 h every 24 h 25°C. The effect of UV irradiation on the toxin production ability and growth of the strains were determined by measuring *Alternaria* toxins and bacterial colony diameter after 7 days.

Statistical analysis

All data were presented as mean ± standard deviation and significance was accepted at $p < 0.05$. The Origin 2019 software (Origin Lab Co., Ltd.; USA) used to express the statistical data and graphs. One-way ANOVA followed by LSD were performed in SPSS 26.0 for Windows (SPSS Inc., Chicago, IL, USA) to determine the significance of the results of the toxigenic ability evaluation and the mycelial diameter.

10.3389/fmicb.2022.1115592

TABLE 1 The information of nine *Alternaria alternata*.

No.	Place of origin	Longitude	Latitude	Crop species	Date of acquisition	Altitude/m
S01-5	Jixiong Town, Gongga County, Shannan City	91.000813°	29.331504°	Wheat	2019	3,577
S05-5	Jixiong Town, Gongga County, Shannan City	90.993080°	29.297055°	Wheat	2018	3,574
2S10-1	Jixiong Town, Gongga County, Shannan City	91.017038°	29.28476°	Wheat	2018	3,588
R01-9	Langazi County, Xigaze City	90.467313°	29.142156°	Hull-less barley	2019	4,429
PL18-4b	Duoyou Village, Pulan Town, Pulan County, Ali District	81.164900°	30.324800°	Hull-less barley	2018	3,964
PL18-5b	Duoyou Village, Pulan Town, Pulan County, Ali District	81.164901°	30.324802°	Hull-less barley	2018	3,964
QBM02-13	Guxianggu village, Bomi County, Nyingchi City	95.470498°	29.907560°	Hull-less barley	2019	2,594
QBM05-10	Guxianggu village, Bomi County, Nyingchi City	95.470498°	29.907561°	Hull-less barley	2019	2,594
QBY06-2	Agriculture and Animal Husbandry College experimental site, Bayi District, Nyingchi City	94.340090°	29.672330°	Hull-less barley	2019	2,976

Results and discussion

The analysis mycotoxins in 145 samples

The mycotoxin contents in 153 hull-less barley and wheat samples were analyzed, the detection targets included AFB_1, AFB_2, AFG_1, AFG_2, OTA, OTB, OTC, ST, ZEN, DON, 3-AcDON, 15-AcDON, HT-2, T-2, FB1, FB2, AME, TeA, AOH, TEN, ALS, and ALT. According to the results, a total of 61 samples contained mycotoxins with overall positive rate was 39.87%, and 5 targets were detected, including TEN, ST, AOH, OTA, and TEA. As was shown in Figure 1, the positive rates of OTA, ST, AOH, TEN, and TEA were 1.31%, 1.96%, 0.65%, 45.41%, and 50.98%, respectively. The statistical results show that the positive rate of TEN and TEA even exceeded 45%, these two mycotoxins had a great risk of contamination of hull-less barley and wheat crops produced on the Tibetan Plateau. The TEN, TEA, and AOH of the five positive mycotoxins were all belonged to the *Alternaria* toxins, produced by *A. alternate*. This indicated that the *Alternaria* toxins should be monitored seriously in order to control mycotoxin contamination in food crops on the Tibetan Platea.

The molecular biology identification

The sequencing results of the nine strains were uploaded to the GenBank data of the NCBI website for alignment, and the phylogenetic tree was constructed using MEGA 6.0 software, which was shown in the following Figure 2. The strains numbered PL18-4b, QBM05-10, QBM02-13, and QBY06-2 were developed from the same branch, which suggested that they were evolved from the same ancestor. The strains numbered 2S10-1, S05-5, R01-9, and S01-5 were developed from another branch, and the strain numbered 2S10-1 shared high homology with the other three strains. The strain numbered PL18-5b was from an independent branch, which indicated that this strain might display different toxigenic capacity properties compared to other two groups. In the subsequent test results, the ALT toxin was only detected in the metabolons of PL18-5b strain, while the other eight strains were not detected, which proved the particularity of PL18-5b to some extent.

The selection of pH

The pH value of the origin environment had a great influence on the biological growth. Due to the presence of carbon dioxide in the air, the pH of the natural water environment was about 5.8, so the experiment was performed at pH 5.8.

The effect of temperature on the toxigenic capacity

Temperature conditions played a crucial role in the life activities of strains. Studies on the growth and toxin-production capacity under different temperatures were important for controlling the fungal contamination of *Alternaria* toxin. Given the climatic conditions on the

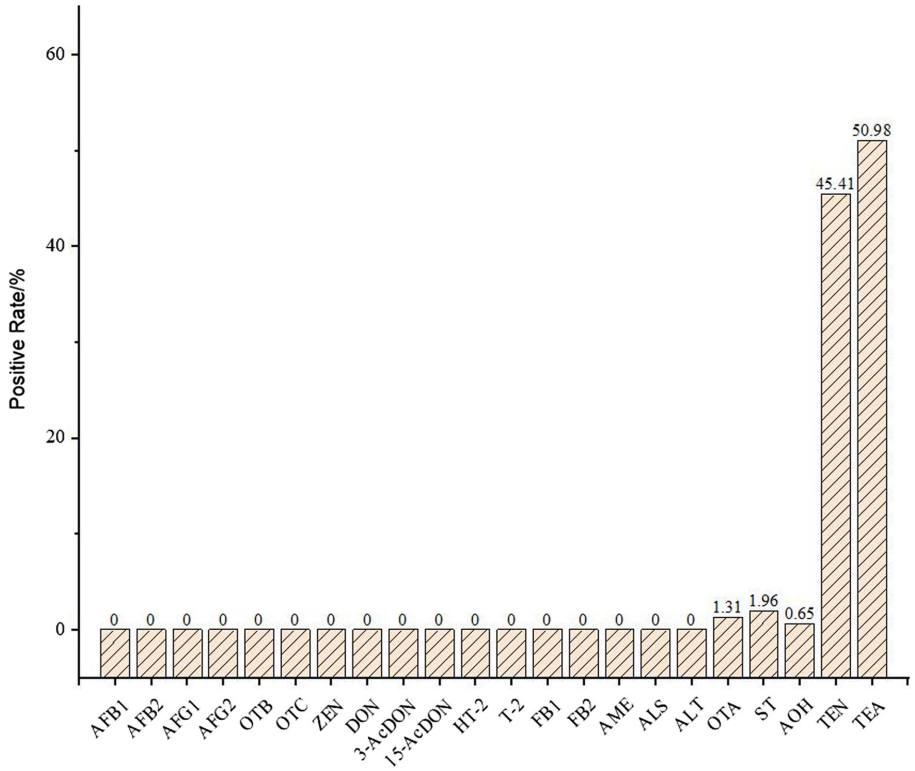

FIGURE 1
The positive rate of mycotoxins in 145 crop samples.

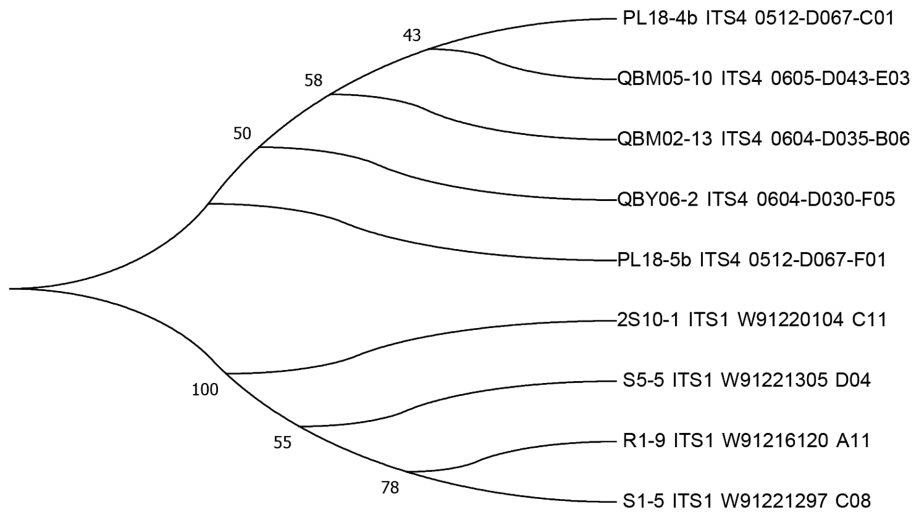

FIGURE 2
The phylogenetic trees of nine strains.

Tibetan Plateau, the temperature generally does not exceed 28°C, as much as possible to ensure that the highland barley and wheat could survive the normal growth period, so the three temperature conditions of 20°C, 25°C, and 28°C were selected for the experiment. Figure 2 showed the growth curves of nine *A. alternate* at different temperatures. As time went on, the results showed that all the nine *A. alternate* had the fastest growth rate at 28°C, with the second growth rate at 25°C and the lowest growth rate at 20°C.

When the nine *A. alternate* were cultured for 7 days at 20°C, 25°C and 28°C, the *Alternaria* toxins in the culture medium was examined qualitatively and quantitatively, and the results were shown in Figure 3. As was shown in Figure 3, a total of five *Alternaria* toxins were detected as positive, which were TEN, AOH, AME, TEA, and ALT. The ALS toxin was not detected in the metabolites of the nine *Alternaria* strains. The TEN and TEA toxins were detected as high values among the metabolites of the nine *Alternaria* strains except for

the strain numbered PL18-4b. This suggested that *A. alternate* had the strongest ability to produce both TEN and TEA toxins. The result could also explain the reasons of the high detection rates of TEN and TEA in the risk assessment to some extent. The AME toxin was detected as positive in eight *Alternaria* strains except for the strain numbered R01-9. This result indicated that the AME toxin has potential hazards in Tibetan crops, and sufficient attention should be paid to it in the future risk assessment. The AOH toxin was found in five *A. alternate*, which were numbered as S05-5, 2S10-1, PL18-4b, PL18-5b, QBM05-10, respectively. And the detected values of AOH toxin were relatively low. It was consistent with the low detection rate of AOH toxin in the risk assessment. The ALT toxin was detected in only one *A. alternate* numbered PL18-5b, and the detected values were very small. The ALS toxins were all negative in the metabolites of the nine *A. alternate*. Combined with the results of the risk assessment, it showed that the ALT and ALS toxins were less harmful than other 4 *Alternaria* toxins in food crops on the Tibetan Plateau.

After 7 days of incubation at 20°C, 25°C, and 28°C, according to Figure 4, a higher amount of toxins was produced at a higher temperature condition for most *Alternaria* toxins, such as the TEA toxins produced by the *A. alternate* numbered R01-9, 2S10-1, PL18-5b, QBM05-10, the TEN toxins produced by the *A. alternate* numbered R01-9, PL18-4b, QBM05-10, QBY06-2, and so on. This result was consistent with the growth of the nine *A. alternate* at different temperatures. However, the production of some toxins did not meet this principle, or even met the principle of relativity, such as the TEA toxins produced by the *A. alternate* numbered QBM02-13. Another phenomenon was found in the production process of many toxins, the production varied little at different culture temperatures, such as the TEN toxins produced by the *A. alternate* numbered R01-9, S01-5, QBM-02-13, the AME toxins produced by the *A. alternate* numbered S05-5, PL18-5b, QBM05-10 and so on. In conclusion, the law of toxicity production with culture temperature was diverse. Depending on the specific situation, the production of a single toxin by a single *A. alternate* was necessary.

The effect of UV irradiation on the toxigenic capacity

During the 7-day culture period at 25°C, after 5 days of UV irradiation treatment under different duration, the detection results of

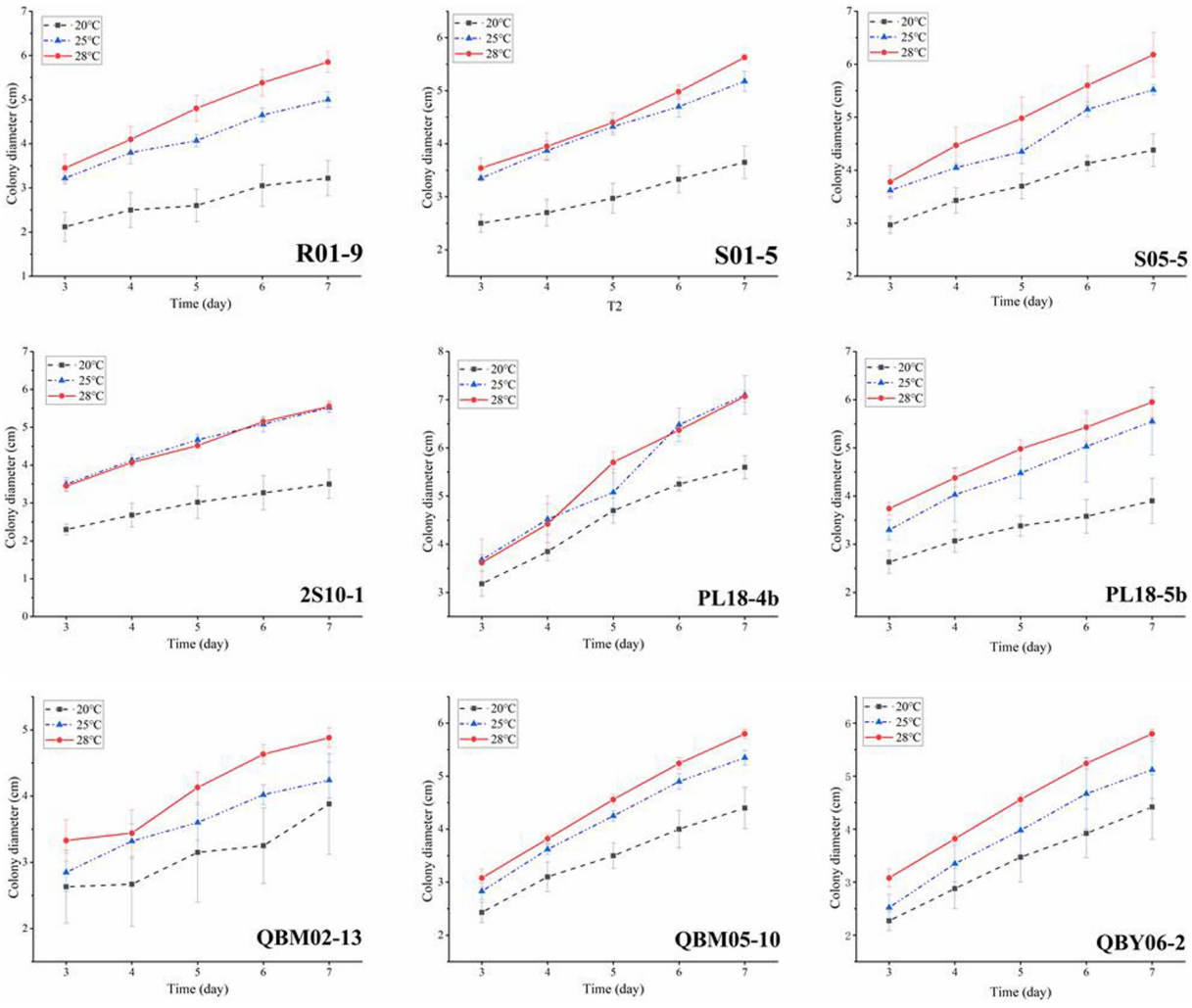

FIGURE 3
The effect of temperature on the growth of nine *Alternaria alternate*.

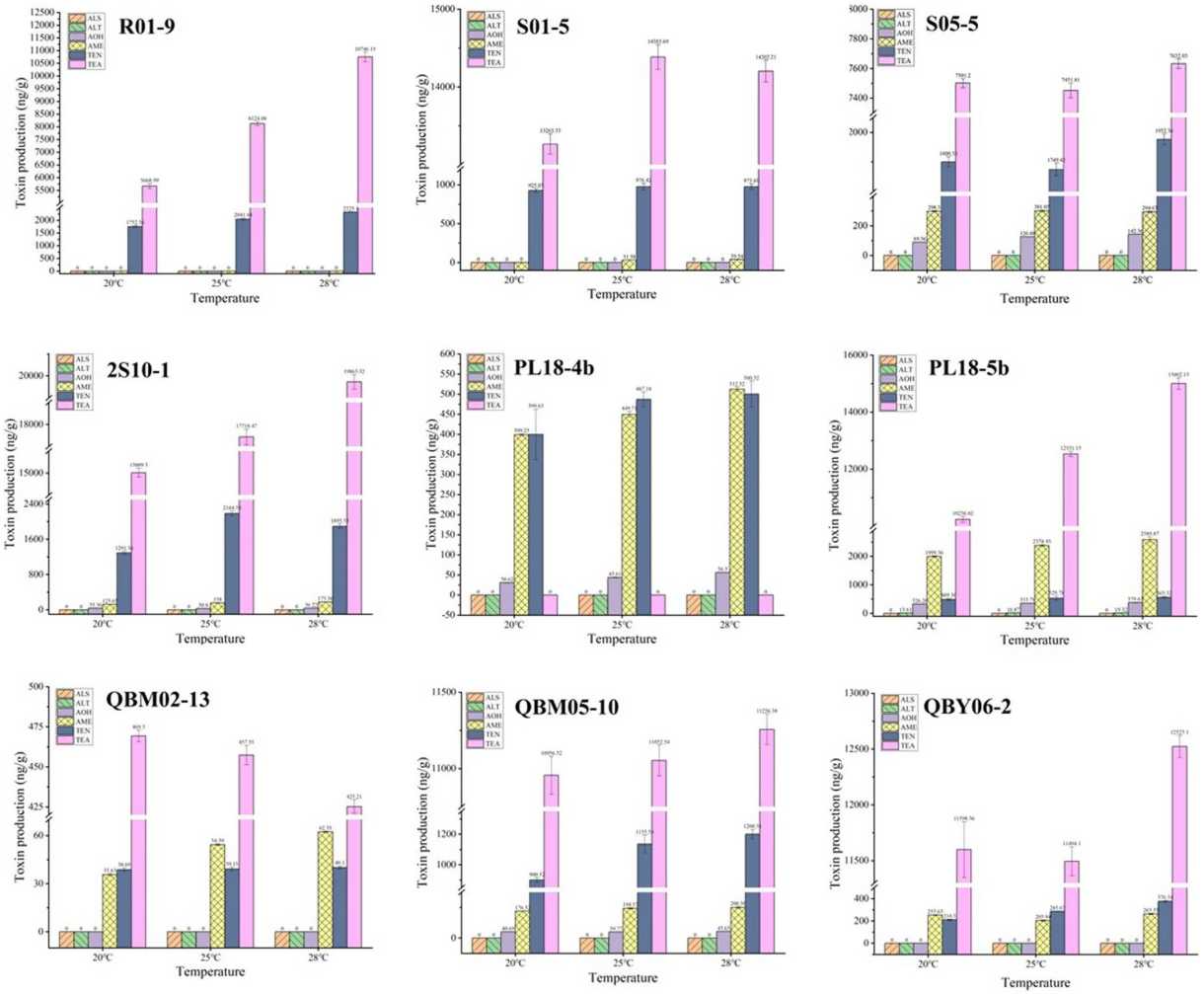

FIGURE 4
The toxin-production ability of nine *Alternaria alternate* at different temperatures.

Alternaria toxins produced in the culture medium were shown in Figure 5. According to the Figure 5, along with the prolonged time of UV irradiation, the trend of toxin production was decreased for most of nine strains. This suggested that the UV irradiation had suppressed the growth of nine strains, but a long duration or even 5 h could not completely kill the strains after 2 days of culture. When the growth of strain was inhibited, the toxin production was also adversely affected. However, the production of some toxins showed different phenomenon, or even presented the principle of relativity. The production of some toxins was not greatly affected by the UV irradiation, Such as the AOH toxins produced by the *A. alternate* numbered S05-5, 2S10-1, PL18-5b, the ALT toxins produced by the *A. alternate* numbered PL18-5b and so on. Moreover, a special phenomenon was discovered, such as the TEA toxins manufactured by the strain numbered S01-5, the toxin production increased with increasing UV irradiation time. When the UV irradiation intensity increased and the strain growth was inhibited, the toxigenic capacity increased. It showed that the production of toxins was not only related to the growth rate of the strains, but also related to the growth environment of the strains. In order to clarify the unclear rules, the subject should be further studied in the future.

Conclusion

Hull-less barley and wheat were the most important *Triticeae* crops on the Tibetan Plateau. Prevention of mycotoxin contamination was of great significance for economic development and people's health. In this study, mycotoxins in the main food crops on the Tibetan Plateau were monitored, and it was found that the main pollutants in the plateau food crops were *Alternaria* toxins, including TEN TEA and AOH. Subsequently, the 65 *A. alternate* were collected, and 9 strains were isolated and identified. The toxin-producing ability under different conditions was evaluated. According to the results, the selected nine *Alternaria alternate* could produce a variety of *Alternaria* toxins, which could not be ignored in terms of the quantity loss and quality reduction of plateau crops. The toxigenic capacity was not only related to the genetic constitution of the strains, but also related to the growth environment. It was necessary to keep monitoring and scientific evaluation of streptomycin in plateau crops, so as to effectively prevent the potential risk of contamination by streptomycin and other mycotoxins.

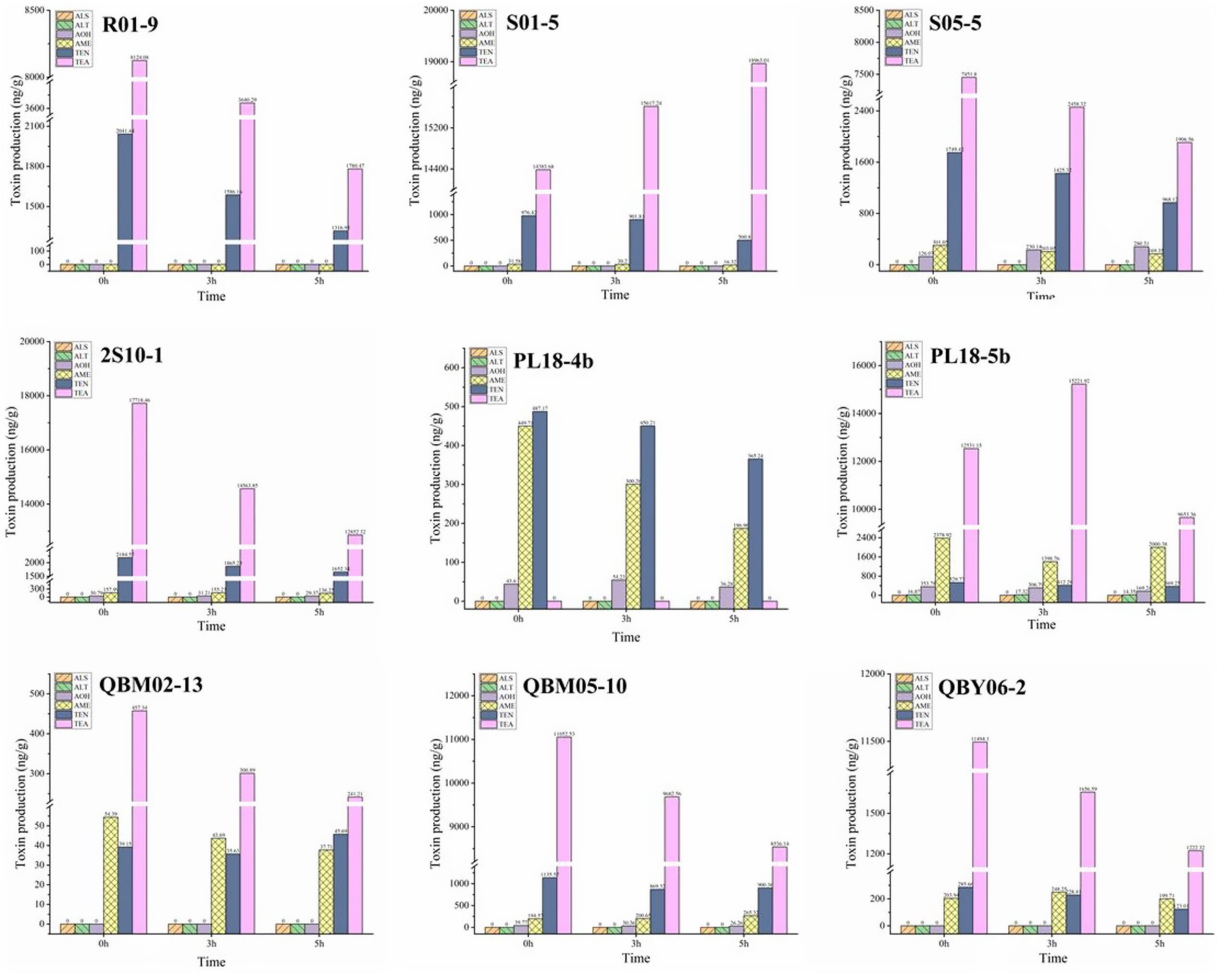

FIGURE 5
The effect of UV irradiation on the toxigenic capacity of nine *Alternaria alternate*.

Data availability statement

The data of 9 *Alternaria alternate* involved in this paper have been submitted and deposited in National Center for Biotechnology Information (https://www.ncbi.nlm.nih.gov/). The strain serial numbers and direct links can be found at: S01-5 - https://www.ncbi.nlm.nih.gov/nuccore/OQ347855, S05-5 - https://www.ncbi.nlm.nih.gov/nuccore/OQ347854, 2S10-1 - https://www.ncbi.nlm.nih.gov/nuccore/OQ347862, R01-9 - https://www.ncbi.nlm.nih.gov/nuccore/OQ347856, PL18-4b - https://www.ncbi.nlm.nih.gov/nuccore/OQ347861, PL18-5b - https://www.ncbi.nlm.nih.gov/nuccore/OQ347860, QBM02-13 - https://www.ncbi.nlm.nih.gov/nuccore/OQ347859, QBM05-10 - https://www.ncbi.nlm.nih.gov/nuccore/OQ347858, and QBY06-2 - https://www.ncbi.nlm.nih.gov/nuccore/OQ347857.

Author contributions

JW and NW conceived and designed the experiments. FZ and TY performed the experiments. JW and NW supervised the project. FZ and YL analyzed the data. JW, NW, and FZ wrote the manuscript. All authors contributed to the article and approved the submitted version.

Funding

This research was supported by National Natural Science Foundation of China (no. 31860473), The Project of the Science and Technology Department of Tibet, China (no. XZ202101ZY0015G), National Natural Science Foundation of Tibet, China (no. XZ202101ZR0067G) and The Doctoral scientific research launch fund project of Nanyang Institute of Technology (no. 510198).

Conflict of interest

The authors declare that the research was conducted in the absence of any commercial or financial relationships that could be construed as a potential conflict of interest.

Publisher's note

All claims expressed in this article are solely those of the authors and do not necessarily represent those of their affiliated organizations, or those of the publisher, the editors and the reviewers. Any product that may be evaluated in this article, or claim that may be made by its manufacturer, is not guaranteed or endorsed by the publisher.

References

Agriopoulou, S., Stamatelopoulou, E., and Varzakas, T. (2020). Advances in analysis and detection of major mycotoxins in foods. *Foods* 9:518. doi: 10.3390/foods9040518

Bryan, D., Richard, E. G., and Gregory, S. L. (2018). Food and feed safety of genetically engineered food crops. *Toxicol. Sci.* 162, 361–371. doi: 10.1093/toxsci/kfx249

Chen, C., Frank, K., Wang, T., and Wu, F. (2021). Global wheat trade and codex Alimentarius guidelines for deoxynivalenol: a mycotoxin common in wheat. *Glob. Food Sec.* 29:100538. doi: 10.1016/j.gfs.2021.100538

Cui, L., Ren, Y., Dmurray, T., Yan, W., Guo, Q., Niu, Y., et al. (2018). Development of perennial wheat through hybridization between wheat and wheatgrasses: a review. *Engineering* 4, 507–513. doi: 10.1016/j.eng.2018.07.003

Estiarte, N., Lawrence, C. B., and Crespo-Sempere, A. (2016). Lae a and VeA are involved in growth morphology, asexual development, and mycotoxin production in *Alternaria alternata*. *Int. J. Food Microbiol.* 238, 153–164. doi: 10.1016/j.ijfoodmicro.2016.09.003

Fillinger, L., Hug, K., and Griebler, C. (2020). Selection imposed by local environmental conditions drives differences in microbial community composition across geographically distinct groundwater aquifers. *FEMS Microbiol. Ecol.* 95:fiz 160. doi: 10.1093/femsec/fiz160

Galli, V., Venturi, M., Guerrini, S., Blandino, M., Luti, S., Pazzagli, L., et al. (2020). Antioxidant properties of sourdoughs made with whole grain flours of Hull-less barley or conventional and pigmented wheat and by selected lactobacilli strains. *Foods* 9:640. doi: 10.3390/foods9050640

Gotthardt, M., Asam, S., Gunkel, K., Moghaddam, A., Baumann, E., Kietzi, R., et al. (2019). Quantitation of six Alternaria toxins in infant foods applying stable isotope labeled standards. *Front. Microbiol.* 10:109. doi: 10.3389/fmicb.2019.00109

Huang, Y., Li, Y., Li, D., Bi, Y., and Liu, Y. (2020). Phospholipase C from *Alternaria alternata* is induced by physiochemical cues on the pear fruit surface that dictate infection structure differentiation and pathogenicity. *Front. Microbiol.* 11:1279. doi: 10.3389/fmicb.2020.01279

Ji, F., Xu, J., Liu, X., Yin, X., and Shi, J. (2014). Natural occurrence of deoxynivalenol and zearalenone in wheat from Jiangsu province. *Food Chem.* 157, 393–397. doi: 10.1016/j.foodchem.2014.02.058

Jiang, Y., Liang, Y., Li, C., Wang, F., Sui, Y., Suvannang, N., et al. (2016). Crop rotations alter bacterial and fungal diversity in paddy soils across East Asia. *Soil Biol. Biochem.* 95, 250–261. doi: 10.1016/j.soilbio.2016.01.007

Li, R., Wen, Y., Wang, F., and He, P. (2021). Recent advances in immunoassays and biosensors for mycotoxins detection in feedstuffs and foods. *J Anim. Sci. Biotechnol.* 12:108. doi: 10.1186/s40104-021-00629-4

Li, X., Zhang, J., Cai, J., Cai, X., Christie, P., and Li, X. (2015). Contribution of arbuscular mycorrhizal fungi of sedges to soil aggregation alongan altitudinal alpine grassland gradient on the Tibetan plateau. *Environ. Microbiol.* 17, 2841–2857. doi: 10.1111/1462_2920.12792

López, P., Venema, D., Mol, H., Spanjer, M., Stoppelaar, J., Pfeiffer, E., et al. (2016). Alternaria toxins and conjugates in selected foods in the Netherlands. *Food Control* 69, 153–159. doi: 10.1016/j.foodcont.2016.04.001

Liu, J.-Q., Li, J.-L., and Lai, Y.-J. (2021). Plant diversity and ecology on the Qinghai–Tibet plateau. *J. Syst. Evol.* 59, 1139–1141. doi: 10.1111/jse.12813

Mitchell, N. J., Bowers, E., Hurburgh, C., and Wu, F. (2016). Potential economic losses to the US corn industry from aflatoxin contamination. *Food Addit. Contam. Part A Chem. Anal. Control Expo. Risk Assess.* 33, 540–550. doi: 10.1080/19440049.2016.1138545

Mukesh, M., Gupta, S. K., Swapnil, P., Zehra, A., Dubey, M. K., and Upadhyay, R. S. (2017). Alternaria toxins: potential virulence factors and genes related to pathogenesis. *Front. Microbiol.* 8:1451. doi: 10.3389/fmicb.2017.01451

Pereira, V. L., Fernandes, J. O., and Cunha, S. C. (2014). Mycotoxins in cereals and related foodstuffs: a review on occurrence and recent methods of analysis. *Trends Food Sci. Technol.* 36, 96–136. doi: 10.1016/j.tifs.2014.01.005

Piacentini, K. C., Rocha, L. O., Savi, G. D., Carnielli-Queiroz, L., Almeida, F. G., Minella, E., et al. (2017). Occurrence of deoxynivalenol and zearalenone in brewing barley grains from Brazil. *Mycotoxin Res.* 34, 173–178. doi: 10.1007/s12550-018-0311-8

Qiu, J. B., Xu, J. H., and Shi, J. R. (2014). Molecular characterization of the fusarium graminearum species complex in eastern China. *Eur. J. Plant Pathol.* 139, 811–823. doi: 10.1007/s10658-014-0435-4

Qiu, J., and Shi, J. (2014). Genetic relationships, Carbendazim sensitivity and mycotoxin production of the fusarium graminearum populations from maize, wheat and rice in eastern China. *Toxins (Basel)* 6, 2291–2309. doi: 10.3390/toxins6082291

Qu, B., Li, H. P., Zhang, J. B., Xu, Y. B., Huang, T., Wu, A. B., et al. (2008). Geographic distribution and genetic diversity of fusarium graminearum and F-asiaticum on wheat spikes throughout China. *Plant Pathol.* 070921225609003–070921225609???. doi: 10.1111/j.1365-3059.2007.01711.x

Ren, C., Zhang, W., Zhong, Z., Han, X., Yang, G., Feng, Y., et al. (2018). Differential responses of soil microbial biomass, diversity, and compositions to altitudinal gradients depend on plant and soil characteristics. *Sci. Total Environ.* 610-611, 750–758. doi: 10.1016/j.scitotenv.2017.08.110

Shun, S., Björn, S., and Takao, K. (2011). The domestication syndrome genes responsible for the major changes in plant form in the Triticeae crops. *Plant Cell Physiol.* 52, 738–749. doi: 10.1093/pcp/pcr025

Yang, J., Sun, C., Zhang, Y., Fu, D., Zheng, X., and Yu, T. (2017). Induced resistance in tomato fruit by γ-aminobutyric acid for the control of alternaria rot caused by *Alternaria alternata*. *Food Chem.* 221, 1014–1020. doi: 10.1016/j.foodchem.2016.11.061

Yao, M., Shao, D., Lv, C., An, R., Gu, W., and Zhou, C. (2021). Evaluation of arable land suitability based on the suitability function - a case study of the Qinghai-Tibet plateau. *Sci. Total Environ.* 787:147414. doi: 10.1016/j.scitotenv.2021.147414

Hassan, Y. I., and Zhou, T. (2018). Promising detoxification strategies to mitigate mycotoxins in food and feed. *Toxins* 10:116. doi: 10.3390/toxins10030116

Zeng, X. Q., Hai, L., Wang, Z., Zhao, S. C., Tang, Y. W., Huang, Z. Y., et al. (2015). The draft genome of Tibetan hulless barley reveals adaptive patterns to the high stressful Tibetan plateau. *PNAS* 112, 1095–1100. doi: 10.1073/pnas.1423628112

Zhang, Y., Dong, S., Gao, Q., Liu, S., Zhou, H., Ganjurjav, H., et al. (2016). Climate change and human activities altered the diversity and composition of soil microbial community in alpine grasslands of the Qinghai-Tibetan plateau. *Sci. Total Environ.* 562, 353–363. doi: 10.1016/j.scitotenv.2016.03.221

Zhao, H., Chen, X., Shen, C., and Qu, B. (2017). Determination of 16 mycotoxins in vegetable oils using a QuEChERS method combined with high-performance liquid chromatography-tandem mass spectrometry. *Food Addit. Contam. Part A* 34, 1–10. doi: 10.1080/19440049.2016.1266096

frontiers | Frontiers in Microbiology

TYPE Original Research
PUBLISHED 13 February 2023
DOI 10.3389/fmicb.2023.1135308

OPEN ACCESS

EDITED BY
Peng Fei,
Nanyang Institute of Technology, China

REVIEWED BY
Smith Etareri Evivie,
University of Benin,
Nigeria
Yunhe Chang,
Guiyang University,
China

*CORRESPONDENCE
Jiaying Xin
✉ xinjiayingvip@163.com

SPECIALTY SECTION
This article was submitted to Food Microbiology, a section of the journal Frontiers in Microbiology

RECEIVED 31 December 2022
ACCEPTED 19 January 2023
PUBLISHED 13 February 2023

CITATION
Song W, Xin J, Yu C, Xia C and Pan Y (2023) Alkyl ferulic acid esters: Evaluating their structure and antibacterial properties. *Front. Microbiol.* 14:1135308. doi: 10.3389/fmicb.2023.1135308

Alkyl ferulic acid esters: Evaluating their structure and antibacterial properties

Wei Song[1], Jiaying Xin[1,2]*, Chong Yu[3], Chungu Xia[2] and Yu Pan[3]

[1]Key Laboratory for Food Science and Engineering, Harbin University of Commerce, Harbin, China, [2]State Key Laboratory for Oxo Synthesis and Selective Oxidation, Lanzhou Institute of Chemical Physics, Chinese Academy of Sciences, Lanzhou, China, [3]Institute of Microbiology Heilongjiang Academy of Sciences, Harbin, China

Ferulic acid (FA) is a natural antibacterial agent rich in plants, FA has excellent antioxidant and antibacterial properties. However, because of its short alkane chain and large polarity, FA is difficult to penetrate the soluble lipid bilayer in the biofilm to enter the cell to play an inhibitory role, limiting its biological activity. To improve the antibacterial activity of FA, with the catalytic condition of Novozym 435, four alkyl ferulic acid esters (FCs) with different alkyl chain lengths were obtained by fatty alcohols (including 1-propanol (C3), 1-hexanol (C6), nonanol (C9), and lauryl alcohol (C12)) modification. The effect of FCs on *P. aeruginosa* was determined by Minimum inhibitory concentrations (MIC), minimum bactericidal concentrations (MBC), Growth curves, alkaline phosphatase (AKP) activity, crystal violet method, scanning electron microscopy (SEM), membrane potential, PI, cell contents leakage. Results showed that the antibacterial activity of FCs increased after esterification, and the antibacterial activity significantly increased and then decreased with the extension of the alkyl chain of the FCs. Hexyl ferulate (FC6) showed the best antibacterial activities against *E. coli* and *P. aeruginosa* (MIC for *E. coli* was 0.5 mg/ml, MIC for *P. aeruginosa* was 0.4 mg/ml). And Propyl ferulate (FC3) and FC6 showed the best antibacterial activities S. aureus and *B. subtilis* (MIC for *S. aureus* was 0.4 mg/ml, The MIC of *B. subtilis* was 1.1 mg/ml). In addition, the growth, AKP activity, bacterial biofilm, bacterial cell morphology, membrane potential and cell contents leakage of *P. aeruginosa* after different FCs were investigated, which found that FCs could damage the cell wall of *P. aeruginosa* and showed different effects on the *P. aeruginosa* cell biofilm. FC6 showed the best inhibition on the biofilm formation of *P. aeruginosa* cells, which caused the surface of *P. aeruginosa* cells to be rough and wrinkled. Some *P. aeruginosa* cells showed aggregation and adhesion, even rupture. The membrane hyperpolarization was obvious, which appeared as holes, leading to cell contents leakage (protein and nucleic acid). All these results concluded that the antibacterial activities FCs against foodborne pathogens depended on different fatty alcohol esterification of FA. FC6 showed the best inhibition on *P. aeruginosa* due to its effect on *P. aeruginosa* cell walls and biofilms and the leak of the cell contents. This study provides more practical methods and a theoretical basis for giving full play to the bacteriostatic effect of plant FA.

KEYWORDS

ferulic acid, alkyl ferulic acid esters, structure, antibacterial properties, foodborne pathogens, bacterial membranes

1. Introduction

Infectious diseases caused by bacteria, fungi and viruses have become a major global health problem (Li et al., 2021). Globally, about 4 million people die each year from acute respiratory infections, about 3 million from intestinal infections, about 1.8 from human immunodeficiency virus (HIV), about 1.3 million from tuberculosis, and about 700,000 from malaria (Lozano et al., 2012; Tang et al., 2021). In addition, increasing microbial resistance to conventional drugs has

informed studies into new antibacterial agents with broad-spectrum antibacterial activity (Malheiro et al., 2018).

Plant antimicrobials were widely used for their safety, environment-friendly, no drug resistance, and low residue, among other advantages. Studies have revealed that some phenolic substances showed antibacterial activities, for example, they be inserted into the phospholipid layer of bacterial membranes, disrupting the van der Waals interaction between the fatty acyl chains and destroying the phospholipid bilayer and membrane integrity (Burt, 2004; Chauhan et al., 2021; Li et al., 2021). As the ion gradient of the cell membrane is disrupted, important components such as ions and macromolecules are released from within the cell, resulting in the death of the bacteria. FA (4-hydroxy-3-methoxy cinnamic acid, $C_{10}H_{10}O_4$) is a natural antibacterial agent rich in plants such as coffee, rice husk, vanilla bean, wheat bran and rice bran. As a phenolic acid, FA has been proven to have various biological activities that can reduce the risk of serious diseases such as diabetes, cholesterol, heart disease and cancer, and it has excellent antioxidant and antibacterial properties (Burcu et al., 2011; Kot et al., 2018; Pernin et al., 2019). As an antimicrobial agent, FA has a broad antibacterial spectrum, and its antibacterial activities against *pneumococcus*, *Escherichia coli*, *Pseudomonas aeruginosa*, *Shigella Sonneri*, *Bacillus*, *Listeria*, and *Staphylococcus aureus* have been reported (Saharkhiz et al., 2012; Barbara et al., 2015; Shi et al., 2016, 2018, 2019).

However, because of its short alkane chain and large polarity, FA is difficult to penetrate the soluble lipid bilayer in the biofilm to enter the cell to play an inhibitory role, limiting its biological activity (Stamatis et al., 2001). It was found that FA esterified by fatty alcohols (Figure 1) can improve the lipid solubility of the molecule and the antibacterial activity of FA, but there is a lack of detailed comparison of ferulic acid and ferulic acid with different alkane chain lengths on the antibacterial activities and the effects on the bacterial cell wall and cell membrane. Bacteria were divided into Gram-positive and Gram-negative bacteria based on Gram staining, with the main difference between the two being the structure of the cell wall, so 2 g-positive and 2 g-negative food-borne pathogens were selected as test bacteria in this experiment. In this study, four FCs with different alkyl chain lengths were prepared by fatty alcohols (C3, C6, C9 and C12) modification, and the effect of FCs molecules with different alkane chains on antibacterial activities against foodborne pathogens (*E. coli*, *P. aeruginosa*, *S. aureus*, and *B. subtilis*) and their mode of action were investigated.

2. Materials and methods

2.1. Materials

Ferulic acid, 1-propanol (C3), 1-hexanol (C6), nonanol (C9), and lauryl alcohol (C12) with >98% purity were purchased from Aladdin Biochemical Technology Co., LTD. (Shanghai, China). Novozym 435 (A Candida antarctica lipase B immobilized on acrylic resin) was purchased from Novozymes Biotechnology LTD. (Denmark). 4 Å molecular sieve and n-hexane (moisture ≤0.02%) were purchased from Guangfu Fine Chemical Research Institute (Tianjin, China). The alkaline phosphatase (AKP) kit and BCA protein quantitative kit were purchased from Dalian Meilun Biotechnology Co., LTD. (Dalian, China). P-Iodonitrotetrazolium Violet (INT) was purchased from Macklin Biochemical Co., LTD. (Shanghai, China). 2.5% glutaraldehyde was purchased from Leagene Biotechnology Co., LTD. (Beijing, China). Rhodamine 123 was purchased from Biotopped Life sciences. (Beijing, China). Propidium iodide (PI) was purchased from Saiguo Biotechnology Co., LTD. (Guangzhou, China). Ferulic acid, 1-propanol, 1-hexanol, nonanol, lauryl alcohol, Novozym435 and other organic solvents were treated with a 4 Å molecular sieve for at least 24 h before use.

2.2. Bacterial strains and culture conditions

Escherichia coli ATCC 25922, *Pseudomonas aeruginosa* ATCC 27853, *Staphylococcus aureus* ATCC 25923 and *Bacillus subtilis* were gift samples from the Institute of Microbiology Heilongjiang Academy of Sciences. The strains preserved in the tube were removed from the −80°C refrigerator and thawed overnight in a 4°C refrigerator. All strains were activated by Tryptone Soy broth (TSB) medium (Hangzhou Microbe 164 Reagent Co., LTD., China) at 37°C in an orbital air shaking bath (180 rpm) for 24 h and maintained on TSA slants at 4°C.

2.3. Preparation of ferulic acid alkyl esters

In this experiment, four fatty alcohols (C3, C6, C9, C12) were selected for esterification with FA to obtain four kinds of FCs with different alkane group lengths. The method described by Shi et al. (2017) was modified slightly. Briefly, FA and fatty alcohol (molar ratio, 1:8) was dissolved in 10 ml n-hexane solvent in a 50 ml triangular bottle, 80 mg of Novozym435 lipase and 10 molecular sieves (4 Å) were added. The reaction was carried out in an orbital air shaking bath (150 rpm) at 50°C for 7 days. The n-hexane solvent was then removed under reduced pressure, and the crude residue was purified by column chromatography on a column (1.5 × 20 cm) packed with silica gel 60 (230–400 mesh, Merck) using hexane: ethyl acetate 8:2 (v/v) as eluent.

2.4. NMR analysis and mass spectrometry

The molecular structure of the FCs was determined by NMR (model AVANCEII400, Swiss-Brock). FCs were weighted with 4 mg for ^{1}H-NMR determination and 15 mg for ^{13}C-NMR determination. After the FCs were dissolved in 0.6 ml deuterium chloroform ($CDCl_{13}$), the solution

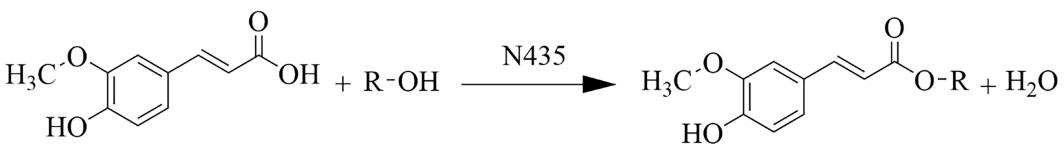

FIGURE 1
Ferulic acid reacts with fatty alcohol to form ferulic ester equation.

was quickly transferred to a clean and dry nuclear magnetic tube (5 mm, 7 inches) for determination. The propyl ferulate (FC3) hexyl ferulate (FC6)nonyl ferulate (FC9) Lauryl ferulate (FC12) of ^{1}H NMR and ^{13}C NMR were all 400 MHz and 100 MHz, respectively (Shi et al., 2019).

Fourier Transform high-resolution mass spectrometry (Velos, ThermoFisher, United States) was used to analyze FCs molecular weight. Five hundred micro liter of methanol was added to a 1.5 mL centrifuge tube, and a trace of the tested sample was dipped into a capillary tube and then dissolved in chromatograde methanol. Methanol solution containing FCs was extracted with an injection needle and injected into the pump for determination. The ESI-MS(m/z) of FC3, FC6, FC9 and FC12 were 237.1[M + H] +, 279.2[M + H]+, 321.2 [M + H]+, 363.3[M + H]+, respectively. The NMR results of FC3, FC6, FC9 and FC12 were shown in Table 1.

2.5. Minimum inhibitory concentrations and minimum bactericidal concentrations determination

The method described by Aljawish et al. (2016) was slightly modified in this step. MIC and MBC were determined by the broth microdilution method combined with the INT indicator method. The FCs solution was prepared with anhydrous ethanol. Single colonies of *P. aeruginosa* were inoculated in TSB medium and cultured at 37°C for 14–16 h. The culture solution was centrifuged(4,000 × g, 4°C, 6 min), and the collected bacteria were washed with sterile 0.01 mol/l PBS (pH 7.4). The cultures obtained were diluted with TSB to obtain a 0.5 MCF (1×10^8 CFU/ml) and diluted 10 times.

Ninety six-well microplates were filled with 160 μL TSB medium, and then 20 μL of diluted bacterial strains and 20 μL of each FCs concentration were added to the wells. Two controls were used in two columns that contained 160 μL TBS medium and 20 μL of diluted bacterial strains: one with 20 μl of sterile distilled water and another with 20 μl of Anhydrous ethanol. Tests were carried out in triplicate. After being cultured at 37°C for 14–16 h, 10 μL 0.4% (w/v) INT was added to the wells as an indicator and cultured at 37°C for 30 min in the dark. The colorless tetrazolium salt acts as an electron acceptor and is reduced to a red-colored formazan product by biologically active organisms. When bacterial growth was inhibited, the solution in the well remained colorless after incubation with INT. When bacterial growth was inhibited (no evidence of growth), MIC values were recorded as the minimal concentration of FCs concentration. For MBC determination, 50 μl from each well without INT was spread on TSA agar plates and incubated at 37°C for 24–48 h. At least two duplicate tests were performed with each strain and antibacterial compound.

2.6. Growth curves

The method described by Campion et al. (2017) has been slightly modified. Single colonies of *P. aeruginosa* were inoculated in TSB medium and cultured at 37°C for 14–16 h in an orbital air shaking bath (180 rpm). The culture solution was centrifuged(4,000 × g, 4°C, 6 min), and the collected bacteria were washed with sterile 0.01 mol/l PBS (pH 7.4). The cultures obtained were diluted with TSB to obtain a 0.5 MCF (1×10^8 CFU/ml) and diluted 100 times. FA, FC3, FC6, FC9 and FC12 were added, respectively, until the final concentration was 0.4 mg/ml, and no drug was added as control. The absorbance values were measured every 2 h at 600 nm after 24 h culture at 37°C. The growth curve was plotted with the culture time as the abscissa and the OD_{600} value as the ordinate.

TABLE 1 Minimum inhibitory concentration MIC (mg/ml) and minimum bactericidal concentration MBC (mg/ml) values of FCs against different pathogens bacterial strains.

Name of compound	*R*	*c* Log *P*[a]		*Escherichia coli* (G^-)	*Pseudomonas aerugino* (G^-)	*Staphylococcus aureus* (G^+)	*Bacillus subtilis* (*G+*)
FA	H	1.4212	MIC	1.2	1.0	0.7	1.4
			MBC	2.5	3.0	1.5	3.5
FC3	$(CH_2)_2CH_3$	2.7052	MIC	0.8	0.7	0.4	1.1
			MBC	3.0	3.0	2.0	4.0
FC6	$(CH_2)_5CH_3$	4.2922	MIC	0.5	0.4	0.4	1.1
			MBC	3.0	3.0	2.0	4.0
FC9	$(CH_2)_8CH_3$	5.8792	MIC	1.0	0.9	0.8	1.3
			MBC	3.5	4.0	2.5	4.5
FC12	$(CH_2)_{11}CH_3$	7.4662	MIC	3.3	2.8	2.6	3.5
			MBC	5.0	4.5	4.0	5.0

[a]ChemDraw 20.0 software was used for theoretical estimation.

FC3: 1H NMR (CDCl3, 400 MHz) δ 7.61 (d, J = 16.0 Hz, 1H), 7.07–7.01 (m, 2H), 6.29 (d, J = 16.0 Hz, 1H), 6.03 (s, 1H), 4.15 (t, J = 8.0 Hz, 1H), 3.90 (s, 1H), 1.76–1.67 (m, 2H), 0.98 (t, J = 8.0 Hz, 3H). 13C NMR (CDCl3, 100 MHz) δ 167.56, 148.09, 148.07, 146.92, 144.81, 126.89, 122.97, 115.39, 114.87, 109.46, 66.05, 55.85, 22.08, 10.44.

FC6: 1H NMR (400 MHz, CDCl3) δ 7.61 (d, J = 16.0 Hz, CH), 7.08–7.03 (m, 2CH), 6.91 (d, J = 7.6 Hz, CH), 6.29 (d, J = 16.0 Hz, CH), 5.88 (s, OH), 4.19 (t, J = 5.6 Hz, CH2), 3.93 (s, CH3), 1.69–1.33 (m, 4CH2), 0.90 (s, CH3). 13C NMR (100 MHz, CDCl3) δ 167.6, 148.0, 146.9, 144.8, 127.2, 123.2, 115.8, 114.8, 109.4, 64.8, 56.1, 31.6, 28.9, 25.8, 22.7, 14.2.

FC9: 1H NMR (400 MHz, CDCl3) δ 7.60 (d, J = 16.0 Hz, CH), 7.08–7.03 (m, 2CH), 6.91 (d, J = 8.4 Hz, CH), 6.29 (d, J = 15.6 Hz, CH), 5.95 (t, OH), 4.18 (t, 6.4 HZ, CH2), 3.92 (s, CH3),1.73–1.27(m, 7CH2). 0.88 (t, 6.8 HZ,CH3). 13C NMR (100 MHz, CDCl3) δ 167.4, 147.9, 146.7, 144.6, 127.0, 123.0, 115.7， 114.7, 109.3, 64.6, 55.9, 31.9, 29.5, 29.3, 29.2, 28.8, 26.0, 22.7,14.1.

FC12: 1H NMR (CDCl3, 400 MHz) δ 7.61 (d, J = 16.0 Hz, 1H), 7.08–7.03 (m, 2H), 6.91 (d, J = 8.0 Hz, 1H), 6.29 (d, J = 16.0 Hz, 1H), 5.89 (s, 1H), 4.19 (t, J = 4.0 Hz, 2H), 3.92 (s, 1H), 1.73–1.66 (m, 2H), 1.26 (s, 18H), 0.88 (t, J = 4.0 Hz, 3H). 13C NMR (CDCl3, 100 MHz) δ 167.59, 148.08, 146.93, 144.82, 127.06, 123.11, 115.61, 114.88, 109.45, 64.74, 55.97, 32.00, 29.74, 29.72, 29.68, 29.63, 29.44, 29.39, 28.84, 26.08, 22.77, 14.20.

2.7. Determination of cell wall integrity

The method described by Shu et al. (2019) was slightly modified for this procedure. FA, FC3, FC6, FC9 and FC12 were, respectively, added into the bacterial suspension (As described in 2.6) to reach the final concentration of 0.4 mg/ml, with no drug added as the control. Under the condition of 37°C and 160 rpm at 0, 1, 2, 4, 6, and 8 h, the culture solution was centrifuged(4,000 × g, 4°C, 6 min), and take the supernatant to detect the AKP activity.

2.8. Determination of bacterial biofilm by crystal violet method

The method described by Djordjevic et al. (2002) has been slightly modified. FA, FC3, FC6, FC9 and FC12 were, respectively, added into the bacterial suspension (As described in 2.6) to reach the final concentration of 0.4 mg/ml, with no drug added as the control. Two hundred microliter was added to the 96-well plate, incubated at 37°C for 48 h, and the single bacterial cells were removed. Each well was gently cleaned with sterile 0.01 mol/l PBS (pH7.4) thrice, and added 200 μL formaldehyde solution to each well to fix for 5 min after drying. Then, 200 μL 0.1%crystal violet solution was added to each well, incubated at room temperature for 10 min, washed with sterile 0.01 mol/LPBS (pH 7.4) thrice to remove excess crystal violet, and dried at room temperature. Finally, 200 μL 95% ethanol was absorbed and added to each well, and the OD value of 600 nm was read. Use the following formula to calculate the percentage inhibition of bacterial biofilm formation.

$$\text{Inhibition rate}(\%) = \left[1 - \frac{E_i}{E_0}\right] \times 100\%$$

where E_i and E_0 are absorbance values treated with or without FCs, respectively.

2.9. Observation of microstructures by scanning electron microscopy

The method described by Shao et al. (2018) has been slightly modified. FA, FC3, FC6, FC9, and FC12 were, respectively, added into the bacterial suspension (As described in 2.6) to reach the final concentration of 0.4 mg/mL, with no drug added as the control. Under the condition of 37°C and 160 rpm at 2 h, the culture solution was centrifuged(4,000 × g, 4°C, 6 min) to take the bacteria. 2.5% glutaraldehyde was used to fix bacteria for more than 1.5 h under a 4°C refrigerator. The collected bacteria were flushed with 0.1 mol/l PBS (pH 7.2) twice (10 min each time), dehydrated with 50, 70, and 90% ethanol once for 10 min, and dehydrated with 100% ethanol twice for 10 min. After dehydration, the bacterial cells were vacuum freeze-dried and coated with gold spray. A scanning electron microscope (model SU8010, Hitachi, Japan) was used to observe the morphological changes of bacteria cells.

2.10. Measurement of membrane potential

This step was performed by slightly modifying the method of Jung et al. (2015). FA, FC3, FC6, FC9, and FC12 were, respectively, added into the bacterial suspension (As described in 2.6) to reach the final concentration of 0.4 mg/mL, with no drug added as the control. Under the condition of 37°C and 160 rpm at 3 h, the bacteria were collected, washed and dissolved with PBS. The Rhodamine 123 (2 μg/mL) was added, and the samples were washed three times and then suspended in PBS after 30 min in the dark. The average fluorescence intensity of the cell suspension was measured with a multi-functional enzyme spectrometer at the excitation wavelength of 489 nm, the emission wavelength of 530 nm and the slit width of 10 nm.

2.11. Evaluation of membrane permeability

2.11.1. Fluorescent detection of PI

The method described by Park and Kang (2013) has been slightly modified. FA, FC3, FC6, FC9 and FC12 were, respectively, added into the bacterial suspension (As described in 2.6) to reach the final concentration of 0.4 mg/ml, with no drug added as the control. Under the condition of 37°C and 160 rpm at 3 h, 0.3 mL PI(1 mg/ml)solution was added to the experimental group and control group, respectively, and incubated at 37°C for 10 min. The bacteria liquid's fluorescence values (excitation light 485 nm, emission light 500–800 nm, slit width 5 nm) with the above concentration gradient were measured successively, and the data were read.

2.11.2. Determination of intracellular protein leakage

FA, FC3, FC6, FC9, and FC12 were, respectively, added into the bacterial suspension (As described in 2.6) to reach the final concentration of 0.4 mg/ml, with no drug added as the control. The supernatant was cultured at 37°C and 160 rpm for 2, 4, 6, and 8 h, filtered by 0.22 μm microporous membrane. The protein content was determined by BCA protein quantitative kit.

2.11.3. Determination of cell contents leakage

The method described by Zhao et al. (2015) was slightly modified. FA, FC3, FC6, FC9, and FC12 were, respectively, added into the bacterial suspension (As described in 2.6) to reach the final concentration of 0.4 mg/mL, with no drug added as the control. Cultured at 37°C and 160 rpm for 4 h, the supernatant was taken, and the value of 260 nm was determined by ultraviolet spectrophotometer.

2.12. Statistical analysis

All experiments were performed in triplicate. Data were presented as mean ± SD. Data were analyzed for analysis of variance (ANOVA) by SPSS software to determine the least significant differences ($p < 0.05$).

3. Results and discussion

3.1. MIC and MBC evaluation

MIC is the lowest inhibitory concentration of the drug that can inhibit the growth of pathogenic bacteria in the culture medium after 14–18 h of bacterial culture *in vitro*. On the other hand, the MBC was defined as the minimal concentration of antibacterial compound that results in 99.9% dead cells in the primary inoculum (no colony was observed on TSA agar plates) (Naraysanan et al., 2021). In this

experiment, the MIC was determined by broth dilution and INT rapid detection method. Aljawish et al. (2016) confirmed that the INT rapid detection results were consistent with the traditional optical density detection results. As shown in Table 1, FA and FCs showed antibacterial activities against four Gram-negative and Gram-positive pathogens. FC6 showed the best antibacterial activity against *E. coli* and *P. aerugino*, with MIC values of 0.5 mg/ml s and 0.4 mg/ml, MBC value of both 3.0 mg/ml. In addition, FC3 and FC6 showed the best antibacterial activity against *S. aureus* and *B. subtilis*, with MIC values of 0.4 mg/ml and 1.1 mg/ml, MBC values of 2.0 mg/ml and 4.0 mg/ml. Borges et al. (2012) used ferulic acid as a bacteriostatic agent to study its bacteriostatic activity on *P. aeruginosa*, *E. coli*, *Listeria*, and *S. aureus* and also confirmed that ferulic acid had an inhibitory effect on *P. aeruginosa*, *E. coli*, and *S. aureus*. In addition, Pinheiro et al. (2021) used ferulic acid and its four esterified derivatives (methyl, ethyl, propyl and butyl) for antibacterial activity against *S. aureus*. These researches confirm our results that FA can have antibacterial functionalities in using FA as a potential preservative in the food industry. In the 4 pathogenic bacteria strains, the determination of antibacterial activity shows that after esterification of FA, bacteriostatic activity increased, but with the extension of antibacterial compounds alkyl chain, the bacteriostatic activity increased first and then, for *E. coli* and *P. aeruginosa*, FC6 bacteriostatic activity of the best, for *S. aureus* and *B. subtilis*, best FC3 and FC6 antibacterial activity.

3.2. Influences on the growth curve of *Pseudomonas aeruginosa*

Using *P. aerugino* as the indicator pathogen, the antibacterial activity of 0.4 mg/ml FA, FC3, FC6, FC9 and FC12, respectively, on the growth were investigated, and the results are shown in Figure 2 *P. aeruginosa* of the control group entered the logarithmic growth stage after culture for 4 h, and showed an increasing trend to the stable stage until 16 h. In the concentration of 0.4 mg/ml FC6 (1 × MIC) treatment group, the growth of the *P. aeruginosa* was completely suppressed—the growth of *P. aeruginosa* treated with FC3 was inhibited, and the logarithmic growth period was prolonged. However, FC9 and FC12 showed insignificant growth inhibition on *P. aeruginosa*. The effect of FCs on the growth curve of *P. aeruginosa* further verified the antibacterial activity of FCs against *P. aeruginosa*. Merkl (2010) reported that phenolic acid fatty alcohol esters could show a broad spectrum of antibacterial activity. In particular, *P. aeruginosa* (G-) and *S. aureus* (G+) were more sensitive to FC6, with MIC values of 0.4 mg/ml. Shi et al. (2017) took ferulic acid and fatty alcohol of ferulic acid from C4 to C12 as bacteriostatic agents to study the bacteriostatic activity against *E. coli* and *L. monocytogenes*, and the results showed that C6 had the best bacteriostatic activity, which was consistent with the results of this study. The possible explanations are as follows: the antibacterial activity of FCs is closely related to the species of bacteria and the length of the carbon chain of FCs (Kubo et al., 2004). We also found that, *E. coli*(G-) (MIC = 0.5 mg/mL), *P. aerugino*(G-) (G-) (MIC = 0.4 mg/ml), *S. aureus*(G+)(MIC = 0.4 mg/mL) was more sensitive to FC6 than *B. subtilis*(G+)(MIC = 1.1 mg/mL). Borges et al. (2012) confirmed that ferulic acid had more effective antibacterial activity against Gram-negative bacteria (*E. coli*, *P. aerugino*) than Gram-positive bacteria.

3.3. Effect on the integrity of *Pseudomonas aeruginosa* cell wall

Cell walls can effectively prevent foreign substances, such as antibiotics and bacteriostatic agents, from entering cells. AKP exists between the cell membrane and the cell wall and plays an important role in the metabolism of substances in organisms. Therefore, the integrity of the cell wall can be reflected by detecting AKP outside the cell (Shu et al., 2019). Figure 3 shows the AKP leakage of *P. aerugino* after being treated by antibacterial agents FA, FC3, FC6, FC9 and FC12. After FA and different FCs were treated with the same inhibitory concentration of *P. aerugino*, AKP activity increased with the extension of culture time. It should be noted that FC6-treated *P. aerugino* rapidly increased AKP activity within 2 h and showed the largest AKP activity at 8 h, with an

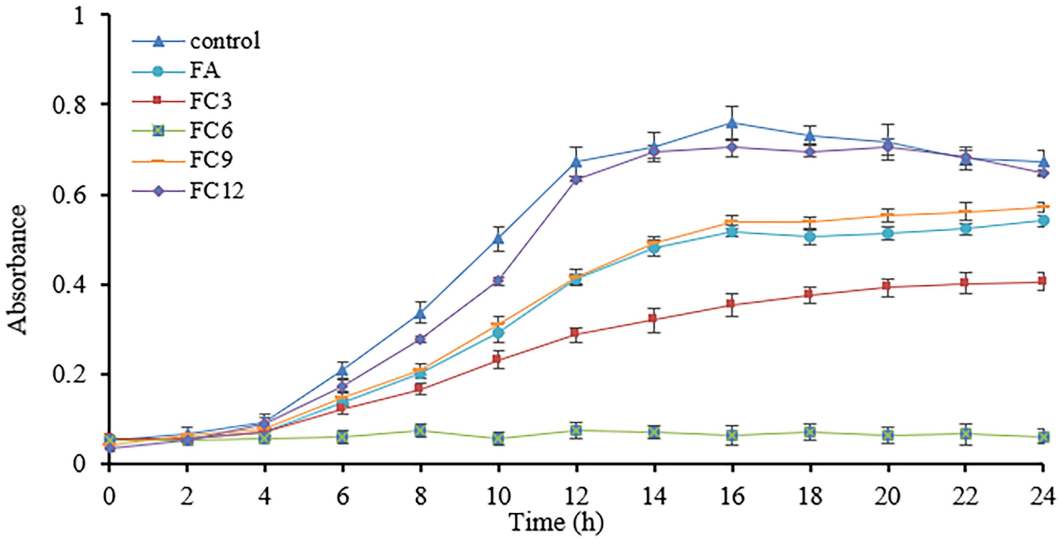

FIGURE 2
Effect on the growth curve of *Pseudomonas aeruginosa*.

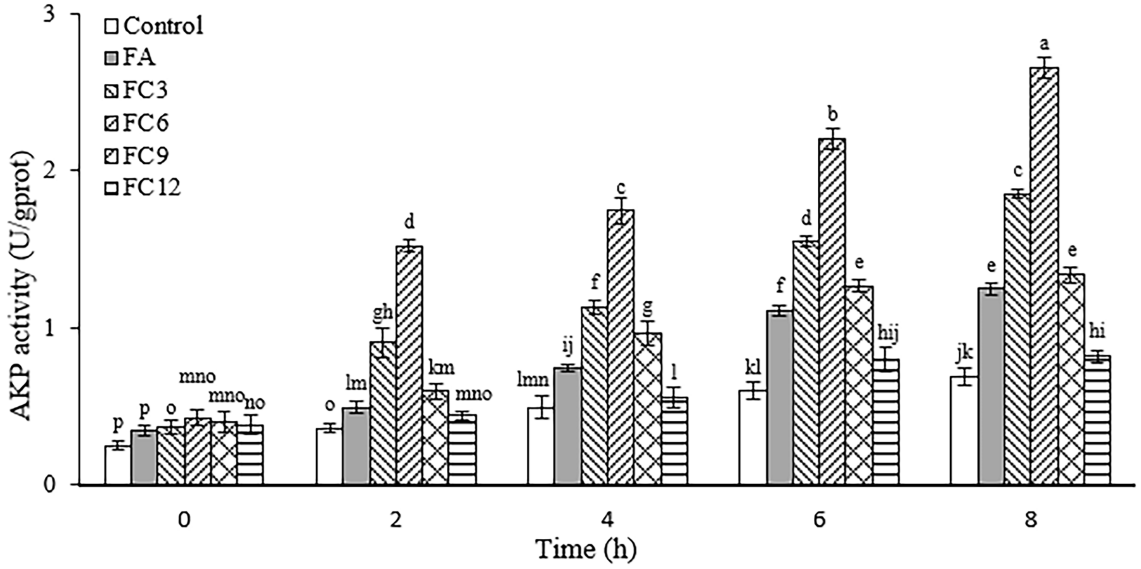

FIGURE 3
Effect on the integrity of *Pseudomonas aeruginosa* cell wall.

activity of 2.66 U/gprot. Based on these results, it was speculated that FCs increased the permeability of the cell wall and damaged the integrity of the cell wall, thus allowing AKP to leak into the cell culture medium. This observation agrees with a recent review by Aldulaimi (2017) that FA acts synergistically with other phenolics like gallic acid against notable pathogens like *P. aerugino* cell wall, resulting in content leakage. Bearing in mind that the threats posed by this and other foodborne pathogens are still major threats to public health, it will be interesting to investigate synergistic antibacterial effects in the future.

3.4. Effects on *Pseudomonas aeruginosa* biofilm formation

The inhibition of FA, FC3, FC6, FC9, and FC12 on FA biofilm formation was evaluated by crystal violet staining. The results are shown in Figure 4. According to the inhibitory effect on biofilm formation, the order is FC6 (78%) > FC3 (43%) > FC9 (27%) > FA (26%) > FC12 (18%). The results indicated that FC6 had the strongest inhibition effect on forming *P. aerugino* biofilm at the same concentration. Floating motion plays an important role in the pathogenic ability of *P. aerugino*, which can initiate the adhesion of bacteria to the adhesive surface and contribute to the formation of *P. aerugino* biofilm. Therefore, these partial results suggest that the inhibition of this motion may be one of the reasons for the reduction of biofilm formation(Diao et al., 2018; Zhao et al., 2019). Furthermore, a recent comparative study by Xu et al. (2022) revealed that FA had a greater biofilm repression effect than *p*-coumaric acid (*p*-CA) against pathogenic *Salmonella enteritidis* by binding to proteins involved in flagella motility. In addition to maintaining high antibiofilm effectiveness in simulated conditions, both phenolics were forwarded as candidates for modifying this notable pathogen's phenotypic and molecular structures. This report supports our observation that further studies will prove valuable in enhancing the pathogen-inhibiting applications of FA.

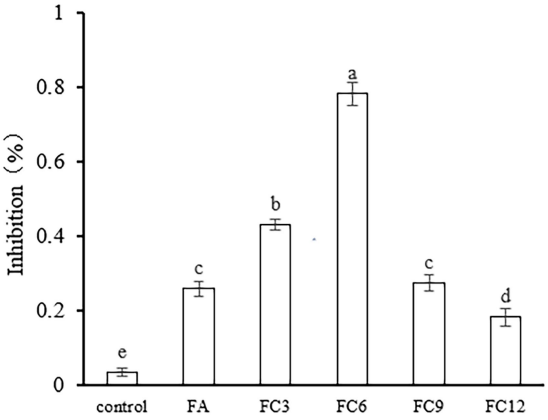

FIGURE 4
Effect on *Pseudomonas aeruginosa* biofilm formation.

3.5. Influence on somatic morphology of *Pseudomonas aeruginosa* bacteria

In order to further observe the effects of FA, FC3, FC6, FC9 and FC12 on the integrity of *P. aerugino* cell wall and membrane, the morphological changes of *P. aerugino* cells treated with an antibacterial agent for 2 h were observed by scanning electron microscopy. As shown in Figure 5, the *P. aerugino* cells in the control group (Figure 5A) were complete, full in shape, clear in outline, rod-shaped, and relatively smooth in surface, showing a typical Gram-negative bacterial morphological structure. In the *P. aerugino* cells treated by FA, FC3 and FC9 (Figures 5B, C, E), thalli were deformed, their surfaces collapsed and crumpled, and their surfaces were rough. The surface of *P. aerugino* treated by FC12 (Figure 5F) showed no change compared with the control group, only some cells were shrunken. The FC6-treated cells (Figure 5D) showed rough

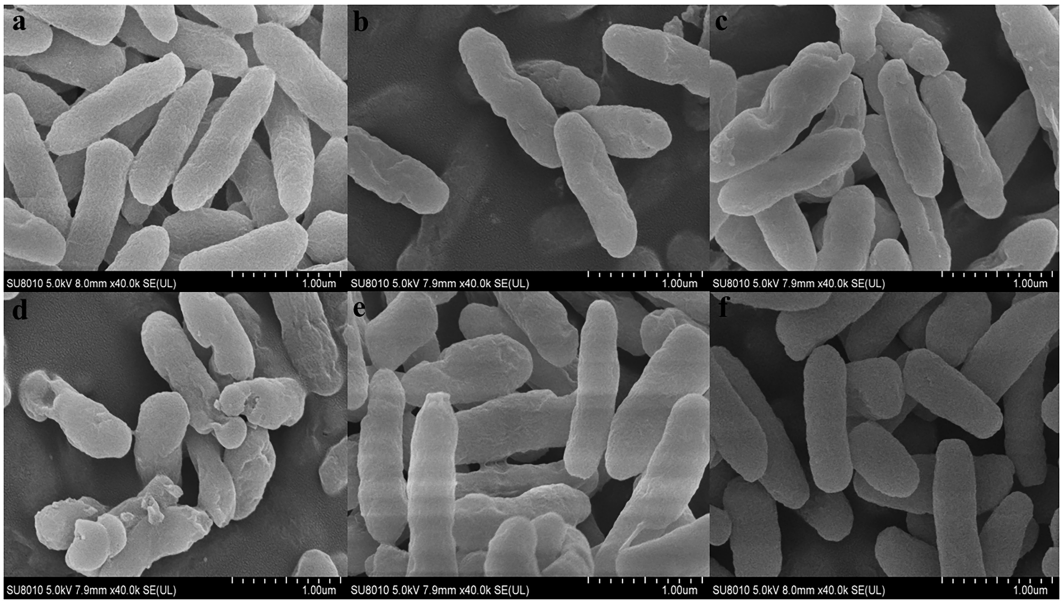

FIGURE 5
Effect on morphology of *Pseudomonas aeruginosa* cells. **(A)** Shows the Control group. **(B)** Shows the experimental group treated with FA. **(C)** Shows the experimental group treated with FC3. **(D)** Shows the experimental group treated with FC6. **(E)** Shows the experimental group treated with FC9. **(F)** Shows the experimental group treated with FC12.

surface, severe shrinkage, aggregation, and adhesion; some cells even ruptured. Dasagrandhi et al. (2018) treated *P. aerugino* cells with ferulic acid-grafted chitosan (CFA) with 1 × MIC concentration to deform the bacterial cells and gather them together in large numbers, causing damage to the bacterial membrane. This agrees with the current study's findings, and thus future experiments may need to investigate if there is a molecular basis for these processes, as previously posited by Xu et al. (2022).

3.6. Influence on FA membrane potential

Membrane potential is the potential difference between the inside and outside of a biological cell membrane, and maintaining normal membrane potential is of great significance for ATP production and cell function maintenance (Xu et al., 2016). Rhodamine 123 is a lipophilic cationic dye that can enter the cell matrix by transmembrane potential, the size of which can be expressed by its fluorescence intensity. Under normal circumstances, the voltage inside the membrane is usually lower than outside the membrane. If the membrane potential decreases, it means that the membrane is depolarized; otherwise, if it increases, it means that hyperpolarization occurs (Kiran and Yarlagadda, 2020. Figure 6 shows the effects of FA and FCs on the membrane potential of *P. aerugino*. As shown in Figure 6, both FA and FCs can hyperpolarize the membrane of *P. aerugino*, and FC3 and FC6 have significant effects on the membrane potential of *P. aerugino*. Control group's fluorescence intensity of 340.33 ± 18.77 on average, after FC3 and FC6 treatment, and the fluorescence intensity increased to 453.67 ± 10.41 and 564.33 ± 14.01 respectively, compared with the control group, with a growth of 33 and 66% respectively, compared with the control group, both were extremely significant differences. The results showed that FC6 had more serious effects on *P. aeruginosa*. Shang et al. (2017) showed that the target of the antibiotic drug chensinin-1b is the plasma

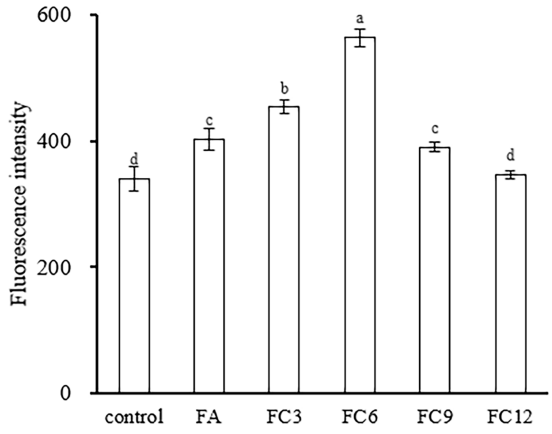

FIGURE 6
Effect on membrane potential of *Pseudomonas aeruginosa*.

membrane through the cell intimal permeability experiment results. Chensinin-1b can increase the membrane potential of MRPA0108, increasing membrane permeability, leakage of contents, and the death of bacteria.

3.7. Evaluation of membrane permeability of *Pseudomonas aeruginosa*

3.7.1. Propidium iodide uptake test

PI can be embedded into DNA double-stranded molecules, making them fluoresce, a fluorescent probe. Under normal physiological conditions, PI cannot enter cells, but when the cell membrane breaks, PI can cross the cell membrane and enter the cell,

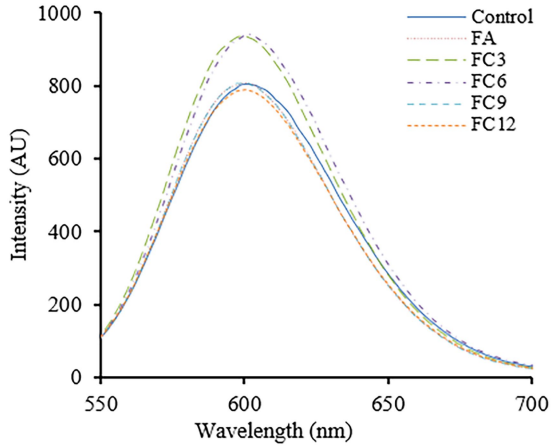

FIGURE 7
Effect on membrane integrity of *Pseudomonas aeruginosa*.

binding to DNA. Therefore, the integrity of the cell membrane can be judged by measuring the fluorescence intensity after PI interacts with DNA (Chakotiya et al., 2017). Figure 7 shows the effects of FA and FCs on cell membrane integrity. As shown in Figure 7, in the range of wavelength 550–700 nm, the fluorescence intensity of FA 4 h under the action of FC3 and FC6 was significantly stronger than that of the control group, indicating that FC3 and FC6 could be effective against *P. aerugino* membrane by damaging its integrity and preventing further disease spread. These observations were similar to earlier findings that FA and other phenolics have growing bactericidal effects against foodborne pathogens (Diao et al., 2018; Xu et al., 2022). Another recent research by Kong et al. (2023) revealed that the FA ester derivatives had substantial *in vitro* and *in vivo* inhibitory effects against *Alternaria alternata,* a major fungal pathogen causing black spot disease of Korla pear has resulted in exponential losses. Thus, further *in vivo* mechanistic studies must be conducted to show more potential for FA and its ester derivatives in the food, agricultural, and biomedical sectors.

3.7.2. Impact on leakage of *Pseudomonas aeruginosa* contents

Nucleic acid, protein, Na^+, K^+ and other cell contents play an important role in maintaining the normal physiological function of cells. In normal cells, cell contents will not cross the cell membrane. When the bacterial cell membrane is destroyed, some macromolecules will enter the external environment through the cell membrane, resulting in the increase of the absorbance of the external environment at 260 and 280 nm wavelengths. Thus, this wavelength range can be used to measure cell content leakage. To determine the permeability of the cell membrane. Figure 8 shows the influence of FA, FC3, FC6, FC9 and FC12 on the leakage of *P. aerugino* contents at different times. Figure 8A shows the leakage of protein, and Figure 8B shows the leakage of nucleic acid. As shown in Figure 8A, the *P. aerugino* treated by FA, FC3, FC6, FC9 and FC12 all have different levels of protein leakage, and the *P. aerugino* protein leakage treated by FC6 is the largest. With the prolongation of the antibacterial agent and *P. aerugino*, the protein content in bacterial suspension increased gradually. At 4 h, the protein content after FC6 action on *P. aerugino* was 0.203 mg/ml, 2.94 times that of the control group (0.069 mg/ml). As shown in Figure 8B, at 4 h, after FC6 acted on *P. aerugino*, the leakage of nucleic acid was significantly higher than that of the control group and other FCs, and the absorbance was 2.48 times that of the control group. Combined with Figures 8A,B, it can be seen that FCs can cause the leakage of macromolecular nucleic acids and proteins in *P. aerugino* cells to varying degrees, indicating that FCs change the permeability and integrity of cell membrane, which is consistent with the above results of cell integrity. Li et al. (2020) reported that the integrity of the cell membrane would be damaged after the antibacterial peptide CM4 was applied to *P. aerugino* cells, resulting in nucleic acid and protein leakage.

4. Conclusion

Antimicrobial resistance posed by foodborne pathogens makes them a constant threat to global public safety, prompting studies into novel ways of overcoming this challenge. In this study, MIC and MBC values of the 4 pathogenic bacteria(*E. coli, P. aerugino, S. aureus*, *and B. subtilis)* showed that after esterification, the antibacterial activity increased, but with the extension of the alkyl chain of antibacterial compounds, the antibacterial activity increased first and then decreased. FCs can destroy the cell wall of Pseudomonas aeruginosa and affect the biofilm of *P. aerugino* cells to varying degrees. Among them, FC6 inhibits the formation of the biofilm of *P. aerugino* cells the most, making the surface of *P. aerugino* cells rough and wrinkled, and showing aggregation and adhesion. Some cells even rupture. The integrity of the cell membrane is damaged, and the contents of the cell (protein, nucleic acid) are leaked. The effect of FCs on the biofilm of *P. aerugino* cells further indicated that the antibacterial activity of FA increased after esterification, but the antibacterial activity increased first and then decreased with the extension of the alkyl chain of antibacterial compounds. However, the application of FCs in the food system needs further research.

Data availability statement

The original contributions presented in the study are included in the article/Supplementary material, further inquiries can be directed to the corresponding author.

Author contributions

WS and JX conceived and designed the experiments. WS and CY performed the experiments. JX and CX supervised the project. WS analyzed the data. WS, JX, CY, and YP wrote the paper. All authors contributed to the article and approved the submitted version.

Funding

This study was supported by the Natural Science Foundation of Heilongjiang Province (LH2020C063).

Conflict of interest

The authors declare that the research was conducted in the absence of any commercial or financial relationships that could be construed as a potential conflict of interest.

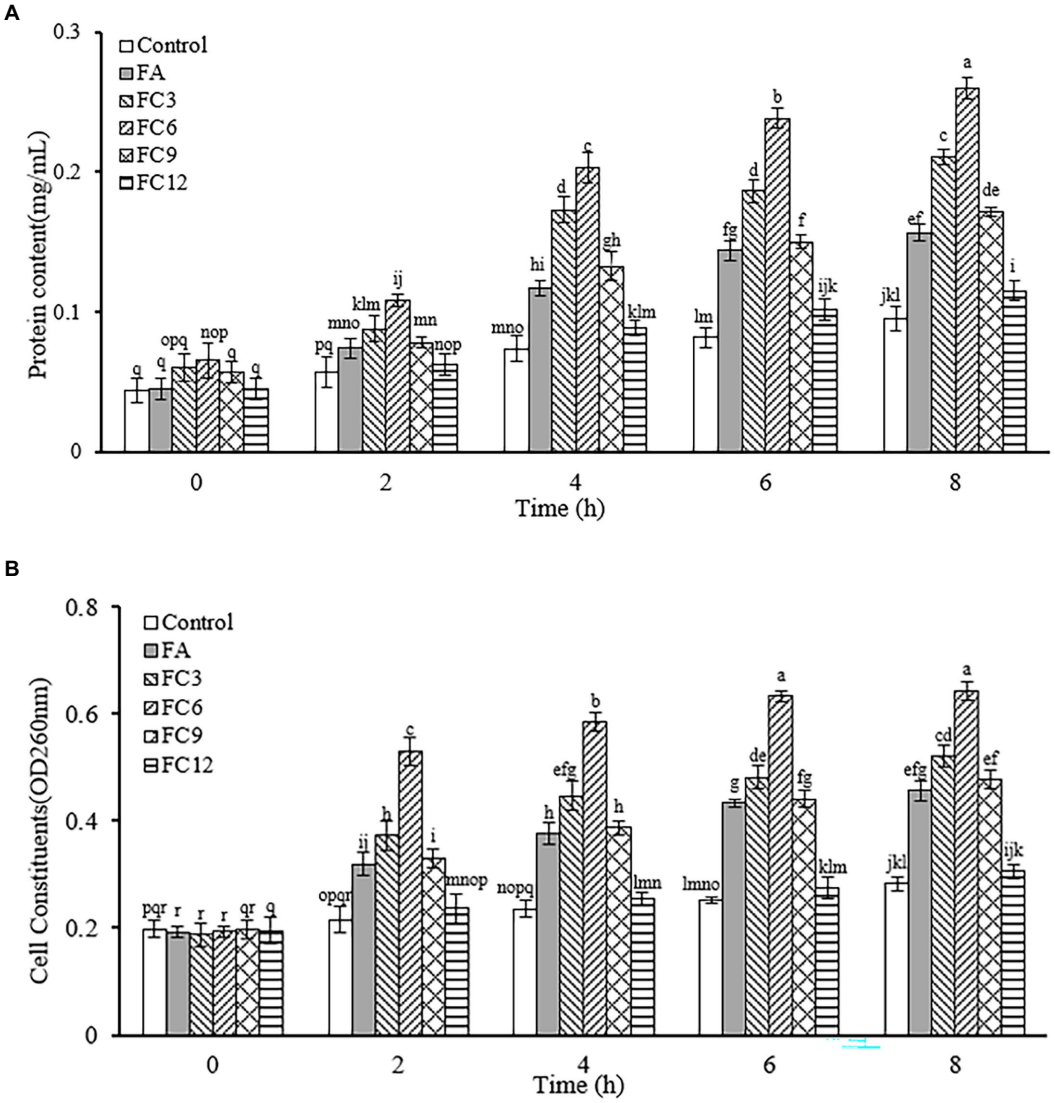

FIGURE 8
Effect on leakage of *Pseudomonas aeruginosa* cell contents. **(A)** Effect on protein leakage in *Pseudomonas aeruginosa* cells. **(B)** Effect on nucleic acid leakage of *Pseudomonas aeruginosa* cells.

Publisher's note

References

Aldulaimi, O. A. (2017). General overview of phenolics from plant to laboratory, good antibacterials or not. *Pharmacogn. Rev.* 11, 123–127. doi: 10.4103/phrev.phrev_43_16

Aljawish, A., Muniglia, L., Klouj, A., Jasniewski, J., Scher, J., and Desobry, S. (2016). Characterization of films based on enzymatically modified chitosan derivatives with phenol compounds. *Food Hydrocoll.* 60, 551–558. doi: 10.1016/j.foodhyd.2016.04.032

Barbara, L., Sofia, C., and Giovanni, M. (2015). Wheat bran phenolic acids: bioavailability and stability in whole wheat-based foods. *Molecules* 20, 15666–15685. doi: 10.3390/molecules200915666

Borges, A., Saavedra, M. J., and Simões, M. (2012). The activity of ferulic and gallic acids in biofilm prevention and control of pathogenic bacteria. *Biofouling* 28, 755–767. doi: 10.1080/08927014.2012.706751

Burcu, E., Çoban, T., Onurdag, F. K., and Banoglu, E. (2011). Synthesis, antioxidant and antimicrobial evaluation of simple aromatic esters of ferulic acid. *Arch. Pharm. Res.* 34, 1251–1261. doi: 10.1021/acs.jafc.8b04429

Burt, S. (2004). Essential oils: their antibacterial properties and potential applications in foods--a review. *Int. J. Food Microbiol.* 94, 223–253. doi: 10.1016/j.ijfoodmicro.2004.03.022

Campion, A., Morrissey, R., Field, D., Cotter, P. D., Hill, C., and Ross, R. P. (2017). Use of enhanced nisin derivatives in combination with food-grade oils or citric acid to control cronobacter sakazakii and escherichia coli 0157:h7. *Food Microbiol.* 65, 254–263. doi: 10.1016/j.fm.2017.01.020

Chakotiya, A. S., Tanwar, A., Narula, A., and Sharma, R. K. (2017). Zingiber officinale: its antibacterial activity on pseudomonas aeruginosa and mode of action evaluated by flow cytometry. *Microb. Pathog.* 107, 254–260. doi: 10.1016/j.micpath.2017.03.029

Chauhan, R., Azmi, W., Bansal, S., and Goel, G. (2021). Multivariate analysis of adaptive response to ferulic acid and poumaric acid after physiological stresses in cronobacter sakazakii. *J. Appl. Microbiol.* 131, 3069–3080. doi: 10.1111/jam.15164

Dasagrandhi, C., Park, S., Jung, W. K., and Kim, Y. M. (2018). Antibacterial and biofilm modulating potential of Ferulic acid-grafted chitosan against human pathogenic bacteria. *Int. J. Mol. Sci.* 19:2157. doi: 10.3390/ijms19082157

Diao, M., Qi, D., Xu, M., Lu, Z., Lv, F., Bie, X., et al. (2018). Antibacterial activity and mechanism of monolauroyl-galactosylglycerol against bacillus cereus – sciencedirect. *Food Control* 85, 339–344. doi: 10.1016/j.foodcont.2017.10.019

Djordjevic, D., Wiedmann, M., and McLandsborough, L. A. (2002). Microtiter plate assay for assessment of listeria monocytogenes biofilm formation. *Appl. Environ. Microbiol.* 68, 2950–2958. doi: 10.1128/AEM.68.6.2950-2958.2002

Jung, S. W., Thamphiwatana, S., Zhang, L., and Obonyo, M. (2015). Mechanism of antibacterial activity of liposomal linolenic acid against helicobacter pylori. *PLoS One* 10:e0116519. doi: 10.1371/journal.pone.0116519

Kiran, K. R. G., and Yarlagadda, V. N. (2020). Alkylimidazolium ionic liquids as antifungal alternatives: antibiofilm activity against candida albicans and underlying mechanism of action. *Front. Microbiol.* 11, 1–15. doi: 10.3389/fmicb.2020.00730

Kong, H., Fu, X., Chang, X., Ding, Z., Yu, Y., Xu, H., et al. (2023). The ester derivatives of ferulic acid exhibit strong inhibitory effect on the growth of Alternaria alternata in vitro and in vivo. *Postharvest Biol. Technol.* 196:112158. doi: 10.1016/j.postharvbio.2022.112158

Kot, B., Wierzchowska, K., Grużewska, A., and Lohinau, D. (2018). The effects of selected phytochemicals on biofilm formed by five methicillin-resistant Staphylococcus aureus. *Nat. Prod. Res.* 32, 1299–1302. doi: 10.1080/14786419.2017.1340282

Kubo, I., Fujita, K., Nihei, K., and Nihei, A. (2004). Antibacterial activity of akyl gallates against Bacillus subtilis. *J. Agric. Food Chem.* 52, 1072–1076. doi: 10.1021/jf034774l

Li, D., Rui, Y. X., Guo, S. D., Luan, F., Liu, R., and Zeng, N. (2021). Ferulic acid: a review of its pharmacology, pharmacokinetics and derivatives. *Life Sci.* 284:119921. doi: 10.1016/j.lfs.2021.119921

Li, J. F., Zhang, J. X., Li, G., Xu, Y. Y., Lu, K., Wang, Z. G., et al. (2020). Antimicrobial activity and mechanism of peptide CM4 against Pseudomonas aeruginosa. *Food Funct.* 11, 7245–7254. doi: 10.1039/d0fo01031f

Lozano, R., Naghavi, M., Foreman, K., Lim, S., Shibuya, K., Aboyans, V., et al. (2012). Global and regional mortality from 235 causes of death for 20 age groups in 1990 and 2010: a systematic analysis for the global burden of disease study 2010. *Lancet (London, England)* 380, 2095–2128. doi: 10.1016/S0140-6736(12)61728-0

Malheiro, J. F., Maillard, J.-Y., Borges, F., and Simoes, M. (2018). Evaluation of cinnamaldehyde and cinnamic acid derivatives in microbial growth control. *Int. Biodeterior. Biodegradation* 141, 71–78. doi: 10.1016/j.ibiod.2018.06.003

Merkl, C. T. (2010). Antimicrobial and antioxidant properties of phenolic acids alkyl esters. *Czech J. Food Sci.* 28, 275–279. doi: 10.1080/19476330903450282

Naraysanan, K. B., Park, G. T., and Han, S. S. (2021). Biocompatible, antibacterial, polymeric hydrogels active against multidrug-resistant Staphylococcus aureus strains for food packaging applications. *Food Control* 123:107695. doi: 10.1016/j.foodcont.2020.107695

Park, I. K., and Kang, D. H. (2013). Effect of electropermeabilization by ohmic heating for inactivation of escherichia coli o157:h7, salmonella enterica serovar typhimurium, and listeria monocytogenes in buffered peptone water and apple juice. *Appl. Environ. Microbiol.* 79, 7122–7129. doi: 10.1128/AEM.01818-13

Pernin, A., Guillier, L., and Dubois-Brissonnet, F. (2019). Inhibitory activity of phenolic acids against listeria monocytogenes: deciphering the mechanisms of action using three different models. *Food Microbiol.* 80, 18–24. doi: 10.1016/j.fm.2018.12.010

Pinheiro, P. G., Santiago, G. M. P., da Silva, F. E. F., de Araújo, A. C. J., de Oliveira, C. R. T., Freitas, P. R., et al. (2021). Antibacterial activity and inhibition against Staphylococcus aureus NorA efflux pump by ferulic acid and its esterified derivatives. *Asian Pac. J. Trop. Biomed.* 11, 405–413. doi: 10.4103/2221-1691.321130

Saharkhiz, M. J., Motamedi, M., Zomorodian, K., Pakshir, K., and Hemyari, K. K. (2012). Chemical composition, antifungal and antibiofilm activities of the essential oil of mentha piperita l. *Isrn Pharmaceutics* 2012:718645. doi: 10.5402/2012/718645

Shang, D., Meng, X., Zhang, D., and Kou, Z. (2017). Antibacterial activity of chensinin-1b, a peptide with a random coil conformation, against multiple-drug-resistant Pseudomonas aeruginosa. *Biochem. Pharmacol.* 143, 65–78. doi: 10.1016/j.bcp.2017.07.017

Shao, S. Y., Shi, Y. G., Wu, Y., Bian, L. Q., Zhu, Y. J., Huang, X. Y., et al. (2018). Lipase-catalyzed synthesis of sucrose Monolaurate and its antibacterial property and mode of action against four pathogenic bacteria. *Molecules (Basel, Switzerland)* 23:1118. doi: 10.3390/molecules23051118

Shi, Y. G., Bian, L. Q., Zhu, Y. J., Zhang, R. R., Shao, S. Y., Wu, Y., et al. (2019). Multi-functional alkyl ferulate esters as potential food additives: antibacterial activity and mode of action against listeria monocytogenes and its application on american sturgeon caviar preservation. *Food Control* 96, 390–402. doi: 10.1016/j.foodcont.2018.09.030

Shi, C., Sun, Y., Zheng, Z., Zhang, X., Song, K., Jia, Z., et al. (2016). Antimicrobial activity of syringic acid against Cronobacter sakazakii and its effect on cell membrane. *Food Chem.* 197, 100–106. doi: 10.1016/j.foodchem.2015.10.100

Shi, Y. G., Wu, Y., Lu, X. Y., Ren, Y. P., Wang, Q., Zhu, C. M., et al. (2017). Lipase-catalyzed esterification of ferulic acid with lauryl alcohol in ionic liquids and antibacterial properties *in vitro* against three food-related bacteria. *Food Chem.* 220, 249–256. doi: 10.1016/j.foodchem.2016.09.187

Shi, Y., Zhu, Y. J., Shao, S. Y., Zhang, R. R., Wu, Y., Zhu, C. M., et al. (2018). Alkyl ferulate esters as multi-functional food additives: antibacterial activity and mode of action against *Escherichia coli in vitro*. *J. Agric. Food Chem.* 66, 12088–12101. doi: 10.1021/acs.jafc.8b04429

Shu, H., Chen, H., Wang, X., Hu, Y., Yun, Y., Zhong, Q., et al. (2019). Antimicrobial activity and proposed action mechanism of 3-carene against brochothrix thermosphacta and pseudomonas fluorescens. *Molecules* 24:3246. doi: 10.3390/molecules24183246

Stamatis, H.,and Sereti, V., & and Kolisis, F.N. (2001). Enzymatic synthesis of hydrophilic and hydrophobic derivatives of natural phenolic acids in organic media. *J. Mol. Catal. B Enzym.*, 11, 323–328. doi: 10.1016/S1381-1177(00)00016-3

Tang, Y., Hao, J., Fan, C., and Cao, X. (2021). Preparative separation of high-purity trans- and cis-ferulic acid from wheat bran by pH-zone-refining counter-current chromatography. *J. Chromatogr. A* 1636:461772. doi: 10.1016/j.chroma.2020.461772

Xu, J. G., Hu, H. X., Chen, J. Y., Xue, Y. S., Kodirkhonov, B., and Han, B. Z. (2022). Comparative study on inhibitory effects of ferulic acid and p-coumaric acid on salmonella Enteritidis biofilm formation. *World J. Microbiol. Biotechnol.* 38, 136–114. doi: 10.1007/s11274-022-03317-1

Xu, C., Li, J., Yang, L., Fang, S., and Ming, Y. (2016). Antibacterial activity and a membrane damage mechanism of lachnum ym30 melanin against vibrio parahaemolyticus and staphylococcus aureus. *Food Control* 73, 1445–1451. doi: 10.1016/j.foodcont.2016.10.048

Zhao, Y., Si, Y., Mei, L., Wu, J., Shao, J., Wang, C., et al. (2019). Effects of sodium houttuyfonate on transcriptome of Pseudomonas aeruginosa. *BMC. Res. Notes* 12:685. doi: 10.1186/s13104-019-4721-2

Zhao, L., Zhang, H., Hao, T., and Li, S. (2015). *In vitro* antibacterial activities and mechanism of sugar fatty acid esters against five food-related bacteria. *Food Chem.* 187, 370–377. doi: 10.1016/j.foodchem.2015.04.108

frontiers | Frontiers in Microbiology

TYPE Original Research
PUBLISHED 22 March 2023
DOI 10.3389/fmicb.2023.1122623

OPEN ACCESS

EDITED BY
Peng Fei,
Nanyang Institute of Technology,
China

REVIEWED BY
Brandan Pedre Perez,
KU Leuven,
Belgium
Chaoxin Man,
Northeast Agricultural University,
China

*CORRESPONDENCE
Chun Fang
✉ fangchun@yangtzeu.edu.cn

†These authors have contributed equally to this work

SPECIALTY SECTION
This article was submitted to Food Microbiology, a section of the journal Frontiers in Microbiology

RECEIVED 13 December 2022
ACCEPTED 07 March 2023
PUBLISHED 22 March 2023

CITATION
Zhang Y, Guo Q, Fang X, Yuan M, Hu W, Liang X, Liu J, Yang Y and Fang C (2023) Destroying glutathione peroxidase improves the oxidative stress resistance and pathogenicity of *Listeria monocytogenes*. *Front. Microbiol.* 14:1122623. doi: 10.3389/fmicb.2023.1122623

Destroying glutathione peroxidase improves the oxidative stress resistance and pathogenicity of *Listeria monocytogenes*

Yu Zhang†, Qian Guo†, Xiaowei Fang, Mei Yuan, Wenjie Hu, Xiongyan Liang, Jing Liu, Yuying Yang and Chun Fang*

Laboratory of Animal Pathogenic Microbiology, College of Animal Science, Yangtze University, Jingzhou, China

Introduction: Glutathione peroxidase is abundant in eukaryotes as an important antioxidant enzyme. However, prokaryotic glutathione peroxidase has not been thoroughly studied. *Listeria monocytogenes* is a facultative intracellular pathogen that is capable of causing listeriosis in animals as well as humans. Despite the fact that *L. monocytogenes* encodes a putative glutathione peroxidase, GSH-Px (encoded by *lmo0983*)), the functions of the enzyme are still unknown. Here we revealed the unusual roles of *L. monocytogenes* GSH-Px in bacterial antioxidants and pathogenicity.

Methods: *L. monocytogenes* Lm850658 was taken as the parental strain to construct the gsh-px deletion strain and related complement strain. The effect of the gsh-px gene on the resistance of *L. monocytogenes* to oxidative stress was determined by measuring the concentrations of glutathione and assaying the stress survival rates under different oxidative conditions. In addition, the pathogenicity of *L. monocytogenes* was determined by cellular adhesion and invasion assays and mice virulence tests, and the expression of virulence factors was determined by Western blot.

Results: Deficiency of GSH-Px not only increased glutathione concentrations in L. monocytogenes but also enhanced its resistance to oxidative stress when exposed to copper and iron ions. In addition, the absence of gsh-px significantly improved the adhesion and invasion efficiency of *L. monocytogenes* to Caco-2 cells. More importantly, *L. monocytogenes* lacking GSH-Px could colonize and proliferate more efficiently in mice livers and spleens, enhancing the pathogenicity of L. monocytogenes by increasing the expression of virulence factors like InlA, InlB, and LLO.

Discussion: Taken together, we confirmed that GSH-Px of *L. monocytogenes* has a counter-intuitive effect on the antioxidant capacity and pathogenicity.

KEYWORDS

***Listeria monocytogenes*, glutathione peroxidase, glutathione, oxidative stress, virulence factor, pathogenicity**

1. Introduction

Listeria monocytogenes is found in plenty of environments and can easily transition from saprophytic organism to intracellular pathogen (Freitag et al., 2009; Xayarath and Freitag, 2012). Humans and animals may develop severe illnesses when they consume contaminated foods containing *L. monocytogenes* (Hedberg, 2011). *L. monocytogenes* faces a variety of stresses to survive in different niches, the most prevalent of which is oxidative stress. The oxidative conditions

L. monocytogenes confronted include reactive oxygen species (ROS), reactive nitrogen species (RNS), and reactive chlorine species (RCS). Cellular components including DNA, proteins and membrane lipids are damaged when cells exposed to ROS, RNS, and RCS (Chakraborty et al., 1992; Ezraty et al., 2017). Consequently, for *L. monocytogenes* to thrive in oxidative environments, it needs to use a sophisticated system to ward off oxidative stress as well as prevent oxidative damage (Mates et al., 1999; Mates, 2000). To combat oxidative stress, *L. monocytogenes* encodes multiple metabolic enzymes like superoxide dismutase (SOD), catalase (CAT), thioredoxin (TRx), glutathione reductase (GR), and glutathione S-transferase (GST; Mains et al., 2021).

Glutathione peroxidases (GSH-Pxs) are a group of antioxidant enzymes found in eukaryotic organisms. In addition to being a vital component of the antioxidant systems, they may be involved in immune defense against pathogen invasion (Bathige et al., 2015). For example, inflammatory signaling cascades are closely linked to GSH-Px1 in mammals (Duong et al., 2010; Brigelius-Flohe and Maiorino, 2013). However, prokaryotic GSH-Px research is lacking. Numerous prokaryotes, including *Staphylococcus aureus*, *Bacillus subtilis*, *Lactococcus lactis*, and *L. monocytogenes*, have been found to possess genes homologous to *gsh-px* (Brenot et al., 2004). To date, there have been no investigations into the biological mechanisms of GSH-Px in bacteria in response to oxidative stress and host infection. GSH-Px reduces the organic hydroperoxides and hydrogen peroxide to the corresponding alcohols (water in the case of hydrogen peroxide) in eukaryotic organisms by utilizing glutathione as an electron donor (Ursini et al., 1995; Kutlu and Susuz, 2004). Whether GSH-Px in prokaryotes is closely linked to glutathione and affects oxidative resistance and pathogenicity, what specific biological functions of GSH-Px in prokaryotes are prompting us to understand the effects of GSH-Px on *L. monocytogenes*.

Glutathione (GSH), one of the glutaredoxin (Grx) systems, is necessary for preserving intracellular redox homeostasis (Masip et al., 2006). *L. monocytogenes* is one of the Gram-positive bacteria capable of synthesizing glutathione (Newton et al., 1996). GSH binds to PrfA at the broad tunnel between the N-terminal and C-terminal domains to make PrfA change conformation and become constitutive activation (Hall et al., 2016). PrfA is a global virulence regulator, which belongs to the Crp/Fnr transcriptional factor family (Scortti et al., 2007). GSH allosterically binds to PrfA results in activation of PrfA and exhibits high affinity to the promoters of PrfA regulated virulent genes (Chakraborty et al., 1992; Freitag et al., 2009; De Las Heras et al., 2011). Therefore, GSH improves the pathogenicity of *L. monocytogenes* by increasing the expression levels of PrfA regulated genes (Reniere et al., 2015; Hall et al., 2016). Moreover, it has been demonstrated that *L. monocytogenes* controlled its biphasic life cycle and transitioned from saprophytic to pathogenic by regulating the concentrations of GSH (Reniere et al., 2015). Hence GSH is indispensable for *L. monocytogenes* not only for its allosteric binding to PrfA to promote expression of the virulence factors but for the ability to resist oxidative stress to produce a reductive environment for life activity (Masip et al., 2006; Ku and Gan, 2019).

Listeria monocytogenes lmo0983 has been identified as a putative glutathione peroxidase in the GenBank database. The purpose of the research is to confirm whether GSH-Px in *L. monocytogenes* is involved in the biological process of bacterial infection and the related molecular mechanisms. As shown by our findings that GSH-Px played unanticipated functions in the antioxidant and pathogenicity of *L. monocytogenes*. The resistance of *L. monocytogenes* to the oxidative condition induced by metal ions was significantly enhanced when the *gsh-px* gene has been deleted, and the virulence of the pathogen in cells and mice was also increased. The findings of this research provide valuable evidence for elucidating the multiple physiological roles of glutathione peroxidase in foodborne pathogens to survive in the external environment and, more importantly, in the successful establishment of infection in the host.

2. Materials and methods

2.1. Bacterial strains and culture conditions

Listeria monocytogenes Lm850658 was taken as a wild-type strain, and the other strains were derived from it. All *L. monocytogenes* strains were incubated in brain-heart infusion (BHI) medium (Oxoid). *E. coli* DH5α was utilized as a plasmid host strain and cultured in Luria-Bertani broth (LB) (Oxoid). Agar was added to solid media at 1% (w/v). All bacteria were incubated at 37°C unless otherwise requested. The following concentrations were used for the antibiotics: ampicillin (100 μg/ml), erythromycin (10 μg/ml), kanamycin (50 μg/ml), or chloramphenicol (10 μg/ml) were added appropriately to the medium. Sangon Biotech supplied the highest purity of all chemicals. Table 1 displays the primers utilized in the research.

2.2. In-frame deletion and complementation of *Listeria monocytogenes*

Construction of gene deletion strain utilizing a homologous recombination strategy (Camilli et al., 1993), and temperature-sensitive plasmid pKSV7 was employed as a shuttle vector. Briefly, PCR amplification yielded the upstream and downstream homologous arms of *lmo0983*. A knock-out plasmid was constructed by connecting the homologous arms to shuttle vector. To promote chromosomal integration, electroporation of the plasmid into Lm850658, and transformants were grown in BHI broth containing 10 μg/ml chloramphenicol at a non-permissive temperature of 42°C. In order to make plasmid excision and curing, the recombinants were continuously passaged without chloramphenicol at a permissive temperature of 30°C. Finally, the chloramphenicol-sensitive recombinant colonies were identified using PCR. The integrative plasmid pIMK2 was utilized to complement the *gsh-px* gene of *L. monocytogenes* (Monk et al., 2008). Briefly, the *gsh-px* gene and its endogenous promoter were obtained using the primer pairs shown in Table 1, which were cloned into the pIMK2 plasmid to create the complementation plasmid. Electroporation of complementary plasmid into *L. monocytogenes* Δ*gsh-px*. The constructed complement strain was named CΔ*gsh-px*.

2.3. Measurement of growth curves

All strains were streaked in advance on BHI plates and individual colonies of each strain were picked into 3 ml broth. All *L. monocytogenes* strains were incubated for an entire night at 37°C in BHI broth. Cultures were gathered by centrifugation at 12,000 rpm

TABLE 1 The PCR primers used in this study.

Primers	Sequeces(5′-3′)	Products(bp)
Δ*gsh-px*-A	CGC*GGATCC*ATAGAAGTAGGCGATTTTGTTTC	566
Δ*gsh-px*-B	GATGATGTCACTACCGAGTCCTTCATG*GAATTC*CTCCTATTTCAATATA	
Δ*gsh-px*-C	GAAGGACTCGGTAGTGACATCATC	563
Δ*gsh-px*-D	CGGGGTACCATTTACGCTTCCCTCCCATGTTTAA	
Δ*gsh-px*-AF	CGCGGATCCTGGTTATGGTGGTAATTCC	
CΔ*gsh-px*-F	TCC*CCCGGG*ATGAATGTCCATGATTTTTC	468
CΔ*gsh-px*-R	TTCGTCGACTTATTTACTTACTTTCGCAAC	

The nucleotides introduced to create restriction enzyme sites are underlined.

for 2 min and washed once in phosphate-buffered saline (PBS, 10 mM, pH 7.4). The optical density of the bacteria was standardized to 1.0. Bacterial cultures were diluted at a ratio of 1:100 with normal BHI broth or with H_2O_2 at sub-lethal concentrations of 10 mM. The diluted bacterial solution was added to 96-well plates at 200 μl per well, 3 parallel wells for each sample, and blank reference using BHI medium. All bacteria were cultivated at 37°C for 12 h. The kinetic growth was conducted and bacterial $OD_{600\ nm}$ was recorded at 1-h interval by a microplate reader.

2.4. Oxidative stress tests

H_2O_2 acted as a direct oxidant in oxidative stress, and the metal ions copper (Cu^{2+}) and iron ions (Fe^{3+}) acted as redox active stress (Birben et al., 2012). The overnight cultured *L. monocytogenes* was harvested by centrifuging at 12000 rpm for 2 min and washed once with PBS, then diluted to $OD_{600\ nm}$ of 1.0 (~10^9 CFU/ml). The bacterial suspension was serially diluted after being resuspended in sterile PBS, and 100 μl bacterial solution was taken into 900 μl BHI broth containing 10 mM H_2O_2, 10 mM $FeCl_3$, and 5 mM $CuSO_4$ for 1 h, respectively. After incubating at 37°C for 1 h, the mixtures were serially diluted and placed on BHI agar plates. Spot plate counts were used to count the number of bacteria after incubation at 37°C for 24 h.

2.5. Determination of glutathione

GSH (reduced glutathione) concentrations were detected under different oxidative conditions. Beyotime Biotechnology provided the commercial measurement kits, which were used in accordance with the manufacturer's instructions. In short, dilution of 10 mM GSSG (oxidized glutathione) stock solution with protein removal reagent M to 15, 10, 5, 2, 1, 0.5 μM sequentially, then the 6 points were taken to make a standard curve. Determination of bacterial samples needed to be performed on the basis of the fresh cells. Bacteria growing to the exponential stage were obtained by centrifugation at 12000 rpm for 5 min, which was weighed and treated with BHI broth containing 10 mM H_2O_2, 10 mM $FeCl_3$, and 5 mM $CuSO_4$ for 3 h, respectively. An equal amount of bacterial pellet was collected from the control group. All samples were treated with lysozyme at 37°C for 30 min, then added with protein removal reagent M 3 times the volume of the cell pellet and mixed thoroughly. The samples were rapidly freeze-thawed twice using liquid nitrogen and a 37°C water bath. The supernatant was gathered by centrifuging at 4°C and 12,000 rpm for 10 min, then the total glutathione concentrations could be determined. Some samples of total glutathione contents to be measured were taken. Adding diluted GSH removal solution proportionally with vortex immediately, then adding GSH scavenging reagent working solution. Immediately vortexed and reacted at 25°C for 60 min. The above reaction could remove GSH from the sample and be used to determine GSSG. The amount of GSH could be calculated by subtracting the amount of GSSG from the total glutathione (GSSG + GSH). GSH concentrations of the parental and mutant strains were measured as described above (Anaya-Sanchez et al., 2021). A 96-well plate was used for measurement, and the standards and samples were added in sequence. 150 μl total glutathione detection working solution was added to the wells, and 50 μl of 0.5 mg/ml NADPH solution was added after incubation at 25°C for 5 min. The absorbance of 412 nm was determined with a plate reader, measured every 10 min for 1 h.

2.6. Adhesion and invasion tests

The human intestinal epithelial Caco-2 cells were used for adhesion and invasion assays (Cheng et al., 2017b). In brief, the Caco-2 cells were cultured in Dulbecco's modified Eagle's medium (DMEM) supplemented with 10% fetal bovine serum (FBS) at 37°C with 5% CO_2. Overnight grown *L. monocytogenes* was washed and resuspended with PBS. A single layer cells infected by bacteria for 30 min at a MOI of 10. For the adhesion assays, cells were lysed after two washes with PBS. As for the invasion assays, the prepared bacterial solution was added to the cells at 37°C with 5% CO_2 for 1 h. To kill extracellular bacteria, DMEM comprising 200 mg/ml gentamicin was used for an additional 1 h after being washed twice with PBS. The cells were lysed after washing twice with PBS. Counting viable bacteria on BHI agar plates after the solution was 10-fold diluted. The adhesion or invasion efficiency was determined by dividing the number of colony-forming units (CFUs) of adherent or invasive cells by the total number of infected bacteria.

2.7. Virulence experiments

The virulence of *L. monocytogenes* parental and mutant strains was detected by the method of bacterial load in mice organs (livers, spleens, and brains; Cheng et al., 2017b). For the bacterial load, overnight-grown *L. monocytogenes* was diluted to concentrations of 1×10^7 CFU/ml after washing once with PBS. The female Kunming mice were divided into 3

groups and 5 mice in each group. 10^6 CFU of each strain were injected intraperitoneally into mice. The mice were euthanized 48 h post infection (pi), and samples of their brains, livers, and spleens were taken and homogenized in 1 ml PBS under sterile condition. In order to count the number of bacteria, after being serially diluted, the homogenate was placed on BHI agar plates and incubated overnight.

2.8. Western blot

Listeria monocytogenes uses a collection of virulence factors to increase its pathogenicity and establish an infection successfully, allosteric binding of GSH to the transcription regulator PrfA is necessary for the expression of the PrfA regulated virulence factors (Ku and Gan, 2019). Therefore, we conjectured that the deletion of *gsh-px* would affect the expression of virulence factors in *L. monocytogenes*. Specifically, the bacteria colonies of the parental strain and mutant strain were picked into 50 ml medium, respectively. Incubation in a shaker at 37°C for one night. For lysates of whole cells (Lenz and Portnoy, 2002), the bacteria was gathered by centrifugation at 12000 rpm for 10 min, bacterial pellet was resuspended with 500 µl extraction solution (2% SDS, 4% triton, 10 mM PBS). The mixture was freeze-thawed twice at −20°C for 1 h and 37°C for 15 min, the supernatant was obtained by centrifugation at 12000 rpm for 10 min as the whole cell extract. After being boiled for 10 min, the protein samples were isolated by SDS-PAGE and incubated with α-InlA, InlB, LLO, and α-GAPDH antisera (prepared in this study). GAPDH served as an internal reference for proteins extracted from whole cells. Referring to the former study, all primary antibodies were produced in our laboratory (Cheng et al., 2017a). Rabbits were injected subcutaneously with 500 µg protein, including InlA, InlB, LLO, and GAPDH separately, with an equivalent volume of complete adjuvant for primary immunization. After 14 days, each rabbit was injected subcutaneously with 250 µg of incomplete adjuvant and an equal volume of protein, the immunization was given three times, once every 2 weeks. Blood was obtained from rabbits 7 days after the last immunization. Primary antibodies were diluted at 1:5,00 – 5,000, including rabbit polyclonal antibodies against InlA, InlB, LLO, and GAPDH, and following the manufacturer's instructions when using the appropriate secondary antibody. The enhanced chemiluminescence detection system was used to visualize all immunoreactions.

2.9. Ethics statement

Animal experiments had approved by the Laboratory Animal Management Committee of Yangtze University (Approval No. 20210301).

2.10. Statistical analysis

All experiments were performed three times with biological replicates. Data was expressed as mean ± standard deviation and statistical analysis was performed with GraphPad Prism 6 (version 6, GraphPad, United States). Unpaired t-tests were used to analyze the statistical significance. p-values <0.05 or 0.01 were considered statistically significant difference and marked with "*" and "**"; p-values >0.05 were considered as statistically, no significant difference and marked with "ns".

3. Results

3.1. *In vitro* growth of *Listeria monocytogenes* was unaffected by the deletion of *gsh-px*

GSH-Px is a vital component of the antioxidant systems in eukaryotes (Margis et al., 2008). To learn more about the specific biological roles of GSH-Px in *L. monocytogenes*, in-frame deletion mutant strain of the *gsh-px* gene was constructed. To understand whether the deletion of *gsh-px* was relevant for the growth of *L. monocytogenes*, the growth capacity of parental strain Lm850658 and the deletion strain Δ*gsh-px* in BHI with or without 10 mM H_2O_2 was determined. After incubating all strains at 37°C for 12 h, it was found that the growth ability of the parental and deletion strains was comparable under the normal condition (Figure 1A). When treated with 10 mM H_2O_2, this phenomenon remained unchanged (Figure 1B), indicating that the absence of *gsh-px* had no effect on H_2O_2. This observation demonstrated that the deletion of *gsh-px* had no influence on the growth of bacteria *in vitro*.

3.2. Deficiency of *gsh-px* dramatically increased tolerance to the copper and iron but not to the hydrogen peroxide

Since it has been shown that GSH-Px is closely related to the antioxidant systems of eukaryotes, further to identify whether GSH-Px of *L. monocytogenes* is correlated with bacterial oxidative resistance, the Lm850658 and *gsh-px* mutant strains (Δ*gsh-px* and CΔ*gsh-px*) were treated with diverse oxidizing media. By comparing the survival rates of the parental strain and deletional strain under the stress of the H_2O_2, the results showed that the survival rates of the parental strain and the mutant were comparable at 10 mM sub-lethal concentrations (Figure 2A). However, when exposed to the same concentrations of Fe^{3+}, the survival rate of the deletion strain was significantly higher than that of the parental strain (Figure 2B), while no viable bacteria were detected in all strains at the same concentrations of Cu^{2+}, so the concentrations of Cu^{2+} were reduced to 5 mM. The deletion of *gsh-px* significantly enhanced the resistance of *L. monocytogenes* to 5 mM Cu^{2+} (Figure 2C). This phenotype could be restored in the complementation strain CΔ*gsh-px*. These findings indicated that GSH-Px played an exceptional role in the antioxidant process of *L. monocytogenes* to metal ions, which was different from the classical fact that GSH-Px plays a role in enhancing antioxidant processes in eukaryotes.

3.3. The GSH concentrations of *Listeria monocytogenes* were significantly increased under the stimulation of metal ions

To understand whether the unusual effects of GSH-Px in *L. monocytogenes* are related to GSH, the concentrations of GSH under different oxidative conditions were measured. According to the measurement results, we found that in contrast to the normal BHI control group, the GSH of *L. monocytogenes* treated with metal

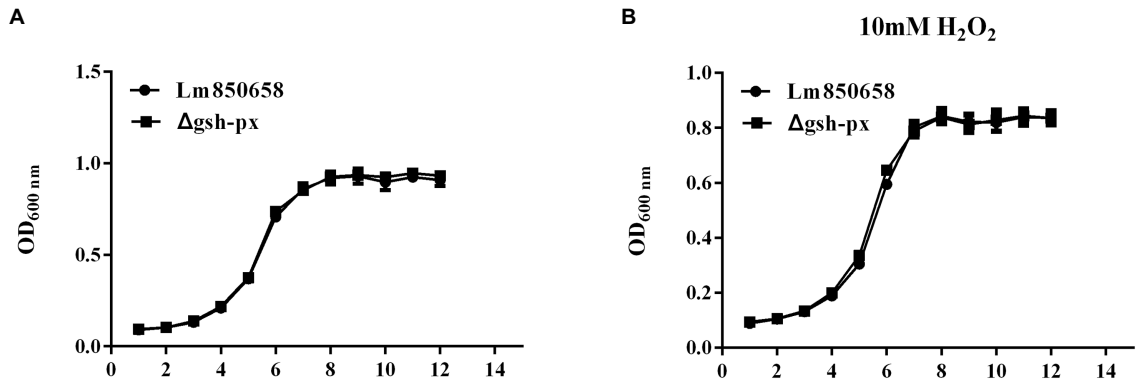

FIGURE 1
Deletion of *gsh-px* did no effect on the growth of *L. monocytogenes in vitro*. Overnight-grown bacteria were washed and diluted (1:100) in fresh BHI broth with **(B)** or without H_2O_2 **(A)**, incubated at 37°C for 12h. Data were expressed as mean±SD.

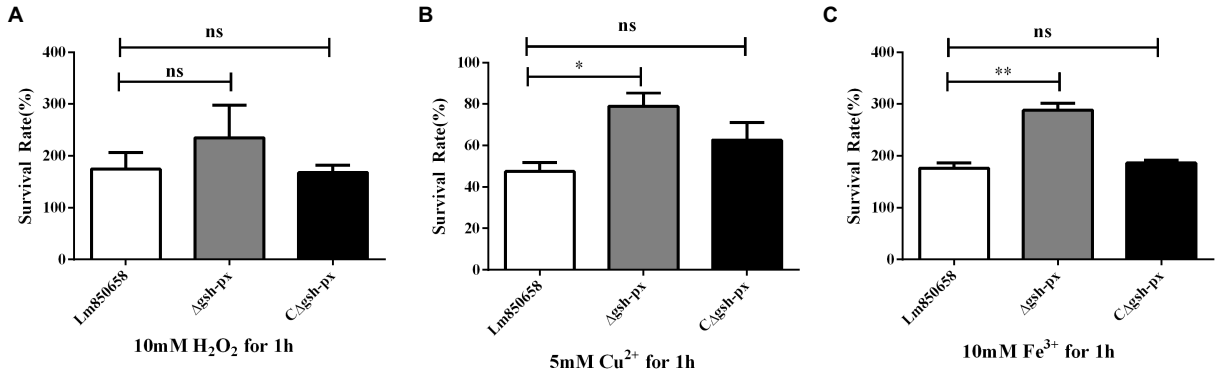

FIGURE 2
Deletion *gsh-px* of *L. monocytogenes* increased the tolerance to copper and iron, but not to hydrogen peroxide. Bacteria were treated with 10mM H_2O_2 **(A)**, 5mM Cu^{2+} **(B)** and 10mM Fe^{3+} **(C)** for 1h, and alive bacteria were counted by plate counting. The experiments were conducted for triplicate and data were expressed as mean±SD. ns, no significance; *, $p<0.05$; **, $p<0.01$.

ions for 3 h was significantly increased (Figure 3). However, after treating the bacteria with H_2O_2 for 3 h, GSH concentrations were essentially the same between the experimental and control groups (Figure 3). Unlike the role of GSH-Px in mammals, GSH concentrations in *L. monocytogenes* did not change significantly when H_2O_2 was used as a stressor, which was consistent with the results of oxidative stress tests.

3.4. Intracellular adhesion and invasion efficiency of *Listeria monocytogenes* was enhanced by the *gsh-px* mutation

Due to the unusual effect of GSH-Px on resistance to oxidative stress in *L. monocytogenes*, we set out to learn more about the role that GSH-Px plays in bacterial intracellular infection. Epithelial cell Caco-2 was used to compare the adhesion and invasion of wild-type and mutant strains. Surprisingly, the Δ*gsh-px* mutant strain was able to adhere and invade cells more effectively than parental strain (Figure 4), suggesting that the *gsh-px* gene was associated with the invasive ability of *L. monocytogenes* and may be redundant in helping the bacteria to invade the host.

3.5. Absence of *gsh-px* upgraded the harmfulness of *Listeria monocytogenes* to mice

The increased cell adhesion and invasion rates of the *gsh-px* mutant strain prompted us to explore more about how the GSH-Px affects virulence of *L. monocytogenes* in mammals. Therefore, we verified the connection between GSH-Px and virulence by measuring the bacterial load in the organs of mice.

The results indicated that the Δ*gsh-px* strain recovered more CFU from the spleens, livers and brains of infected mice compared to the wild-type strain (Figure 5). According to the findings, enhanced virulence of the Δ*gsh-px* mutant strain in mice, which was consistent with the consequence of cellular assays. The remarkable role of GSH-Px in the pathogenicity of *L. monocytogenes* was demonstrated by the discovery of the *gsh-px* mutant that increased virulence.

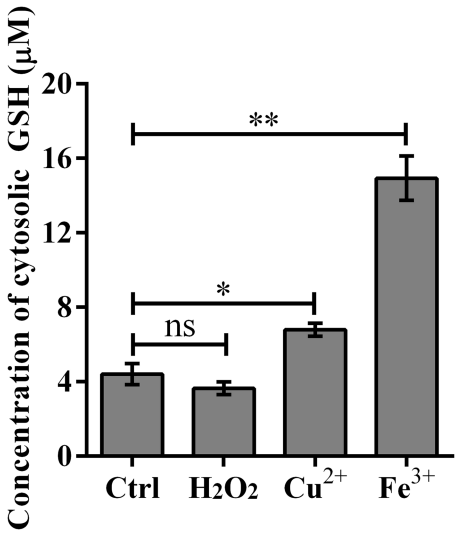

FIGURE 3
Cytosolic GSH concentration was significantly improved upon copper and iron treatment. Wild type strain Lm850658 was treated with BHI containing 10mM hydrogen peroxide, 5mM copper or 10mM iron for 3h and then bacteria were collected and lysed with lysozyme for 30min. The concentrations of GSH were measured with commercial kit supplied by Beyotime Biotechnology as manufacturer's instruction. The experiments were conducted for triplicate and data were expressed as mean±SD. ns, no significance; *, $p<0.05$; **, $p<0.01$.

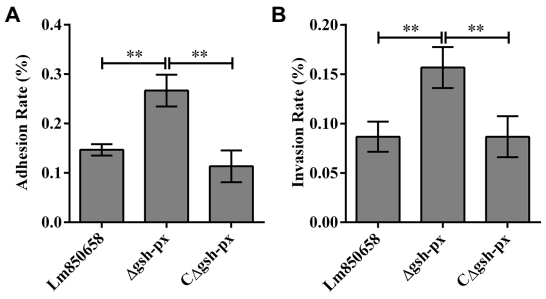

FIGURE 4
Mutation of *gsh-px* increased the adhesion **(A)** and invasion **(B)** ability of *L. monocytogenes* to Caco-2 cells. Epithelial cells Caco-2 were incubated with Lm850658, Δ*gsh-px* and CΔ*gsh-px* for 1h, the adhesive bacteria were collected and counted by plate counting and the invasive bacteria collected after killing the extracellular bacteria with gentamycin. Finally, the adhesion and adhesion rates were calculated using the adherent and invasive bacteria divided by the initial bacteria. The experiments were conducted for triplicate and data were expressed as mean±SD. ns, no significance; *, $p<0.05$; **, $p<0.01$.

3.6. Deletion of *gsh-px* upregulated the expression of major virulence factors in *Listeria monocytogenes*

The InlA and InlB are vital members of the virulence factors and the adhesion and invasion of *L. monocytogenes* into cells are crucially influenced by the InlA and InlB. By rupturing phagocytic vesicles, LLO makes it possible for bacteria to enter the cytoplasm. Western blotting was used to examine the expression of the major virulence factors in order to expand our understanding of how GSH-Px affects these factors. We discovered that *L. monocytogenes* was capable of invading the host more effectively in the absence of *gsh-px* in cellular experiments and virulence assays on mice. Based on this, we hypothesized that the increased expression of virulence factors might result from the deletion of *gsh-px*. The blotting validation results indicated that the expression of InlA, InlB and LLO in *L. monocytogenes* was remarkably increased when *gsh-px* was lacking, further to confirm the regulatory role of *gsh-px* on virulence factors in *L. monocytogenes* (Figure 6). This also supported our hypothesis that the deletion of *gsh-px* enhanced the adhesion and invasion ability of *L. monocytogenes* by enhancing the expression of virulence factors.

3.7. Deletion of *gsh-px* increased the GSH levels in *Listeria monocytogenes*

Due to the fact that intracellular GSH levels are required for PrfA activation, it is necessary to maintain high intracellular GSH concentrations for *L. monocytogenes*. We hypothesized that the effective intracellular GSH levels of the *gsh-px* deficient mutant were higher than that of the parental strain, resulting in enhanced virulence of the deletion strain. To validate the assumption, we tested the levels of GSH in the wild-type, Δ*gsh-px* and CΔ*gsh-px* strains. The results showed that the GSH concentrations of deletion strain were higher than that of parental strain, and this phenotype could be restored in the complementation strain CΔ*gsh-px* (Figure 7), suggesting that *L. monocytogenes* no longer consumed GSH or the rates of GSH consumption slowed down when the *gsh-px* was deleted, leading to GSH accumulation and enhanced virulence of *L. monocytogenes*.

4. Discussion

In normal circumstances, intracellular pro-oxidant agents and antioxidant stressors are in a dynamic equilibrium. However, when the host is infected with bacteria, host cells promote the synthesis of hydrogen peroxide, superoxide, and hydroxyl radicals to prevent bacterial invasion (Mates, 2000; van der Oost et al., 2003). The accumulation of pro-oxidant agents that cause oxidative damage in activated cells turns the cytoplasm into a risky location. Protein damage, oxidative degradation of lipids, DNA denaturation, apoptosis and necrosis are all outcomes of oxidative damage (Limon-Pacheco and Gonsebatt, 2009), because specialized phagocytes like macrophages can prevent pathogens from becoming viable through an oxidative burst of NADPH oxidase complexes assembled on phagocytic vesicles. Furthermore, some metals can also mediate the production of oxidative stimuli. In order to safeguard themselves from oxidative stressors and prevent essential virulent proteins from damaging, bacteria have naturally developed numerous antioxidant defense mechanisms, both enzymatic and non-enzymatic (Mates et al., 1999; Mates, 2000). As a foodborne pathogen, *L. monocytogenes* also contains several antioxidant enzymes to combat the strict conditions from both outside and inside environments of host. Superoxide dismutase (SOD) easily breaks down superoxide into peroxides, which indirectly causes the accumulation of H_2O_2 within the cell. Peroxides can be broken down by catalase (CAT) and peroxidase (PER), or the Fenton reaction with

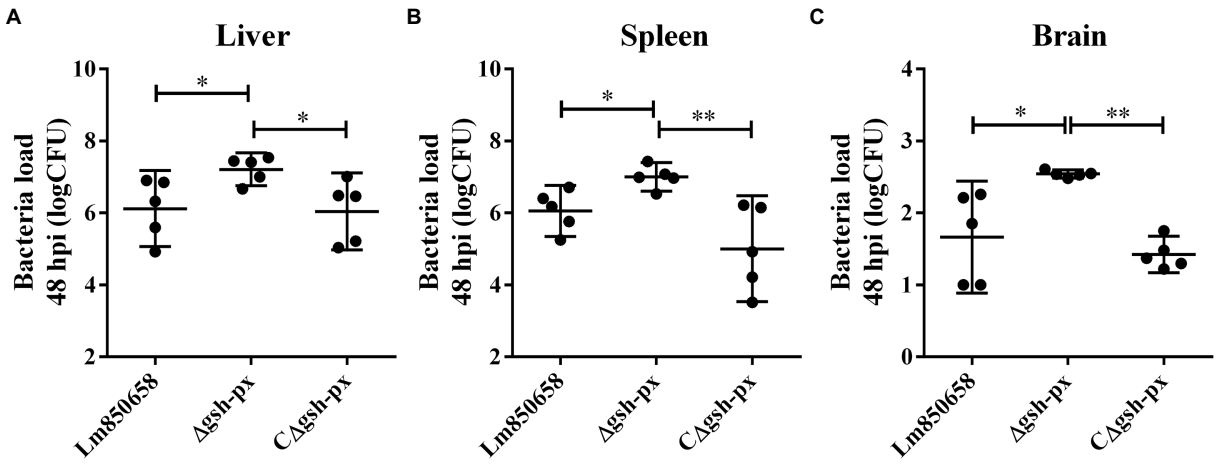

FIGURE 5
Deletion of *gsh-px* enhanced the virulence of *L. monocytogenes* to mice. Mice were infected with 10^7CFU by intraperitoneal injection with Lm850658, Δ*gsh-px* and CΔ*gsh-px*. Bacteria load in the livers **(A)**, spleens **(B)** and brains **(C)** were counted by plate counting after mice were euthanasia at 48h post infection. Data were expressed as mean±SD. ns, no significance; *, $p<0.05$; **, $p<0.01$.

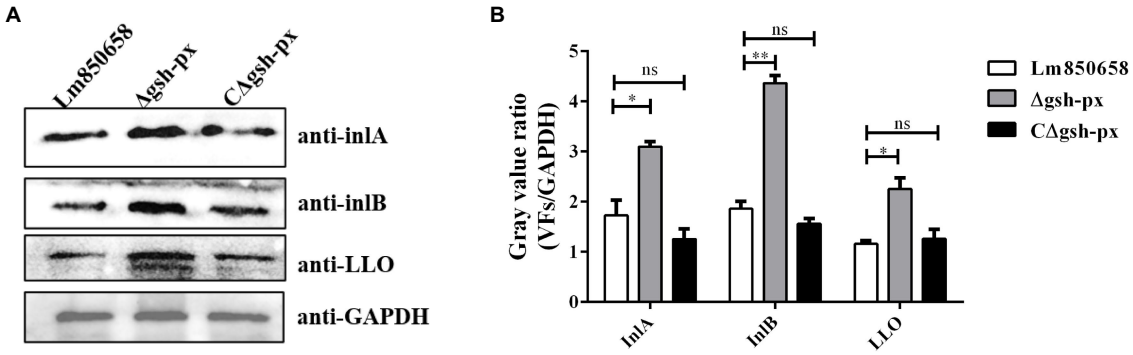

FIGURE 6
Deletion of *gsh-px* upregulated the expression of major virulence factors in *L. monocytogenes*. Overnight cultured bacteria were collected and the expression levels of the major virulence factor InlA, InlB and LLO were measured by western blot **(A)**. The gray value ratio was calculated by the band gray value of virulence factor relative to that of GAPDH **(B)**. Data were expressed as mean±SD. ns, no significance; *, $p<0.05$; **, $p<0.01$.

metal ions (Fe^{2+} and Cu^{2+}) can turn them into hydroxyl radicals (Reichmann et al., 2018). However, the products of the Fenton reaction can also damage cells, through DNA or protein repair mechanisms, this can be reduced by removing or synthesizing new substances to replace the damaged cellular components.

By using GSH as an electron donor and catalyzing the conversion of organic hydroperoxides and hydrogen peroxide to the corresponding alcohols, GSH-Pxs in eukaryotes play a crucial role in mediating antioxidant defense (Arthur, 2000). However, prokaryotic GSH-Px is poorly understood, in contrast to the extensive research on eukaryotic GSH-Px. A previous report on the *gsh-px* gene in prokaryotes, *Neisseria meningitidis*, was published (Moore and Sparling, 1995, 1996). The susceptibility of *N. meningitidis* to oxidative stress caused by the redox cyclist paraquat was increased when the *gpxA* gene was inactivated (Moore and Sparling, 1996). Eukaryotic cells lacking GSH-Px activity experienced a similar phenomenon (Arthur, 2000). With the increased knowledge of prokaryotic GSH-Px, the *btuE* gene from *E. coli* and the *gpoA* gene from *Streptococcus pyogenes* are genes encoding various bacterial GSH-Px (Aho and Kelly, 1995; Moore and Sparling, 1996; King et al., 2000; Brenot et al., 2004). In *E. coli*, GSH-Px encoded by *btuE* suggests that this enzyme reduces cell oxidative stress and prevents cells from being damaged by a variety of oxidants (Arenas et al., 2010). Increased susceptibility of eukaryotic cells to paraquat is indeed present in *N. meningitidis gpoA* deletion mutant (Brenot et al., 2005), indicating that GSH-Px does aid in oxidative stress resistance. Surprisingly, in present research the tolerance of *L. monocytogenes* to metal ion-induced oxidative stress was significantly improved when *gsh-px* was not present, suggesting that GSH-Px has a remarkable effect in *L. monocytogenes*, contrary to the classical finding that the existence of GSH-Px in *E. coli* and *N. meningitidis* contributes to the antioxidant processes. However, the *gsh-px* deletion strain in *L. monocytogenes* was not affected by H_2O_2-induced oxidative stress. This may be due to additional antioxidant enzymes like CAT and SOD are present, which are so powerful and sensitive to H_2O_2-induced oxidative stress that GSH-Px did not respond significantly to it.

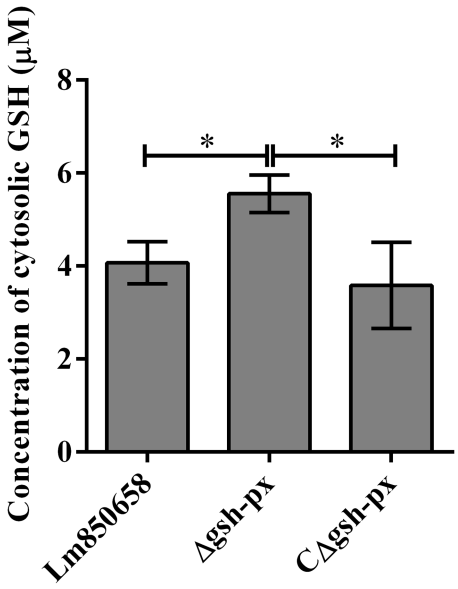

FIGURE 7
Deletion of *gsh-px* increased the glutathione levels in *L. monocytogenes*. Lm850658, Δ*gsh-px* and CΔ*gsh-px* were collected and lysed with lysozyme for 30min. The concentrations of GSH were measured with commercial kit supplied by Beyotime Biotechnology as manufacturer's instruction. The experiments were conducted for triplicate and data were expressed as mean±SD. ns, no significance; *, $p<0.05$; **, $p<0.01$.

Audrey found that knock out *gsh-px* resulted in significantly impaired virulence of *S. pyogenes* in mice subcutaneous infection model, which provided the first concrete evidence that GSH-Px contributed to the pathogenicity of bacteria (Brenot et al., 2004, 2007). In the present work, we found enhanced virulence of *L. monocytogenes* when lacking the *gsh-px* gene, together with its adhesion and invasion efficiency, which could be accomplished by binding GSH to PrfA allosterically (Wang et al., 2017). GSH is a necessary small-molecule cofactor for PrfA, which is directly charged with the transcription of 10 essential virulence factors and has an indirect impact on the expression of over 140 other genes in *L. monocytogenes*. As a result, PrfA is regarded as the regulator of the major virulence factors, including *Listeria* pathogenic island 1 (LIPI-1) and LIPI-2, which contain *plcA-prfA-hly-mpl-actA-plcB* gene cluster and *inlA-inlB* gene cluster, respectively (De Las Heras et al., 2011). Due to the possibility of ROS, RNS and RCS being present in the phagocytic vesicles, glutathione dimers to form oxidized glutathione disulfide (GSSG), which does not bind to PrfA. However, since the host cytoplasm is a highly reduced state, once *L. monocytogenes* escape into the cytoplasm, all thiols are present in reduced form and the GSH is able to bind PrfA and trigger transcription of PrfA regulatory genes (PRG). Therefore, GSH acts as an irreplaceable element in the metabolic activation of PrfA (Reniere et al., 2015; Hall et al., 2016). Deletion of *gsh-px* gene increased concentrations of GSH in the mutant, which improved the efficiency of allosteric binding of PrfA to GSH and enhanced the regulation of virulence proteins like InlA, InlB and LLO (Kim et al., 2005), increasing pathogenicity of the *gsh-px* deletion strain. Moreover, transcriptome data analysis in a study revealed that the *lmo0983* (*gsh-px*) gene was apparently down-regulated in Δ*grx* strains of *L. monocytogenes* (Sun et al., 2019). The absence of *grx* contributed to improve survival of *L. monocytogenes* when exposed to copper and cadmium ions (Sun et al., 2019), it is speculated that the resistance to oxidative stress in *L. monocytogenes* should be up-regulated when *gsh-px* was absent, which was consistent with our experimental results.

The resistance of GSH-Px to oxidative stress is linked to virulence and other bacterial species as previously mentioned. We hypothesized that increased oxidative stress resistance might be the cause of an unexpected change in the pathogenicity of *gsh-px* mutants. This prompts us to consider how GSH-Px of *L. monocytogenes* perceives and reacts to the presence of metal ions. Perhaps conformation of GSH-Px is altered or the activity of GSH-Px is changed after stimulation by metal ions, which affects the expression of GSH-Px. Figuring out the mechanisms involved is the goal of our subsequent research. In conclusion, we provided worthwhile insight into a role of GSH-Px in bacterial infections by demonstrating the *L. monocytogenes* GSH-Px acts a counter-intuitive agent in bacterial oxidative tolerance and intracellular infection.

Data availability statement

The original contributions presented in the study are included in the article/Supplementary material, further inquiries can be directed to the corresponding author.

Ethics statement

The animal study was reviewed and approved by Animal Ethics Committee of Yangtze University.

Author contributions

YZ and CF planned the experimental protocol and finished the manuscript. YZ and QG accomplished the main part of the study. XF, MY, and WH involved in the cell assay and animal assay. XL and JL participated in the gathering of experimental data. CF and YY participated in revising the manuscript. CF funded and oversaw the entire project. All authors contributed to the article and approved the submitted version.

Funding

The work was sponsored by the National Natural Science Foundation of China (31802208) and the Science and Technology Research Project of Education Department of Hubei Province (Q20221302).

Conflict of interest

The authors declare that the research was conducted in the absence of any commercial or financial relationships that could be construed as a potential conflict of interest.

Publisher's note

References

Aho, E. L., and Kelly, L. P. (1995). Identification of a glutathione peroxidase homolog in *Neisseria meningitidis*. *DNA Seq.* 6, 55–60. doi: 10.3109/10425179509074701

Anaya-Sanchez, A., Feng, Y., Berude, J. C., and Portnoy, D. A. (2021). Detoxification of methylglyoxal by the glyoxalase system is required for glutathione availability and virulence activation in listeria monocytogenes. *PLoS Pathog.* 17:e1009819. doi: 10.1371/journal.ppat.1009819

Arenas, F. A., Diaz, W. A., Leal, C. A., Perez-Donoso, J. M., Imlay, J. A., and Vasquez, C. C. (2010). The Escherichia coli btuE gene, encodes a glutathione peroxidase that is induced under oxidative stress conditions. *Biochem. Biophys. Res. Commun.* 398, 690–694. doi: 10.1016/j.bbrc.2010.07.002

Arthur, J. R. (2000). The glutathione peroxidases. *Cell. Mol. Life Sci.* 57, 1825–1835. doi: 10.1007/pl00000664

Bathige, S. D., Umasuthan, N., Godahewa, G. I., Thulasitha, W. S., Whang, I., Won, S. H., et al. (2015). Two variants of selenium-dependent glutathione peroxidase from the disk abalone *Haliotis discus discus*: molecular characterization and immune responses to bacterial and viral stresses. *Fish Shellfish Immunol.* 45, 648–655. doi: 10.1016/j.fsi.2015.05.028

Birben, E., Sahiner, U. M., Sackesen, C., Erzurum, S., and Kalayci, O. (2012). Oxidative stress and antioxidant defense. *World Allergy Organ. J.* 5, 9–19. doi: 10.1097/WOX.0b013e3182439613

Brenot, A., King, K. Y., and Caparon, M. G. (2005). The PerR regulon in peroxide resistance and virulence of streptococcus pyogenes. *Mol. Microbiol.* 55, 221–234. doi: 10.1111/j.1365-2958.2004.04370.x

Brenot, A., King, K. Y., Janowiak, B., Griffith, O., and Caparon, M. G. (2004). Contribution of glutathione peroxidase to the virulence of streptococcus pyogenes. *Infect. Immun.* 72, 408–413. doi: 10.1128/IAI.72.1.408-413.2004

Brenot, A., Weston, B. F., and Caparon, M. G. (2007). A PerR-regulated metal transporter (PmtA) is an interface between oxidative stress and metal homeostasis in streptococcus pyogenes. *Mol. Microbiol.* 63, 1185–1196. doi: 10.1111/j.1365-2958.2006.05577.x

Brigelius-Flohe, R., and Maiorino, M. (2013). Glutathione peroxidases. *Biochim. Biophys. Acta* 1830, 3289–3303. doi: 10.1016/j.bbagen.2012.11.020

Camilli, A., Tilney, L. G., and Portnoy, D. A. (1993). Dual roles of plcA in listeria monocytogenes pathogenesis. *Mol. Microbiol.* 8, 143–157. doi: 10.1111/j.1365-2958.1993.tb01211.x

Chakraborty, T., Leimeister-Wächter, M., Domann, E., Hartl, M., Goebel, W., Nichterlein, T., et al. (1992). Coordinate regulation of virulence genes in listeria monocytogenes requires the product of the prfA gene. *J. Bacteriol.* 174, 568–574. doi: 10.1128/jb.174.2.568-574.1992

Cheng, C., Dong, Z., Han, X., Wang, H., Jiang, L., Sun, J., et al. (2017a). Thioredoxin a is essential for motility and contributes to host infection of listeria monocytogenes via redox interactions. *Front. Cell. Infect. Microbiol.* 7:287. doi: 10.3389/fcimb.2017.00287

Cheng, C., Jiang, L., Ma, T., Wang, H., Han, X., Sun, J., et al. (2017b). Carboxyl-terminal residues N478 and V479 required for the Cytolytic activity of Listeriolysin O play a critical role in listeria monocytogenes pathogenicity. *Front. Immunol.* 8:1439. doi: 10.3389/fimmu.2017.01439

De Las Heras, A., Cain, R. J., Bielecka, M. K., and And Vazquez-Boland, J. A. (2011). Regulation of listeria virulence: PrfA master and commander. *Curr. Opin. Microbiol.* 14, 118–127. doi: 10.1016/j.mib.2011.01.005

Duong, C., Seow, H. J., Bozinovski, S., Crack, P. J., Anderson, G. P., and Vlahos, R. (2010). Glutathione peroxidase-1 protects against cigarette smoke-induced lung inflammation in mice. *Am. J. Physiol. Lung Cell. Mol. Physiol.* 299, L425–L433. doi: 10.1152/ajplung.00038.2010

Ezraty, B., Gennaris, A., Barras, F., and Collet, J. F. (2017). Oxidative stress, protein damage and repair in bacteria. *Nat. Rev. Microbiol.* 15, 385–396. doi: 10.1038/nrmicro.2017.26

Freitag, N. E., Port, G. C., and Miner, M. D. (2009). Listeria monocytogenes - from saprophyte to intracellular pathogen. *Nat. Rev. Microbiol.* 7, 623–628. doi: 10.1038/nrmicro2171

Hall, M., Grundstrom, C., Begum, A., Lindberg, M. J., Sauer, U. H., Almqvist, F., et al. (2016). Structural basis for glutathione-mediated activation of the virulence regulatory protein PrfA in listeria. *Proc. Natl. Acad. Sci. U. S. A.* 113, 14733–14738. doi: 10.1073/pnas.1614028114

Hedberg, C. W. (2011). Foodborne illness acquired in the United States. *Emerg. Infect. Dis.* 17:1338. doi: 10.3201/eid1707.110019

Kim, H., Marquis, H., and Boor, K. J. (2005). SigmaB contributes to listeria monocytogenes invasion by controlling expression of inlA and inlB. *Microbiology (Reading)* 151, 3215–3222. doi: 10.1099/mic.0.28070-0

King, K. Y., Horenstein, J. A., and Caparon, M. G. (2000). Aerotolerance and peroxide resistance in peroxidase and PerR mutants of streptococcus pyogenes. *J. Bacteriol.* 182, 5290–5299. doi: 10.1128/JB.182.19.5290-5299.2000

Ku, J. W., and Gan, Y. H. (2019). Modulation of bacterial virulence and fitness by host glutathione. *Curr. Opin. Microbiol.* 47, 8–13. doi: 10.1016/j.mib.2018.10.004

Kutlu, M., and Susuz, F. (2004). Biochemical properties of glutathione peroxidase in *Gammarus pulex*. *Bull. Environ. Contam. Toxicol.* 73, 432–436. doi: 10.1007/s00128-004-0447-4

Lenz, L. L., and Portnoy, D. A. (2002). Identification of a second listeria secA gene associated with protein secretion and the rough phenotype. *Mol. Microbiol.* 45, 1043–1056. doi: 10.1046/j.1365-2958.2002.03072.x

Limon-Pacheco, J., and Gonsebatt, M. E. (2009). The role of antioxidants and antioxidant-related enzymes in protective responses to environmentally induced oxidative stress. *Mutat. Res.* 674, 137–147. doi: 10.1016/j.mrgentox.2008.09.015

Mains, D. R., Eallonardo, S. J., and Freitag, N. E. (2021). Identification of listeria monocytogenes genes contributing to oxidative stress resistance under conditions relevant to host infection. *Infect. Immun.* 89:e00700. doi: 10.1128/IAI.00700-20

Margis, R., Dunand, C., Teixeira, F. K., and Margis-Pinheiro, M. (2008). Glutathione peroxidase family-an evolutionary overview. *FEBS J.* 275, 3959–3970. doi: 10.1111/j.1742-4658.2008.06542.x

Masip, L., Veeravalli, K., and Georgiou, G. (2006). The many faces of glutathione in bacteria. *Antioxid. Redox Signal.* 8, 753–762. doi: 10.1089/ars.2006.8.753

Mates, J. M. (2000). Effects of antioxidant enzymes in the molecular control of reactive oxygen species toxicology. *Toxicology* 153, 83–104. doi: 10.1016/s0300-483x(00)00306-1

Mates, J. M., Perez-Gomez, C., and Nunez de Castro, I. (1999). Antioxidant enzymes and human diseases. *Clin. Biochem.* 32, 595–603. doi: 10.1016/s0009-9120(99)00075-2

Monk, I. R., Gahan, C. G., and Hill, C. (2008). Tools for functional postgenomic analysis of listeria monocytogenes. *Appl. Environ. Microbiol.* 74, 3921–3934. doi: 10.1128/AEM.00314-08

Moore, T. D., and Sparling, P. F. (1995). Isolation and identification of a glutathione peroxidase homolog gene, gpxA, present in Neisseria meningitidis but absent in Neisseria gonorrhoeae. *Infect. Immun.* 63, 1603–1607. doi: 10.1128/iai.63.4.1603-1607.1995

Moore, T. D., and Sparling, P. F. (1996). Interruption of the gpxA gene increases the sensitivity of *Neisseria meningitidis* to paraquat. *J. Bacteriol.* 178, 4301–4305. doi: 10.1128/jb.178.14.4301-4305.1996

Newton, G. L., Arnold, K., Price, M. S., Sherrill, C., Delcardayre, S. B., Aharonowitz, Y., et al. (1996). Distribution of thiols in microorganisms: mycothiol is a major thiol in most actinomycetes. *J. Bacteriol.* 178, 1990–1995. doi: 10.1128/jb.178.7.1990-1995.1996

Reichmann, D., Voth, W., and Jakob, U. (2018). Maintaining a healthy proteome during oxidative stress. *Mol. Cell* 69, 203–213. doi: 10.1016/j.molcel.2017.12.021

Reniere, M. L., Whiteley, A. T., Hamilton, K. L., John, S. M., Lauer, P., Brennan, R. G., et al. (2015). Glutathione activates virulence gene expression of an intracellular pathogen. *Nature* 517, 170–173. doi: 10.1038/nature14029

Scortti, M., Monzo, H. J., Lacharme-Lora, L., Lewis, D. A., and Vazquez-Boland, J. A. (2007). The PrfA virulence regulon. *Microbes Infect.* 9, 1196–1207. doi: 10.1016/j.micinf.2007.05.007

Sun, J., Hang, Y., Han, Y., Zhang, X., Gan, L., Cai, C., et al. (2019). Deletion of glutaredoxin promotes oxidative tolerance and intracellular infection in listeria monocytogenes. *Virulence* 10, 910–924. doi: 10.1080/21505594.2019.1685640

Ursini, F., Maiorino, M., Brigelius-Flohe, R., Aumann, K. D., Roveri, A., Schomburg, D., et al. (1995). Diversity of glutathione peroxidases. *Methods Enzymol.* 252, 38–53. doi: 10.1016/0076-6879(95)52007-4

van der Oost, R., Beyer, J., and Vermeulen, N. P. (2003). Fish bioaccumulation and biomarkers in environmental risk assessment: a review. *Environ. Toxicol. Pharmacol.* 13, 57–149. doi: 10.1016/s1382-6689(02)00126-6

Wang, Y., Feng, H., Zhu, Y., and Gao, P. (2017). Structural insights into glutathione-mediated activation of the master regulator PrfA in listeria monocytogenes. *Protein Cell* 8, 308–312. doi: 10.1007/s13238-017-0390-x

Xayarath, B., and Freitag, N. E. (2012). Optimizing the balance between host and environmental survival skills: lessons learned from listeria monocytogenes. *Future Microbiol.* 7, 839–852. doi: 10.2217/fmb.12.57

frontiers | Frontiers in Microbiology

TYPE Original Research
PUBLISHED 06 April 2023
DOI 10.3389/fmicb.2023.1141043

OPEN ACCESS

EDITED BY
Stephen Forsythe,
Foodmicrobe.com, United Kingdom

REVIEWED BY
Abasiofiok Mark Ibekwe,
United States Department of Agriculture (USDA), United States
Zhao Chen,
University of Maryland, College Park, United States

*CORRESPONDENCE
Laurel S. Burall
✉ Laurel.Burall@fda.hhs.gov

†PRESENT ADDRESSES
Christopher Grim,
Karen Jarvis,
Office of Regulatory Science,
Center for Food Safety and Applied Nutrition,
U.S. Food and Drug Administration,
College Park, MD, United States

SPECIALTY SECTION
This article was submitted to Food Microbiology, a section of the journal Frontiers in Microbiology

RECEIVED 09 January 2023
ACCEPTED 14 March 2023
PUBLISHED 06 April 2023

CITATION
Ferguson M, Hsu C-K, Grim C, Kauffman M, Jarvis K, Pettengill JB, Babu US, Harrison LM, Li B, Hayford A, Balan KV, Freeman JP, Rajashekara G, Lipp EK, Rozier RS, Zimeri AM and Burall LS (2023) A longitudinal study to examine the influence of farming practices and environmental factors on pathogen prevalence using structural equation modeling.
Front. Microbiol. 14:1141043.
doi: 10.3389/fmicb.2023.1141043

A longitudinal study to examine the influence of farming practices and environmental factors on pathogen prevalence using structural equation modeling

Martine Ferguson[1], Chiun-Kang Hsu[2], Christopher Grim[2†], Michael Kauffman[3], Karen Jarvis[2†], James B. Pettengill[1], Uma S. Babu[2], Lisa M. Harrison[2], Baoguang Li[2], Alice Hayford[2], Kannan V. Balan[2], Josefina P. Freeman[2], Gireesh Rajashekara[3], Erin K. Lipp[4], Ralph Scott Rozier[4], Anne Marie Zimeri[4] and Laurel S. Burall[2*]

[1]Office of Analytics and Outreach, Center for Food Safety and Applied Nutrition, U.S. Food and Drug Administration, College Park, MD, United States, [2]Office of Applied Safety and Research Assessment, Center for Food Safety and Applied Nutrition, U.S. Food and Drug Administration, Laurel, MD, United States, [3]Center for Food Animal Health, The Ohio State University, Wooster, OH, United States, [4]Department of Environmental Health Science, University of Georgia, Athens, GA, United States

The contamination of fresh produce with foodborne pathogens has been an on-going concern with outbreaks linked to these commodities. Evaluation of farm practices, such as use of manure, irrigation water source, and other factors that could influence pathogen prevalence in the farming environment could lead to improved mitigation strategies to reduce the potential for contamination events. Soil, water, manure, and compost were sampled from farms in Ohio and Georgia to identify the prevalence of *Salmonella*, *Listeria monocytogenes* (*Lm*), *Campylobacter*, and Shiga-toxin-producing *Escherichia coli* (STEC), as well as *Arcobacter*, an emerging human pathogen. This study investigated agricultural practices to determine which influenced pathogen prevalence, i.e., the percent positive samples. These efforts identified a low prevalence of *Salmonella*, STEC, and *Campylobacter* in soil and water (< 10%), preventing statistical modeling of these pathogens. However, *Lm* and *Arcobacter* were found in soil (13 and 7%, respectively), manure (49 and 32%, respectively), and water samples (18 and 39%, respectively) at a comparatively higher prevalence, suggesting different dynamics are involved in their survival in the farm environment. *Lm* and *Arcobacter* prevalence data, soil chemical characteristics, as well as farm practices and weather, were analyzed using structural equation modeling to identify which factors play a role, directly or indirectly, on the prevalence of these pathogens. These analyses identified an association between pathogen prevalence and weather, as well as biological soil amendments of animal origin. Increasing air temperature increased *Arcobacter* and decreased *Lm*. *Lm* prevalence was found to be inversely correlated with the use of surface water for irrigation, despite a high *Lm* prevalence in surface water suggesting other factors may play a role. Furthermore, *Lm* prevalence increased when the microbiome's Simpson's Diversity Index decreased, which occurred as soil fertility increased, leading to an

indirect positive effect for soil fertility on *Lm* prevalence. These results suggest that pathogen, environment, and farm management practices, in addition to produce commodities, all need to be considered when developing mitigation strategies. The prevalence of *Arcobacter* and *Lm* versus the other pathogens suggests that multiple mitigation strategies may need to be employed to control these pathogens.

KEYWORDS

farm management practices, fresh produce, *Listeria*, *Salmonella*, *Campylobacter*, STEC, *Arcobacter*, structural equation modeling

1. Introduction

Foodborne illness associated with the consumption of fresh produce, particularly leafy greens, tomatoes, cantaloupes, tree fruit, and peppers, continues to be a major health concern with numerous outbreaks linked to these commodities (Iwu and Okoh, 2019). This diversity in product type suggests that common risk factors should be considered when evaluating farming practices or developing on-farm risk-mitigation approaches, not just produce-specific factors. Numerous studies have identified bacterial pathogens in agricultural environments, clearly indicating the potential for contamination of produce during cultivation and harvest (Cooley et al., 2007; Jeyaletchumi et al., 2011; Micallef et al., 2012; Strawn et al., 2013a,b; Marine et al., 2015; Belias et al., 2021). An evaluation of bacterial pathogens linked to foodborne illness, conducted by the Interagency Food Safety Analytics Collaboration (IFSAC) implicated four key bacterial pathogens, non-typhoidal *Salmonella*, *E. coli* O157, *Listeria monocytogenes (Lm)*, and *Campylobacter* spp., based on frequency and severity of illness. These findings agree with other efforts identifying these four bacterial pathogens as the primary concerns for foodborne illness (Scallan et al., 2011; IFSAC, 2018).

Non-typhoidal *Salmonella* and Shiga-toxin-producing *E. coli* (STEC) are associated with a large proportion of the burden associated with foodborne outbreaks. *Salmonella* causes an estimated one million cases and is responsible for over a third of the hospitalizations, annually (Scallan et al., 2011). Furthermore, from data derived from an active and passive surveillance study between 2000 and 2008, it was estimated that STEC cause roughly 265,000 illnesses annually in the United States (US), resulting in over 3,600 hospitalizations and 30 deaths (Scallan et al., 2011). Many serovars of non-typhoidal *Salmonella* and STEC are also enteric pathogens to a wide range of wild and domesticated animals (Hoelzer et al., 2011; Persad and LeJeune, 2015). Due to this burden, research has evaluated the potential of these pathogens to survive in manure and in the field environment (Himathongkham et al., 1999; Sharma and Reynnells, 2016; Hruby et al., 2018; Gu et al., 2019; Sharma et al., 2019). The presence of animal hosts in the pre-harvest environment and the application of manure or compost as a soil amendment may facilitate the dissemination and survival of *Salmonella*, as well as other pathogens, in soil (Shah et al., 2019; Bardsley et al., 2021).

Lm is well-characterized as a saprophytic bacterium and considered ubiquitous in soil and the environment and the causative agent of invasive listeriosis, a comparatively rare illness that causes ~19% of foodborne illness deaths (Ivanek et al., 2006; Scallan et al., 2011; Vivant et al., 2013; Iwu and Okoh, 2019). Due to its established role as a saprophytic organism, *Lm* may be better adapted to soil and soil microbiome competition than STEC and *Salmonella* (Freitag, 2009). Data have shown an association of *Lm* with wet soil environments and rain, but longitudinal studies evaluating *Lm* in agricultural fields are limited (Locatelli et al., 2013; Falardeau et al., 2018; Harrand et al., 2020). Watershed studies have also demonstrated that *Lm*, if found in water and sediment samples, could be introduced into the field environment if contaminated water is used for irrigation (Gorski et al., 2014; Stea et al., 2015). Additionally, it has been demonstrated that soil type can impact *Lm* survival and/or growth (Dowe et al., 1997; Jiang et al., 2004; Brennan et al., 2014). Furthermore, manure usage can further support *Lm* survival, depending on manure type (Dowe et al., 1997; Jiang et al., 2004; Brennan et al., 2014). These observations indicate the need for risk assessments using a variety of conditions to better understand the factors at play in *Lm* agricultural prevalence.

Campylobacter species are the leading cause of human bacterial gastroenteritis (EFSA and ECDC, 2021), and are predominantly associated with the consumption and handling of improperly cooked poultry, raw milk, and water. However, *Campylobacter* outbreaks have been associated with row crops and other produce, representing 6 and 1.7% of *Campylobacter* outbreaks, respectively (Gardner et al., 2011; IFSAC, 2018; Sher et al., 2021). Similarly, *Arcobacter* spp., which belong to the family *Campylobacteraceae* are classified as a serious hazard to human health by the International Commission on Microbiological Specifications for Foods (ICMSF) (Hoa et al., 2006; Ramees et al., 2017). Recently, *Arcobacter* prevalence was reported in fresh produce (Abay et al., 2022, Ma et al., 2022), and they are widely distributed among animals and environmental water (Collado and Figueras, 2011; Ramees et al., 2017; Niedermeyer et al., 2020). Furthermore, *Arcobacter* spp. have been associated with foodborne outbreaks (Lappi et al., 2013; EFSA and ECDC, 2021; Uljanovas et al., 2021). There are few longitudinal

Abbreviations: AT, 24 h average of air temperature; BSA, biological soil amendment; BSAAO, biological soil amendments of animal origin; CFI, comparative fit index; h, hour; DM, dairy manure; LOI, loss-on-ignition; PM, poultry manure; PR, precipitation; QLR, Quandt likelihood ratio; RMSEA, root mean square error of approximation; SDI, Simpson's diversity index; SEM, structural equation model; SR, solar radiation; VBNC, viable but non-culturable cells; WS, wind speed.

studies assessing *Campylobacter* prevalence in farm environments and in produce, and none for *Arcobacter* (Chai et al., 2009; Guevremont et al., 2017). Thus, there is limited understanding of the presence of these pathogens in the produce farm environment, and transmission to humans.

Farm practices, including irrigation, soil amendment types, pest control, and worker hygiene, have been highlighted as potential sources of pathogen introduction to the farm environment and/or produce. For example, biological soil amendments of animal origin (BSAAO) have been associated with higher risk of pathogen introduction, in particular, when not properly treated prior to use (i.e., composted), (Iwu and Okoh, 2019). In addition to the application of BSAAO to the field, dispersal of pathogen-containing fecal material in the produce preharvest environment could occur *via* surface water runoff and/or animal intrusion (Atwill et al., 2012; Pandey et al., 2014; Sharma and Reynnells, 2016; Alegbeleye and Sant'Ana, 2020). Enteric pathogens have also been detected in source water or distribution systems of irrigation water used in produce farms in multiple US coastal states (Gu et al., 2013, 2020; Draper et al., 2016; Allard et al., 2019; Weller et al., 2020).

This study evaluated pathogen prevalence and survival in the pre-harvest environment in two US geographic regions. These data provide critical information to compare and evaluate the role of soil characteristics, climate, and farm management practices on pathogen prevalence, and improve the understanding of pathogen ecology in agricultural settings. This knowledge, especially when coupled with commodity-specific risk assessments, may aid in the development of targeted mitigation strategies to enhance the microbial safety of fresh produce.

2. Materials and methods

2.1. Farm characteristics

The study was initiated in the 2018 growing season as a small pilot study to evaluate potential regional differences in pathogen prevalence, alongside evaluating the effect of some farm management practices on pathogen prevalence. In 2019, the study was expanded to include more pathogens, increased sampling, and the contribution of irrigation water sources. The study ended in 2020 due to COVID-19 restrictions preventing monthly sampling, with the heaviest restrictions coinciding with amendment application.

Farms were recruited in both Georgia (GA) and Ohio (OH) by voluntary agreement of the farmers. All farms were blinded for the purposes of this study. Four farms in GA elected to participate in 2018, two of which also participated in 2019. Two new farms participated in GA in 2019, for a total of six participating farms in GA over both years. In each year a single, but different, farm was removed from the study due to circumstances unrelated to the study. All GA farms were certified organic farms, growing mixed commodities. During the 2018 growing season, limited sampling occurred on three GA farms/fields, with samples (amendment and soil) collected pre-amendment, post-amendment, mid-season and at harvest. In 2019, to expand the study as noted earlier, fields associated with certified organic farms were selected based on amendment type (BSAAO or green compost). Green compost was a BSA of non-animal origin, e.g., plant-based. BSAAO samples included both raw and composted manure samples, which were not analyzed separately in this study due to the limited number of composted manure samples. Composite samples were collected monthly from each field, starting prior to amendment application, and continuing through harvest. GA fields were subdivided into four sections that were sampled at each site visit. Some of these sections had differing amendment types but the sections were defined by the commodity grown within each section. Each of these sections were considered separate fields in the analysis.

In OH, 18 farms, using a variety of farm management approaches, were similarly recruited with six farms for each amendment type, dairy manure (DM)-amended, poultry manure (PM)-amended, and non-BSAAO-amended. The farm management approaches in OH ranged from conventional to organic with most using a hybrid approach. None of the OH farms were certified organic. The study included fields in rotation (i.e., fields that were cultivating a crop with the intention of restoring soil health). As these fields had crops growing and were not fallow, these fields are referred to as rotating fields. The OH farms are characterized as small, ranging from 80 to 120 acres; each grew mixed commodities on a staggered schedule, and often had animals residing on the farm, including work animals, or on neighboring farms.

2.2. Metadata collection

Metadata on farm management practices were collected *via* an interview with each farmer at the end of the growing season. Observations were recorded where available but complete metadata were not always available due to differences in reporting by farmers. These metadata include the use of organic management practices, use and type of fertilizers and pesticides, presence of domestic animals, evidence of intrusion from wild animals, and other events of note.

Daily meteorological data, provided by the Ohio Agricultural Research and Development Center weather system, were obtained from a local weather station in OH, located within an ~24 km radius of all sampled fields. The data included total liquid precipitation (inches of accumulation, collected midnight to midnight, melted in case of ice or snow), average/minimum/maximum air temperature (°F, average determined with the 24 hourly readings for each day), global solar radiation measured at 6 m (Langleys units, 1 Ly = 1 cal/cm^2, sum of 5 min readings in 24 h, average/minimum/maximum soil temperature (°F, top 2 and top 4 inches) (**Supplementary Table 1**). Wind speed and relative humidity were excluded from this study due to errors in data collection.

In GA, daily meteorological data were collected from the University of Georgia Climatology Research Laboratory and included maximum rain gauge (inches), i.e., total precipitation, average air temperature (°F), average solar radiation (watts per square meter), and average 10 min wind gust (mph), i.e., wind speed (WS) (**Supplementary Table 2**). Soil temperature was not collected in GA. Solar radiation was measured differently in GA and OH. To correct for this, when comparing GA and OH weather, solar radiation data were standardized by subtracting the observed

value from the observed state mean value and then dividing by the observed state standard deviation.

2.3. Sample collection and processing

2.3.1. Biological soil amendments and manure

A single composite biological soil amendment (BSA, green compost) or BSAAO sample, consisting of 3–4 sub-samples, was taken from the compost or manure at the time of application to the field. DM, which was applied only to fields in OH, was comprised of a combination of straw/corn fodder and dairy heifer manure that had accumulated for several months, in the pen housing the animals, before being transferred to a manure spreader. Three to four sub-samples were collected from one of the manure spreaders and combined into a single composite sample for testing. PM was purchased by the farmers from a local broiler house and delivered to the farm as a pile with no covering. Time between delivery and sample collection varied from farm to farm. In the OH region, monthly DM samples were collected from farms using DM amendments to evaluate the longitudinal pathogen prevalence in the herds beyond the manure that was applied to the field. These samples were formed by combining 8–10 fresh manure pats into a composite DM sample and were often found in the housing facilities or grass pasture areas. Samples were shipped at temperatures consistent with environmental conditions to minimize changes. The received samples were aliquoted (25 g) aseptically into sterile, filter Whirl-Pak® bags and then processed for pathogen detection. The samples were tested for the presence of five pathogens, *Lm*, *Arcobacter*, *Salmonella*, STEC, and *Campylobacter*. STEC analyses were added in the 2018–2019 growing season as part of the expansion mentioned in Section "2.1 Farm characteristics."

2.3.2. Water

In OH and GA, water samples were collected in 2019 from the water source (pond, well, or creek/stream) and from the end of the drip tape. Stream water samples were collected within 3 to 4 ft from the edge of the stream and near the irrigation system's pump. Pond water samples were collected 3 to 10 ft from the shore and near the irrigation pump. Well source water samples were either sampled at the well head, directly from the pump, or after the water had travelled through an irrigation pipe from the well to the field. While all GA fields used well water for irrigation, water samples were also collected from surface water adjacent to the GA farms.

Ten liters of source water were filtered using Modified Moore Swabs (MMS) for pathogen testing including *Lm*, *Arcobacter*, *Campylobacter*, *Salmonella* and STEC, as well as for 16S rRNA gene sequencing analysis. Additionally, two liters of water samples, collected from the end of the dripline, were filtered through MMS. The MMS were maintained at refrigeration prior to pathogen testing. All MMS were then bisected using a disposable sterile scalpel to ensure open exchange during processing. The bisected MMS were transferred to sterile, filter Whirl-Pak® bags and 250 mL of sterile distilled water was added to each. The MMS were manually massaged for 15–30 s to evenly distribute the swabs within the Whirl-Pak® bags and then stomached at 300 rpm for 2 min in 30 s increments, with manual massaging between intervals to redistribute the MMS. Aliquots of 25 mL were collected from each sample, with manual agitation between samples to redistribute any sediment that had settled and processed according to the appropriate pathogen protocol.

2.3.3. Soil

In the 2017–2018 season, four composite samples were collected from each field representing pre-amendment, post amendment, mid-season, and harvest time. Preliminary analysis indicated more frequent sampling was needed. For this reason, in the 2018–2019 growing season, one composite sample was collected monthly per field in OH and GA. Each composite sample was comprised of three random sub-samplings from different locations in the field, all collected from between the rows of growing crop, which were combined as a composite sample weighing ∼2 kg. Each sub-sample entailed collection of soil from an area of 6" x 6" x 1" (width x length x depth) by spade, treated with 70% ethanol between sampling, with visible debris removed.

The soil samples were shipped and processed for pathogen detection and 16S rRNA gene sequencing analysis in the same way described above for the BSA and manure samples. A portion (∼0.5 kg) of soil samples, collected pre-amendment, post-amendment, mid-season, and at harvest, was shipped to The Maine Agricultural and Forest Experiment Station Analytical Laboratory and Maine Soil Testing Service[1] for analysis by their comprehensive soil test using the Mehlich 3 extraction method (Rutter et al., 2022). This comprehensive soil test assessed pH, total organic matter, available nitrogen (nitrate plus ammonium), phosphorus, potassium, calcium, magnesium, sulfur, boron, copper, iron, manganese, sodium, and zinc. Separately, 25 g samples were processed for pathogen detection and an additional 250 mg was used for DNA extraction for 16S rRNA sequencing gene analysis.

2.4. Pathogen detection methods

2.4.1. *Listeria monocytogenes*

Cultural enrichment and detection of *Lm* largely followed ISO 11290, with one modification (Gnanou Besse et al., 2019). Ferric citrate, which serves as a screening tool, was omitted from the medium as early testing found limited association with *Lm* presence (data not shown) (Donnelly, 2002; Leclercq, 2004; Parsons et al., 2019). Antibiotics were obtained from MilliporeSigma (Sigma-Aldrich®, St. Louis, MO). Samples were processed according to ISO 11290 with manual massage, due to the presence of rocks. Detection was performed by plating 10 μL on Rapid L'mono (RLM) agar (Bio-Rad, Hercules, CA), according to manufacturer's procedures, and then subcultured on RLM to mitigate media changes due to background flora. Presumptive *Lm* colonies were then cultured on Brain Heart Infusion (BHI) agar (Becton, Dickinson and Company, Sparks, MD) and confirmed *via* qPCR analysis (Burall et al., 2021).

2.4.2. *Arcobacter* and *Campylobacter*

Soil and manure samples were pre-enriched in 75 mL Bolton broth (ThermoFisher Scientific Oxoid limited, Hampshire, UK) containing amphotericin B (5 mg/L) in filter Whirl-Pak® bags at 37°C for 3–4 h. This was followed by enrichment of 3 mL

1 https://umaine.edu/soiltestinglab/

pre-enriched sample in 7 mL Bolton broth containing 5 mg/L amphotericin B, 20 mg/L vancomycin, 5 mg/L cefsulodin, and 10 mg/L trimethoprim for 48 h under microaerobic (MA) conditions (5% O_2, 7.6% CO_2, 7.6% H_2, 79.2% N_2). Each MMS rinsate was enriched with 25 mL 2X Bolton broth containing antibiotics (as above), under MA conditions at 37°C for 48 h.

After enrichment, samples were screened microscopically for the presence of spiral to rod or curved shaped bacteria and by PCR using *Campylobacter* (16S rRNA)- and *Arcobacter* (23S rRNA)-specific primers (Linton et al., 1996; Kim et al., 2019). Dilutions of the presumptive positive samples were inoculated (100 μL) onto 0.65 μm mixed cellulose ester filters (Hiett, 2017) placed on Brucella Blood Agar (ThermoFisher Scientific Remel, Lenexa, KS) supplemented with lysed Horse blood (Lampire biological laboratories, Pipersville, PA) for 15 min and/or streaked (20 μL) onto modified charcoal-cefoperazone-deoxycholate (mCCDA) plates. Isolated colonies were screened microscopically and confirmed by PCR.

2.4.3. *Salmonella*

Pre-enrichment of samples was conducted by resuspending each sample in a Whirl-Pak® bag with 225 mL modified buffered peptone water. Each bag was slowly swirled for 1 h in a shaking incubator at 30°C before continuing incubation at 35°C for 24 h (± 2 h). Enrichment for *Salmonella* was performed as described in the FDA Bacteriological Analytical Manual (BAM) (Andrews et al., 2022) with Rappaport-Vassiliadis (RV) medium and Tetrathionate (TT) broth, followed by isolation of black single colonies on XLT-4 agar and confirmation using the VITEK® 2 system (BioMérieux, Inc, Marcy-l'Étoile, France).

2.4.4. Isolation of STEC

Samples were pre-enriched by resuspending each sample in a filter bag with 225 mL modified buffered peptone water with pyruvate (mBPWp) and incubated at 37°C for 5 h (± 1 h). Acriflavin–Cefsulodin-Vancomycin supplement (3 mL) (Feng et al., 2020) was added and the samples were incubated at 42°C for 18 h (± 2 h). Then, two 1 mL replicate aliquots of the enrichments were collected from each sample. One was for screening for STEC by qPCR. The aliquot was centrifuged at 2,500 x g for 3 min for DNA extraction.

The other aliquot was for isolation. When tested positive by PCR, three 10 μL replicates from each culture were streaked onto ChromAgar STEC plates (CHROMagar™, Paris, France) and incubated at 37°C for 18 h. Pink colonies were selected for STEC verification. The colonies were grown in mBPWp in a 96-well plate at 37°C for 5–8 h. Half of the culture was used for DNA purification and the other half was saved as a seed culture for later use. DNA was purified and qPCR analysis was performed to detect STEC as described elsewhere (Li et al., 2017). Wells positive for STEC were tracked to the seed plate, which was used for secondary culture on CHROMagar™ STEC plates for further isolation and purification.

2.4.5. 16S rRNA gene sequencing and analysis

Water samples were centrifuged at 7,200 rpm for 30 min. Cell pellets were then resuspended in DNA/RNA Shield solution (Zymo Research, Irvine, CA) and stored before batch processing for DNA extraction. DNA was extracted from environmental samples with the ZymoBIOMICS DNA Miniprep kit (Zymo Research, Irvine, CA) utilizing the lysis bead bashing tubes and validated lysis protocols on either the FastPrep-24 5G homogenizer (MP Biomedicals, Santa Ana, CA) or a Vortex Genie with Horizontal-(24) Microtube Adaptor. 16S rRNA gene amplicon library preparation and sequencing was performed on the MiSeq benchtop sequencer (Illumina, San Diego, CA) targeting the V4 variable region of the 16S rRNA gene, following the manufacturer's recommended protocol with the modification of using Omni Klentaq polymerase (DNA Polymerase Technology, St. Louis, MO) in place of KAPA HiFi HotStart Ready Mix, as described elsewhere (Daquigan et al., 2016). The amplification primers used were 515F-Y and 926R (Parada et al., 2016). Nextera XT dual indices were used to allow multiplex sequencing using 600 cycle V3 paired-end chemistry. Each sequencing run contained 60 to 80 multiplexed libraries and estimated equimolar library pools were sequenced at 8 pM. with a 15% phiX spike-in.

Taxonomic classification of 16S V4 amplicon microbiome datasets were processed using an in-house bioinformatics pipeline written in R, Bash, and Python. Preprocessing and classification of reads were performed as follows. First, paired-end reads were merged using FLASH (Magoc and Salzberg, 2011). In cases where reads could not be merged, either due to insufficient overlapping base pairs or poor quality within the overlapping region, read 1 was retained in the dataset. This approach allowed retention of more sequencing data. Next, the paired-merged and read 1 dataset was then processed using USEARCH (Edgar, 2010; Edgar and Flyvbjerg, 2015) to perform quality filtering and prepare reads for taxonomic classification. This included using the fastx_truncate option to remove the 16S rRNA PCR primers, fastq_filter to filter based on a minimum fragment length of 150 bp and ee (expected error) value of 1.0 quality, fastx_uniques to get unique sequences per sample, and unoise3 to check for and remove chimeric sequences. The resulting datasets were then classified with MAPseq (Matias Rodrigues et al., 2017), utilizing their default curated database. Briefly, this was created using NCBI GenBank and RefSeq reference sequence databases, extracting any sequences annotated as ribosomal RNA with 16S or 18S in the annotation. The data presented in the study are deposited in the NCBI repository, accession number PRJNA894200.

2.5. Statistical methods

2.5.1. Soil amendment and water

Associations between *Lm*, *Arcobacter*, *Campylobacter*, *Salmonella*, and STEC prevalence and type of soil amendment (DM, PM, and green compost) or water source (surface, including streams and ponds, or well) were assessed using Fisher's exact test, performed in SAS 9.4 (SAS Institute, Cary, NC). Associations between pathogen prevalence and season were also assessed using Fisher's exact test. Small sample sizes prohibited multivariate modeling analyses.

2.5.2. OH soil

A structural equation model (SEM) was postulated specifying direct and/or indirect influence of local meteorological data, soil fertility data, farm management practices (soil amendment

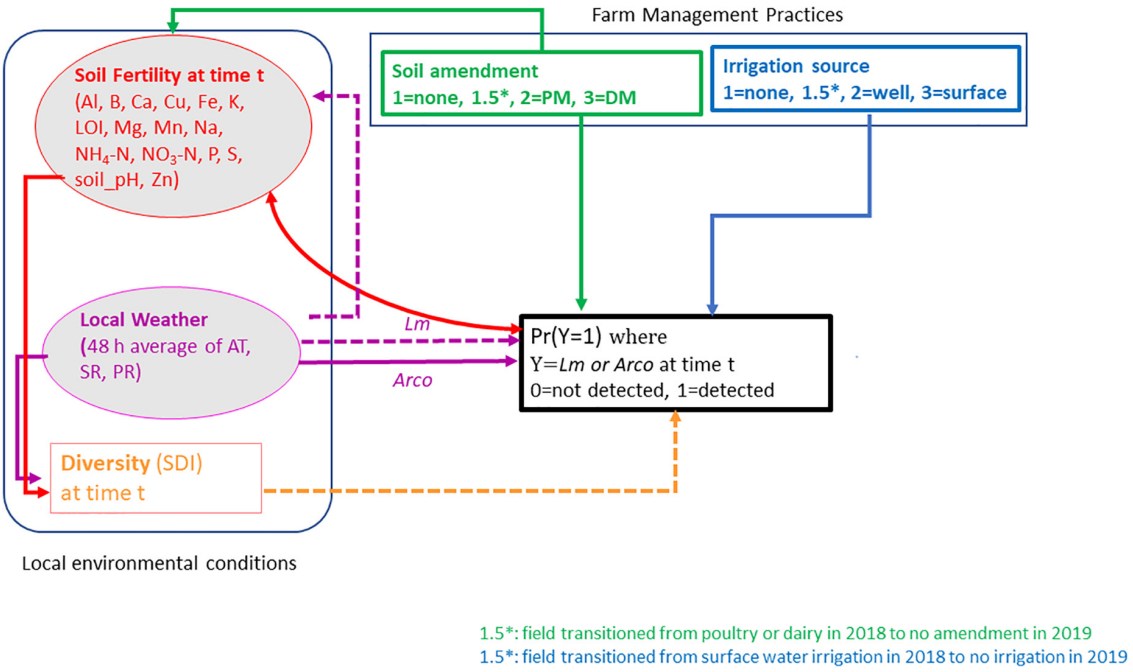

FIGURE 1
Conceptual model for *Lm* and *Arcobacter* (*Arco*) prevalence in OH soil. Square boxes are observed variables, Farm management practices (soil amendment and irrigation source) and Simpson's diversity index (SDI). Ovals are latent variables, soil fertility and local weather at time t. Arrows represent the flow of causality. Solid-line arrows indicate positive effects on the *to* variable, dash-line arrows indicate negative effects on the to variable. Double-headed curved arrows are covariances (i.e., no causality). Al, aluminum; B, boron; Ca, calcium; Cu, copper; Fe, iron; K, potassium; Mg, magnesium; Mn, manganese; Na, sodium; P, phosphorus; S, sulfur; Zn, zinc; LOI, loss-on-ignition; PM, poultry manure; DM, dairy manure; AT, air temperature; SR, solar radiation; PR, precipitation.

and source of irrigation water) and taxonomic diversity on the presence of the most prevalent pathogens, *Lm* and *Arcobacter* (**Supplementary Tables 1, 2**, and **5**). The conceptual model, evaluating OH soil data, is outlined in **Figure 1**, specifying indicators and direction of causality. There were insufficient data to inform the model for *Salmonella*, *Campylobacter*, and STEC. Soil samples that were positive for *Lm* or *Arcobacter* after culture enrichment were considered "positive." The farm management variables, soil amendment and irrigation water source, were ordinalized with increasing scores corresponding to greater observed *Lm* or *Arcobacter* prevalence. The water data were thus coded: 1 = non-irrigated, 2 = well water-irrigated, 3 = surface water-irrigated. Similarly, the manure data were coded as: 1 = no BSAAO, 2 = PM (including composted PM), and 3 = DM (including composted DM). To account for transition from soil amendment to no BSA amendment in a field from one year to another, i.e., if a field transitioned from PM or DM soil amendment in 2018 to no BSA amendment in 2019, the assigned amendment score was adjusted to 1.5 to account for possible lingering PM or DM effects. Similarly, if a field was irrigated with surface water in 2018 and then transitioned to no irrigation in 2019, that field was assigned an irrigation score of 1.5. This allowed the potential to capture carryover risk from one treatment to another during the SEM analysis.

The soil elements tested in this study were known to influence plant and microbial growth and considered indicators of soil fertility Lines-Kelly, 1992 (Gardner, 1985). These elements, in the collective, are referred to as "soil fertility" in this manuscript, despite no direct assessment of fertility *via* crop growth or yield. Soil fertility was modeled as a latent variable. Soil fertility was defined as the underlying driver of the soil chemical profile values: soil pH, phosphorus, potassium, calcium, magnesium, aluminum, manganese, boron, copper, iron, sodium, ammonium nitrogen (NH_4-N), nitrate nitrogen (NO_3-N), sulfur, zinc, and loss-on-ignition, which estimates the organic matter content of the soil. Increasing values of nutrients and soil pH were considered as indicators of increased soil fertility (i.e., positive loadings). In a secondary analysis, both nitrogen analytes (NH_4-N and NO_3-N) were analyzed separately from soil fertility to examine their relationship with *Nitrospira*, *Nitrosospira*, *Lm*, and *Arcobacter*. The relative abundance of *Nitrospira* and *Nitrosospira*, the measured values of NH_4-N and NO_3-N, and the prevalence of both *Lm* and *Arcobacter* were plotted versus time to assess if prevalence tracked synchronically or asynchronically with the nitrogen analytes and nitrifying bacteria.

Weather was incorporated in the model as a latent variable observed through precipitation (PR), air temperature (AT), and solar radiation (SR), with increasing temperature and radiation values (i.e., positive loading) and decreasing precipitation (i.e., negative loading) representing increasing "weather" across time. Minima and maxima measures were not included to avoid collinearity issues with average daily measures and to reflect the center rather than the extremes of the data. Due to the high

TABLE 1 Overall pathogen prevalence by sample type and state.

		Lm			*Salmonella*			*Campylobacter*			*Arcobacter*			STEC		
		GA	OH	Overall	GA	OH	Overall	GA	OH	Overall	GA	OH	Overall	GA	OH	Overall
Water	Positive n (%)	2 (7)	15 (22)	17 (18)	1 (4)	6 (9)	7 (7)	1 (4)	0	1 (1)	5 (22)	31 (45)	36 (39)	0	2 (3)	2 (2)
	# samples tested	26	69	95	26	69	95	23	69	92	23	69	92	26	69	95
Soil	Positive n (%)	10 (9)	45 (15)	55 (13)	0	0	0	0	0	0	1 (2)	21 (8)	22 (7)	0	1 (0.4)	1 (0.3)
	# samples tested	106	311	417	106	310	416	84	260	344	67	260	327	89	235	324
BSA	Positive n (%)	1 (6)	35 (51)	36 (42)	0	2 (3)	2 (2)	0	21 (31)	21 (24)	1 (20)	23 (34)	24 (33)	0	9 (16)	9 (15)
	# samples tested	18	69	87	18	69	87	18	68	86	5	68	73	5	57	62

BSA refers to all amendment samples, those associated with field application, as well as those not associated with field application. Positive n, the number of samples in which the pathogen indicated was detected; %, percent of samples positive for the pathogen indicated.

collinearity ($corr_{Pearson}$ = 0.93) between soil and air temperatures, soil temperature was not included.

The literature indicated a delayed, or lagged, effect of weather on *Lm* prevalence, with a peak increase in *Lm* prevalence 24 h after a rain event but rain amounts over the preceding 2 days also increased *Lm* prevalence (Weller et al., 2015a,b; Harrand et al., 2020). Based on these data, a 48 h lag was used in this study to evaluate effects linked to precipitation. The term "lag" is used to indicate the timeframe prior to sample collection. The choice of lag (or no lag) or moving average span for the remaining weather parameters was informed by (1) published results and (2) visual examination of loess-smoothed plots.

There are two main components to an SEM. The structural component quantifies potential dependencies (pathways) between the variables in the model. The measurement component quantifies how well the latent variables are represented by the observed indicators (e.g., how well is soil fertility represented by the soil measurements Al, B, Ca, . . ., Zn). A SEM must have a sound theoretical basis and is only as successful as the researcher-hypothesized *a priori* model, based on researcher knowledge and/or published results.

The hypothesized OH conceptual model, guided by observed manure and water prevalence in **Table 1** and prior research, is presented in **Figure 1**. As the SEM is a model approach driven by theory and prior research, it was postulated that the use of BSAAO, the use of surface water for irrigation, increasing soil fertility, decreasing AT and SR, increasing PR, and decreasing microbiome diversity would result in an increase in *Lm* prevalence. It was also hypothesized that the use of BSAAO, increasing soil fertility, increasing AT and SR, decreasing PR, and decreasing Simpson's Diversity Index (SDI) would result in an increase in *Arcobacter* prevalence. SDI is a measure of alpha, or within-sample, diversity which takes into account the number of species present and the relative abundance of each species (Roswell et al., 2021). In both approaches, DM was hypothesized to have a larger effect than PM. Microbiome diversity, measured as SDI, was hypothesized to increase with increasing AT, SR, and soil fertility assuming nutrients in the soil can be utilized by bacteria and plants.

Diagonally weighted least squares was implemented using the *sem* function in the R lavaan package, version 0.6.9 (Rosseel, 2012) and the probit link function, Φ () where Φ is the cumulative standard normal distribution function. The model was fit by fixing the variances of the latent variables to unity. As observed weather and soil parameters, SDI, and prevalence data were on different scales, they were standardized to the same scale.

The fit of the SEM was assessed by the Bentler Comparative Fit Index (CFI) and the root mean square error of approximation (RMSEA). Covariances between the soil or weather manifest variables, as suggested by large modification indices (MI), MI > 10 (i.e., $\chi^2_{df=1}$ p < 0.002), and fitting the model paradigm, were included in the model. The model was tuned by removing regression parameters and pathways with Wald z-test P-value > 0.15.

2.5.3. GA soil

A more parsimonious SEM was conducted to model *Lm* prevalence in GA soil samples due to insufficient soil fertility panel data. No analysis was performed for the other pathogens, due to limited soil positive samples. Furthermore, all GA fields were well-irrigated, and no GA fields were amended with DM, eliminating irrigation source as a variable and reducing the soil amendment variable to two levels, 1 = green compost, 2 = PM. The hypothesized conceptual model, used to evaluate GA soil data, is presented in **Figure 2A** with local weather incorporated, as in the OH soil model, with the addition of WS as an indicator. Decreasing AT and SR, increasing PR and WS, and the use of PM amendment were hypothesized to result in increased *Lm* prevalence, similar to the model evaluating OH data.

2.5.4. Bacterial diversity of OH soil

Metataxonomic analysis of the bacterial community was conducted on OH soil samples, targeting the V4 region of the 16S rRNA gene. Families occurring in less than five of the samples were excluded. SDI was calculated, at the family level, using the R *diversity* function in the vegan package Oksanen et al., 2019. SDI is a measure of taxonomic diversity with 1 representing maximum diversity and 0 representing no diversity. SDI was included in the *Lm* and *Arcobacter* prevalence models as the measure of microbiome diversity.

2.5.5. *Lm* and *Arcobacter* co-occurrence in OH soil

Analyses of co-occurrence with *Lm* or *Arcobacter* were conducted to assess which soil genera correlated with the presence or absence of *Lm* or *Arcobacter*. *Lm* culture positive samples that were undetected in the 16S analysis were included by setting a value at half the minimum percent hit versus those positive by

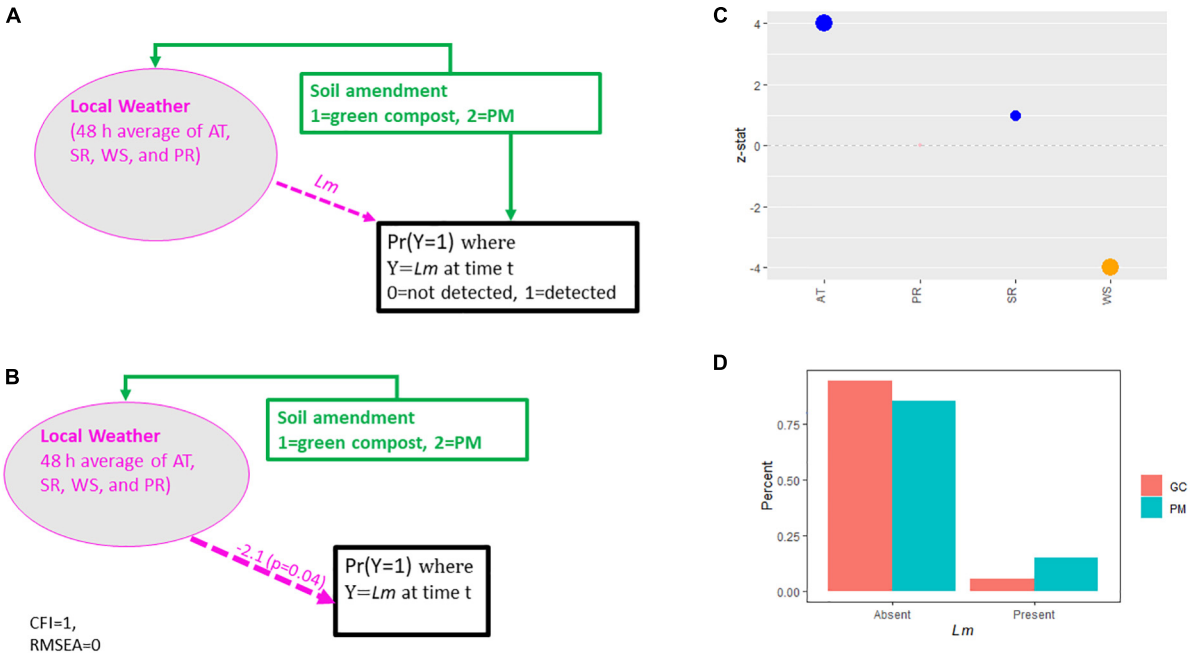

FIGURE 2
(A) Conceptual model for *Lm* prevalence in GA soil. **(B)** Final estimated model for *Lm* prevalence in GA soil. **(C)** Weather effect sizes. GC, green compost. **(D)** *Lm* prevalence in GA soil by soil amendment type. PM, poultry manure; AT, air temperature; SR, solar radiation; PR, precipitation; WS, wind speed; CFI, comparative fit index; RMSEA, root mean square error of approximation.

16S analysis. The relative abundances of genera in the *Lm*+ (or *Arcobacter*+) OH soil samples were compared to those in *Lm*- (or *Arcobacter*-) OH soil samples. Non-parametric bootstrap 95% confidence intervals (CI) were calculated for the mean relative abundance of each genus for *Lm*- (or *Arcobacter*-) samples and *Lm*+ (or *Arcobacter*+) samples. CIs were calculated using the *np.boot* function in the R nptest package Helwig, 2021.

3. Results

3.1. Amendment pathogen prevalence

Amendment samples (n = 87) were tested for the prevalence of *Salmonella*, *Arcobacter*, *Campylobacter*, STEC, and *Lm* (Supplementary Table 3). When comparing pathogen prevalence in OH and GA, all five pathogens were lower in GA amendments (0–20% positive samples) than OH (3–51% positive samples) (P-values, not significant), though this may be due to the absence of DM in GA (Table 1). *Lm*, *Salmonella*, and *Arcobacter* were detected in DM and PM samples while *Campylobacter* was only detected in DM samples (Table 2). No pathogens were detected in the green (non-animal) compost samples. The presence of *Campylobacter* and *Lm* was significantly associated with manure type ($P_{Campylobacter}$ = 0.0002, P_{Lm} < 0.0001), being most prevalent in DM samples (Table 2). To assess seasonal trends in OH, pathogen prevalence was compared across season (winter, spring, summer and fall). *Lm* (P = 0.05) and *Campylobacter* (P = 0.001) were most prevalent in the summer and *Arcobacter* (P < 0.0001) was most prevalent in the fall, followed by the summer (Figure 3). There were comparatively fewer samples analyzed for STEC, as STEC was added in the second year, and a low prevalence was observed, reducing confidence in the observed results; however, we note that STEC was only detected in DM samples and appeared most prevalent in the fall.

3.2. Pathogen prevalence in irrigation water

Water samples (n = 95) were tested for pathogen prevalence (Table 1, Supplementary Table 4). Thirty-nine samples (n_{OH} = 31; n_{GA} = 8) were collected from the end of the dripline, and 56 samples (n_{GA} = 18, n_{OH} = 38) were collected from the water source. *Lm* and *Arcobacter* were by far the most frequently detected pathogens. Comparisons of pathogen prevalence of GA and OH water samples, using Fisher's exact test, found that *Arcobacter* was more prevalent in water from OH than GA (P = 0.05). However, no significant regional differences in prevalence for *Lm*, *Salmonella*, *Campylobacter*, and STEC were observed for water samples (Table 1).

Arcobacter was detected in both surface and well source water, with a higher prevalence in surface water ($P_{Overall}$ < 0.0001, P_{OH} = 0.05), whereas *Lm*, *Salmonella*, *Campylobacter*, and STEC were detected only in surface water (pond or stream) (Table 2). *Campylobacter* and STEC were only detected in source samples whereas *Lm*, *Salmonella* and *Arcobacter* were detected in both source and dripline samples (Table 2).

To assess seasonal trends, pathogen prevalence in OH surface water was compared across seasons (spring, fall, or summer). *Lm* was significantly more prevalent in the summer OH water samples (P = 0.02; Figure 3). Some of the subgroups within Figure 3

10.3389/fmicb.2023.1141043

TABLE 2 Pathogen prevalence by sample type and subtype.

		Positive n (%)						Positive n (%)				
		Lm	*Salm.*	*Campy.*	*Arco.*	STEC		*Lm*	*Salm.*	*Campy.*	*Arco.*	STEC
Water type (# tested)	All surface* (66)	17 (26)	7 (11)	1 (2)	34 (52)	2 (3)	Drip	7 (18)	1 (3)	0	14 (39)	0
	OH surface only (57)	15 (26)	6 (11)	0	29 (51)	2 (4)						
	All well (29)	0	0	0	2 (8)	0	Source	10 (18)	6 (11)	1 (2)	22 (39)	2 (4)
	OH well only (12)	0	0	0	2 (17)	0						
Soil by amendment or irrigation practice (# tested)	GA no BSA (20)	0	0	0	0	0	Non-irrigated					
	GA poultry-amended (52)	7 (14)	0	0	1 (3)	0	Well-irrigated (108)	10 (9)	0	0	1 (1.5)	0
	GA GC-amended (36)	3 (8.5)	0	0	0	0	Surface-irrigated					
	OH dairy-amended (103)	19 (18)	0	0	10 (11)	1 (1)	Non-irrigated (94)	18 (19)	0	0	7 (10)	1 (1)
	OH poultry-amended (94)	18 (19)	0	0	7 (8)	0	Well-irrigated (125)	14 (11)	0	0	6 (6)	0
	OH no BSA (114)	8 (7)	0	0	4 (4)	0	Surface-irrigated (92)	13 (14)	0	0	8 (10)	0
Amendment (# tested)	Green compost (13)	0	0	0	0	0						
	PM or poultry compost (17)	2 (12)	1 (6)	0	2 (13)	0						
	DM or dairy compost (57)	34 (60)	1 (2)	21 (38)	22 (39)	9 (18)						

All, includes samples from OH and GA; *, stream and pond. *Salm.*, *Salmonella*; *Campy.*, *Campylobacter*; *Arco.*, *Arcobacter*; # tested, the number of samples tested; Dairy-amended, soils amended with BSA of dairy origin; Poultry-amended, soils amended with BSA of poultry origin; GC-amended, soils amended with green compost (GC).

had sample sizes too small for any conclusions to be drawn and are considered observational. No significant seasonal trend was observed for the other pathogens, either due to the absence of a significant difference or the dataset's size preventing statistical analysis.

3.3. Soil pathogen prevalence

OH soil samples were tested for *Salmonella* (n = 310), *Campylobacter* (n = 260), STEC (n = 235), *Lm* (n = 311), and *Arcobacter* (n = 260; Table 1). These samples were collected from 21 farms/fields in 2018 and 29 farms/fields in 2019, for a total of 29 different farms/fields across both years with 20 of them sampled in both years. All OH soil samples were negative for *Salmonella* and *Campylobacter*, and only one was positive for STEC. Given the low yield for those three pathogens, prevalence analyses focused on *Lm* and *Arcobacter*. There were 154 (for *Lm*) and 144 (for *Arcobacter*) complete cases, i.e., samples which had complete data on soil fertility, weather, farm management data, and metagenomic to model the pathogen prevalence. Rotating fields (n_{OH} = 13) were included in the analysis as non-amended fields (SA = 1) or previously amended fields (SA = 1.5) unless amendment was applied to the rotating field (n = 3, DM-amended). Fifteen percent of OH soil samples tested positive for *Lm* and 8% tested positive for *Arcobacter* (Table 1). However, when limited to the 154 (*Lm*) OH soil samples with complete data, 26 (20%) samples tested positive for *Lm*. Likewise, limiting the analysis to the 144 (*Arcobacter*) OH soil samples with complete data, 12 (8%) samples tested positive for *Arcobacter*.

Among the GA soil samples, 106 were tested for *Lm* and *Salmonella*, 89 for STEC, 84 for *Campylobacter*, and 67 for *Arcobacter* (Table 1). While no GA soil samples tested positive for *Salmonella*, *Campylobacter*, or STEC, one (2%) tested positive for *Arcobacter* and ten (9%) tested positive for *Lm*. Of the 10 *Lm*+ GA soil samples, seven were from PM-amended fields (14% of PM-amended fields) and 3 were from green compost-amended fields (6% of green compost-amended fields), indicating increased *Lm* prevalence in GA PM-amended fields versus green compost-amended fields (Table 2). There were 99 complete GA soil cases to model *Lm* prevalence.

Lm and *Arcobacter* prevalence of GA and OH soil samples were compared using Fisher's exact test. *Arcobacter* was more prevalent in OH soil than GA soil (P = 0.06), while no differences were observed in *Lm* soil prevalence between the two regions.

Trends of OH soil *Lm* and *Arcobacter* prevalence and GA *Lm* prevalence versus weather were explored, with weather parameters observed at various hours (24, 48, 72, 96, and 120 h) prior to the day of soil collection or averaged across various moving averages (spanning 48, 72, 96, and 120 h) (data not shown). PR averaged over the 48 h prior to and including the day of soil collection correlated most closely with *Lm* prevalence in GA and OH soil and inversely correlated with *Arcobacter* prevalence in OH soil. AT and SR, also averaged over 48 h, inversely correlated with *Lm* prevalence in OH and GA soil and directly correlated with *Arcobacter* prevalence in OH soil. These findings largely agreed with prior literature results for *Lm* (Strawn et al., 2013a,b; Weller et al., 2015a; Harrand et al., 2020). WS averaged over the 48 h prior to and including the day

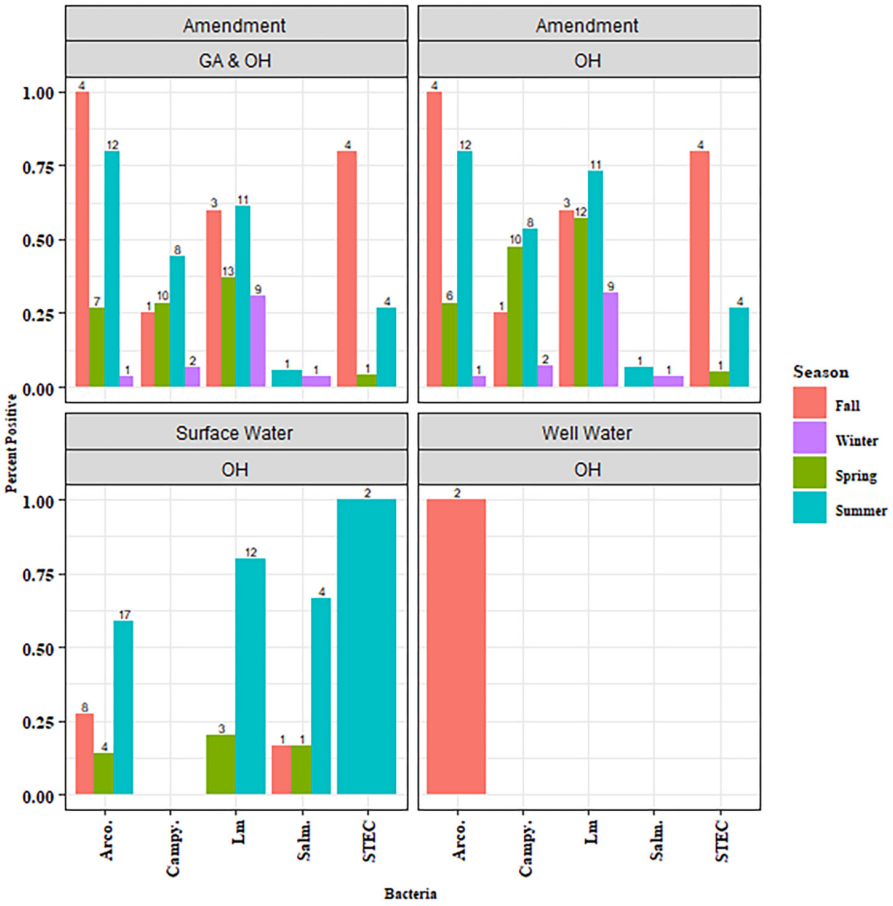

FIGURE 3
Pathogen prevalence in amendment and water samples by season. Amendment includes the actual BSA applied to fields as well as dairy manure samples that were not associated with field application. Data is plotted to show the percent of the samples tested that were positive for the indicated pathogen evaluated within each season.

of soil collection was observed to correlate most closely with *Lm* prevalence in GA soil.

3.3.1. Effects of environmental conditions on *Lm* and *Arcobacter* prevalence

Most soil characteristics analyzed in OH soil samples were good indicators of soil fertility, as defined in the methods, i.e., had large effect sizes (large, standardized regression coefficients), with the exceptions of Ca, Na, and S. Soil characteristics with larger size effects were considered as good indicators of soil fertility. All indicators had positive loadings, i.e., increasing values indicated increasing "fertility," except for NO_3-N and S, which had negative loadings, i.e., increasing NO_3-N and S indicated decreasing fertility (Figure 4).

The strongest indicators of local weather's ability to predict *Lm* and *Arcobacter* prevalence in OH soil were AT and SR (Figures 4C, D), which is expected given seasonal patterns associated with changes in temperature due to increased solar radiation. AT and WS were significant indicators in predicting *Lm* prevalence in GA soil but SR and soil amendments were not (Figure 2). *Lm* prevalence in GA soil was directly impacted by weather ($P_{GA} = 0.04$; Figure 2B) and, in OH, the impact of weather on soil *Lm* prevalence was mediated by soil fertility, with decreasing fertility correlating with decreasing *Lm* prevalence ($P = 0.05$; Figure 5). Observed *Lm* prevalence was highest during the coolest part of the year, winter and spring (Figure 6A and Supplementary Figure 1). *Arcobacter* prevalence in OH soil was directly impacted by weather ($P = 0.04$; Figure 5) but in an opposite direction, with observed *Arcobacter* prevalence highest during the warmest part of the year (summer and fall) (Figure 6A). The observed effect of PR was not nearly as prominent as AT or SR in OH or GA (effect $size_{Lm,} = 0$ in GA, effect $size_{Lm,} = -1$ and effect $size_{Arcobacter} = -2$ in OH).

OH soil fertility itself was significantly impacted by both soil amendment ($P_{Lm} = 0.02$, $P_{Arcobacter} = 0.01$) and local weather ($P_{Lm} < 0.0001$, $P_{Arcobacter} = 0.003$; Figure 5). Soil fertility was highest when a DM-BSAAO was used, followed by PM-BSAAO. Increasing AT and SR and, to a lesser extent, decreasing PR were correlated with decreasing soil fertility in the summer. Soil fertility was highest in winter when AT was low and PR was largely in the form of snow and ice. Altogether, these factors contributed to improved soil fertility in the winter. AT and SR had a more pronounced effect on soil fertility than PR (Figure 4C and D). Soil fertility had a correlative effect on *Lm* but not *Arcobacter* prevalence, but had a direct effect on diversity ($P_{Lm} = 0.005$; Figure 5) in OH, where diversity decreased as soil fertility increased. Decreasing diversity, in turn, was correlated with higher

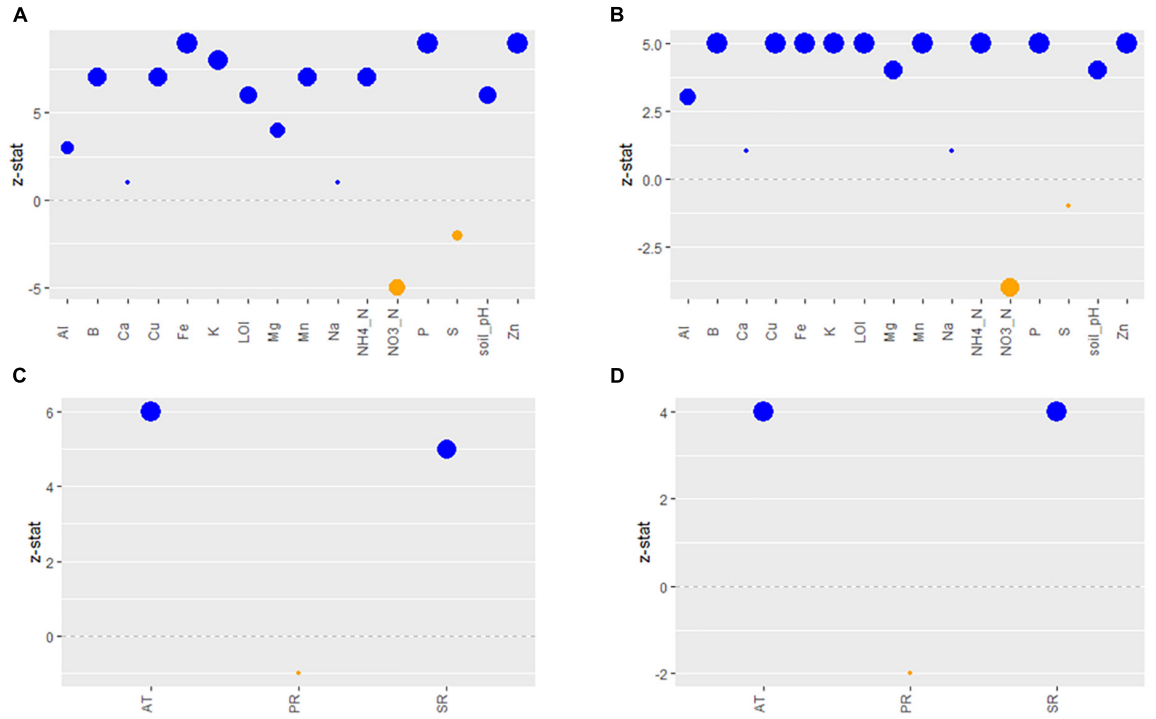

FIGURE 4
Effect sizes (z-statistic) of the observed soil chemistry variables composing the predicted (standardized) soil fertility latent variable for the *Lm* **(A)** and *Arcobacter* **(B)** models. Effect sizes (z-statistic) of the observed weather variables composing the predicted (standardized) Weather latent variable for the *Lm* **(C)** and *Arcobacter* **(D)** models. Blue dots are positive effect sizes and orange dots are negative effect sizes. The larger the dot, the larger the effect size, i.e., the more important the indicator. Al, aluminum; B, boron; Ca, calcium; Cu, copper; Fe, iron; K, potassium; Mg, magnesium; Mn, manganese; Na, sodium; P, phosphorus; S, sulfur; Zn, zinc; LOI, loss-on-ignition; AT, 24 h average of air temperature; PR, precipitation; SR, solar radiation.

Lm prevalence ($P = 0.02$), indicating an indirect effect of soil fertility on *Lm* prevalence. These results were in line with the expected results, suggesting the observations that informed the model overall were likely consistent with environmental factors.

While the role of plant nitrogen utilization could not be properly evaluated in this study, some intriguing patterns were observed between the levels of ammonium and nitrate, local weather, and soil amendment in OH with *Lm* showing an increased prevalence late in the year in PM-amended fields compared to DM- and non-BSAAO-amended fields (Figure 7). Evaluation of the presence of *Nitrospira* and *Nitrosospira*, along with *Lm* prevalence, nitrate levels, and ammonium levels, showed a potential relationship between these factors, possibly initiated by the large increase in ammonium levels observed only in PM-amended fields (Figure 7). Two genera associated with nitrification are *Nitrospira* and *Nitrosospira* (Daims, 2014). Their role in nitrogen processing may be affected by the nitrogen source provided based on the use of DM or PM, the latter with a higher content of ammonium Herbert et al.,[2] and could explain the observed inverse relationship between the levels of ammonium (high to low) and nitrate (low to high) during the growing season in OH (Figure 7). PM, rich in urea and uric acids, was shown to boost ammonium levels, as expected, when (Figure 7). In these fields, an increase in *Lm* prevalence was observed late in the year, but not in non-BSAAO-amended fields, and was lower in DM-amended fields (Figures 6B, 7). Additionally, there are marked differences between these field groups when evaluating the relative abundance of *Nitrospira* and *Nitrosospira*.

To concentrate on regional differences in *Lm* soil prevalence, possibly due to different weather patterns, the GA and OH weather was compared. The AT and SR values for GA and OH (Figure 8A), and PR data for OH (Figure 8B) were cross-plotted. PR trends were similar cross year (2018, 2019) and were analogous cross both states (GA, OH). The SR trends were also similar cross year (2018, 2019) but the GA SR peaked around May, about two months before the OH SR peaked, around July. To ascertain when the prevalence of *Lm* in soil first significantly decreased, a structural change analysis was conducted. The mean monthly *Lm* prevalence in OH soil was calculated, over both years aggregated. Unlike OH, where soil was sampled throughout the year, the soil in GA was only sampled March through October, due to different amendment application times, resulting in insufficient longitudinal samples to conduct a structural change analysis in GA as mentioned earlier for other analyses.

The Quandt Likelihood Ratio (QLR) statistic (Quandt, 1960) was used to detect the presence of structural breaks in the OH data and was calculated using the *Fstats* function in the strucchange R package (Zeileis et al., 2002, 2003). To determine when the structural break(s) occurred, the *breakpoints* function in the same

2 Herbert, S., Hashemi, M., Chickering-Sears, C., Weis, S. M., Carlevale, J., Campbell-Nelson, K., et al. Conserving Ammonia in Manure. UMass Extension Crops, Dairy, Livestock and Equine Program. Available online at: https://ag.umass.edu/crops-dairylivestock-equine/fact-sheets/conserving-ammonia-in-manure

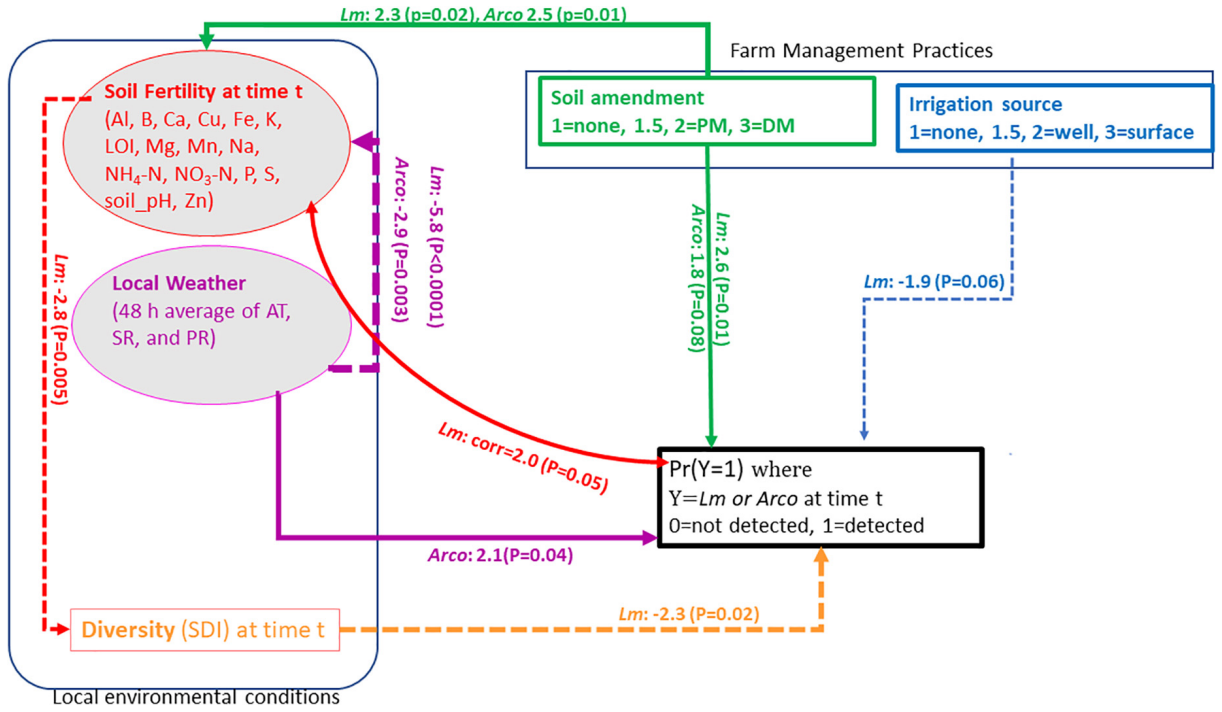

FIGURE 5
Final (parsimonious) model for OH soil *Lm* and *Arcobacter* (*Arco*) prevalence. Numbers on single-headed arrows are the standardized regression path estimates (*z*-statistic) and *p*-values (in parentheses). The thickness of the arrow reflects the strength of the relationship, with solid-line arrows indicating positive relationships and dash-line arrows indicating negative relationships. For plot simplicity, the soil nutrient covariances are provided in **Supplementary Figure 2**. Al, aluminum; B, boron; Ca, calcium; Cu, copper; Fe, iron; K, potassium; Mg, magnesium; Mn, manganese; Na, sodium; P, phosphorus; S, sulfur; Zn, zinc; LOI, loss-on-ignition; PM, poultry manure; DM, dairy manure; AT, air temperature; SR, solar radiation; PR, precipitation; SDI, Simpson's diversity index.

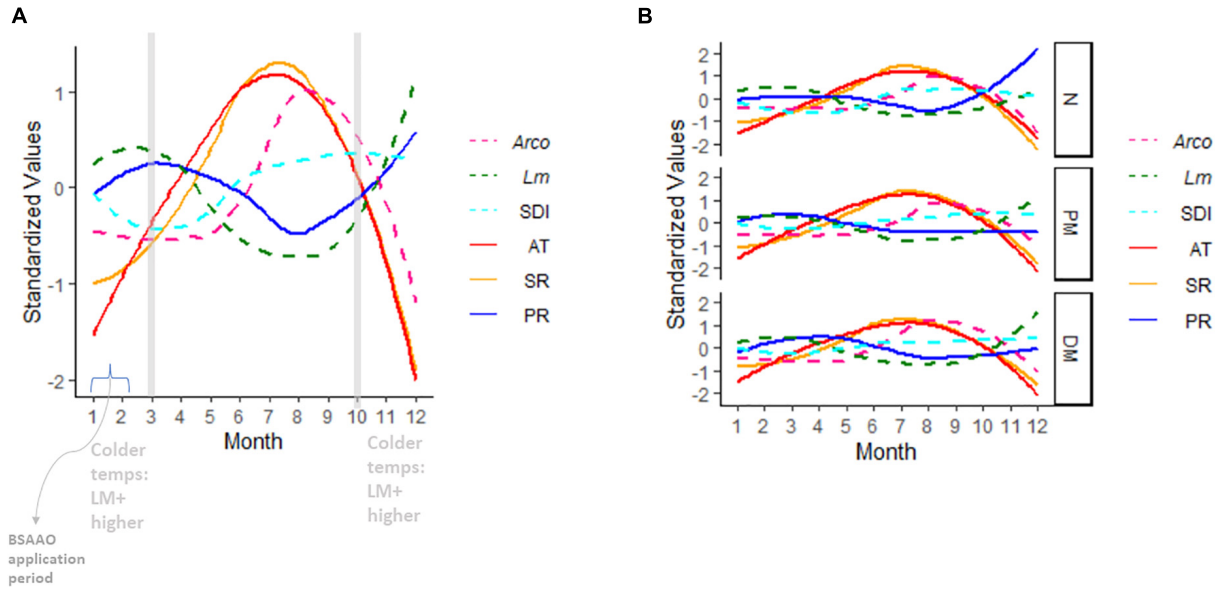

FIGURE 6
Seasonal trends in OH air temperature (AT), precipitation (PR), and solar radiation (SR). Overlaid are *Lm* soil prevalence, *Arcobacter* (*Arco*) prevalence, and Simpson's diversity index (SDI) in OH soil. AT, PR, and SR are 48 h moving averages. All variables are standardized to the same scale using the R standardize function in the robustHD package (Alfons, 2019). Soil amendment groups are aggregated in **(A)** and grouped in **(B)**. BSA, biological soil amendment; BSAAO, biological soil amendments of animal origin; PM, poultry manure; DM, dairy manure; N, not amended with BSA or BSAAO; AT, 24 h average of air temperature; SR, solar radiation; PR, precipitation; SDI, Simpson's diversity index.

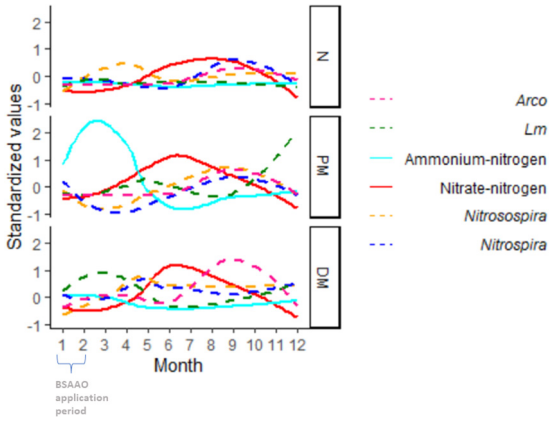

FIGURE 7
Seasonal Trends in *Lm* and *Arcobacter* (*Arco*) prevalence, *Nitrosospira* relative abundance, *Nitrospira* relative abundance, ammonium-nitrogen and nitrate-nitrogen levels in Ohio soil, grouped by soil amendment. All variables are standardized to the same scale using the R standardize function in the robustHD package. BSA, biological soil amendment; BSAAO, biological soil amendments of animal origin; PM, poultry manure; DM, dairy manure; N, not amended with BSA or BSAAO.

R package was used. The QLR tests detects structural changes of a regression of the *Lm* soil prevalence at month j regressed on the previous month's (month j-1) prevalence, i.e., detects month-to-month prevalence changes. Only one structural break in OH was detected in March (P_{QLR} = 0.05) and is evident in Figure 6A.

3.3.2. *Listeria monocytogenes* and *Arcobacter*

The final parsimonious *Lm* and *Arcobacter* model for OH revealed a causality effect associated with the type of soil amendment (P_{Lm} = 0.01, $P_{Arcobacter}$ = 0.08) with prevalence highest for DM-amended fields (Figures 5, 9). Although the direct effect of soil amendment on *Lm* prevalence in GA was not significant, the observed *Lm* prevalence in PM-amended fields was marginally higher than for green compost-amended fields. A causal effect of irrigation source in OH (P = 0.06) on *Lm* prevalence was observed with prevalence highest for non-irrigated OH fields (Figures 5, 9A). Although, in OH, surface water samples presented the highest observed *Lm* prevalence and well water samples presented zero observed *Lm* prevalence (Table 2), soil samples from surface water-irrigated fields had similar *Lm* prevalence to well-irrigated fields, while the soil samples from non-irrigated fields had the highest *Lm* prevalence (Figure 9A). Since the decision regarding whether to irrigate may be influenced by known on-farm risk factors, such as resident animals, amendment practices were evaluated to determine if they might influence irrigation practices. When evaluating whether amendment choice might correlate with irrigation choice, it was found that: PM-amended fields were equally likely to be irrigated with surface or well water; DM-amended fields were more likely to be irrigated with well water; and non-amended fields were more likely to not be irrigated.

3.3.3. Diversity of bacterial community in soil

Metataxonomic sequence analysis was performed for 305 of the 311 OH soil samples. For purposes of informing the model, samples that were positive for *Lm* after enrichment (culture positive) were considered positive for *Lm*, even if the culture-independent sequencing results did not indicate the presence of *Lm*. In fact, an evaluation of the sensitivity of microbiome metataxonomics when detecting *Lm* in soil samples, only two OH soil samples were found to contain *Lm* by 16S rRNA sequencing analysis whereas 45 OH soil samples were culture-positive for *Lm*. Additionally, the two samples from which *Lm* levels were detected by metataxonomics, were culture-negative for *Lm*. These data highlight the need for culture enrichment of foodborne pathogens from environmental samples. Furthermore, the two samples which were *Lm* culture-negative but contained detectable levels of *Lm* in the metataxonomic analysis were included as *Lm*-containing samples in the analysis. The detection of *Arcobacter* using metataxonomics was also incongruous with culture results. Four OH soil samples had levels of *Arcobacter* detected by metataxonomics, three of which were culture-negative for *Arcobacter* and one of which was not cultured for *Arcobacter*.

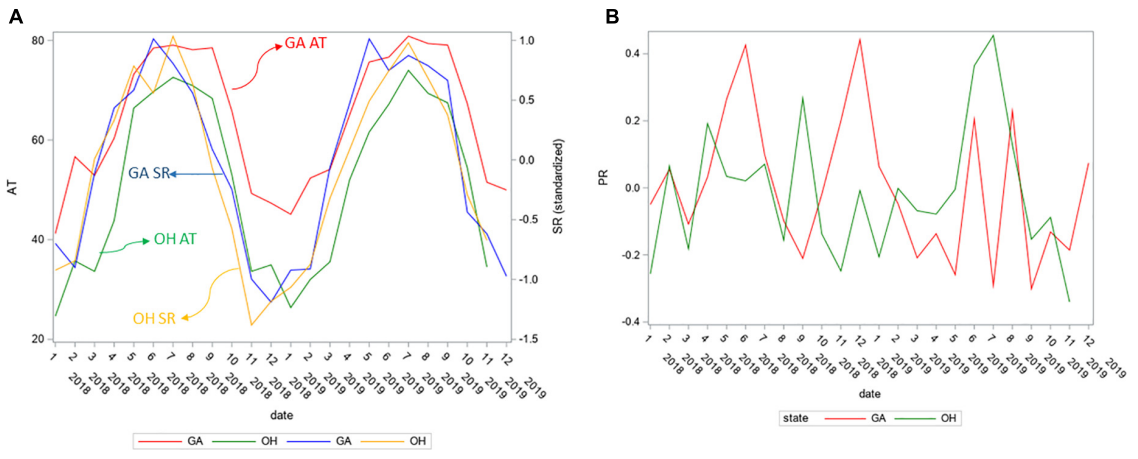

FIGURE 8
(A) GA and OH monthly average air temperature (AT) and average solar radiation (SR) for study years 2018 and 2019. **(B)** GA and OH monthly average precipitation (PR) for study years 2018 and 2019. SR and PR were standardized to the same scale as they were measured differently in GA and OH.

10.3389/fmicb.2023.1141043

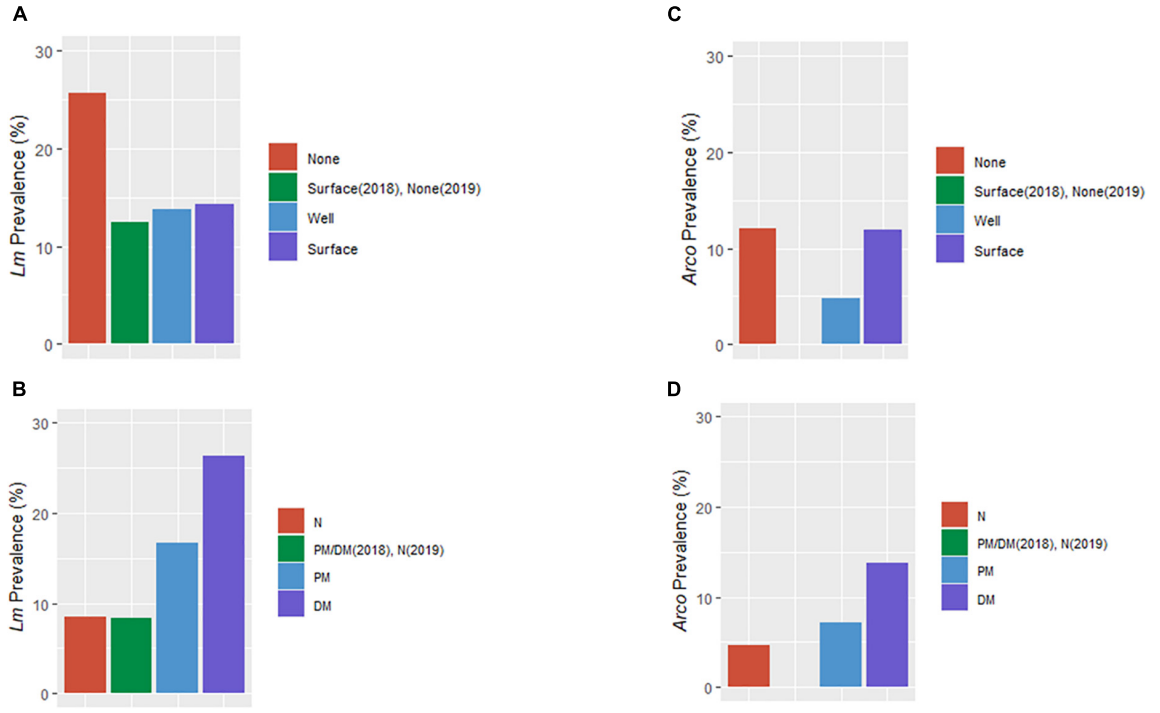

FIGURE 9
Distribution of *Lm* and *Arcobacter* (*Arco*) prevalence in OH soil by irrigation source **(A,C)** and soil amendment **(B,D)**. BSA, biological soil amendment; BSAAO, biological soil amendments of animal origin; None, no irrigation of the field; Surface, irrigation performed with surface water; Well, irrigation *via* well water; N, not amended with BSA or BSAAO; PM, poultry manure; DM, dairy manure.

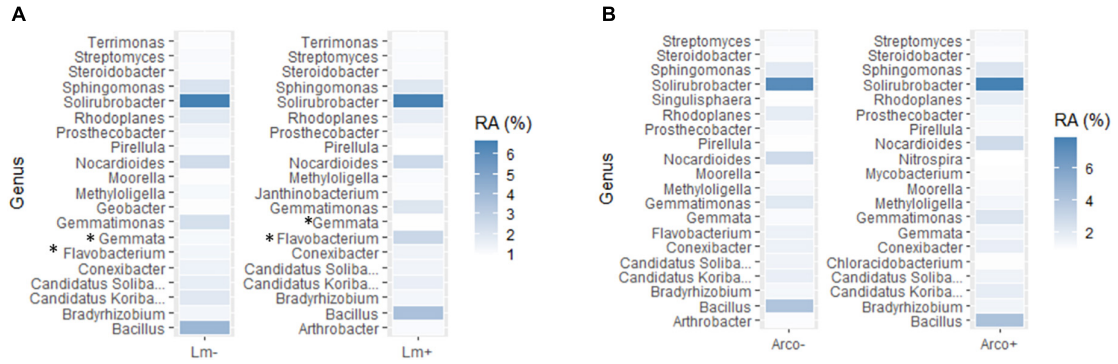

FIGURE 10
(A) Top (most abundant) twenty genera detected (16S) in *Lm* negative (−) samples vs. top 20 genera detected in *Lm* positive (+) samples in OH soil. **(B)** Top twenty genera detected in *Arcobacter* negative (−) samples vs. top 20 genera detected in *Arcobacter* positive (+) samples in OH soil. The darker the color, the more abundant the genus, i.e., the higher the relative abundance (%). An asterisk (*) denotes genera with significantly different mean relative abundance between positive and negative samples. RA, mean relative abundance.

Of the 21 OH soil samples, which were culture-positive for *Arcobacter*, none had levels of *Arcobacter* detected by 16S rRNA gene amplicon sequencing. These 21 samples were included in the analysis as containing *Arcobacter* and the *Arcobacter* relative abundance (percent hit) was set to half the minimum relative abundance of the four *Arcobacter* containing metataxonomic samples, 0.002.

Diversity of the microbiome was calculated at the family level with the SDI ranging from 0.89 to 0.98. The type of soil amendment did not appear to influence bacterial diversity (Figure 6B). Although weather did not have a direct impact on bacterial diversity, diversity was visibly lower in the winter through spring, reaching its nadir in April/May (Figure 6A). This observation indicated that April/May represented an inflection point in bacterial diversity, perhaps due to increased temperatures that were disadvantageous for cold-adapted bacteria, while growth of more warm-adapted microorganisms had not yet occurred to levels detectable by metataxonomics. Diversity increased significantly with decreasing soil fertility in the *Lm* model (P_{Lm} = 0.005; Figure 5). As previously mentioned, fertility decreased with increasing AT and SR; as such, the effect of weather on diversity appeared mediated through soil fertility.

3.3.4. Co-occurrence in OH soil

The top twenty most abundant genera in *Lm* and *Arcobacter* negative (–) samples were compared to the top twenty most abundant genera detected in *Lm* and *Arcobacter* positive (+) samples (**Figure 10**). In general, the top twenty genera are similarly abundant in positive and negative samples for *Lm* and *Arcobacter* (**Figure 10**) with two exceptions, mentioned below. As such, the profiles of dominant genera in soil appeared similar and their influence on pathogen prevalence did not appear substantial. The relative abundances of *Flavobacterium* and *Gemmata*, however, were significantly different (i.e., non-overlapping 95% CI, **Table 3**) between *Lm*+ and *Lm*-samples, with the former more abundant in *Lm*+ samples and the latter more abundant in *Lm*- samples. Regarding the genera with significantly different mean relative abundances between pathogen negative and positive samples in the *Arcobacter* co-occurrence analysis, the mean relative abundances (**Figure 11A**) were much lower (max∼0.5) than the mean relative abundances for *Lm* co-occurrence analysis (**Figure 11B**), max = 2.5); this signifies that for *Arcobacter* the genera differences observed between positive and negative samples were generated by genera that represented a smaller proportion of the soil microbiome than those genera associated with *Lm* presence or absence.

4. Discussion

4.1. Pathogen prevalence in dairy manure

While green compost, PM, and DM were evaluated in this study, there was a higher prevalence of the evaluated pathogens in DM. Additionally, as green compost and PM were only collected around the time of application, analysis of seasonality trends was not possible. However, due to the collection of DM throughout the growing season, it was possible to determine the prevalence data for *Arcobacter* and *Lm* and evaluate potential patterns associated with season, leading to a possible explanation for the observed pattern. In the spring and summer, dairy herds associated with this study shifted to grazing in pastures around the farm. A similar shift likely occurred at other farms in the region. As a result, there was likely increased interaction of cattle with surface water that could lead to transmission of *Lm* to or from neighboring animals. This exposure could be by drinking contaminated surface water, which could occur independent of pasture access, as well as by the animals entering surface water that cross through the pasture, transmitting pathogens to and from pastures. This increased potential for exposure and transmission could explain the observed increase in *Lm* prevalence in OH DM in the spring that continued through the fall but declined in the winter (**Figure 3**) when herds were generally kept within barns, which could potentially reduce direct interaction with surface water. However, the possibility remains that dietary shifts associated with these seasonal shifts could be affecting *Lm* prevalence in DM as well. Although *Lm* DM prevalence was lowest in the winter, the regional herd, encompassing all cattle evaluated for *Lm via* manure testing, carried some level of *Lm* year-round. This presence of *Lm* in some cattle within the region would provide an opportunity for re-introduction of *Lm* to the agricultural region in the spring. Higher *Lm* prevalence in DM and surface water (**Figure 3**) samples during the summer was not observed in OH soil (**Figure 6A**). Soil *Lm* prevalence, instead, was higher in the spring than the summer. This reduced prevalence could be due to reduced runoff in the summer as precipitation was lowest in the summer and/or increased competition with other soil organisms in the warmer months. Similarly, *Arcobacter* prevalence in DM was much higher in warmer months than in the winter. Others have similarly reported higher frequency of *Arcobacter* in feces from cows in southern dairy herds than in those in the northern states, which may reflect higher transmission in warmer climates (Wesley et al., 2000).

4.2. Pathogen prevalence in water

Surface water had a higher pathogen prevalence when compared to well water. Although some ponds and streams evaluated were not used directly for agricultural irrigation, their relatively high *Lm* and *Arcobacter* prevalence should be considered since they could still be sources of pathogen introduction. Pathogens could be introduced into the field *via* animal movement and/or precipitation events could lead to flooding of surface water, introducing contaminated water into the field. This study did not examine surface water during the winter since it was not used for irrigation. However, an assessment of *Lm* prevalence in winter water samples could provide better information about how *Lm* survives and circulates in an agricultural region and how those factors contribute to the potential for *Lm* contamination of fresh produce. This is of particular interest after the observations of *Lm* prevalence in DM, indicating the potential for circulation between the regional herd and surface water. *Lm* prevalence in OH surface water was observed to peak in the summer when the domestic animals were more likely to be outside with possible direct interaction with surface water. This prevalence decreased to undetectable levels in the fall (**Figure 3**). Unlike *Lm* prevalence, *Arcobacter* presence in surface water was not significantly different in spring, summer and fall seasons. Similarly, others have shown that the prevalence of *Arcobacter* and five associated virulence genes in water samples from various sources were not impacted by weather in the Kathmandu Valley in Nepal (Ghaju Shrestha et al., 2019). These results, revealing differences in how each pathogen survives and persists in the agricultural environment, highlighted the need to consider pathogen-specific risk assessment models and mitigation strategies in agricultural practices.

4.3. Pathogen prevalence in soil

The SEM approach used to evaluate factors associated with pathogen prevalence in soil is in line with the exploratory and confirmatory attitude of this study. Lam and Maguire provided a good description of SEM and its uses (Lam and Maguire, 2012). *Lm* and *Arcobacter* were both directly impacted by soil amendment, with pathogen prevalence being highest for DM amendment, second highest for PM amendment and lowest for no amendment (**Figures 5**, **9B, D**). *Lm* presence in non-amended fields was marginally higher than *Arcobacter* presence (**Table 2**), suggesting *Arcobacter* prevalence in soil was primarily driven by BSAAO usage. BSAAO usage may serve as either the vehicle for *Arcobacter* introduction or provide a more favorable environment for pathogen survival. Other factors (e.g., irrigation

TABLE 3 Top thirty genera whose mean relative abundance was most significantly different between (A) samples with no detectable *Lm* (*Lm*-) and samples with detectable *Lm* (*Lm*+) and (B) samples with no detectable *Arcobacter* (*Arco*-) and samples with detectable *Arcobacter* (*Arco*+).

A							B						
	Lm+			*Lm-*				*Arco+*			*Arco-*		
Genus	Mean	Lower CL	Upper CL	Mean	Lower CL	Upper CL	Genus	Mean	Lower CL	Upper CL	Mean	Lower CL	Upper CL
Aeromicrobium	0.0945	0.0745	0.1589	0.0524	0.0451	0.0595	*Acinetobacter*	0.0063	0.0030	0.0129	0.3052	0.1552	1.3559
Aerosphaera	0.0669	0.0238	0.4378	0.0065	0.0027	0.0194	*Agrococcus*	0.0057	0.0019	0.0131	0.0169	0.0137	0.0227
Anaeromyxobacter	0.1799	0.1457	0.2210	0.2572	0.2355	0.2864	*beta proteobacter.*	0.0223	0.0129	0.0480	0.0071	0.0048	0.0106
Azospirillum	0.2054	0.1701	0.2372	0.2627	0.2461	0.2831	*Chitinophaga*	0.1874	0.1535	0.2548	0.3065	0.2602	0.4093
Bacteroides	0.0009	0.0003	0.0027	0.0889	0.0223	1.0358	*Coxiella*	0.0098	0.0060	0.0148	0.0191	0.0155	0.0222
Candidatus Accumu.	0.0382	0.0323	0.0459	0.0559	0.0475	0.0681	*Cupriavidus*	0.3111	0.2750	0.3656	0.2323	0.2189	0.2463
Candidatus Koriba.	1.6213	1.4506	1.8140	1.8997	1.8285	1.9825	*Enhygromyxa*	0.0171	0.0081	0.0263	0.0503	0.0338	0.0958
Chitinimonas	0.0272	0.0209	0.0352	0.0416	0.0378	0.0469	*Halothiobacillus*	0.0540	0.0382	0.0694	0.0319	0.0281	0.0360
Chthonomonas	0.1749	0.1479	0.2040	0.2384	0.2278	0.2526	*Herbiconiux*	0.0088	0.0050	0.0180	0.0249	0.0195	0.0323
Corynebacterium	0.5816	0.1749	2.2222	0.0662	0.0455	0.1005	*Hippea*	0.0054	0.0034	0.0090	0.0017	0.0013	0.0024
Cyanothece	0.0291	0.0186	0.0414	0.0544	0.0449	0.0730	*Janibacter*	0.0378	0.0288	0.0471	0.0808	0.0644	0.1051
Edaphobacter	0.2888	0.2295	0.3304	0.3829	0.3605	0.4106	*Leucobacter*	0.0085	0.0043	0.0147	0.0417	0.0296	0.0825
Flavobacterium	2.6550	1.7939	3.9411	1.3286	1.0864	1.6932	*Lewinella*	0.0268	0.0140	0.0392	0.0464	0.0392	0.0632
Gemmata	0.9593	0.8502	1.1113	1.2336	1.1648	1.3119	*Magnetospirillum*	0.0044	0.0024	0.0074	0.0133	0.0102	0.0157
Geoalkalibacter	0.1516	0.1210	0.1856	0.1960	0.1872	0.2091	*Methylovorus*	0.0274	0.0070	0.4757	0.0039	0.0032	0.0057
Geobacter	0.7395	0.5791	0.9095	0.9872	0.9373	1.0455	*Microterricola*	0.0228	0.0145	0.0346	0.0625	0.0470	0.0804
Geopsychrobacter	0.0584	0.0491	0.0676	0.0820	0.0763	0.0885	*Mucilaginibacter*	0.0090	0.0035	0.0250	0.0660	0.0500	0.1124
Labrys	0.0341	0.0279	0.0420	0.0474	0.0432	0.0576	*Novispirillum*	0.1357	0.0937	0.1881	0.0739	0.0658	0.0813
Lachnoclostridium	0.0232	0.0174	0.0311	0.0518	0.0324	0.0926	*Oerskovia*	0.0074	0.0043	0.0134	0.0231	0.0146	0.0379
Nitrosospira	0.5063	0.4379	0.5947	0.6386	0.6055	0.6780	*Polaromonas*	0.0171	0.0054	0.0460	0.0944	0.0784	0.1305
Paraclostridium	0.0499	0.0395	0.0605	0.0782	0.0638	0.0989	*Ramlibacter*	0.4620	0.3519	0.5496	0.2794	0.2470	0.3084
Pelobacter	0.5541	0.4913	0.6278	0.6886	0.6513	0.7335	*Rhodopseudomonas*	0.0578	0.0401	0.0684	0.1059	0.0970	0.1155
Pseudoxanthomonas	0.0550	0.0351	0.0882	0.0255	0.0198	0.0301	*Rubinisphaera*	0.1719	0.1428	0.2007	0.1181	0.1083	0.1269
Rhodocyclus	0.1117	0.0912	0.1407	0.1495	0.1409	0.1574	*Salinirepens*	0.0209	0.0141	0.0330	0.0069	0.0056	0.0084
Rhodoferax	0.2179	0.1186	0.4360	0.0879	0.0804	0.1029	*Sanguibacter*	0.0194	0.0091	0.0586	0.1479	0.0671	0.4369
Roseiflexus	0.3678	0.3107	0.4119	0.4701	0.4288	0.5204	*Skermanella*	0.1631	0.1376	0.1893	0.2035	0.1893	0.2168
Ruminiclostridium	0.0268	0.0191	0.0355	0.1216	0.0523	0.6547	*Tepidimonas*	0.1730	0.1096	0.2612	0.0735	0.0617	0.0945
Spongiibacter	0.1220	0.1017	0.1511	0.1668	0.1519	0.1858	*Thermodesulfatator*	0.0819	0.0602	0.1164	0.0477	0.0418	0.0532
Terriglobus	0.0754	0.0562	0.0922	0.1169	0.1091	0.1284	*Thiorhodococcus*	0.0388	0.0222	0.0661	0.0147	0.0111	0.0182
Thermobaculum	0.4798	0.4055	0.5699	0.6090	0.5878	0.6370	*Turneriella*	0.0067	0.0035	0.0134	0.0012	0.0008	0.0017

Lower CL, lower limit of 95% CI; Upper CL, upper limit of 95% CI; CL, confidence limit.

10.3389/fmicb.2023.1141043

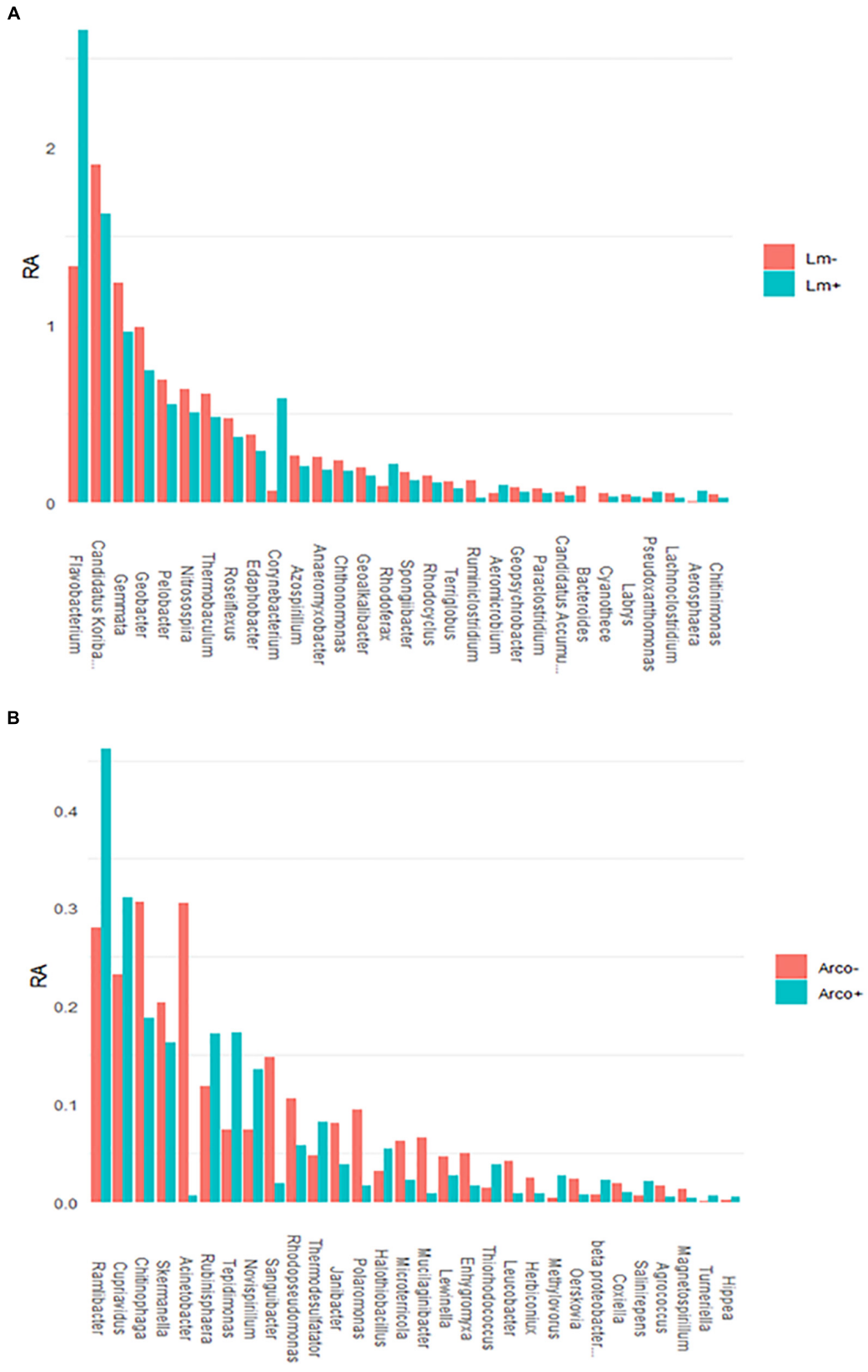

FIGURE 11
Top thirty genera detected (16S) with significant differences between their mean relative abundance (%) when comparing *Arcobacter* negative (−) and positive (+) OH soil samples **(A)** and between *Lm* negative (−) and *Lm* positive (+) OH soil samples **(B)**. Genera names were truncated at twenty characters. *Bacteriodes* RA in Lm+ samples was 0.000883. RA, mean relative abundance.

source) appeared to have critical influence on *Lm* prevalence, though BSAAO usage did contribute to *Lm* prevalence. BSAAO serving as a primary driver for *Arcobacter* prevalence may explain the differences in prevalence observed between GA and OH farms in this study, with the former having reduced BSAAO usage and no use of DM and a concurrent reduction in *Arcobacter* prevalence. It is intriguing that this difference was also seen in surface water, suggesting added factors may be reducing *Arcobacter* prevalence in GA though it could simply be the absence of introduction from reduced BSAAO applications, potentially limited to the lack of DM.

Lm prevalence in soil was highest during the winter and spring when AT was lowest and precipitation amounts were marginally higher (**Figures 6A, B**). The impact of increasing AT (|effect size| ~6) on decreasing *Lm* prevalence appeared more salient than the impact of increasing PR (|effect size| ~1) on increasing *Lm* prevalence (**Figure 4C**). Although this study found, as others did (Strawn et al., 2013a,b; Weller et al., 2015a; Falardeau et al., 2018; Harrand et al., 2020), that *Lm* positivity increased with increased rainfall or soil moisture, AT appeared to suppress *Lm* more (i.e., higher effect size) than the moisture supported *Lm*. This observation is intriguing however, as GA weather had higher AT and similar PR compared to OH, but GA *Lm* prevalence was only slightly lower than that of OH in both soil and water samples. This suggests the possibility that AT alone may not be suppressing *Lm* or that temperatures during winter may provide a basal level of support for *Lm* prevalence throughout the year. However, it may also be that the microbiome population dynamics or other factors, such as soil texture, may vary between the different regions resulting in equivalent *Lm* prevalence despite the differences in temperature. SDI was highest during the summer and fall (**Figure 6A**), the same seasons where *Lm* prevalence is at its lowest, and the model (**Figure 5**) showed a direct role for diversity in the reduction of *Lm*, suggesting that competition played a role in suppression of *Lm*. It should be considered that AT, therefore, could impact *Lm* directly and indirectly.

Weather had a stronger direct effect on *Arcobacter* with prevalence increasing as AT increased and PR decreased (**Figure 6A**). A predictive model to measure the growth rate of *A. butzleri* showed that growth was directly proportional to increasing temperature, achieving maximum growth at a storage temperature of 40°C (Park and Ha, 2015). A more recent study has shown optimal growth of the three major human pathogenic *Arcobacter* species (*A. butzleri*, *A. cryaerophilus*, and *A. skirrowii*) at 35°C, followed by growth on agar plates at 30°C under microaerophilic conditions (Nguyen et al., 2021). Given average temperatures never exceeded 95°F (35°C), these prior data support the findings of this study, which indicated warmer temperatures supported *Arcobacter* prevalence, potentially by improved growth.

Soil fertility was directly impacted by both weather and soil amendment, as expected. Soil fertility decreased with rising AT and decreasing PR and was highest in DM-amended fields, with a slight decrease in PM-amended fields and a substantial decrease in non-amended fields. While some elements (anions) in the fertility panel may naturally leach out of soil through water percolating through soil column or surface erosion (water/wind whose speed increased through the growing season), all the elements in the panel are affected by weather through plant/crop uptake. Greater AT and SR enhance crop growth and thereby nutrient consumption, resulting in decreased soil fertility as the growing season progresses. While soil fertility was only correlated with *Lm* prevalence, the improvement of soil fertility associated with soil amendment usage could have indirectly affected *Lm* and *Arcobacter* prevalence *via* improved nutrient content. Although there are no studies to test the effect of soil fertility on the prevalence of *Arcobacter*, it is important to recognize its global presence in water bodies and various animals, including food and farm animals, domestic birds, wildlife, and zoo animals (Hsu and Lee, 2015).

The preliminary assessment, evaluating NO_3-N and NH_4-N separate from soil fertility, indicated the possibility of a relationship between ammonium, nitrate, *Nitrospira*, *Nitrosospira*, and *Lm* prevalence, though this observation requires further analysis since AT or other variables could play a role as well. However, within this study, given that manure was applied at a set time in the year and AT varies throughout the year and correlates with the season, it was not possible to disconnect these variables to evaluate their impact on nitrifying bacteria and *Lm* prevalence independently. The observed increase in *Lm* prevalence in PM-amended fields late in the year suggested the possibility that the ammonium increase associated with PM might impact nitrifying microorganisms, with one nitrifying genus, *Nitrosospira*, found to have a significant difference in relative abundance between *Lm*+ and *Lm*- fields (**Figure 11A**).

There are hypotheses that a healthy, robust soil, i.e., high soil fertility, may limit pathogen prevalence (Devarajan et al., 2021; Jayaraman et al., 2021). In fact, one recent study found that the use of cover crops and compost boosted soil diversity, improving suppression of *Salmonella* and *Lm* (Devarajan et al., 2021). However, in our study, while we found soils with higher SDI had reduced *Lm* prevalence, soils with higher soil fertility, which was improved with the use of BSAAO, which included both raw and composted manure, had a decreased SDI (**Figure 5** and 6A). Additionally, the use of BSAAO was associated with an increased prevalence of *Arcobacter* and *Lm*, suggesting added complexity within these relationships. In particular, the *Lm* model showed that increased soil fertility resulted in decreased SDI, which could indirectly increase *Lm* prevalence as decreased SDI was correlated with higher *Lm* prevalence, though the same was not true for *Arcobacter* (**Figure 5**). Therefore, careful consideration of the attributes of a pathogen is important when testing how farm management practices could impact its prevalence.

This finding that there could be differing impacts on pathogens was further highlighted when evaluating the impact of irrigation on pathogen prevalence. Irrigation was found to have no impact on *Arcobacter* prevalence (**Figures 5**, **9C**). However, irrigation source had a direct impact on *Lm* prevalence, though the result was counter to the expected results. *Lm* prevalence was highest for non-irrigated fields when compared to both well and surface water-irrigated fields (**Figures 5**, **9A**). One explanation could be that farm management practices could have been impacted by observable risks, such as known proximity to animals, when deciding whether to use surface water for irrigation. Evaluation of farm practices found that non-BSA amended fields were more likely to not be irrigated, suggesting that other factors, such as economics or neighboring animals, may have influenced these decisions. However, metadata to evaluate what factors farmers used to inform their irrigation choice were not available. It is important to note, though, that the soil evaluated was not the soil directly irrigated but adjacent so it is possible that a different observation

would have been made closer to the dripline. These possibilities suggest that more studies are needed to understand what could be creating the observed result, given that *Lm* prevalence was highest in surface water samples.

4.4. Evaluation of study

SEMs are uniquely suited for (1) identifying relationships (pathways) between latent variables (weather and soil fertility), (2) modeling complex (intermediary) relationships between factors and (3) explicitly identifying covariances between indicators and factors (Nachtigall et al., 2003). SEMs directly estimate both the effect sizes and direction of the effects, simultaneously for all factors, a notable strength of this analysis.

Some factors that indicated possible associations with soil pathogen prevalence but were not included in the soil analyses due to insufficient or incomplete data include comparing organic and non-organic farming, equipment hygiene, insecticide/fungicide application, presence of animal activity, water additives, and soil moisture measurements. The impact of these candidate factors would need a much larger study to be evaluated. Broader and more complete metadata collection was desirable for the study but attaining such on a voluntary basis was challenging, especially with potential for differences in memory to recall specific practices and/or events.

Year to year variability also cannot be eliminated as a factor in this study given 2018 and 2019 were not evaluated to determine if weather related factors were representative of overall weather trends.

5. Conclusion

Pathogen prevalence in soil, for both *Lm* and *Arcobacter*, was found to be associated with the use of BSAAO but not the use of surface water as an irrigation source. In fact, the *Lm* model indicated that not irrigating increased *Lm* prevalence, suggesting that other factors that might be linked to the decision to not irrigate, such as animals residing at neighboring farms, wildlife presence, equipment sanitation activities, land topography, or unidentified/unknown variables may be contributing to increased *Lm* prevalence in non-irrigated fields. As noted earlier, BSAAO usage was not correlated with the practice of not irrigating fields. This indirectly suggests that the presence of cattle on farms, which served as the source of DM, did not impact irrigation choices. AT appeared to play a more significant role on pathogen prevalence in soil rather than the use of BSAAO, although the effect of AT was in opposing directions for *Arcobacter* and *Lm*. Additionally, data showed key differences in how environmental conditions impacted pathogen prevalence, indicating that a one size fits all approach to risk mitigation would not control certain pathogens. While the sample size was small and metadata were limited, this real-world comparison of multiple farms in two regions based on BSAAO and irrigation provided critical data to inform and validate controlled studies. The results of this study have identified other factors, i.e., not irrigating could increase pathogen prevalence, that may need further study and the need to better understand how pathogens are established and circulated within the agricultural environment.

Data availability statement

The data presented in the study are deposited in the NCBI repository, accession number PRJNA894200.

Author contributions

EL, GR, MK, CG, KJ, LB, CH, KB, LH, UB, BL, and AZ contributed to the conception and design of the study. CH and MF organized the database. JP, MF, CG, and KJ worked on bioinformatics and sequence analysis. MF performed the statistical analysis. CH, LB, CG, UB, LH, BL, AH, KB, JF, MK, KJ, and RR were involved in sample processing. MF, CH, CG, UB, LB, and BL wrote the manuscript. KB was responsible for the revision and proofreading of this work. All authors contributed to the article and approved the submitted version.

Funding

This work was funded by the U.S. Food and Drug Administration, Center for Food Safety and Applied Nutrition.

Acknowledgments

We thank Hugh Rand, at the U.S. Food and Drug Administration, for his helpful insight and input to this study and manuscript; Marianne Sawyer, Surasri Sahu, Mira Rakic-Martinez, and Mohammad S. Alam, at the U.S. Food and Drug Administration, for their assistance on soil sample preparation for fertility testing, and DNA extraction; and Jennifer Schrock and Nick Anderson, at the Ohio State University, for sample collection.

Conflict of interest

The authors declare that the research was conducted in the absence of any commercial or financial relationships that could be construed as a potential conflict of interest.

Publisher's note

Supplementary material

The Supplementary Material for this article can be found online at: https://www.frontiersin.org/articles/10.3389/fmicb.2023.1141043/full#supplementary-material

SUPPLEMENTARY FIGURE 1
Seasonal trends in GA air temperature (AT), precipitation (PR), solar radiation (SR), and wind speed (WS). Overlaid is *Lm* soil prevalence GA soil. AT, PR, SR and WS are 48 h moving averages. All variables are standardized to the same scale using the R *standardize* function in the robustHD package. Soil amendment groups are aggregated in **(A)** and grouped in **(B)**. GC, green compost; PM, poultry manure; AT, 24 h average of air temperature; PR, precipitation; SR, solar radiation; WS, wind speed.

SUPPLEMENTARY FIGURE 2
Covariances between the soil nutrient covariances included in the OH *Lm* and *Arcobacter* (*Arco*) soil prevalence models. Ca, calcium; Mg, magnesium; Mn, manganese; P, phosphorus; S, sulfur; Zn, zinc; LOI, loss-on-ignition; NO_3_N, nitrate nitrogen; NH_4_N, ammonium nitrogen.

References

Abay, S., Yaman, A., Karakava, E., and Fuat, A. (2022). Prevalence and antibacterial susceptibilities of *Arcobacter* spp. and Campylobacter spp. from fresh vegetables. *World J. Microbiol. Biotechnol.* 38:132. doi: 10.1007/s11274-022-03315-3

Alegbeleye, O. O., and Sant'Ana, A. S. (2020). Manure-borne pathogens as an important source of water contamination: an update on the dynamics of pathogen survival/transport as well as practical risk mitigation strategies. *Int. J. Hyg. Environ. Health* 227:113524. doi: 10.1016/j.ijheh.2020.113524

Alfons, A. (2019). *robustHD: Robust Methods for High-Dimensional Data. R package version 0.6.1.*

Allard, S. M., Callahan, M. T., Bui, A., Ferelli, A. M. C., Chopyk, J., Chattopadhyay, S., et al. (2019). Creek to table: tracking fecal indicator bacteria, bacterial pathogens, and total bacterial communities from irrigation water to kale and radish crops. *Sci. Total Environ.* 666, 461–471. doi: 10.1016/j.scitotenv.2019.02.179

Andrews, W. H., Wang, H., Jacobson, A., Ge, B., Zhang, G., and Hammack, T. (2022). *BAM Chapter 5: Salmonella*. Silver Spring, MA: U.S. Food and Drug adminstration.

Atwill, E. R., Jay-Russell, M., Li, X., Vivas, E., Kilonzo, C., and Mandrell, R. (2012). "Methodological and epidemiological concerns when comparing microbial food safety risks from wildlife, livestock, and companion animals," in *Proceedings of the 25th Vertebrate Pest Conference*, (Davis, CA: Western Center for Food Safety, University of California). doi: 10.5070/V425110514

Bardsley, C. A., Weller, D. L., Ingram, D. T., Chen, Y., Oryang, D., Rideout, S. L., et al. (2021). Strain, soil-type, irrigation regimen, and poultry litter influence *Salmonella* survival and die-off in agricultural soils. *Front. Microbiol.* 12:590303. doi: 10.3389/fmicb.2021.590303

Belias, A., Strawn, L. K., Wiedmann, M., and Weller, D. (2021). Small produce farm environments can harbor diverse *Listeria monocytogenes* and *Listeria* spp. populations. *J. Food Prot.* 84, 113–121. doi: 10.4315/JFP-20-179

Brennan, F. P., Moynihan, E., Griffiths, B. S., Hillier, S., Owen, J., Pendlowski, H., et al. (2014). Clay mineral type effect on bacterial enteropathogen survival in soil. *Sci. Total Environ.* 46, 302–305. doi: 10.1016/j.scitotenv.2013.08.037

Burall, L. S., Sepehri, S., Srinivasan, D., Grim, C. J., Lacher, D. W., Ferguson, M., et al. (2021). Development and validation of a quantitative pcr method for species verification and serogroup determination of *Listeria monocytogenes* isolates. *J. Food Prot.* 84, 333–344. doi: 10.4315/JFP-20-178

Chai, L. C., Ghazali, F. M., Bakar, F. A., Lee, H. Y., Suhaimi, L. R., Talib, S. A., et al. (2009). Occurrence of thermophilic *Campylobacter* spp. contamination on vegetable farms in Malaysia. *J. Microbiol. Biotechnol.* 19, 1415–1420. doi: 10.4014/jmb.0901.0002

Collado, L., and Figueras, M. J. (2011). Taxonomy, epidemiology, and clinical relevance of the genus *Arcobacter*. *Clin. Microbiol. Rev.* 24, 174–192. doi: 10.1128/CMR.00034-10

Cooley, M., Carychao, D., Crawford-Miksza, L., Jay, M. T., Myers, C., Rose, C., et al. (2007). Incidence and tracking of *Escherichia coli* O157:H7 in a major produce production region in California. *PLoS One* 2:e1159. doi: 10.1371/journal.pone.0001159

Daims, H. (2014). "The family nitrospiraceae," in *The Prokaryotes*, eds D. E. F. Rosenberg, S. Lory, E. Stackebrandt, and F. Thompson (Berlin: Springer), 733–749. doi: 10.1007/978-3-642-38954-2_126

Daquigan, N., Grim, C. J., White, J. R., Hanes, D. E., and Jarvis, K. G. (2016). Early recovery of *Salmonella* from food using a 6-hour non-selective pre-enrichment and reformulation of tetrathionate broth. *Front. Microbiol.* 7:2103. doi: 10.3389/fmicb.2016.02103

Devarajan, N., McGarvey, J. A., Scow, K., Jones, M. S., Lee, S., Samaddar, S., et al. (2021). Cascading effects of composts and cover crops on soil chemistry, bacterial communities and the survival of foodborne pathogens. *J. Appl. Microbiol.* 131, 1564–1577. doi: 10.1111/jam.15054

Donnelly, C. W. (2002). Detection and isolation of *Listeria monocytogenes* from food samples: implications of sublethal injury. *J. AOAC Int.* 85, 495–500. doi: 10.1093/jaoac/85.2.495

Dowe, M. J., Jackson, E. D., Mori, J. G., and Bell, C. R. (1997). *Listeria monocytogenes* survival in soil and incidence in agricultural soils (dagger). *J. Food Prot.* 60, 1201–1207. doi: 10.4315/0362-028X-60.10.1201

Draper, A. D., Doores, S., Gourama, H., and LaBorde, L. F. (2016). Microbial survey of pennsylvania surface water used for irrigating produce crops. *J. Food Prot.* 79, 902–912. doi: 10.4315/0362-028X.JFP-15-479

Edgar, R. C. (2010). Search and clustering orders of magnitude faster than BLAST. *Bioinformatics* 26, 2460–2461. doi: 10.1093/bioinformatics/btq461

Edgar, R. C., and Flyvbjerg, H. (2015). Error filtering, pair assembly and error correction for next-generation sequencing reads. *Bioinformatics* 31, 3476–3482. doi: 10.1093/bioinformatics/btv401

EFSA, and ECDC (2021). The European union one health 2019 zoonoses report. *EFSA J.* 19:6406. doi: 10.2903/j.efsa.2021.6406

Falardeau, J., Walji, K., Haure, M., Fong, K., Taylor, G., Ma, Y., et al. (2018). Native bacterial communities and *Listeria monocytogenes* survival in soils collected from the Lower Mainland of British Columbia, Canada. *Can. J. Microbiol.* 64, 695–705. doi: 10.1139/cjm-2018-0115

Feng, P., Weagant, S. D., and Jinneman, K. (2020). "BAM: chapter 4a: diarrheagenic *Escherichia coli*," in *Bacteriological Analytical Manual*, eds K. W. B. Jinneman, M. Davidson, P. Feng, B. Ge, G. Gharst, T. Hammack, et al. (Silver Spring, MA: U.S. FDA).

Freitag, N. E. (2009). *Listeria monocytogenes* – from saprophyte to intracellular pathogen. *Nat. Rev. Microbiol.* 7, 623–628. doi: 10.1038/nrmicro2171

Gardner, H. (1985). *Soil Fertility*, ed. O. Natural Resources Conservation Service (Washington, DC: United States Department of Agriculture).

Gardner, T. J., Fitzgerald, C., Xavier, C., Klein, R., Pruckler, J., Stroika, S., et al. (2011). Outbreak of campylobacteriosis associated with consumption of raw peas. *Clin. Infect Dis.* 53, 26–32. doi: 10.1093/cid/cir249

Ghaju Shrestha, R., Tanaka, Y., Sherchand, J. B., and Haramoto, E. (2019). Identification of 16S rRNA and virulence-associated genes of *Arcobacter* in water samples in the Kathmandu valley. *Nepal. Pathogens* 8:110. doi: 10.3390/pathogens8030110

Gnanou Besse, N., Lombard, B., Guillier, L., Francois, D., Romero, K., Pierru, S., et al. (2019). Validation of standard method EN ISO 11290 - Part 1 - detection of *Listeria monocytogenes* in food. *Int. J. Food Microbiol.* 288, 13–21. doi: 10.1016/j.ijfoodmicro.2018.03.024

Gorski, L., Walker, S., Liang, A. S., Nguyen, K. M., Govoni, J., Carychao, D., et al. (2014). Comparison of subtypes of *Listeria monocytogenes* isolates from naturally contaminated watershed samples with and without a selective secondary enrichment. *PLoS One* 9:e92467. doi: 10.1371/journal.pone.0092467

Gu, G., Luo, Z., Cevallos-Cevallos, J. M., Adams, P., Vellidis, G., Wright, A., et al. (2013). Occurrence and population density of *Campylobacter jejuni* in irrigation ponds on produce farms in the Suwannee River Watershed. *Can. J. Microbiol.* 59, 339–346. doi: 10.1139/cjm-2013-0027

Gu, G., Strawn, L. K., Ottesen, A. R., Ramachandran, P., Reed, E. A., Zheng, J., et al. (2020). Correlation of *Salmonella enterica* and *Listeria monocytogenes* in irrigation water to environmental factors, fecal indicators, and bacterial communities. *Front. Microbiol.* 11:557289. doi: 10.3389/fmicb.2020.557289

Gu, G., Strawn, L. K., Zheng, J., Reed, E. A., and Rideout, S. L. (2019). Diversity and dynamics of *Salmonella enterica* in water sources, poultry litters, and field soils amended with poultry litter in a major agricultural area of Virginia. *Front. Microbiol.* 10:2868. doi: 10.3389/fmicb.2019.02868

Guevremont, E., Lamoureux, L., Genereux, M., and Cote, C. (2017). Irrigation water sources and time intervals as variables on the presence of *Campylobacter* spp.

and *Listeria monocytogenes* on romaine lettuce grown in muck soil. *J. Food Prot.* 80, 1182–1187. doi: 10.4315/0362-028X.JFP-16-551

Harrand, A. S., Strawn, L., Illas-Ortiz, P. M., Wiedmann, M., and Weller, D. (2020). *Listeria monocytogenes* prevalence varies more within fields than between fields or over time on conventionally farmed New York produce fields. *J. Food Prot.* 83, 1958–1966. doi: 10.4315/JFP-20-120

Helwig, N. E. (2021). *nptest: Nonparametric Bootstrap and Permutation Tests. R package version 1.0-3*.

Herbert, S., Hashemi, M., Chickering-Sears, C., Weis, S. M., Carlevale, J., Campbell-Nelson, K., et al. *Conserving Ammonia in Manure. UMass Extension Crops, Dairy, Livestock and Equine Program*. Available online at: https://ag.umass.edu/crops-dairy-livestock-equine/fact-sheets/conserving-ammonia-in-manure.

Hiett, K. L. (2017). *Campylobacter jejuni* isolation/enumeration from environmental samples. *Methods Mol. Biol.* 1512, 1–8. doi: 10.1007/978-1-4939-6536-6_1

Himathongkham, S., Bahari, S., Riemann, H., and Cliver, D. (1999). Survival of *Escherichia coli* O157:H7 and *Salmonella typhimurium* in cow manure and cow manure slurry. *FEMS Microbiol. Lett.* 178, 251–257. doi: 10.1111/j.1574-6968.1999.tb08684.x

Hoa, T. K. H., Lipman, L. J. A., and Gaastra, W. (2006). Arcobacter, what is known and unknown about a potential foodborne zoonotic agent! *Vet. Microbiol.* 115, 1–13. doi: 10.1016/j.vetmic.2006.03.004

Hoelzer, K., Moreno Switt, A. I., and Wiedmann, M. (2011). Animal contact as a source of human non-typhoidal salmonellosis. *Vet. Res.* 42:34. doi: 10.1186/1297-9716-42-34

Hruby, C. E., Soupir, M. L., Moorman, T. B., Pederson, C., and Kanwar, R. (2018). *Salmonella* and fecal indicator bacteria survival in soils amended with poultry manure. *Water Air Soil Pollut.* 229:32. doi: 10.1007/s11270-017-3667-z

Hsu, T. T., and Lee, J. (2015). Global distribution and prevalence of *Arcobacter* in food and water. *Zoonoses Public Health* 62, 579–589. doi: 10.1111/zph.12215

IFSAC (2018). *Foodborne Illness Source Attribution Estimates for 2016 for Salmonella, Escherichia coli O157, Listeria monocytogenes, and Campylobacter using Multi-Year Outbreak Surveillance Data, United States*, ed. T. I. F. S. A. Collaboration (Atlanda, GA: CDC).

Ivanek, R., Grohn, Y. T., and Wiedmann, M. (2006). *Listeria monocytogenes* in multiple habitats and host populations: review of available data for mathematical modeling. *Foodborne Pathog. Dis.* 3, 319–336. doi: 10.1089/fpd.2006.3.319

Iwu, C. D., and Okoh, A. I. (2019). Preharvest transmission routes of fresh produce associated bacterial pathogens with outbreak potentials: a review. *Int. J. Environ. Res. Public Health* 16:4407. doi: 10.3390/ijerph16224407

Jayaraman, S., Naorem, A. K., Lal, R., Dalal, R. C., Sinha, N. K., Patra, A. K., et al. (2021). Disease-suppressive soils-beyond food production: a critical review. *J. Soil Sci. Plant Nutr.* 21, 1437–1465. doi: 10.1007/s42729-021-00451-x

Jeyaletchumi, P., Tunung, R. S., Margaret, S., Chai, L. C., Radu, S., Farinazleen, M. G., et al. (2011). Evaluation of *Listeria* spp. and *Listeria monocytogenes* in selected vegetable farms. *J. Trop. Agric. Fd Sci.* 39, 255–266.

Jiang, X., Islam, M., Morgan, J., and Doyle, M. P. (2004). Fate of *Listeria monocytogenes* in bovine manure-amended soil. *J. Food Prot.* 67, 1676–1681. doi: 10.4315/0362-028X-67.8.1676

Kim, N. H., Park, S. M., Kim, H. W., Cho, T. J., Kim, S. H., Choi, C., et al. (2019). Prevalence of pathogenic *Arcobacter* species in South Korea: comparison of two protocols for isolating the bacteria from foods and examination of nine putative virulence genes. *Food Microbiol.* 78, 18–24. doi: 10.1016/j.fm.2018.09.008

Lam, T. Y., and Maguire, D. A. (2012). Structural equation modeling: theory and applications in forest management. *Intl. J. For. Res.* 2012:263953. doi: 10.1155/2012/263953

Lappi, V., Archer, J. R., Cebelinski, E., Leano, F., Besser, J. M., Klos, R. F., et al. (2013). An outbreak of foodborne illness among attendees of a wedding reception in Wisconsin likely caused by *Arcobacter butzleri*. *Foodborne Pathog. Dis.* 10, 250–255. doi: 10.1089/fpd.2012.1307

Leclercq, A. (2004). Atypical colonial morphology and low recoveries of *Listeria monocytogenes* strains on Oxford, PALCAM, Rapid'L.mono and ALOA solid media. *J. Microbiol. Methods* 57, 251–258. doi: 10.1016/j.mimet.2004.01.011

Li, B., Liu, H., and Wang, W. (2017). Multiplex real-time PCR assay for detection of *Escherichia coli* O157:H7 and screening for non-O157 Shiga toxin-producing *E. coli*. *BMC Microbiol.* 17:215. doi: 10.1186/s12866-017-1123-2

Lines-Kelly, R. (1992). *Plant Nutrients in the Soil [Online]*. Available online at: https://www.dpi.nsw.gov.au/agriculture/soils/improvement/plant-nutrients (accessed July 29 2021).

Linton, D., Owen, R. J., and Stanley, J. (1996). Rapid identification by PCR of the genus *Campylobacter* and of five *Campylobacter* species enteropathogenic for man and animals. *Res. Microbiol.* 147, 707–718. doi: 10.1016/S0923-2508(97)85118-2

Locatelli, A., Spor, A., Jolivet, C., Piveteau, P., and Hartmann, A. (2013). Biotic and abiotic soil properties influence survival of *Listeria monocytogenes* in soil. *PLoS One* 8:e75969. doi: 10.1371/journal.pone.0075969

Ma, Y., Ju, C., Zhou, G., Yu, M., Chen, H., He, J., et al. (2022). Genetic characteristics, antimicrobial resistance, and prevalence of *Arcobacter* spp. isolated from various sources in Shenzhen. *China. Front. Microbiol.* 13:1004224. doi: 10.3389/fmicb.2022.1004224

Magoc, T., and Salzberg, S. L. (2011). FLASH: fast length adjustment of short reads to improve genome assemblies. *Bioinformatics* 27, 2957–2963. doi: 10.1093/bioinformatics/btr507

Marine, S. C., Pagadala, S., Wang, F., Pahl, D. M., Melendez, M. V., Kline, W. L., et al. (2015). The growing season, but not the farming system, is a food safety risk determinant for leafy greens in the mid-Atlantic region of the United States. *Appl. Environ. Microbiol.* 81, 2395–2407. doi: 10.1128/AEM.00051-15

Matias Rodrigues, J. F., Schmidt, T. S. B., Tackmann, J., and von Mering, C. (2017). MAPseq: highly efficient k-mer search with confidence estimates, for rRNA sequence analysis. *Bioinformatics* 33, 3808–3810. doi: 10.1093/bioinformatics/btx517

Micallef, S. A., Rosenberg Goldstein, R. E., George, A., Kleinfelter, L., Boyer, M. S., McLaughlin, C. R., et al. (2012). Occurrence and antibiotic resistance of multiple *Salmonella* serotypes recovered from water, sediment and soil on mid-Atlantic tomato farms. *Environ. Res.* 114, 31–39. doi: 10.1016/j.envres.2012.02.005

Nachtigall, C., Kroehne, U., Funke, F., Steyer, R., and Schiller, F. (2003). (Why) should we use sem? pros and cons of structural equation modeling. *MethPsychol Res. Online* 8, 1–22.

Nguyen, P. T., JuArez, O., and Restaino, L. (2021). A new method for detection of *Arcobacter butzleri*, *Arcobacter cryaerophilus*, and *Arcobacter skirrowii* using a novel chromogenic agar. *J. Food Prot.* 84, 160–168. doi: 10.4315/JFP-20-245

Niedermeyer, J. A., Miller, W. G., Yee, E., Harris, A., Emanuel, R. E., Jass, T., et al. (2020). Search for *Campylobacter* spp. reveals high prevalence and pronounced genetic diversity of *Arcobacter butzleri* in floodwater samples associated with Hurricane Florence in North Carolina, USA. *Appl. Environ. Microbiol.* 86, e1118–e1120. doi: 10.1128/AEM.01118-20

Oksanen, J., Guillaume Blanchet, F., Friendly, M., Kindt, R., Legendre, P., McGlinn, D., et al. (2019). *vegan: Community Ecology Package. R package version 2.5-6*.

Pandey, P. K., Kass, P. H., Soupir, M. L., Biswas, S., and Singh, V. P. (2014). Contamination of water resources by pathogenic bacteria. *AMB Express* 4:51. doi: 10.1186/s13568-014-0051-x

Parada, A. E., Needham, D. M., and Fuhrman, J. A. (2016). Every base matters: assessing small subunit rRNA primers for marine microbiomes with mock communities, time series and global field samples. *Environ. Microbiol.* 18, 1403–1414. doi: 10.1111/1462-2920.13023

Park, S. Y., and Ha, S. D. (2015). Development of an absorbance-based response model for monitoring the growth rates of *Arcobacter butzleri* as a function of temperature, pH, and NaCl concentration. *Poult. Sci.* 94, 136–143. doi: 10.3382/ps/peu022

Parsons, C., Jahanafroozi, M., and Kathariou, S. (2019). Requirement of lmo1930, a gene in the menaquinone biosynthesis operon, for esculin hydrolysis and lithium chloride tolerance in *Listeria monocytogenes*. *Microorganisms* 7:539. doi: 10.3390/microorganisms7110539

Persad, A. K., and LeJeune, J. T. (2015). "Animal reservoirs of shiga toxin-producing *Escherichia coli*," in *Enterohemorrhagic Escherichia coli and Other Shiga Toxin-Producing E. coli*, ed. V. H. Sperandio (Washington, DC: ASM Press), 211–230. doi: 10.1128/9781555818791.ch11

Quandt, R. E. (1960). Tests of the hypothesis that a linear regression system obeys two separate regimes. *J. Am. Stat. Assoc.* 55, 324–330. doi: 10.1080/01621459.1960.10482067

Ramees, T. P., Dhama, K., Karthik, K., Rathore, R. S., Kumar, A., Saminathan, M., et al. (2017). *Arcobacter*: an emerging food-borne zoonotic pathogen, its public health concerns and advances in diagnosis and control - a comprehensive review. *Vet. Q.* 37, 136–161. doi: 10.1080/01652176.2017.1323355

Rosseel, Y. (2012). lavaan: an r package for structural equation modeling. *J. Stat. Softw.* 48, 1–36. doi: 10.18637/jss.v048.i02

Roswell, M. E., Dushoff, J., and Winfree, R. (2021). A conceptual guide to measuring species diversity. *Oikos* 130, 321–338. doi: 10.1111/oik.07202

Rutter, E. B., Diaz, D. R., and Hargrave, L. M. (2022). Evaluation of Mehlich-3 for determination of cation exchange capacity in Kansas soils. *Soil Sci. Soc. Am. J.* 86, 146–156. doi: 10.1002/saj2.20354

Scallan, E., Hoekstra, R. M., Angulo, F. J., Tauxe, R. V., Widdowson, M. A., Roy, S. L., et al. (2011). Foodborne illness acquired in the United States-major pathogens. *Emerg. Infect Dis.* 17, 7–15. doi: 10.3201/eid1701.P11101

Shah, M. K., Bradshaw, R., Nyarko, E., Handy, E. T., East, C., Millner, P. D., et al. (2019). *Salmonella enterica* in soils amended with heat-treated poultry pellets survived longer than bacteria in unamended soils and more readily transferred to and persisted on spinach. *Appl. Environ. Microbiol.* 85:e334–19. doi: 10.1128/AEM.00334-19

Sharma, M., and Reynnells, R. (2016). Importance of soil amendments: survival of bacterial pathogens in manure and compost used as organic fertilizers. *Microbiol. Spectr.* 4, 1–13. doi: 10.1128/microbiolspec.PFS-0010-2015

Sharma, M., Millner, P. D., Hashem, F., Vinyard, B. T., East, C. L., Handy, E. T., et al. (2019). Survival of *Escherichia coli* in manure-amended soils is affected by spatiotemporal, agricultural, and weather factors in the Mid-Atlantic United States. *Appl. Environ. Microbiol.* 85:e2392–18. doi: 10.1128/AEM.02392-18

Sher, A. A., Ashraf, M. A., Mustafa, B. E., and Raza, M. M. (2021). Epidemiological trends of foodborne *Campylobacter* outbreaks in the United States of America, 1998-2016. *Food Microbiol.* 97:103751. doi: 10.1016/j.fm.2021.103751

Stea, E. C., Purdue, L. M., Jamieson, R. C., Yost, C. K., and Truelstrup Hansen, L. (2015). comparison of the prevalences and diversities of *Listeria* species and *Listeria monocytogenes* in an urban and a rural agricultural watershed. *Appl. Environ. Microbiol.* 81, 3812–3822. doi: 10.1128/AEM.00416-15

Strawn, L. K., Fortes, E. D., Bihn, E. A., Nightingale, K. K., Grohn, Y. T., Worobo, R. W., et al. (2013a). Landscape and meteorological factors affecting prevalence of three food-borne pathogens in fruit and vegetable farms. *Appl. Environ. Microbiol.* 79, 588–600. doi: 10.1128/AEM.02491-12

Strawn, L. K., Grohn, Y. T., Warchocki, S., Worobo, R. W., Bihn, E. A., and Wiedmann, M. (2013b). Risk factors associated with *Salmonella* and *Listeria monocytogenes* contamination of produce fields. *Appl. Environ. Microbiol.* 79, 7618–7627. doi: 10.1128/AEM.02831-13

Uljanovas, D., Golz, G., Bruckner, V., Grineviciene, A., Tamuleviciene, E., Alter, T., et al. (2021). Prevalence, antimicrobial susceptibility and virulence gene profiles of *Arcobacter* species isolated from human stool samples, foods of animal origin, ready-to-eat salad mixes and environmental water. *Gut Pathog.* 13:76. doi: 10.1186/s13099-021-00472-y

Vivant, A.-L., Garmyn, D., and Piveteau, P. (2013). *Listeria monocytogenes*, a down-to-earth pathogen. *Front. Cell Infect. Microbiol.* 3:87. doi: 10.3389/fcimb.2013.00087

Weller, D., Belias, A., Green, H., Roof, S., and Wiedmann, M. (2020). Landscape, water quality, and weather factors associated with an increased likelihood of foodborne pathogen contamination of New York streams used to source water for produce production. *Front. Sustain. Food Syst.* 3:124. doi: 10.3389/fsufs.2019.00124

Weller, D., Wiedmann, M., and Strawn, L. K. (2015a). Spatial and temporal factors associated with an increased prevalence of *Listeria monocytogenes* in New York State spinach fields. *Appl. Environ. Microbiol.* 81, 6059–6069. doi: 10.1128/AEM.01286-15

Weller, D., Wiedmann, M., and Strawn, L. K. (2015b). Irrigation is significantly associated with an increased prevalence of *Listeria monocytogenes* in produce production environments in New York State. *J. Food Prot.* 78, 1132–1141. doi: 10.4315/0362-028X.JFP-14-584

Wesley, I. V., Wells, S. J., Harmon, K. M., Green, A., Schroeder-Tucker, L., Glover, M., et al. (2000). Fecal shedding of *Campylobacter* and *Arcobacter* spp. in dairy cattle. *Appl. Environ. Microbiol.* 66, 1994–2000. doi: 10.1128/AEM.66.5.1994-2000.2000

Zeileis, A., Kleiber, C., Kraemer, W., and Hornik, K. (2003). Testing and dating of structural changes in practice. *Comput. Stat. Data Anal.* 44, 109–123. doi: 10.1016/S0167-9473(03)00030-6

Zeileis, A., Leisch, F., Hornik, K., and Kleiber, C. (2002). strucchange: an r package for testing for structural change in linear regression models. *J. Stat. Softw.* 7, 1–38. doi: 10.18637/jss.v007.i02

frontiers | Frontiers in Microbiology

TYPE Original Research
PUBLISHED 06 April 2023
DOI 10.3389/fmicb.2023.1130891

OPEN ACCESS

EDITED BY
Peng Fei,
Nanyang Institute of Technology, China

REVIEWED BY
Dorota Witkowska,
University of Warmia and Mazury in Olsztyn, Poland
Stephen Forsythe,
Foodmicrobe.com, United Kingdom

*CORRESPONDENCE
Sabrina Cadel-Six
✉ sabrina.cadelsix@anses.fr

SPECIALTY SECTION
This article was submitted to Food Microbiology, a section of the journal Frontiers in Microbiology

RECEIVED 23 December 2022
ACCEPTED 13 March 2023
PUBLISHED 06 April 2023

CITATION
De Sousa Violante M, Michel V, Romero K, Bonifait L, Baugé L, Perrin-Guyomard A, Feurer C, Radomski N, Mallet L, Mistou M-Y and Cadel-Six S (2023) Tell me if you prefer bovine or poultry sectors and I'll tell you who you are: Characterization of *Salmonella enterica* subsp. *enterica* serovar Mbandaka in France.
Front. Microbiol. 14:1130891.
doi: 10.3389/fmicb.2023.1130891

Tell me if you prefer bovine or poultry sectors and I'll tell you who you are: Characterization of *Salmonella enterica* subsp. *enterica* serovar Mbandaka in France

Madeleine De Sousa Violante[1,2], Valérie Michel[2], Karol Romero[3], Laetitia Bonifait[4], Louise Baugé[4], Agnès Perrin-Guyomard[5], Carole Feurer[6], Nicolas Radomski[7], Ludovic Mallet[8], Michel-Yves Mistou[1] and Sabrina Cadel-Six[3]*

[1]INRAE, MaIAGE, Université Paris-Saclay, Jouy-en-Josas, France, [2]ACTALIA, La Roche-sur-Foron, France, [3]Salmonella and Listeria Unit (SEL), ANSES, Laboratory for Food Safety, Maisons-Alfort, France, [4]Hygiene and Quality of Poultry and Pork Products Unit, ANSES, Ploufragan-Plouzané-Niort Laboratory, Ploufragan, France, [5]ANSES, Fougères Laboratory, National Reference Laboratory for Antimicrobial Resistance, Fougères, France, [6]IFIP–Institut du Porc, Le Rheu, France, [7]Istituto Zooprofilattico Sperimentale dell'Abruzzo e del Molise "Giuseppe Caporale" (IZSAM), National Reference Centre (NRC) for Whole Genome Sequencing of Microbial Pathogens: Data-Base and Bioinformatics Analysis (GENPAT), Teramo, Italy, [8]Institut Universitaire du Cancer de Toulouse–Oncopole, Toulouse, France

Introduction: In north-western France, *Salmonella enterica* susp. *enterica* serovar Mbandaka (*S.* Mbandaka) is most frequently isolated from bovine and dairy samples. While this serovar most often results in asymptomatic carriage, for a number of years it has caused episodes of abortions, which have serious economic consequences for the sector. Interestingly, this serovar is also isolated from *Gallus gallus* in the same geographic zone. Despite its prevalence in bovines in north-western France, *S.* Mbandaka has not been broadly studied at the genomic level, and its prevalence and host adaptation are still not fully understood.

Methods: In this study, we analyzed the genomic diversity of 304 strains of *S.* Mbandaka isolated from the bovine and poultry sectors in this area over a period of 5 years. A phylogenetic analysis was carried out and two approaches were followed to identify conserved genes and mutations related to host associations. The first approach targeted the genes compiled in the MEGARESv2, Resfinder, VFDB and SPI databases. Plasmid and phage contents were also investigated. The second approach refers to an in-house algorithm developed for this study that computes sensitivity, specificity, and accuracy of accessory genes and core variants according to predefined genomes groups.

Results and discussion: All the analyzed strains belong to the multi-locus sequence type profile ST413, and the phylogenomic analysis revealed main clustering by host (bovine and poultry), emphasizing the circulation of 12 different major clones, of which seven circulate in poultry and five in the bovine sector in France and a likely food production chain adaptation of these clones. All strains present resistance determinants including heavy metals and biocides

that could explain the ability of this serovar to survive and persist in the environment, within herds, and in food processing plants. To explore the wild animal contribution to the spread of this serovar in north-western France, we retrieved *S.* Mbandaka genomes isolated from wild birds from EnteroBase and included them in the phylogenomic analysis together with our collection. Lastly, screening of accessory genes and major variants allowed us to identify conserved specific mutations characteristic of each major cluster. These mutations could be used to design useful probes for food safety surveillance.

KEYWORDS

***S.* Mbandaka, bovine and poultry sectors, genomic analysis, clone characterization, genomic markers, host adaptation**

1. Introduction

Non-typhoidal *Salmonella* spp. is one of the most important foodborne pathogens. The bacterium *Salmonella* is commonly found in the intestines of birds and mammals where it most frequently results in asymptomatic carriage. However, it can cause disease and abortion in bovines, with resulting economic losses (Jawor et al., 2021). In food, the bacterium is mostly found in eggs, dairy products, and raw meat from chickens, turkeys, and pigs. To protect the consumer and to avoid contamination in humans, the European Parliament has implemented regulations that require the control of all foodstuffs and the absence of *Salmonella* in 25 g of test sample. Contaminated animals or food must be destroyed or withdrawn from the market if accidentally already marketed. According to the European Food Safety Authority (EFSA), there were 91,857 confirmed human salmonellosis cases in 2018 in the European Union (EU) (EFSA and ECDC, 2019). The overall economic burden is about 3 billion Euros annually (EFSA, 2014). In France, data collected by the national *Salmonella* Network in 2020 by the French Food Safety Laboratory shows that the sectors most affected by *Salmonella* are the poultry and bovine sectors, and the most frequently isolated serovars are Senftenberg, Montevideo, Livingstone, Dublin, and Mbandaka (*Salmonella* Network Data Report, 2020[1] and Leclerc et al., 2019). The first four of these serovars have been discussed in the literature (Acosta et al., 2017; Guillen et al., 2020; Sekhon et al., 2020, 2021; Bonifait et al., 2021; Kent et al., 2021), but Mbandaka is a poorly studied serovar even though it is the fifth most frequently isolated serovar in livestock and in the animal production sector in France. *Salmonella* Mbandaka, *S.* Montevideo, and *S.* Dublin account for 66% of the strains isolated in the bovine sector (n = 422/639 strains in 2020) (*Salmonella* Network Data Report, 2020)[1]. The *Salmonella* strains collected in the bovine sector originate mainly from samples taken from sick animals and their breeding environment (Peek and Divers, 2016). In adult bovines, clinical signs include fever followed by going off feed, diarrhea with varying amounts of blood, mucus, and shreds of intestinal lining. In milking animals, milk production drops severely (Peek and Divers, 2016). Clinical illness usually lasts for 7–10 days, with recovery in 2 to 3 weeks. Some animals, however, never resume full production. Sick cows that recover may become carriers that shed *Salmonella* for varying periods (e.g., *S.* Typhimurium is shed from 3 to 6 + months, while *S.* Dublin is shed for life) (Kirchner et al., 2012; Holschbach and Peek, 2018). Abortions may occur in infected bovines (Holschbach and Peek, 2018). In north-western France (ISO 3166-2 Metropolitan departments 22 and 35), starting from the spring of 2018, strains of *S.* Mbandaka have also been associated with cases of abortion (personal data). In addition to the economic losses for cow breeders linked to the presence of sick animals on the farm, the presence of *S.* Mbandaka is an additional constraint for producers of milk, dairy products, and cheese in France. According to data from the *Salmonella* Network, 32% (n = 480/1,489) of the isolates collected between 2010 and 2020 originated from dairy cows and 14% (n = 210/1,489) from milk, dairy products, and cheese (Personal data from the *Salmonella* network, **Supplementary Figure 1**).

The *S.* Mbandaka serovar is also associated with the poultry sector in France. Since 2010, it has appeared among the top 10 most isolated serovars in poultry from animals and from the production sector. However, it is mainly found in the breeding sector and is rarely isolated from meat and egg products. According to data from the *Salmonella* Network, 98% (n = 4,741/4,837) of the isolates collected between 2010 and 2020 comes from animal and poultry breading environment and only 2% (n = 96/4,837) from poultry meat and egg products (Personal data from the *Salmonella* network, **Supplementary Figure 1**). Unlike bovines, poultry are asymptomatic carriers of *Salmonella*. Affected animals may therefore contaminate bovines on mixed farms. Furthermore, recent studies conducted in the United States and Japan on the persistence of *Salmonella* in feces from bovines and various wild animals (crows, deer, feral pigs, raccoons, and waterfowl) have shown that wild animals can also represent a risk of contamination for producers. *Salmonella* can in fact survive in feces for several months and contaminate the farm environment and pastures (Topalcengiz et al., 2020; Yamaguchi et al., 2022).

Certain serovars are able to adapt to several hosts (Stevens and Kingsley, 2021). For example, we have shown that the *S.* Derby serovar isolated in France has adapted to both porcine and *Gallus gallus* hosts, with different genomic clones circulating in the pork and poultry sectors. These clones are characterized by different

1 https://www.anses.fr/fr/content/inventaire-des-salmonella-dorigine-non-humaine

sequence types (STs): *S.* Derby ST40 is most frequently isolated in the pork sector, and *S.* Derby ST71 in the poultry sector (Sevellec et al., 2018a). The genomic differences between the lineages mainly concern the presence or absence of *Salmonella* pathogenicity islands (SPIs), characteristic substitutions in the *fim*H alleles, and heterogeneity in prophage sequence content (Zheng et al., 2017; Sevellec et al., 2018b).

The aim of this study was to investigate the genomic diversity of the *S.* Mbandaka serovar using a large dataset (n = 304) representative of the bovine and poultry production sectors in the north-western production area of France, where this serovar is frequently isolated. The collection was investigated by multi-locus sequence type (MLST) and single nucleotide polymorphism (SNP) analyses. Because resistance of *Salmonella* to antimicrobial agents is a worldwide problem, identification of acquired antimicrobial resistance gene was investigated. We also explored the detection and characterization of SPIs, coding for virulence factors involved in adhesion and invasion of the host, and of the *fim*H gene, known to be a marker of host specificity within *Salmonella*. Genes conferring resistance to heavy metals and biocides, phage sequences, and plasmid content were also evaluated to characterize this poorly studied serovar and to identify potential genome signatures responsible for host specificity of *S.* Mbandaka for bovines and poultry. To increase the chances of finding differences in this serovar's genome, a host pattern investigation analysis was carried out with an in-house pipeline developed in this study, to identify accessory genes and core variants according to predefined groups of genomes.

2. Materials and methods

2.1. Strain dataset for France

The panel of 304 *Salmonella enterica* subsp. *enterica* Mbandaka strains analyzed in this study with their metadata (ID, sample name, ID owner, country, collection year, and origin) is presented in **Supplementary Table 1** ("Sample DATA" tab). These strains were isolated over a period of 6 years, from 2016 to 2021. Among the panel selected, 140 strains were isolated from the bovine sector and 164 from poultry. All the bovine strains were collected from north-western France, in the *Normandie* region where this serovar is prevalent for bovine sector. The poultry strains, to be compared with bovine strains, were collected mainly (70%) from north-western France to can compare the genomic poultry profiles with the bovine ones but also in the *Pays de la Loire* (n = 47), *Bretagne* (n = 34), and *Normandie* (n = 32) regions. The resting 51 poultry strains were collected elsewhere in France, such as in the *Hauts-de-France*, *Auvergne-Rhône-Alpes*, *Grand Est* or *Occitanie* regions. The number of poultry strains in each region was selected proportionally to its production level compared to the total national production for the poultry sector, with samples isolated both from broilers and layers. One strain of duck and five strains of turkey isolated in north-western France were also included in the panel. The strains from bovine sector come from self-checks carried out at the producers, the ones from poultry sector come from the national surveillance plans carried out for *Salmonella* by the regulation (EC) 2,160/2,003. In both cases, the strains were isolated according to the standard ISO 6579-1 or NF U 47-100 with the scheme of White-Kauffman Le-Minor (Grimont and Weill, 2007).

2.2. Sequencing and assembly

All strains were sequenced using Illumina chemistry producing paired end reads as described by Radomski et al. (2019).

Genome assemblies were generated using an in-house workflow called ARTwork (Vila Nova et al., 2019).[2] The raw reads were normalized to 100× with Bbnorm using the *S.* Mbandaka SA20026234 reference complete genome (NCBI ID CP022489). Then, Trimmomatic (Bolger et al., 2014) was used for the trimming step. The applied quality rules were: (1) length of read higher than or equal to 50 base pairs (bp) otherwise excluded, (2) phred score per base higher than or equal to 30×, and (3) filter away adapters based on an internal database with Illumina adapters. FastQC version 0.11.5 was used to check the read quality and ConFindr to identify intra- and cross-species contamination (Low et al., 2019). SPAdes 3.11.05 was then used to perform *de novo* assembly (Bankevich et al., 2012). Medusa and Gapcloser were used to optimize and finish the assembly (Kremer et al., 2017). Subsequently, QUAST was used to evaluate the quality of *de novo* assemblies by identifying misassemblies and determining error rates (Gurevich et al., 2013). All assemblies were confirmed as belonging to the *S.* Mbandaka serovar with the SeqSero2 tool (Zhang et al., 2019).

Read and assembly quality of the 304 genomes retained in the study is reported in **Supplementary Table 1** ("Genome DATA" tab).

2.3. Core genome analysis

2.3.1. Multi-locus sequence typing (MLST)

All genomes were characterized by *in silico* MLST using the seven housekeeping gene sequences (*aro*C, *dna*N, *hem*D, *his*D, *pur*E, *suc*A, and *thr*A) described in the PubMLST database (Jolley and Maiden, 2010). The sequence type (ST) of each genome was obtained with the MLST tseeman tool.[3]

2.3.2. Variant calling (SNPs)

The core genome SNPs and small InDels were detected based on the variant caller HaplotypeCaller implemented in the iVARCall2 workflow (Felten et al., 2017). The *S.* Mbandaka strain SA20026234 (accession number CP022489.1) was used as reference complete genome referring to the studies previously published by Cherchame et al. (2022b), and following the best practices proposed by the Genome Analysis ToolKit (GATK) (McKenna et al., 2010). More precisely, secondary alignments around small InDels were performed, and duplications were excluded before variant calling analysis

2 https://github.com/afelten-Anses/ARtWORK

3 https://github.com/tseemann/mlst

via local *de novo* assembly of haplotypes in active regions. The matrices of pairwise SNP differences and pseudogenomes were computed using the scripts called "VCFtoMATRIX" and "VCFtoPseudoGenome."[4]

2.3.3. Phylogenomic inference and calculation of bootstrap support

Phylogenomic inferences were performed by maximum likelihood based on SNP alignment produced by the iVARCall2 workflow and the transversional model TVM + F implemented in the IQ-TREE program (Nguyen et al., 2015). Node support was evaluated with 1,000 rapid bootstrap inferences (Nguyen et al., 2015). Phylogenetic trees were visualized and annotated using interactive Tree Of Life[5] (Letunic and Bork, 2016).

2.4. Accessory genome analysis

2.4.1. Identification of virulence factors and resistance genes

All genomes from France were screened for the presence/absence of genes mediating resistance and virulence using ABRICATE.[6] ABRICATE was used against the VFDB database (Chen et al., 2016) available at the Institute of Pathogen Biology (Beijing, China), MEGAResV2 (Doster et al., 2020), ResFinder (Zankari et al., 2012), and SPIFinder (Roer et al., 2016), available at the Center for Genomic Epidemiology (CGE) (Denmark). The ABRICATE outputs displayed only the genes detected in at least one genome of the analyzed panel. The threshold was set at 90% identity over at least 3/5 of the length of the gene or genomic region.

Particular attention was paid to the FimH sequence. The *fim*H gene sequence was isolated from the PRJNA297164 project and searched in all 304 *S.* Mbandaka genomes using the BLAST tool (Camacho et al., 2009). All nucleotide sequences found were translated and compared to determine SNP differences between poultry and bovine hosts.

2.4.2. Plasmid identification

All the assemblies were further analyzed to characterize the presence of mobile genetic elements (MGE). MOB-suite tools (Robertson and Nash, 2018) were used to identify plasmid markers. Putative plasmids were blasted against the NCBI nucleotide archive to identify the closest plasmid neighbors.

2.4.3. Phage identification

The presence of phage sequences in the assemblies of French *S.* Mbandaka strains was investigated using the PHASTER online application (Arndt et al., 2016). Only prophages identified as "intact" were considered.

2.5. Genome association analysis

Unique markers (genes and variants) and combinations were both investigated to find a genomic pattern of host adaptation (bovine and poultry).

For unique genes, GFF files of all genomes produced by Prokka[7] were computed by Panaroo (Tonkin-Hill et al., 2020), a graph-based pangenome clustering tool that is able to account for errors introduced during annotation. The clustering identity threshold was increased to 90%. For unique variants, VCF files from iVARCall2 were merged to identify the presence and absence of variants in each genome. The position of variants was identified in *S.* Mbandaka SA20026234. Genes identified by Panaroo or genes containing discriminating variants were annotated using BLAST and UniProt (UniProt, 2021).

To explore possible combinations of markers for host adaptation, we developed a python 3 script called MarkerFinder. MarkerFinder computes the combination of maximum 3 genes or variants with the best discrimination accuracy score according to a phenotypic criterion (in this study, the host origin). MarkerFinder needs two input files: a csv file with the list of genes or variants (produced as described above as outputs by Panaroo and iVarCall2, respectively) and the Excel file compiled with the corresponding phenotype (bovine and poultry in this study). The MarkerFinder output txt file compiles the best combination of maximum three genes or variants found, with accuracy scores, as well as specificity and sensitivity values. The accuracy score was calculated as follow: (TP + TN)/(TP + TN + FP + FN) with TP corresponding to "true-positive result," TN to "true-negative result," FP to "false-positive result," and FN to "false-negative result." Sensitivity was calculated as TP/(TP + FN) and specificity as TN/(FP + TN). A false-positive result is defined as a positive signal for an identification assay for a gene or variant belonging to a non-targeted phenotype. A false-negative result is defined as a negative result for a gene or variant belonging to the targeted phenotype.

The MarkerFinder tool developed is available at https://github.com/madeleinevlt/MarkerFindr.

2.6. Worldwide wild animal genome dataset and phylogenetic analysis

To explore the hypothesis of possible cross-contamination between wild and farm animals, we extracted, from the open access Salmonella EnteroBase database, 2,465 genomes in row reads (on October 2021) whose serovar was confirmed as S. Mbandaka, the MLST profile as ST413, and epidemiologic information-host or country of isolation-available. Among these genomes, 42 were retained because they were isolated from wild animals, with 10 genomes from "Avian," 2 from "Canine," 2 from "Marsupial," 4 from "Reptile," and 23 "No-determined." Among these 42 genomes, none were isolated from France or Europe. Finally, considering that only Aves could have been physically responsible for contamination between different continents, we chose nine of the ten genomes from strains isolated from wild birds ("Avian"). One genome was

4 https://github.com/afelten-Anses/VARtools/tree/master/iVARCall2

5 iTOL https://itol.embl.de/

6 https://github.com/tseemann/abricate

7 https://github.com/tseemann/prokka

retried due to read errors. Among the final nine genomes selected, six were from coastal regions with five genomes coming from strains isolated along the east coast of North America and one from the west coast. Six genomes were from the United States, two from Canada, and one from Mexico. The accession numbers and epidemiologic information for these genomes are reported in **Supplementary Table 1** ("Wild animal DATA" tab).

The variant calling (SNPs) phylogenetic analysis was carried out as described above with the nine genomes from North America and a subset of 214 genomes from France. These 214 genomes (n = 100 bovine, n = 114 poultry) were selected from the total panel of 304 genomes so that they were representative of the different groups identified by the phylogenetic analysis of bovine and avian strains from France. All singletons were also included (n = 41). The S. Mbandaka 100,727 strain (NCBI ID SRR6860551, uploaded at 11/01/2022) belonging to ST506 was also included to root the tree.

3. Results

3.1. Sequence type genetic diversity and SNP core genome phylogenetic analysis

All 304 *S.* Mbandaka genomes belong to the MLST profile ST413. To investigate the genome diversity of the dataset and identify clustering revealing possible host adaptation, a maximum likelihood phylogenetic tree was built taking into account core genome SNP distances. The tree was rooted using the strain *S.* Mbandaka 100,727 (NCBI ID SRR6860551) belonging to ST506. This ST was identified as genetically closest to ST413 according to hierarchical clustering (HC) cgMLST EnteroBase analysis (Zhou et al., 2020) (data not shown). The phylogenetic analysis revealed 12 major groups supported by 100% bootstrap values and each containing more than five strains. Among these 12 groups, seven groups (A, B, C, D, F, H, and K) contained 118 out of a total of 164 (72%) analyzed genomes sampled from poultry. These seven groups were characterized by genome distances comprised between 5 and 68 SNPs. The other five groups (E, G, I, J, and L) contained 134 bovine genomes over the total 140 bovine genomes analyzed (95%). These five groups were characterized by genome distances comprised between 12 and 34 SNPs (**Figure 1**). Among poultry samples, 40 did not cluster in any group, while among bovine samples, only 1 genome did not cluster. The maximum SNP distance between all 140 bovine samples was 163 SNPs, whereas all 164 poultry samples had a maximum SNP distance up to 214 SNPs. Interestingly, poultry samples were collected from a wider geographic zone than bovine samples (**Supplementary Figure 2**). This could explain the higher SNP differences calculated between poultry genomes. Finally, only six poultry samples clustered in bovine groups, while five bovine samples clustered in poultry groups. The six poultry samples clustering within bovine groups were all isolated in the same geographic region (*Normandie,* ISO 3166-2 FR-NOR). Of these six poultry samples, two (S17LNR0975 and S16LNR1497) were genetically close to bovine samples isolated from feces and four (S17LNR0564, S19LNR1916, S18LNR1821, and S17LNR0496) were close to bovine samples isolated from milk. The SNP differences between these samples and the closest bovine samples were comprised between 20 and 38 SNPs. The five bovine samples clustered in poultry groups were all isolated from the same geographic region (*Normandie*). Of these five bovine samples, four (ACT1919926, ACT1919928, ACT1919929, and ACT1919833) were isolated from manure and feces. The last bovine sample (ACT20SMb25) was isolated from bovine feed. The SNP differences between these bovine samples and the closest poultry samples were comprised between 10 and 45 SNPs (**Figure 1** and **Supplementary Figure 2**).

Among the seven poultry groups identified (A, B, C, D, F, H, and K) only group H was characterized by samples isolated from the same region (*Hauts-de-France*). For the bovine groups identified (E, G, I, J, and L), all the samples were isolated in the same region (*Normandie*). Interestingly, in group L, one isolate from cheese (ACT20SMb44) displays only 3 SNP difference with a milk isolate (ACT20SMb64), suggesting likely contamination through the food chain. In the same way, in group J, samples from different matrices (manure, milk, processing plant, and cheese) isolated between 2019 and 2020 clustered together with a mean distance of 12 SNPs (**Figure 1** and **Supplementary Figure 2**).

3.2. Accessory genome analyses

The virulome and accessory genome were analyzed to better characterize this serovar and to identify possible genomic differences between strains isolated from the bovine and poultry sectors. Two approaches were followed to identify conserved genes and mutations related to possible bovine and poultry host associations within *S.* Mbandaka strains. The first approach, described in this paragraph, explores the presence/absence of virulence and resistance genes compiled in open access databases targeting known virulence factors, SPI genes, multi-drug resistance genes, and genes conferring heavy metal or biocide resistance. Plasmid and phage sequences were also queried. The second approach, described below, refers to a genomic pattern analysis that computes statistical sensitivity, specificity, and accuracy of accessory genes and core variants according to host associations and specific phylogenetic groups identified.

3.2.1. Virulome analysis

Infection of cells by *Salmonella* requires different steps. After moving to reach epithelial intestine target cells with its flagella, adhesion factors, such as fimbriae and adhesins present on the *S.* Mbandaka surface, enabling strong attachment to the surface of host cells. Gene clusters *csg*, *fim*, *bcf,* and *lpf*, coding for both curli and chaperonne/placier type fimbriae were found in all analyzed strains from France and, although genes coding for SPI-3 were not observed as a whole, *mis*L and *mgt*CB genes coding for adhesins were also observed in the dataset (**Supplementary Table 2**, "SPI" and "vfdb" tabs). The *fim*H gene was identified in all genomes, and comparison of translated sequences revealed no mutations that could be associated with any bovine or avian host. Only one sequence revealed 1 SNP mutation (i.e., poultry ACT20SMb17 *fim*H nucleotide sequence), but this mutation is synonymous.

Combined analysis of the BLAST results obtained by the SPIFinder and VFDB databases with both thresholds set at 90% identity and 80% identity (data not shown) revealed that SPI-1, SPI-2, SPI-4, and SPI-9, coding for type III (T3SS-1 and T3SS-2)

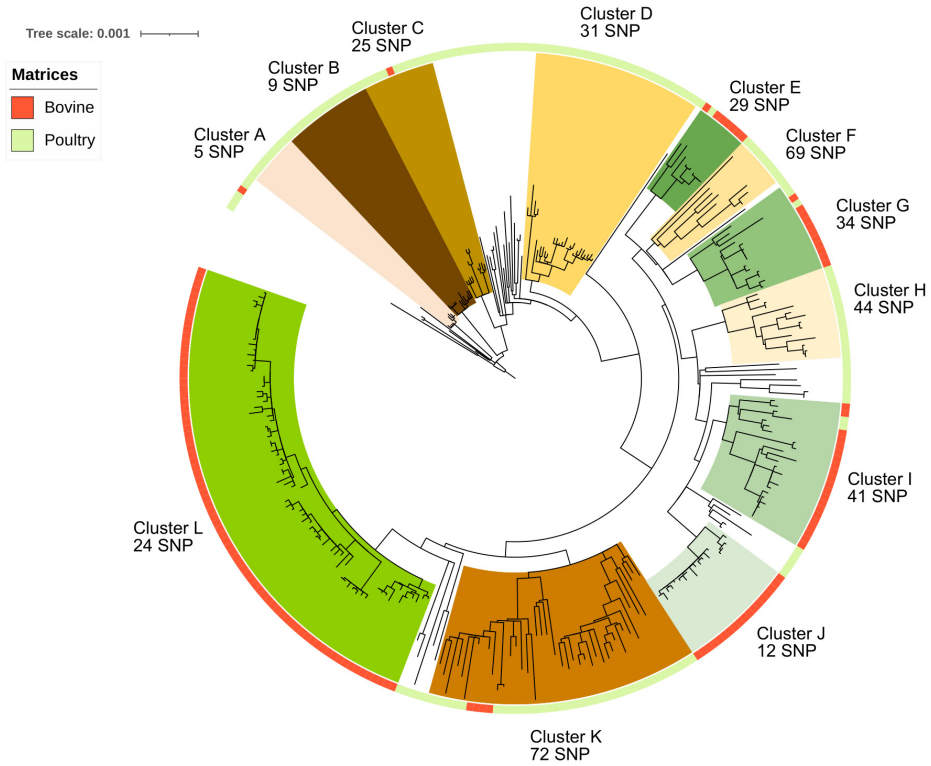

FIGURE 1
Phylogenetic reconstruction based on core-genome single nucleotide polymorphism substitutions of the 304 *Salmonella* Mbandaka strains isolated in France between 2016 and 2021 from the bovine and poultry sectors. The maximum likelihood criterion and the transversional model TVM + F model were applied. *Salmonella* Mbandaka SA20026234 was used as the reference complete genome. The source of the strains (bovine and poultry) is indicated in the ring around the tree. The 12 genomic groups identified with their intergenomic mean SNP values are indicated by different names and colors for a better visualization.

and type I secretory apparatus (T1SS) responsible for survival and proliferation in various intracellular environments, were identified in all the *S.* Mbandaka genomes (**Supplementary Table 2**, "SPI" and "VFDB" tabs).

SPI-1 genes, encoding T3SS-1 apparatus that is required for invasion of intestinal epithelium cells, such as *inv, prg*, and *org* gene clusters and *sic*A, *sip*ABCD, *ssp*ABC, *sop*B, *sop*E, and *sop*E2 regulator/effector genes were identified in all genomes. In the same way, SPI-2 genes encoding components of the T3SS-2 apparatus required for bacterial virulence and proliferation in macrophages, such as *ssa*, *ssc*, and *sse* gene clusters and *pip*B, *pip*B2, and *sox*S regulator genes were also identified within all genomes from France (**Supplementary Table 2**, "SPI" and "VFDB" tabs). Interestingly, the *sii*ABCDEF SPI-4 gene cluster, encoding a type I secretion apparatus that contributes to the colonization of bovine intestines, was also observed in the dataset, with the exception of five out of the 164 poultry genomes. The few inconsistencies between BLAST results of SPIFinder and VFDB could be explained by the use of different alleles for the same gene in the two databases. It is also important to take into account the identity percentage applied to the analyses. Likewise, only an in-depth analysis of the sequences of these gene clusters within each genome could highlight either SNP or indell type differences between the strains or possible recombination events. Additionally, even though SPI-9 was identified by the SPIFinder database BLAST analysis, operon STY2876, STY2877, STY2878, and STY2875 were not displayed by VFDB BLAST analysis. This inconsistency could be explained by the fact that the ORFs of SPI-9, STY2876, STY2877, and STY2878 present 98% identity with type 1 secretory apparatus (T1SS) genes of SPI-1, inducing likely confusing results. However, further in-depth sequence analyses would be needed to corroborate or rule out this hypothesis (**Supplementary Table 2**, "SPI" and "VFDB" tabs).

3.2.2. Biocide and heavy metal resistance analysis

At least four of the six genes (*ydd*G, *baeR, bae*S, *sod*A, *rpo*S, and *smv*A) involved in biocide resistance activity were identified within all genomes. Of these six genes, three (*ydd*G, *baeR*, and *bae*S) are described in the literature as involved in methyl viologen dichloride hydrate (paraquat herbicide) resistance (Baranova and Nikaido, 2002; Santiviago et al., 2002). All 140 bovine genomes have these three genes, one poultry genome lacks the *ydd*G gene (S20LNRO591), and one lacks the *bae*R and *bae*S genes (S16LNR1426). The other three genes (*sod*A, *rpo*S, and *smv*A) code for peroxide, hydrogen peroxide, and monochloramine-cation biocide resistances, respectively (Gao et al., 2019; Wand et al., 2019). All genomes have the *sod*A gene coding for peroxide resistance. Only one poultry genome lacks *smv*A (S20LNR0591) coding for monochloramine, and 14 genomes (7 poultry and 7 bovine genomes) have the *rpo*S gene coding for hydrogen peroxide.

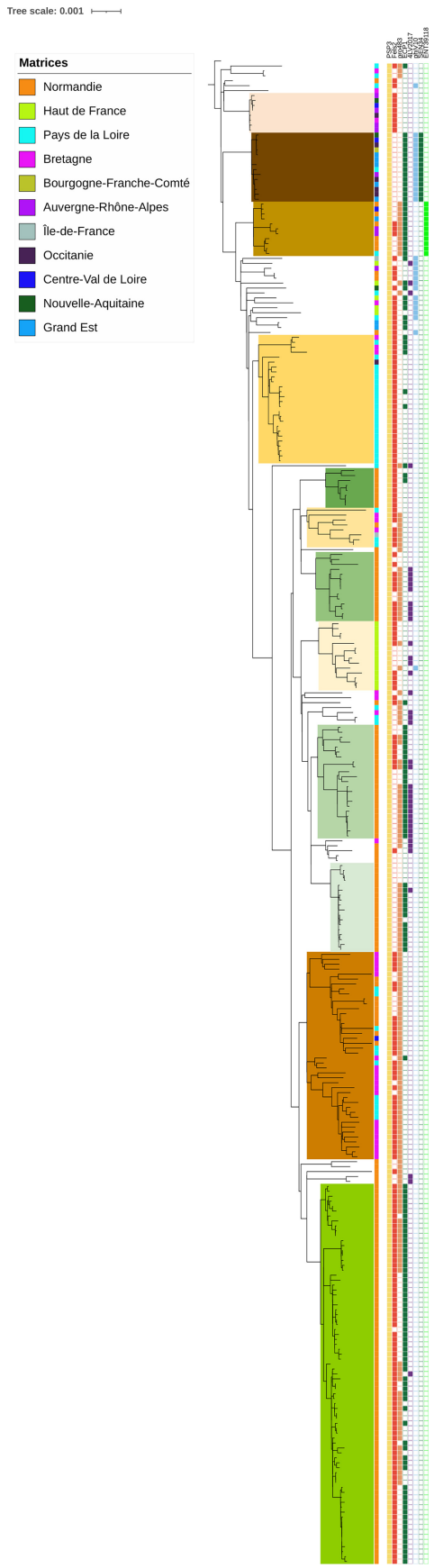

FIGURE 2
Continued

FIGURE 2
Phylogenetic reconstruction based on core-genome single nucleotide polymorphism substitutions of 304 *Salmonella* Mbandaka strains including the genomic groups identified, geographic origin, and phage profiles. The maximum likelihood criterion and the transversional model TVM + F model were applied. *Salmonella* Mbandaka SA20026234 was used as the reference complete genome.

The *Salmonella* iron transporter gene cluster *sit*ABCD, coding for a periplasmic ATP-binding- protein, previously identified in *S.* Typhimurium (Kehres et al., 2002) was also identified in all genomes. Interestingly, in line with iron cytoplasm starvation, the *ent*B gene coding for the *Escherichia coli* catecholate siderophore enterobactin (Pakarian and Pawelek, 2016) was identified in all genomes with 80% identity (data not showed), such as the *fep*CG genes that code for ferric enterobactin transport ATP-binding proteins.

Several heavy metal resistance genes were identified. Genes implied in cobalt/magnesium resistance (*cor*ABCD), gold resistance (*ges*ABC and *gol*ST), arsenic (*pst*B), and copper (*cui*D and *cue*P) resistances were found in all genomes. The *mer*CRT genes implied in mercury resistance were also found in only one strain isolated from poultry (S18LNR1211). This last strain also presents the tetracycline, sulphonamide, and aminoglycoside resistance genes *tet*AB, *sul*1, and *ant*3-D, respectively (**Supplementary Table 2**, "MEGAResV2" tab).

3.2.3. Antibiotic resistance gene analysis

All genomes possessed the cryptic aminoglycoside resistance gene aac(6′)-Iaa (**Supplementary Table 2**, "ResFinder" tab). The ten poultry samples of genomic group D present the plasmid p15ODMR carrying genes conferring resistance to ampicillin (*bla*TEM-1b), sulfonamide (*sul*2), streptomycin (*aph*(6)-Id), tetracycline (*tet*(A)), and trimethoprim (*dfr*A14). The poultry strain S18LNR1211 presents tetracycline, sulfonamide, and aminoglucoside resistance genes *tet*AB, *sul*1, and *ant*3-D' (**Supplementary Table 2**, "ResFinder" and "MOB-suite tool–Plasmid" tabs). Mutations on the topoisomerase genes *gyr*A, *gyr*B, and *par*C were identified by MEGAResV2 analysis within all genomes, but they were not associated with fluoroquinolone resistance (**Supplementary Table 2**, "ResFinder" and "MEGAResV2" tabs). The phenotype of six strains (2021LSAL06158, 2021LSAL06159, 2021LSAL06162, 2019LSAL01500, 2021LSAL06165, and 2021LSAL06166) were analyzed by antimicrobial susceptibility tests confirming these results (data not shown).

3.2.4. Plasmid analysis

The plasmid identification carried out by MOB-suite allows for identification of the plasmid contents in genomes and their mobility. In all, 36 mobilizable, 23 conjugative, and 159 non-mobilizable plasmids were identified. The p15ODMR plasmid present in ten poultry strains of genomic group D carrying multi-drug resistance genes, was characterized as non-mobilizable missing both relaxase and the *oriT* gene. The non-mobilizable plasmid p-F219, previously associated with the epidemic multi-drug-resistance strain of *S.* Infantis isolated from a small farm in

the southern region of Peru in 2017 (Vallejos-Sanchez et al., 2019), was identified in 285 genomes in our panel (122 bovines and 163 poultry). The pSLU-1913 conjugative plasmid previously described in *S.* Montevideo strains was identified in 27 strains in our panel, 18 from the bovine sector and 9 from poultry (Bugarel et al., 2019; **Supplementary Table 2**, "MOB-suite tool–Plasmid" tab).

3.2.5. Phage analysis

Eight phages were identified among the *S.* Mbandaka genomes in our panel (**Figure 2**; **Supplementary Table 2**, "Phage" tab). One of them, *Salmonella* phage PSP3 was detected in all samples. This phage, belonging to the P2-like phage family, is widely spread within other *Salmonella* serovars (Bullas et al., 1991). The other phages identified were Fels2 (in 207 genomes), pro483 (in 161 genomes), ECP1 (148 genomes), 4LV2017 (41 genomes), phiV10 (29 genomes), SEN34 (14 genomes), and ENT39118 (11 genomes). All these phages are known among *Salmonella* serovars, but some of them such as phiV10 have a high number of genes in common with *E. coli* specific phages (Kim et al., 2017 Phage). Interestingly, the three phages phiV10, SEN34, and ENT39118 were observed only in the genomes of strains isolated from poultry, with the exception of one strain (ACT20SMb25 presenting the phage ENT39118), which was isolated from animal feed on a bovine farm. We did not observe geographic distribution of the phages within the genomes analyzed; however, some of the groups identified were characterized by specific phage profiles such as groups A, D, and E, characterized by phages PSP3 and Fels2, group B characterized by phages PSP3, ECP1, phiV10, and SEN34, or group F characterized by phages PSP3, Fels2, and pro483.

3.3. Genes and variants as discrimination markers for hosts

Unique markers and combination of genes or variants were investigated to discriminate host source (bovines and poultry) within our panel of 304 genomes. Any unique marker (gene or variant) was searched among the 5,833 genes and the 3,922 variants identified by the Panaroo analysis. Combinations of genes and variants were identified, allowing us to discriminate the bovine and poultry host source of strains (**Table 1**). For gene contents, the best combination of genes proposed to discriminate samples from bovines from those originating from poultry hosts was composed of three genes with an accuracy of 0.92, with 91% inclusivity (127/140 bovines identified) and 96% exclusivity (11 false positives) (**Table 1**).

The genes identified for the combinations correspond to genes acquired by phages and belong to the accessory genome. For variants content, the best combination identified with two variants has an accuracy of 0.91 and the best combination with three variants displays an accuracy of 0.95, with 95% inclusivity and 97% exclusivity. The three variants identified are in position 199,204, 1,567,699, and 3,213,391 in the genome of *Salmonella* Mbandaka SA20026234. All these variants are located in coding *Salmonella* chromosome sequences. Interestingly, the variant at position 199,204 is located on a gene of SPI2, coding for the type III secretion system protein, which is known to be directly involved in invasion by the bacterium (Jennings et al., 2017). The variant at position 1,567,699 is located on a gene involved in alkyl hydroperoxide resistance, and the variant at position 3,213,391 on a gene coding for a methyl-accepting chemotaxis protein. Further analyses would be needed to determine whether these SNP variations have an impact on the coded proteins.

Finally, with the aim of tracking the *S.* Mbandaka genomic clones belonging to the 12 phylogenomic groups identified in our panel, and without resorting to whole-genome sequencing, we explored the possibility of identifying each group with unique markers of genes and variants (**Supplementary Table 3**). Using gene content, groups A, B, C, and E can be identified by one unique gene, with 100% inclusivity and 100% exclusivity. Groups F and J can be identified by one unique gene, with 100% inclusivity and 99.7% exclusivity. Group G can be identified with one unique gene with 78% inclusivity and 100% exclusivity. Other groups could not been identified by one unique gene but by unique variants that are able to discriminate these groups and display 100% inclusivity and 100% exclusivity (**Supplementary Table 3**).

3.4. Investigation of wild animal contamination in French herds

The nine North American genomes from wild birds selected from the *Salmonella* EnteroBase database clustered together with six genomes from France (five poultry samples and one bovine) (**Figure 3**). Interestingly, the genomes from France were from strains isolated on farms close to the west coast or along a river that flows to this coast. Among the five poultry samples, strains S18LNR1211 and S16LNR3059 were isolated from farms located close to the Atlantic coast in *Bretagne*. Strain 2019LSAL01500 was sampled in the same region and the last two strains S18LNR0214 and S18LNR1879 were isolated further inland, but along a river that flows to the Atlantic coast. Bovine sample ACT1919846 was isolated from manure close to the north-western coast in the *Normandie* region. The mean SNP difference between all these 13 genomes was 57 SNPs (with values ranging from a minimum of 39 to a maximum of 105 SNPs).

4. Discussion and conclusion

Phylogenetic analyses carried out on the 304 genomes of *S.* Mbandaka isolated from the bovine and poultry sectors in north-western France revealed strong MLST profile homogeneity. All the bovine isolates belonged to the ST413 profile and, among all poultry strains, isolated in the same period and geographic zone, only five were of different MLST profiles (data not shown). Despite this homogeneity, our panel of strains revealed twelve different clones with a likely degree of adaptation to bovine and avian hosts: 95% of bovine genomes (134/140) clustered into five groups characterized by genome distances of between 12 and 34 SNPs, and 72% of the poultry genomes (118/164) clustered into seven genomic groups characterized by genome distances of between 5 and 68 SNPs. All these twelve groups were supported by 100% bootstrap values. The higher number of genomic groups identified among poultry strains (i.e., 7 poultry groups vs. 5 bovine groups) is likely due to the higher geographic heterogeneity of the samples

TABLE 1 Duo and trio combinations of genes and variants for host identification (bovine and poultry) within *S.* Mbandaka strains of sequence type ST413 from France.

	Panaroo name	Source		Accurancy	Inclusivity	Exclusivity	Annotation by Uniprot	Definition/Function	Position[b]	Gene length (bp)	References
		Bovine	Poultry								
Gene	group_716	+	–	0.92	91%	96%	nd	Phage tail protein of *Klebsiella* phage 4LV2017 and *Salmonella* phage RE2010		486	Villa et al., 2017
	group_2947	+	–				*mEp*235_051	Portal protein/uncharacterized protein found in *Enterobacteriaceae* phage mEp235		270	https://www.ncbi.nlm.nih.gov/nuccore/428781810
	group_2909	+	–				AMBK_57	DNA replication protein O found in *Salmonella* phage vB_SosS_Oslo		279	Ho et al., 2012
Variants[a]	1567699_G_T	+	–	0.91	87%	96%	STM1546[a]	Protein involved in DNA protection against damage by alkyl hydroperoxides	1,566,277–1,567,785	1,508	McClelland et al., 2001
	3213391_T_C	+	–				*tsr*	Serine sensor receptor / methyl-accepting chemotaxis protein I	3,212,787–3,214,448	1,661	McClelland et al., 2001
	199204_C_T	+	–	0.95	95%	97%	*prg*H	SPI2 Type III secretion system inner membrane ring protein PrgH	198,059–199,237	1,178	Burkinshaw and Strynadka, 2014

The duo of genes or variants is framed by a black dotted line as well as the corresponding accuracy, inclusivity, and exclusivity values.
The trio of genes or variants is framed by a gray line as well as the corresponding accuracy, inclusivity, and exclusivity values.
[a]99% identity found.
[b]Reference genome *Salmonella* Mbandaka SA20026234.
nd: Gene name not determined.

10.3389/fmicb.2023.1130891

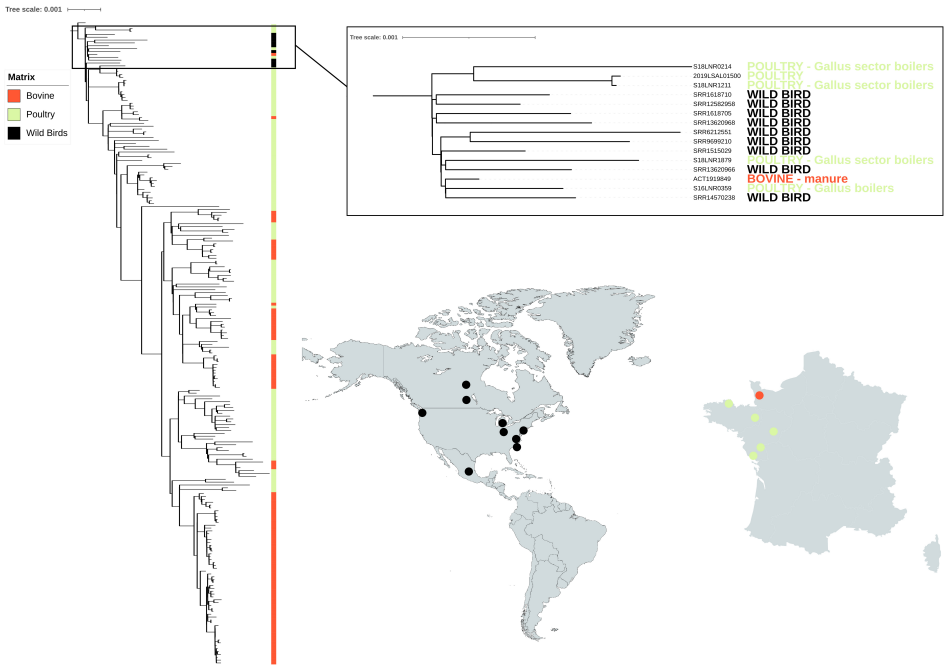

FIGURE 3
Phylogenetic reconstruction based on core-genome single nucleotide polymorphism substitutions of the 214 *Salmonella* Mbandaka strains from France isolated from the bovine and poultry sectors and nine North American strains isolated from wild birds. The genomes (n = 100 bovine, n = 114 poultry) were selected so that they were representative of the different groups identified by the phylogenetic analysis of the 304 bovine and avian strains (see **Figure 1**). All singletons were also included (n = 41). The maximum likelihood criterion and the transversional model TVM + F model were applied. *Salmonella* Mbandaka SA20026234 was used as the reference complete genome.

(i.e., seven different regions versus one for bovine samples) and to the higher number of sample analyzed (i.e., 164 poultry sample versus 140 bovine ones). Given that the samples were isolated over a period of 6 years (between 2016 and 2021) from different matrices, the differences in SNPs observed between the samples within the same group are consistent with those observed for other *Salmonella* serovars such as Typhimurium, Derby or Welikade (Sevellec et al., 2020; Cadel-Six et al., 2021; Cherchame et al., 2022a). The pathways that bacterial pathogens take from farm to fork can be complex, and bacteria can undergo evolutionary changes, especially over long periods. The scientific community agrees that few SNP differences (usually 10 SNPs maximum) closely define related isolates, increasing the likelihood that they arose from the same source (Pightling et al., 2018). The presence of many (hundreds or more) SNPs indicates that isolates are distantly related, implying that they did not originate from the same reservoir population. Interestingly, within bovine strains, in a genomic group identified (i.e., cluster J), only 12 SNPs were recorded between samples from different matrices (manure, milk, processing plant, and cheese) isolated between 2019 and 2020 and only three SNPs were observed between two samples (i.e., cluster L), one from cheese (ACT20SMb44), and one from milk (ACT20SMb64) isolated in 2018 and 2019, respectively. These results suggest an epidemiologic link between these strains and possible contamination/recontamination of the same *Salmonella* clone through this dairy food production chain. This could be due to asymptomatic carriage by animals or use of inappropriate hygiene measures. Within poultry strains, we observed only 5 SNPs between samples belonging to the same genomic group (i.e., cluster A), isolated in 2020 from five different regions (and production). However, it is difficult to interpret these results without having epidemiologic data such as movement of animals between farms, and information on the feed given in breeding or even on the purchase address of primary production chicks and veal.

Nevertheless, what this study shows is that the *S.* Mbandaka clones circulating in France, both in the bovine and poultry sectors, have several multi-resistance genes, likely conferring them the ability to survive several biocides, heavy metals, and drugs. The genomes analyzed carry genes such as *ydd*G, *bae*SR, *omp*D, *smv*A, *par*C, and *mdt*ABCK, conferring resistance to the herbicide paraquat (i.e., methyl viologen dichloride hydrate), peroxide, hydrogen peroxide, and monochloramine (Baranova and Nikaido, 2002; Santiviago et al., 2002). Paraquat, also known under the trade name Gramoxone, was first manufactured and sold by Imperial Chemical Industries in 1962. The European Union authorities banned its use in Court of First Instance of the European Communities (2007) stating that there were indications of neurotoxicity associated with paraquat and a possible link between paraquat and Parkinson's disease. Peroxide is currently used as a biocide on farms today again. Although there is no standard or protocol imposed by the European Union authorities, peroxide is used in poultry chiller water to reduced aerobic organisms and cross-contamination of poultry carcasses during immersion chilling (Lillard and Thomson, 1983). This compound is also used to clean the claw sleeves between two dairy cows in order to avoid the transmission of mastitis from one cow to another. In general, farm animal drinking water is disinfected with this compound. The advantage of peroxide is that it is used cold and has an immediate effect. Monochloramine is used to disinfect milking machine waters on many farms. Interestingly, it has been

demonstrated that the *bae*SR genes are part of a putative operon *mdt*ABCD-*bae*SR that in *Escherichia coli* increases its resistance to novobiocin and deoxycholate (Baranova and Nikaido, 2002). Further experimental tests should be conducted to enable us to assess similar activity in *S.* Mbandaka strains.

This study showed that *S.* Mbandaka can have plasmidic or chromosomic genes conferring resistance to several antibiotics frequently used in the agri-food sector, such as ampicillin (*bla*TEM-1b), sulfonamide (*sul*2), streptomycin (*aph*(6)-Id), tetracycline (*tet*(A and B)), trimethoprim (*dfr*A14), and aminoglycoside (*ant*3-D). Of course, further phenotypical analyses would be needed to confirm the ability of the 304 *S.* Mbandaka strains analyzed to resist paraquat, different biocides, detergents, and antibiotic drugs.

Interestingly, several metal resistance genes were also identified in all genomes conferring to this serovar likely resistance to cobalt/magnesium (*cor*ABCD), gold (*ges*ABC and *gol*ST), arsenic (*pst*B), copper (*cui*D and *cue*P), and iron (*sit*ABCD). Some of these metals, such as copper, are authorized in the European Union as feed additives for breeding and pets animal (Commission Implementing Regulation (EU) 2018/1,039 of 23 July 2018), and are used to treat lameness in dairy bovines (Bolan et al., 2003). Others, such as arsenic, are present in the general environment as a result of human activity such as burning of treated wood (Mandal, 2017) (USGS data 2020). Nonetheless, our results highlight that the evolution of this serovar is driven by anthropogenic selection, as recently observed for other *Salmonella* serovars such as Typhimurium and its monophasic variant *S.* 4,5,12:i:- (Bawn et al., 2020; Cadel-Six et al., 2021).

The *mer*CRT cluster, involved in mercury resistance, was also found in only one strain isolated from poultry (S18LNR1211). This strain also presents the tetracycline, sulphonamide, and aminoglycoside resistance genes *tet*AB, *sul*1, and *ant*3-D,' respectively. Mercuric resistance was previously described in the epidemic *S.* 4,5,12:i:- clone ST34 associated with resistance to ampicillin, streptomycin/spectinomycin, sulphonamides, and tetracyclines in a composite transposon of the Tn21-family (Petrovska et al., 2016). Similarly, genes conferring resistance to mercury have also been shown in the epidemic *Salmonella* serovar Derby clone ST40 responsible for 70% of human *S.* Derby infections in France (Sevellec et al., 2020). In *S.* Derby, the mercury resistance cluster is located on the transposon of the Tn7-family carried by the *Salmonella* genomic island SGI-1, also encoding the *aadA2* and *sul1* genes mediating aminoglycoside and sulphonamide resistance (Sevellec et al., 2018b). Further tests should be conducted to understand the possible transfer of heavy metal resistance clusters between different *Salmonella* serovars and co-evolution with drug resistance genes.

Gene clusters coding for both curli and chaperon-placier type fimbriae (*csg*, *fim*, *bcf*, and *lpf*) were found in all the *S.* Mbandaka strains analyzed. Interestingly, it was previously shown that *S.* Typhimurium requires Lpf fimbriae for biofilm formation, and other genes such as *mis*L and *mgt*CB involved in biofilm formation (Ledeboer et al., 2006; Wang et al., 2018) that were identified in all *S.* Mbandaka genomes suggesting its likely biofilm formation ability. Finally, despite the analysis carried out on the *FimH* sequence, we were unable to highlight any mutations that could justify speciation to bovine or avian hosts. We were also unable to demonstrate a difference in SPI composition because all genomes analyzed had SPI-1, SPI-2, SPI-4, and SPI-9 coding for type III (T3SS-1 and T3SS-2) and type I secretory apparatus (T1SS), responsible for survival and proliferation in various intracellular environments.

Our genomic analyses revealed that, within their complex, the *S.* Mbandaka ST143 strains analyzed, there was no deep speciation for bovine or avian hosts, but rather different clones circulating within the two sectors. To follow these clones within the different food production chains we identified genomic markers candidate for sub-typing identification analyses. The differences between these clones are manifested by specific genomic variants that rather characterize one clone or the other within one or the other sector. Host pattern analysis carried out allowed us to identify specific sequences for each of the 12 French clusters identified in this study, and a combination of five genes and three variants (i.e., with an accuracy comprised between 0.92 and 0.95) that can identify, within their complex, all the clones belonging to the five bovine phylogenetic clusters circulating in the bovine sector in France. Among the genes, there are some acquired by phages RE2010, mEp235 and vB_SosS_Oslo. Among the three variants, there is a mutation in the sequence of the *prg*H gene that codes for a membrane protein of SPI-2, a mutation in the sequence of the STM1546 gene that codes for a protein involved in protecting DNA from damage caused by alkyl hydroperoxides, and a mutation in the sequence of the *trs* gene cluster that encodes the signaling and chemotaxis complex activated by serine sensing (McClelland et al., 2001; Ho et al., 2012; Burkinshaw and Strynadka, 2014; Villa et al., 2017). Among the genes and variants that are characterized by high performance (i.e., inclusivity 100% and exclusivity comprised between 99.7 and 100%), in each of the twelve phylogenetic clusters identified, six genes and 12 variants were selected. All these sequences constitute ideal sites for the design of genetic markers that could be used for *in silico* or experimental genomic identification analyses such as PCR. There is a clear demand for relevant schemes that are capable of typing and subtyping *Salmonella* and its epidemic clones, ideally with a single technological approach. DNA sequence-based typing methods offer faster, more portable results that allow for a more informative analysis than phenotypic tests or whole-genome sequencing (Wattiau et al., 2011; Bishop et al., 2012). It is clearly useful for producers in the agri-food sector to be able to follow the clones of *S.* Mbandaka throughout the production chain in the event of contamination, but it may also be beneficial to trace these clones in the case of outbreak investigations. Although there have not yet been any associated cases of food poisoning in France, *S.* Mbandaka recently caused human infections in Finland due to contaminated chicken products (FoodSafetyNews, 2022). In 2018, an investigation by the Kalamazoo County Health and Community Services Department and the Michigan Department of Health and Human Services revealed that environmental samples and stool specimens from asymptomatic restaurant employees tested positive for the *S.* Mbandaka outbreak strains (Nettleton et al., 2021). Among the genetic differences that could be used for source tracing, phages such as ΦV10, SEN34, and ENT39118 could also be used. The analysis carried out on the search for phages in the 304 genomes allowed us to highlight that these three phages are present only on clones circulating in the poultry sector. Bacteriophage ΦV10 is a temperate phage, which specifically infects *Escherichia coli* O157:H7 and is closely related to *S.* Anatum (Group E1) phage ∈15 (Perry et al., 2009). Phages SEN34 and ENT39118 were previously described as infecting *Salmonella* strains belonging

to *S. enterica* subspecies *enterica*, *salamae*, *arizonae*, *diarizonae*, and *houtenae* (Mikalova et al., 2017; Burnett et al., 2021). It was also previously shown how the presence of phages, such as phage mTmV2, in the *Salmonella* genome constitutes a signature that can contribute to an enhanced ability to track the dissemination of specific clones (Palma et al., 2018).

Geographical segregation and contact with wild animals can also play an important role in the microevolution of emerging clones. In the present study, we tested this hypothesis by focusing on identifying possible wild animal contamination in the geographic and temporal related set of *S.* Mbandaka, all obtained from north-western France between 2016 and 2021. To mine phylogenetic relationships between isolates from different parts of the world, we applied a naïve approach by comparing 214 isolates from France with nine genomes selected from a large set (>2,000) of publicly available genomes of *S.* Mbandaka ST413 isolated from wild animals using the variant calling methodology. The nine North American wild animal genomes selected were all from birds such as gulls, the only wild animals considered able to have entered into contact with livestock animals in France. A recent study by Ahlstrom et al. (2021) provides evidence that gulls can migrate across and between continents and disperse antimicrobial resistant bacteria acquired from anthropogenic sources. In this study, satellite telemetry results of gulls inhabiting Alaska landfills demonstrated autumn migration to Russia, Canada, and California to reach warmer coasts (Ahlstrom et al., 2021). Among the nine genomes of wild birds, six were from the United States, two were from Canada, and one was from Mexico. The isolates were taken over a period of 12 years (between 2007 and 2019) which overlaps with the period of isolation of the French strains. Six French genomes clustered together with these nine North American wild bird genomes, with mean SNP differences of 57 SNPs, a minimum of 39 and a maximum of 105. Interestingly, the mean SNP differences between genomes of the 12 French clusters are comprised between a minimum of 5 and 72 SNPs, with four clusters F, H, I, and K having more than 39 mean SNP differences (i.e., 69, 44, 41, and 72, respectively). The genomes from France that clustered with wild birds were from strains isolated from farms close to the coast or along a river that flows to the coast. The values of SNP differences calculated and the geographic localization of the French samples genomically related to those of wild animals could suggest possible cross-contamination between wild birds and farms. However, further analyses and more genomes such as genomes from wild gulls in France would be needed to confirm this hypothesis. It is known that naturally, the prevalence of *Salmonella* spp. in wild animals is lower than on the farm, despite the fact that wild animals can be asymptomatic carriers of *Salmonella* spp., with the bacterium remaining in equilibrium with the intestinal microbiota (dos Santos et al., 2022). A study carried out on 518 free-living wild animals including mammals, birds, and reptiles in forest fragments in Brazil from 2015 to 2021 showed that only three mammals and one bird were tested positive for *Salmonella* spp (dos Santos et al., 2022). Further investigations would be needed to calculate the frequency of likely contamination of *S.* Mbandaka from wild birds to farm animals in France.

Finally, this is the first genomic study on *S.* Mbandaka. It allowed us to acquire new knowledge about this serovar, both in terms of epidemiology and genomics. The results of the genomic analyses carried out on the 304 *S.* Mbandaka strains underline how the genetic potential of this serovar (i.e., biocide, heavy metal, and drug resistances) could explain why this serovar is present in France in the bovine and poultry sectors. The phylogenetic analyses revealed the presence of 12 major clones, of which seven circulate in poultry and five in the bovine sector in France. The genomic markers study allowed us to determine specific and sensitive sequences that could be used to develop *in silico* or experimental PCRs to trace these clones along the poultry and bovine production chains, or in investigations of foodborne contamination. The MarkerFinder pipeline developed in this study is pathogen-independent and could be used in the future to identify specific and sensitive genes or variants for other foodborne organisms. The 304 genomes that are made available on public databases such as EnteroBase may therefore prove useful for future studies on this poorly referenced serovar. In conclusion, this study has brought to light new aspects of *S.* Mbandaka genomic biodiversity and provides a preliminary overview of the epidemiologic dynamics of this serovar on the farms in north-western France.

Data availability statement

The datasets presented in this study can be found in online repositories. The names of the repository/repositories and accession number(s) can be found in this article/**Supplementary material**.

Author contributions

SC-S, VM, CF, and M-YM: conceptualization. SC-S and MDSV: methodology, formal analysis, data curation, and writing—original draft preparation. SC-S, VM, LBo, and AP-G: strains collection. KR and LBa: experimental analyses. MDSV and NR: bioinformatic development. SC-S, VM, and CF: resources. SC-S, MDSV, VM, AP-G, and LBo: review and editing. SC-S, VM, M-YM, NR, and LM: supervision. All authors contributed to the article and approved the submitted version.

Funding

This study was supported by funding from the French Ministry of Agriculture, Food and Forestry, through the grant CASDAR–RT EMISSAGE (No. 1710). MDSV was the recipient of a doctoral fellowship co-funded by the grant CASDAR–RT EMISSAGE (No. 1710) and two French Agrifood Institutes (ACTALIA and IFIP-Institut du Porc).

Acknowledgments

We thank colleagues from the *Salmonella* Network, Vincent Leclerc, Fréderique Moury, and Viviane Morel for their advice on

selection of collections, and Véronique Noel for prevalence data on *S.* Mbandaka in France.

Conflict of interest

The authors declare that the research was conducted in the absence of any commercial or financial relationships that could be construed as a potential conflict of interest.

Publisher's note

All claims expressed in this article are solely those of the authors and do not necessarily represent those of their affiliated organizations, or those of the publisher, the editors and the reviewers. Any product that may be evaluated in this article, or claim that may be made by its manufacturer, is not guaranteed or endorsed by the publisher.

Supplementary material

The Supplementary Material for this article can be found online at: https://www.frontiersin.org/articles/10.3389/fmicb.2023.1130891/full#supplementary-material

SUPPLEMENTARY FIGURE 1
French *Salmonella* Network data. *Salmonella* Mbandaka data from the French *Salmonella* Network database of the Food Safety Laboratory of the French Agency for Food, Environmental and Occupational Health and Safety (ANSES). **(A)** Distribution of *S.* Mbandaka data from 2010 to 2020. **(B)** Data from *Salmonella* strains isolated from animals and the poultry and bovine production sectors from 2010 to 2020. In the poultry sector, *S.* Mbandaka isolates account for 3,950 entries out of 110,591 (3.5%). In the bovine sector, *S.* Mbandaka isolates account for 1,300 entries out of 17,151 (7.6%).

SUPPLEMENTARY FIGURE 2
Phylogenetic reconstruction based on core-genome single nucleotide polymorphism substitutions of the 304 *S.* Mbandaka isolated in France from the bovine and poultry sectors, including strain ID, matrix source, and geographic distribution. The maximum likelihood criterion and the transversional model TVM + F model were applied. *Salmonella* Mbandaka SA20026234 was used as the reference complete genome. In all, 12 groups were identified and are highlighted in different colors. Bootstraps comprised between 80 and 100% are shown as triangles at the node's position.

References

Acosta, O., Usaga, J., Churey, J. J., Worobo, R. W., and Padilla-Zakour, O. I. (2017). Effect of water activity on the thermal tolerance and survival of *Salmonella enterica* serovars tennessee and senftenberg in goat's milk caramel. *J. Food Prot.* 80, 922–927. doi: 10.4315/0362-028X.JFP-16-191

Ahlstrom, C. A., van Toor, M. L., Woksepp, H., Chandler, J. C., Reed, J. A., and Reeves, A. B. (2021). Evidence for continental-scale dispersal of antimicrobial resistant bacteria by landfill-foraging gulls. *Sci. Total Environ.* 764:144551. doi: 10.1016/j.scitotenv.2020.144551

Arndt, D., Grant, J. R., Marcu, A., Sajed, T., Pon, A., Liang, Y., et al. (2016). PHASTER: A better, faster version of the PHAST phage search tool. *Nucleic Acids Res.* 44, W16–W21. doi: 10.1093/nar/gkw387

Bankevich, A., Nurk, S., Antipov, D., Gurevich, A. A., Dvorkin, M., Kulikov, A. S., et al. (2012). SPAdes: A new genome assembly algorithm and its applications to single-cell sequencing. *J. Comput. Biol.* 19, 455–477. doi: 10.1089/cmb.2012.0021

Baranova, N., and Nikaido, H. (2002). The baeSR two-component regulatory system activates transcription of the yegMNOB (mdtABCD) transporter gene cluster in *Escherichia coli* and increases its resistance to novobiocin and deoxycholate. *J. Bacteriol.* 184, 4168–4176. doi: 10.1128/JB.184.15.4168-4176.2002

Bawn, M., Alikhan, N. F., Thilliez, G., Kirkwood, M., Wheeler, N. E., Petrovska, L., et al. (2020). Evolution of *Salmonella enterica* serotype Typhimurium driven by anthropogenic selection and niche adaptation. *PLoS Genet.* 16:e1008850. doi: 10.1371/journal.pgen.1008850

Bishop, C., Honisch, C., Goldman, T., Mosko, M., Keng, S., Arnold, C., et al. (2012). Combined genomarkers approach to *Salmonella* characterization reveals that nucleotide sequence differences in the phase 1 flagellin gene fliC are markers for variation within serotypes. *J. Med. Microbiol.* 61, 1517–1524. doi: 10.1099/jmm.0.047431-0

Bolan, N., Khan, M., Donaldson, J., Adriano, D., and Matthew, C. (2003). Distribution and bioavailability of copper in farm effluent. *Sci. Total Environ.* 309, 225–236. doi: 10.1016/S0048-9697(03)00052-4

Bolger, A. M., Lohse, M., and Usadel, B. (2014). Trimmomatic: A flexible trimmer for Illumina sequence data. *Bioinformatics* 30, 2114–2120. doi: 10.1093/bioinformatics/btu170

Bonifait, L., Thepault, A., Bauge, L., Rouxel, S., Le Gall, F., and Chemaly, M. (2021). Occurrence of *Salmonella* in the cattle production in France. *Microorganisms* 9:872. doi: 10.3390/microorganisms9040872

Bugarel, M., Cook, P. W., den Bakker, H. C., Harhay, D., Nightingale, K. K., and Loneragan, G. H. (2019). Complete genome sequences of four *Salmonella enterica* strains (including those of serotypes Montevideo, Mbandaka, and Lubbock) isolated from peripheral lymph nodes of healthy cattle. *Microbiol. Resour. Announc.* 8, e01450–18. doi: 10.1128/MRA.01450-18

Bullas, L. R., Mostaghimi, A. R., Arensdorf, J. J., Rajadas, P. T., and Zuccarelli, A. J. (1991). *Salmonella* phage PSP3, another member of the P2-like phage group. *Virology* 185, 918–921. doi: 10.1016/0042-6822(91)90573-T

Burkinshaw, B. J., and Strynadka, N. C. (2014). Assembly and structure of the T3SS. *Biochim. Biophys. Acta* 1843, 1649–1663. doi: 10.1016/j.bbamcr.2014.01.035

Burnett, E., Ishida, M., de Janon, S., Naushad, S., Duceppe, M. O., Gao, R., et al. (2021). Whole-genome sequencing reveals the presence of the blaCTX-M-65 gene in extended-spectrum beta-lactamase-producing and multi-drug-resistant clones of *Salmonella* serovar infantis isolated from broiler chicken environments in the Galapagos Islands. *Antibiotics* 10:267. doi: 10.3390/antibiotics10030267

Cadel-Six, S., Cherchame, E., Douarre, P. E., Tang, Y., Felten, A., Barbet, P., et al. (2021). The spatiotemporal dynamics and microevolution events that favored the success of the highly clonal multidrug-resistant monophasic *Salmonella* Typhimurium circulating in Europe. *Front. Microbiol.* 12:651124. doi: 10.3389/fmicb.2021.651124

Camacho, C., Coulouris, G., Avagyan, V., Ma, N., Papadopoulos, J., Bealer, K., et al. (2009). BLAST+: Architecture and applications. *BMC Bioinformatics* 10:421. doi: 10.1186/1471-2105-10-421

Chen, L., Zheng, D., Liu, B., Yang, J., and Jin, Q. (2016). VFDB 2016: Hierarchical and refined dataset for big data analysis–10 years on. *Nucleic Acids Res.* 44, D694–D697. doi: 10.1093/nar/gkv1239

Cherchame, E., Ilango, G., and Cadel-Six, S. (2022b). Retrieving good-quality *Salmonella* genomes from the genbank database using a python tool, SalmoDEST. *Bioinform. Biol. Insights* 16:11779322221080264. doi: 10.1177/11779322221080264

Cherchame, E., Guillier, L., Lailler, R., Vignaud, M. L., Jourdan-Da Silva, N., Le Hello, S., et al. (2022a). *Salmonella enterica* subsp. *enterica* welikade: Guideline for phylogenetic analysis of serovars rarely involved in foodborne outbreaks. *BMC Genomics* 23:217. doi: 10.1186/s12864-022-08439-2

Court of First Instance of the European Communities, (2007). *Court of first instance of the European Communities*. Available online at: https://curia.europa.eu/en/actu/communiques/cp07/aff/cp070045en.pdf (accessed March 23, 2023).

dos Santos, E., Sampaio, Lopes, A., and Bianca, M. M. (2022). *Salmonella in wild animals: A public health concern*. London: IntechOpen.

Doster, E., Lakin, S. M., Dean, C. J., Wolfe, C., Young, J. G., Boucher, C., et al. (2020). MEGARes 2.0: A database for classification of antimicrobial drug, biocide and metal resistance determinants in metagenomic sequence data. *Nucleic Acids Res.* 48, D561–D569. doi: 10.1093/nar/gkz1010

EFSA (2014). *European food safety authority. EFSA explains zoonotic diseases: Salmonella*. Available online at: https://www.efsa.europa.eu/en/corporate/pub/factsheetsalmonella

EFSA and ECDC (2019). *European food safety authority and european centre for disease prevention and control. The European Union one health 2018 Zoonoses report*. doi: 10.2903/j.efsa.2019.5926

Felten, A., Vila Nova, M., Durimel, K., Guillier, L., Mistou, M. Y., and Radomski, N. (2017). First gene-ontology enrichment analysis based on bacterial coregenome variants: Insights into adaptations of *Salmonella* serovars to mammalian- and avian-hosts. *BMC Microbiol.* 17:222. doi: 10.1186/s12866-017-1132-1

FoodSafetyNews (2022). *FoodSafetyNews*. Available online at: https://www.foodsafetynews.com/?s=salmonella+mbandaka (accessed March 23, 2023).

Gao, Q., Xia, L., Wang, X., Ye, Z., Liu, J., and Gao, S. (2019). SodA contributes to the virulence of avian pathogenic *Escherichia coli* O2 strain E058 in experimentally infected chickens. *J. Bacteriol.* 201, e00625–18. doi: 10.1128/JB.00625-18

Grimont, P., and Weill, F.-X. (2007). *Antigenic formulae of the Salmonella serovars*, 9th Edn. Paris: WHO Collaborating Center.

Guillen, S., Marcen, M., Alvarez, I., Manas, P., and Cebrian, G. (2020). Stress resistance of emerging poultry-associated *Salmonella* serovars. *Int. J. Food Microbiol.* 335:108884. doi: 10.1016/j.ijfoodmicro.2020.108884

Gurevich, A., Saveliev, V., Vyahhi, N., and Tesler, G. (2013). QUAST: Quality assessment tool for genome assemblies. *Bioinformatics* 29, 1072–1075. doi: 10.1093/bioinformatics/btt086

Ho, N., Erika, L., Andre, V., Cole, L., and Andrew, M. K. (2012). Genomic Characterization of two new *Salmonella* bacteriophages: vB_SosS_Oslo AND vB_SemP_Emek. *Ann. Agrar. Sci.* 10.

Holschbach, C. L., and Peek, S. F. (2018). *Salmonella* in dairy cattle. *Vet. Clin. North Am. Food Anim. Pract.* 34, 133–154. doi: 10.1016/j.cvfa.2017.10.005

Jawor, P., Mee, J. F., and Stefaniak, T. (2021). Role of infection and immunity in bovine perinatal mortality: Part 2. fetomaternal response to infection and novel diagnostic perspectives. *Animals.* 11:2102. doi: 10.3390/ani11072102

Jennings, E., Thurston, T. L. M., and Holden, D. W. (2017). *Salmonella* SPI-2 Type III secretion system effectors: Molecular mechanisms and physiological consequences. *Cell Host Microbe* 22, 217–231. doi: 10.1016/j.chom.2017.07.009

Jolley, K. A., and Maiden, M. C. (2010). BIGSdb: scalable analysis of bacterial genome variation at the population level. *BMC Bioinformatics* 11:595. doi: 10.1186/1471-2105-11-595

Kehres, D. G., Janakiraman, A., Slauch, J. M., and Maguire, M. E. (2002). SitABCD is the alkaline Mn(2+) transporter of *Salmonella enterica* serovar Typhimurium. *J. Bacteriol.* 184, 3159–3166. doi: 10.1128/JB.184.12.3159-3166.2002

Kent, E., Okafor, C., Caldwell, M., Walker, T., Whitlock, B., and Lear, A. (2021). Control of *Salmonella* Dublin in a bovine dairy herd. *J. Vet. Intern. Med.* 35, 2075–2080. doi: 10.1111/jvim.16191

Kim, J., Kim, M., Kim, S., and Ryu, S. (2017). Sensitive detection of viable *Escherichia coli* O157:H7 from foods using a luciferase-reporter phage phiV10lux. *Int. J. Food Microbiol.* 254, 11–17. doi: 10.1016/j.ijfoodmicro.2017.05.002

Kirchner, M., McLaren, I., Clifton-Hadley, F. A., Liebana, E., Wales, A. D., and Davies, R. H. (2012). A comparison between longitudinal shedding patterns of *Salmonella* Typhimurium and *Salmonella* Dublin on dairy farms. *Vet. Rec.* 171:194. doi: 10.1136/vr.100865

Kremer, F. S., McBride, A. J. A., and Pinto, L. S. (2017). Approaches for in silico finishing of microbial genome sequences. *Genet. Mol. Biol.* 40, 553–576. doi: 10.1590/1678-4685-gmb-2016-0230

Leclerc, V., Moury, F., Morel, V., Noel, V., and Lailler, R. (2019). Le réseau *Salmonella*, un dispositif de surveillance des salmonelles de la fourche à la fourchette: Bilan 2016. *Bull. Épidémiol.* 89, 1–8. Available online at: https://be.anses.fr/sites/default/files/N_SSA14_2019-24-10_MaqVF.pdf (accessed March 24, 2023).

Ledeboer, N. A., Frye, J. G., McClelland, M., and Jones, B. D. (2006). *Salmonella enterica* Serovar Typhimurium Requires the Lpf, Pef, and Tafi fimbriae for biofilm formation on HEp-2 tissue culture cells and chicken intestinal epithelium. *Infect. Immun.* 74, 3156–3169. doi: 10.1128/IAI.01428-05

Letunic, I., and Bork, P. (2016). Interactive tree of life (iTOL) v3: An online tool for the display and annotation of phylogenetic and other trees. *Nucleic Acids Res.* 44, W242–W245. doi: 10.1093/nar/gkw290

Lillard, H. S., and Thomson, J. E. (1983). Efficacy of hydrogen peroxide as a bactericide in poultry chiller water. *J. Food Sci.* 48, 125–126. doi: 10.1111/j.1365-2621.1983.tb14804.x

Low, A. J., Koziol, A. G., Manninger, P. A., Blais, B., and Carrillo, C. D. (2019). ConFindr: Rapid detection of intraspecies and cross-species contamination in bacterial whole-genome sequence data. *PeerJ* 7:e6995. doi: 10.7717/peerj.6995

Mandal, P. (2017). An insight of environmental contamination of arsenic on animal health. *Emerg. Contam.* 3, 17–22. doi: 10.1016/j.emcon.2017.01.004

McClelland, M., Sanderson, K. E., Spieth, J., Clifton, S. W., Latreille, P., Courtney, L., et al. (2001). Complete genome sequence of *Salmonella enterica* serovar Typhimurium LT2. *Nature* 413, 852–856. doi: 10.1038/35101614

McKenna, A., Hanna, M., Banks, E., Sivachenko, A., Cibulskis, K., Kernytsky, A., et al. (2010). The genome analysis toolkit: A MapReduce framework for analyzing next-generation DNA sequencing data. *Genome Res.* 20, 1297–1303. doi: 10.1101/gr.107524.110

Mikalova, L., Bosak, J., Hribkova, H., Dedicova, D., Benada, O., Smarda, J., et al. (2017). Novel Temperate Phages of *Salmonella enterica* subsp. salamae and subsp. diarizonae and Their Activity against Pathogenic *S. enterica* subsp. *enterica* isolates. *PLoS One* 12:e0170734. doi: 10.1371/journal.pone.0170734

Nettleton, W. D., Reimink, B., Arends, K. D., Potter, D., Henderson, J. J., Dietrich, S., et al. (2021). Protracted, intermittent outbreak of *Salmonella* Mbandaka linked to a restaurant–Michigan, 2008–2019. *Morb. Mortal. Wkly. Rep.* 70, 1109–1113. doi: 10.15585/mmwr.mm7033a1

Nguyen, L. T., Schmidt, H. A., von Haeseler, A., and Minh, B. Q. (2015). IQ-TREE: A fast and effective stochastic algorithm for estimating maximum-likelihood phylogenies. *Mol. Biol. Evol.* 32, 268–274. doi: 10.1093/molbev/msu300

Pakarian, P., and Pawelek, P. D. (2016). Intracellular co-localization of the *Escherichia coli* enterobactin biosynthetic enzymes EntA, EntB, and EntE. *Biochem. Biophys. Res. Commun.* 478, 25–32. doi: 10.1016/j.bbrc.2016.07.105

Palma, F., Manfreda, G., Silva, M., Parisi, A., Barker, D. O. R., Taboada, E. N., et al. (2018). Genome-wide identification of geographical segregated genetic markers in *Salmonella enterica* serovar Typhimurium variant 4,[5],12:i. *Sci. Rep.* 8:15251. doi: 10.1038/s41598-018-33266-5

Peek, S., and Divers, T. J. (2016). *Rebhun's diseases of dairy cattle*, 3rd Edn. Amsterdam: Elsevier.

Perry, L. L., SanMiguel, P., Minocha, U., Terekhov, A. I., Shroyer, M. L., Farris, L. A., et al. (2009). Sequence analysis of *Escherichia coli* O157:H7 bacteriophage PhiV10 and identification of a phage-encoded immunity protein that modifies the O157 antigen. *FEMS Microbiol. Lett.* 292, 182–186. doi: 10.1111/j.1574-6968.2009.01511.x

Petrovska, L., Mather, A. E., AbuOun, M., Branchu, P., Harris, S. R., Connor, T., et al. (2016). Microevolution of monophasic *Salmonella* Typhimurium during epidemic, United Kingdom, 2005–2010. *Emerg. Infect. Dis.* 22, 617–624. doi: 10.3201/eid2204.150531

Pightling, A. W., Pettengill, J. B., Luo, Y., Baugher, J. D., Rand, H., and Strain, E. (2018). Interpreting whole-genome sequence analyses of foodborne bacteria for regulatory applications and outbreak investigations. *Front. Microbiol.* 9:1482. doi: 10.3389/fmicb.2018.01482

Radomski, N., Cadel-Six, S., Cherchame, E., Felten, A., Barbet, P., Palma, F., et al. (2019). A simple and robust statistical method to define genetic relatedness of samples related to outbreaks at the genomic scale - application to retrospective *Salmonella* foodborne outbreak investigations. *Front. Microbiol.* 10:2413. doi: 10.3389/fmicb.2019.02413

Robertson, J., and Nash, J. H. E. (2018). MOB-suite: Software tools for clustering, reconstruction and typing of plasmids from draft assemblies. *Microb. Genom.* 4:e000206. doi: 10.1099/mgen.0.000206

Roer, L., Hendriksen, R. S., Leekitcharoenphon, P., Lukjancenko, O., Kaas, R. S., Hasman, H., et al. (2016). Is the evolution of *Salmonella enterica* subsp. *enterica* linked to restriction-modification systems?. *mSystems* 1, e00009–e16. doi: 10.1128/mSystems.00009-16

Santiviago, C. A., Fuentes, J. A., Bueno, S. M., Trombert, A. N., Hildago, A. A., Socias, L. T., et al. (2002). The *Salmonella enterica* sv. Typhimurium smvA, yddG and ompD (porin) genes are required for the efficient efflux of methyl viologen. *Mol. Microbiol.* 46, 687–698. doi: 10.1046/j.1365-2958.2002.03204.x

Sekhon, A. S., Singh, A., and Michael, M. (2020). Short communication: Decimal log reductions of *Salmonella* Senftenberg 775 W and other *Salmonella* serovars in nonfat milk and powder. *J. Dairy Sci.* 103, 6894–6899. doi: 10.3168/jds.2019-17844

Sekhon, A. S., Singh, A., Unger, P., Babb, M., Yang, Y., and Michael, M. (2021). Survival and thermal resistance of *Salmonella* in dry and hydrated nonfat dry milk and whole milk powder during extended storage. *Int. J. Food Microbiol.* 337:108950. doi: 10.1016/j.ijfoodmicro.2020.108950

Sevellec, Y., Granier, S. A., Le Hello, S., Weill, F. X., Guillier, L., Mistou, M. Y., et al. (2020). Source attribution study of sporadic *Salmonella* derby cases in France. *Front. Microbiol.* 11:889. doi: 10.3389/fmicb.2020.00889

Sevellec, Y., Granier, S. A., Radomski, N., Felten, A., Le Hello, S., Feurer, C., et al. (2018a). Complete genome sequence of *Salmonella enterica* subsp. *enterica* serotype derby, associated with the pork sector in France. *Microbiol. Resour. Announc.* 7, e01027–18. doi: 10.1128/MRA.01027-18

Sevellec, Y., Vignaud, M. L., Granier, S. A., Lailler, R., Feurer, C., Le Hello, S., et al. (2018b). Polyphyletic nature of *Salmonella enterica* serotype derby and lineage-specific host-association revealed by genome-wide analysis. *Front. Microbiol.* 9:891. doi: 10.3389/fmicb.2018.00891

Stevens, M. P., and Kingsley, R. A. (2021). *Salmonella* pathogenesis and host-adaptation in farmed animals. *Curr. Opin. Microbiol.* 63, 52–58. doi: 10.1016/j.mib.2021.05.013

Tonkin-Hill, G., MacAlasdair, N., Ruis, C., Weimann, A., Horesh, G., Lees, J. A., et al. (2020). Producing polished prokaryotic pangenomes with the Panaroo pipeline. *Genome Biol.* 21:180. doi: 10.1186/s13059-020-02090-4

Topalcengiz, Z., Spanninger, P. M., Jeamsripong, S., Persad, A. K., Buchanan, R. L., Saha, J., et al. (2020). Survival of *Salmonella* in various wild animal feces that may contaminate produce. *J. Food Prot.* 83, 651–660. doi: 10.4315/0362-028X.JFP-19-302

UniProt, C. (2021). UniProt: The universal protein knowledgebase in 2021. *Nucleic Acids Res.* 49, D480–D489.

Vallejos-Sanchez, K., Tataje-Lavanda, L., Villanueva-Perez, D., Bendezu, J., Montalvan, A., Zimic-Peralta, M., et al. (2019). Whole-genome sequencing of a *Salmonella enterica* subsp. *enterica* serovar infantis strain isolated from broiler chicken in Peru. *Microbiol. Resour. Announc.* 8, e00826–19. doi: 10.1128/MRA.00826-19

Vila Nova, M., Durimel, K., La, K., Felten, A., Bessieres, P., Mistou, M. Y., et al. (2019). Genetic and metabolic signatures of *Salmonella enterica* subsp. *enterica* associated with animal sources at the pangenomic scale. *BMC Genomics* 20:814. doi: 10.1186/s12864-019-6188-x

Villa, L., Feudi, C., Fortini, D., Brisse, S., Passet, V., Bonura, C., et al. (2017). Diversity, virulence, and antimicrobial resistance of the KPC-producing *Klebsiella pneumoniae* ST307 clone. *Microb. Genom.* 3:e000110. doi: 10.1099/mgen.0.000110

Wand, M. E., Jamshidi, S., Bock, L. J., Rahman, K. M., and Sutton, J. M. (2019). SmvA is an important efflux pump for cationic biocides in *Klebsiella pneumoniae* and other *Enterobacteriaceae*. *Sci. Rep.* 9:1344. doi: 10.1038/s41598-018-37730-0

Wang, S., Yang, D., Wu, X., Wang, Y., Wang, D., Tian, M., et al. (2018). Autotransporter MisL of *Salmonella enterica* serotype typhimurium facilitates bacterial aggregation and biofilm formation. *FEMS Microbiol. Lett.* 365:365. doi: 10.1093/femsle/fny142

Wattiau, P., Boland, C., and Bertrand, S. (2011). Methodologies for *Salmonella enterica* subsp. enterica subtyping: Gold standards and alternatives. *Appl. Environ. Microbiol.* 77, 7877–7885. doi: 10.1128/AEM.05527-11

Yamaguchi, E., Fujii, K., Kayano, M., Sakurai, Y., Nakatani, A., Sasaki, M., et al. (2022). Is *Salmonella enterica* shared between wildlife and cattle in cattle farming areas? An 11-year retrospective study in Tokachi district, Hokkaido, Japan. *Vet. Med. Sci.* 8, 758–770. doi: 10.1002/vms3.685

Zankari, E., Hasman, H., Cosentino, S., Vestergaard, M., Rasmussen, S., Lund, O., et al. (2012). Identification of acquired antimicrobial resistance genes. *J. Antimicrob. Chemother.* 67, 2640–2644. doi: 10.1093/jac/dks261

Zhang, S., den Bakker, H. C., Li, S., Chen, J., Dinsmore, B. A., Lane, C., et al. (2019). SeqSero2: Rapid and improved *Salmonella* serotype determination using whole-genome sequencing data. *Appl. Environ. Microbiol.* 85, e01746–19. doi: 10.1128/AEM.01746-19

Zheng, J., Luo, Y., Reed, E., Bell, R., Brown, E. W., and Hoffmann, M. (2017). Whole-genome comparative analysis of *Salmonella enterica* serovar newport strains reveals lineage-specific divergence. *Genome Biol. Evol.* 9, 1047–1050. doi: 10.1093/gbe/evx065

Zhou, Z., Alikhan, N. F., Mohamed, K., Fan, Y., Agama Study, G., and Achtman, M. (2020). The enterobase user's guide, with case studies on *Salmonella* transmissions, *Yersinia pestis* phylogeny, and *Escherichia* core genomic diversity. *Genome Res.* 30, 138–152. doi: 10.1101/gr.251678.119

frontiers | Frontiers in Microbiology

TYPE Original Research
PUBLISHED 14 April 2023
DOI 10.3389/fmicb.2023.1175912

OPEN ACCESS

EDITED BY
Peng Fei,
Nanyang Institute of Technology,
China

REVIEWED BY
Panxue Wang,
Shaanxi University of Science and Technology,
China
Qinnan Yang,
University of Nebraska-Lincoln,
United States

*CORRESPONDENCE
Xiaodong Xia
✉ foodscixiaodong@dlpu.edu.cn
Qinggang Xie
✉ xieqinggang@feihe.com

SPECIALTY SECTION
This article was submitted to
Food Microbiology,
a section of the journal
Frontiers in Microbiology

RECEIVED 28 February 2023
ACCEPTED 27 March 2023
PUBLISHED 14 April 2023

CITATION
Xu Y, Guo W, Luo D, Li P, Xiang J, Chen J, Xia X and Xie Q (2023) Antibiofilm effects of punicalagin against *Staphylococcus aureus in vitro*.
Front. Microbiol. 14:1175912.
doi: 10.3389/fmicb.2023.1175912

Antibiofilm effects of punicalagin against *Staphylococcus aureus in vitro*

Yunfeng Xu[1], Weiping Guo[1], Denglin Luo[1], Peiyan Li[1], Jinle Xiang[1], Junliang Chen[1], Xiaodong Xia[2]* and Qinggang Xie[3]*

[1]College of Food and Bioengineering, Henan University of Science and Technology, Luoyang, Henan, China, [2]School of Food Science and Technology, Dalian Polytechnic University, Dalian, Liaoning, China, [3]Heilongjiang Feihe Dairy Co. Ltd., Beijing, China

Staphylococcus aureus is a common foodborne pathogen which can form biofilms to help them resist to antimicrobials. It brings great harm to human health. Punicalagin has good antimicrobial activities against *S. aureus*, but its effect on biofilm formation has not been clearly illustrated. The aim of this study was to explore the antibiofilm effects of punicalagin against *S. aureus*. Results showed that punicalagin did not significantly interfere with the growth of *S. aureus* at the concentrations of 1/64 MIC to 1/16 MIC. The biomass and metabolic activity of biofilms were significantly reduced when exposed to sub-inhibitory concentrations of punicalagin. The number of viable cells in the biofilms was also decreased after punicalagin treatment. Scanning electron microscopy and confocal laser scanning microscopy images confirmed that punicalagin damaged the structure of biofilms. The antibiofilm mechanism was partly due to the modification of the cell surface which led to the reduction of cell surface hydrophobicity. These findings suggest that punicalagin has the potential to be developed as an alternative to control *S. aureus* biofilms.

KEYWORDS

punicalagin, *Staphylococcus aureus*, antibiofilm, microscopy, hydrophobicity

Introduction

Most bacteria adhere to a surface in the form of biofilm in nature. In comparison with planktonic bacteria, biofilm bacteria have stronger resistance to disinfectants, ultraviolet rays, heavy metals, antibiotics, acids, alkalis and salts owing to genetic and metabolic adaptations (Phuong et al., 2017). Biofilm also brings great potential safety hazards to food industry. Some pathogenic bacteria can colonize, grow and form biofilm on food surface, food processing machinery surface and pipeline, food processing environment and packaging materials, which often lead to pipeline corrosion or product pollution, thus bringing huge economic losses. *Staphylococcus aureus* is a common pathogen which can form biofilm and bring serious safety risks to medical and food fields. There is an urgent need to search for safe and effective antimicrobials for the treatment of the bacteria.

In recent years, many researchers have turned their attention to natural products, especially plant-derived active substances (Bouarab Chibane et al., 2019). Punicalagin, the main component of pomegranate peel polyphenols, is a high molecular weight (1084.72) water-soluble compound (Aqil et al., 2012). It is known for various biological properties, including antioxidant, anti-inflammatory, anti-cancer and immunomodulatory activities (Benchagra et al., 2021; Berdowska et al., 2021; Čolić et al., 2022; Xu et al., 2022). It has also been reported to

possess antimicrobial activities against several pathogenic bacteria such as *S. aureus*, *Salmonella*, and *Vibrio parahaemolyticus* (Li et al., 2014; Mun et al., 2016; Liu et al., 2022). Our previous study has shown that punicalagin exhibited a good bacteriostatic effect on *S. aureus* with the minimum inhibitory concentration (MIC) of 0.25 mg/ml (Xu et al., 2017). However, the effect of punicalagin on the biofilm formation of *S. aureus* and its action mechanism is unclear. Therefore, this study was aimed to investigate the antibiofilm effects of punicalagin against *S. aureus*. It provides a theoretical and experimental basis for the development and utilization of punicalagin and the control of *S. aureus* biofilm.

Materials and methods

Bacterial strains and cultural conditions

Staphylococcus aureus ATCC 29213, obtained from the American Type Culture Collection, was stored in tryptone soybean broth (TSB; Land Bridge Technology Co. Ltd., Beijing, China) containing 25% glycerol at −80°C. It was taken out from the refrigerator and inoculated on tryptone soybean agar (TSA; Land Bridge Technology Co. Ltd., Beijing, China) plate before each experiment. Single colony of the strain was picked out, inoculated into TSB, and cultured at 37°C for about 12 h. The absorbance of the bacterial suspension was measured by a spectrophotometer (Smart Spec™ plus, Bio-Rad Laboratories, Hercules, CA) to obtain the optical density about 0.5 at 600 nm.

Growth curves

The growth curves of *S. aureus* were detected when treated with or without punicalagin using the Bioscreen C automated microbiology growth curve analysis system (Labsystems, Helsinki, Finland) as described by Zheng et al. (2020). Punicalagin (≥98%, CAS 65995–63-3, Must Bio-Technology Co. Ltd., Chengdu, China) was added into the wells to obtain the final concentrations of 0 (control), 1/64, 1/32, 1/16 and 1/8 MIC, respectively. The above bacterial suspension was inoculated at a ratio of 1% containing about 10^6 colony-forming units (CFU)/mL. Sterile TSB containing corresponding concentrations of punicalagin was taken as negative control. The microplate was incubated statically at 37°C and the absorbance at 600 nm wavelength was measured in 1 h intervals for 24 h.

Biofilm formation assay

The effect of punicalagin on biofilm biomass was conducted by crystal violet staining method referred to Fan et al. (2022b). Briefly, *S. aureus* suspensions exposure to punicalagin at 0 (control), 1/64, 1/32 and 1/16 MIC were incubated in a 96-well microplate at 37°C for 24 h. After removing the planktonic cells, wells were washed with sterile phosphate buffered saline (PBS) for three times and fixed with methanol for 15 min. Then crystal violet solution (1%) was added to stain biofilms and the wells were rinsed thrice with distilled water, followed by the addition of acetic acid (33%, vol/vol). After shaking at low speed for 5 min, the absorbance at 570 nm was measured using a microplate reader (model 680; Bio-Rad). The relative biofilm formation was calculated by the $OD_{treatment}$ normalized with $OD_{control}$.

Biofilm metabolic activity assay

The effect of punicalagin on biofilm metabolism was examined by the method of Jadhav et al. (2013). The prepared bacterial suspensions containing different concentrations of punicalagin (0, 1/64, 1/32 and 1/16 MIC) were separately added to a 96-well plate and incubated at 37°C for 24 h. Then the bacterial suspensions were removed. The plate was gently rinsed three times with PBS. A total of 250 µl of 3-[4, 5-dimethylthiazol-2-yl]-2, 5-diphenyltetrazolium bromide (MTT; Beijing Solarbio Science and Technology Co., Ltd., Beijing, China) solution at the concentration of 0.5 mg/ml was added to each well, and incubated at 37°C for 3 h. The insoluble purple formazan was further dissolved in dimethyl sulfoxide (DMSO) and the absorbance was measured at a wavelength of 570 nm using a microplate spectrophotometer (model 680; Bio-Rad).

Counting of viable bacteria in biofilms

The number of viable bacteria in biofilms was counted as previously reported with some modifications (Amalaradjou and Venkitanarayanan, 2011). Briefly, the bacterial suspensions containing different concentrations of punicalagin (0, 1/64, 1/32 and 1/16 MIC) were inoculated into a 24-well polystyrene plate at 2 ml per well and cultured at 37°C for 24 h. Then the wells were carefully washed three times with sterile PBS, followed by the addition of another 2 ml of PBS. The biofilms were wiped off and mixed thoroughly. After a series of 10-fold dilution, the suspensions were spread on TSA, and cultured at 37°C overnight before the colonies were counted.

Field-emission scanning electron microscopy observation

FESEM was performed as described by Li et al. (2021) with some modifications. The bacterial suspensions containing punicalagin at different concentrations (0, 1/64, 1/32 and 1/16 MIC) were added to a 12-well plate pre-placed with sterile glass sheets. After incubated at 37°C for 24 h, the glass sheets were rinsed gently with 2 ml of PBS for three times to wash off the planktonic bacteria. Then they were placed in 2.5% glutaraldehyde solution (prepared in PBS) at 4°C for 5 h, followed by fixation with 1% osmic acid solution for 5 h. Samples were washed with PBS and dehydrated with different concentrations of ethanol solution (30, 50, 70, 80, 90 and 100%). After naturally air dried in a fume hood overnight, the samples were immobilized on a support, and sprayed with Au-Pd under vacuum. Finally, the morphology of the biofilm was observed and photographed by a scanning electron microscope (S-4800, Hitachi, Tokyo, Japan).

Confocal laser scanning microscopy observation

CLSM was carried out according to Fan et al. (2022a) with minor changes. As described above, *S. aureus* biofilm was formed on glass sheets with or without the treatment of punicalagin (0, 1/64, 1/32 and 1/16 MIC) at 37°C for 24 h. After gently rinsed three times with PBS, the glass sheets were transferred to a new 12-well plate. A total of 1 ml of SYTO 9 and propidium iodide (PI) fluorescent dye mixture was

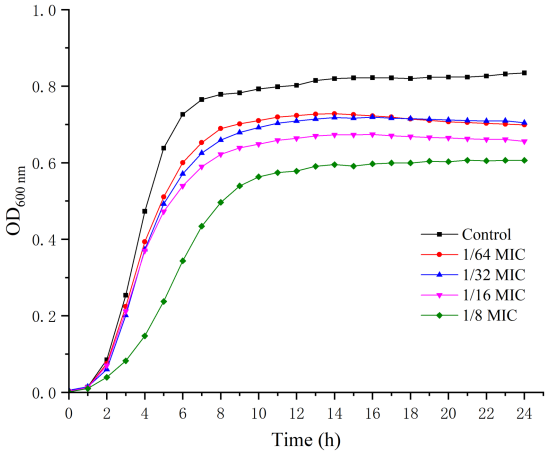

FIGURE 1
Growth curves of *S. aureus* in the absence or presence of punicalagin (0, 1/64 MIC, 1/32 MIC, 1/16 MIC and 1/8 MIC).

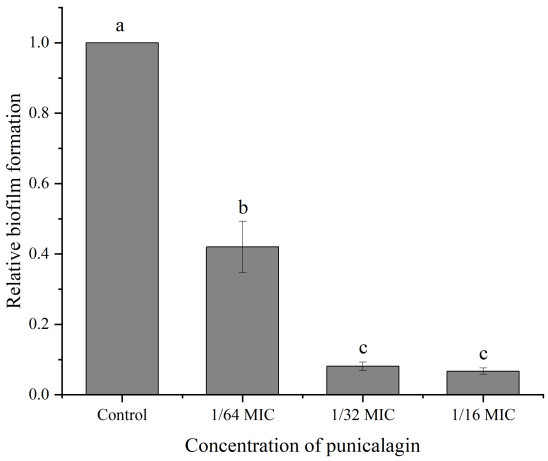

FIGURE 2
Inhibition of punicalagin (0, 1/64 MIC, 1/32 MIC, and 1/16 MIC) on *S. aureus* biofilm formation by crystal violet staining assay. Each bar indicates means ± the standard deviation. Different letters represent a significant difference compared to the control (p<0.05).

added to the wells, followed by the incubation at room temperature in the dark for 15 min. The biofilms were observed under a confocal laser scanning fluorescence microscope (A1; Nikon, Tokyo, Japan). Live bacteria with intact cell membranes emitted green fluorescence, while dead or damaged bacteria emitted red fluorescence.

Determination of bacterial surface hydrophobicity

The effect of punicalagin on the cell surface hydrophobicity of *S. aureus* was assessed by the method of microbial adhesion to hydrocarbons (MATH) as reported previously (Tang et al., 2020). In brief, overnight *S. aureus* culture was collected, washed, and resuspended in PBS. Punicalagin was added to reach the concentrations of 0, 1/64, 1/32 and 1/16 MIC. The absorbance of each sample was detected at 600 nm. Then, 1 ml of hexadecane was added to 2 ml of the bacterial suspension and mixed thoroughly for 1 min. The absorbance of aqueous phase was detected again after incubated for 15 min at 37°C. The hydrophobicity was calculated as follow.

$$\text{Hydrophobic rate}(\%) = (\text{Aa} - \text{Ab}) / \text{Aa} \times 100\%$$

Where Aa is the initial absorbance at 600 nm, and Ab is the absorption value after the treatment of punicalagin. Control groups were those without punicalagin treatment.

Statistical analysis

Mean values and standard deviations were obtained from three replicate experiments. Statistical analysis was performed by the analysis of variance (ANOVA) with SPSS 20.0 software. Tukey's multiple range test was used to calculate the significant differences (p < 0.05) between the control and treatment groups.

Results

Effect of punicalagin on bacterial growth

The effect of punicalagin on the growth of *S. aureus* was shown in Figure 1. After about 2 h of lag, the strains of control groups quickly entered the logarithmic growth phase and reached a stationary phase within 8 h. The growth of *S. aureus* was obviously inhibited by punicalagin at 1/8 MIC compared to the control. However, punicalagin has minor effect on the growth of *S. aureus* at 1/64 MIC to 1/16 MIC. Therefore, the concentrations of punicalagin from 1/64 MIC to 1/16 MIC were considered as sub-inhibitory concentrations (SICs) against *S. aureus* which were chosen for the following experiments.

Effect of punicalagin on biofilm formation

As shown in Figure 2, the relative biofilm formation by *S. aureus* on polystyrene microplate was markedly decreased after punicalagin treatment. The biomass of the biofilm was decreased to 42.0% at the presence of punicalagin at 1/64 MIC compared to the control. And a higher reduction to 8.1% occurred as the concentration of punicalagin increased to 1/32 MIC. There was no significant difference between the 1/32 MIC and 1/16 MIC groups. This result indicated that punicalagin prevented biofilm formation effectively at SICs.

Effect of punicalagin on metabolic activity of biofilms

MTT staining method reflects the metabolism of live bacteria in the biofilm and the result was depicted in Figure 3. At 1/64 MIC, punicalagin has a significant inhibitory effect on the metabolism of bacteria in the biofilm. The inhibitory effect increased with the

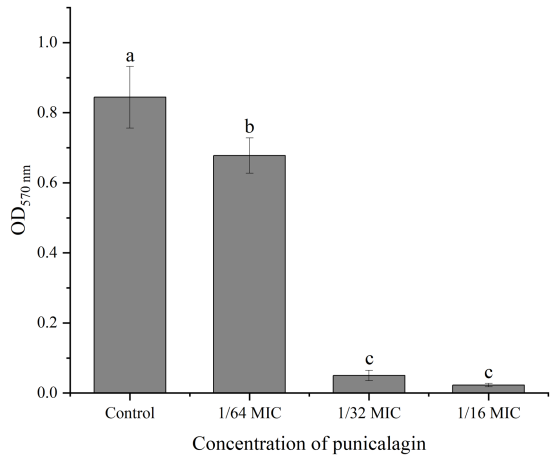

FIGURE 3
The effect of punicalagin on biofilm metabolic activity by MTT staining assay. Each bar indicates means ± the standard deviation. Different letters represent a significant difference compared to the control (p<0.05).

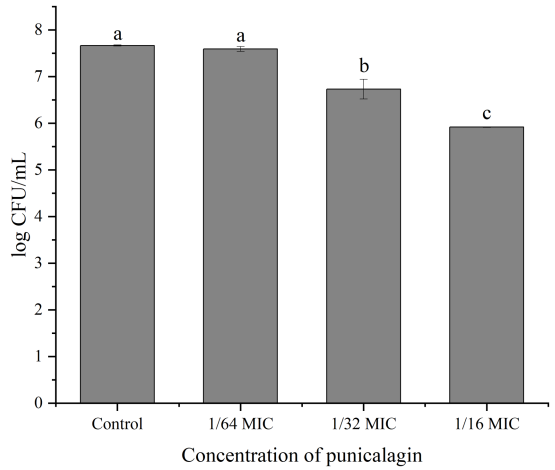

FIGURE 4
Cell enumeration of biofilms after exposed to various concentrations of punicalagin. Error bars represent standard deviations from triplicate analyzes of each sample. Different letters represent a significant difference compared to the control (p<0.05).

increase of the concentration of punicalagin. At the highest concentration tested (1/16 MIC), the optical density was reduced by 97.3% in comparison with the control.

Number of viable bacteria in biofilm

Figure 4 shows the number of viable bacteria in biofilm. It can be observed that the biofilm-associated population of *S. aureus* was reduced by the treatment of punicalagin and higher concentrations of punicalagin lead to more reduction in viable bacteria. Specifically, the viable cell counts were decreased by 0.94 and 1.75 log CFU/mL in comparison with the control after incubated with punicalagin at the 1/32 MIC and 1/16 MIC, respectively.

Effect of punicalagin on biofilm of *Staphylococcus aureus* under FESEM

FESEM was used to observe the effect of punicalagin on the structure of biofilm. The results are shown in Figure 5. In Figure 5A, the cells are tightly adhered to each other on the surface of the glass slide and stacked on top of each other, suggesting the strong biofilm formation ability of the strain. The cells in Figures 5B–D are under the action of SICs of punicalagin. The adhesion between the cells became looser and the distribution became sparser than the control. This experiment visually illustrates the inhibitory effect of punicalagin on the biofilm formation of *S. aureus*. It also can be clearly seen that the surface of the control cells was smooth, while the surface of the punicalagin-treated cells was rough, indicating that punicalagin disrupted the cell surface morphology.

Effect of punicalagin on biofilm of *Staphylococcus aureus* by CLSM

The inhibitory effect of punicalagin on the biofilm formation of *S. aureus* was also observed by CLSM. As can be seen from Figure 6, the fluorescence intensity of the control group was significantly higher than that of the experimental group after the action of punicalagin. A large number of *S. aureus* aggregates can be seen in the control group. After the treatment of punicalagin, the ability of *S. aureus* to form biofilm was significantly reduced. The amount of biofilm formation decreased as the concentration of punicalagin increased. The proportion of viable bacteria in all groups accounted for the majority (green). Only a few bacteria emitted red fluorescence, suggesting impaired cell membranes.

Effect of punicalagin on *Staphylococcus aureus* surface hydrophobicity

The result of bacterial surface hydrophobicity was shown in Figure 7. No significant difference was seen on the hydrophobic rates between the control and 1/64 MIC groups with the result of 70.9 and 69.6%, respectively. But the hydrophobic rates were significantly reduced to 55.5 and 37.2% after treated with 1/32 MIC and 1/16 MIC of punicalagin.

Discussion

In this study, the antibiofilm activity of punicalagin against *S. aureus* was investigated. Punicalagin at SICs could significantly inhibit the production of biofilm biomass. Many antibiofilm agents have been reported to possess similar activities against *S. aureus*. Shikimic acid was confirmed to reduce the biomass of the biofilm dose-dependently at its sub-MICs (Bai et al., 2019). Thymol exhibited a concentration-dependent antibiofilm activity with maximum biofilm inhibition of 88% at 100 μg/ml without affecting growth (Valliammai et al., 2020). The metabolic activity of *S. aureus* biofilm was significantly reduced when treated with punicalagin from 1/64 MIC to 1/16 MIC. There are some other compounds that inhibited the biofilm formation of *S. aureus* coupled with the

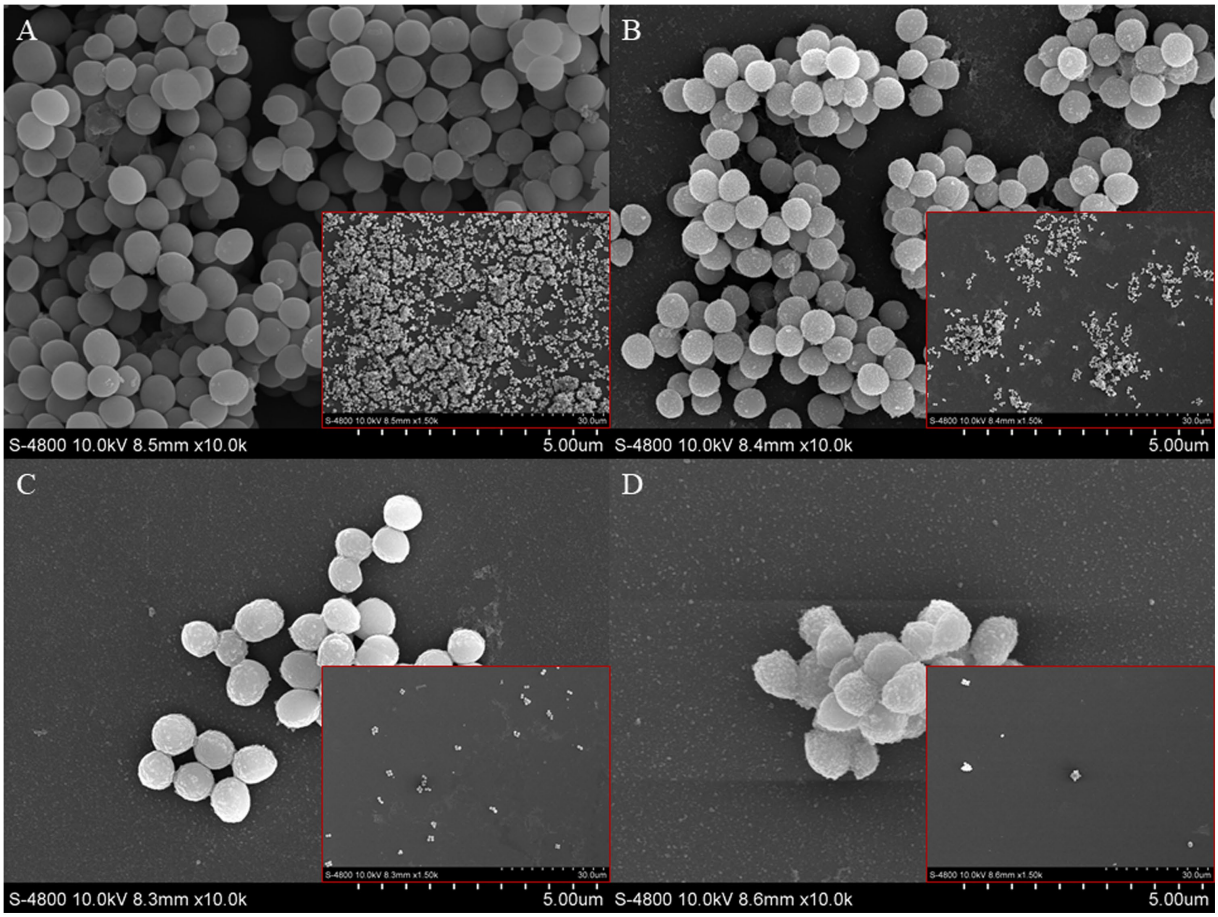

FIGURE 5
Scanning electron microscopic images of *S. aureus* biofilm in the presence of punicalagin at concentrations of 0 **(A)**, 1/64 MIC **(B)**, 1/32 MIC **(C)** and 1/16 MIC **(D)**. Biofilm images in small red boxes are at 10,000×magnification, and the large images are 1,500×magnified.

reduction in cellular metabolic activity of biofilm. Kannappan et al. (2017) reported the inhibitory effect on the biofilm formation and metabolic activity of *S. aureus* by *Vetiveria zizanioides* root extract. Parai et al. (2020) found reserpine stopped the metabolic activity of 50.6% bacterial cells at 1/2 MIC. Punicalagin also induced a reduction of the number of bacteria in the biofilm. But this result was not exactly the same as the biofilm biomass and metabolic activity due to the difference of experimental principles and methods.

Microscopic visualization of punicalagin induced alterations on biofilm architecture of *S. aureus* was made through FESEM analyzes. The biofilm without punicalagin treatment was observed to adhere on the surface of glass slide and form thick aggregates, while the biofilms exposed to SICs of punicalagin gradually decreased. This result was in accordance with previous reports that many natural compounds were able to destroy the structure of biofilm. For instance, Gu et al. (2022) observed the biofilm of *S. aureus* USA300 on slides decreased as the concentration of geraniol increased. The morphological changes of *S. aureus* biofilm treated with punicalagin was also confirmed by CLSM. The fluorescent images were well correlated with the measured antibiofilm effects. It was reported that kaempferol dose-dependently inhibited the biofilm formation of *S. aureus* as observed by the fluorescence microscopy (Ming et al., 2017). Similarly, a reduction in the thickness of biofilm formation was noticed in myrtenol treated samples compared to the control (Selvaraj et al., 2019).

Adhesion is the initial and key step of biofilm formation. Bacterial adhesive ability is closely relevant to cell surface hydrophobicity (Zhu et al., 2022). Generally, the higher hydrophobicity, the stronger adhesive ability. The ability of bacterial hydrophobicity was decreased by the treatment of punicalagin, which resulted in the decrease of cell attachment, and eventually interfered with biofilm formation. Wen et al. (2021) reported the significant dose-related reduction in cell surface hydrophobicity of *S. aureus* with increasing concentrations of naringenin. Wang et al. (2017) found that hydrophobic rates of *S. aureus* decreased to 32.1 and 28.1% after exposed to MIC and MBC level of *Dodartia orientalis* L. essential oil, respectively. However, the mechanism of *S. aureus* biofilm formation is complex (Peng et al., 2023). The effect of punicalagin on the expression of genes critical for biofilm formation needs to be determined in the future.

Besides, how to apply punicalagin to food industry is another unaddressed issue. Tayel et al. (2012) added the ethanol extract of pomegranate peel into the meat steaks for decontamination. Andrade et al. (2023) incorporated pomegranate peel extract (85.84 mg/g punicalagin, 6.67 mg/g ellagic acid) into polylactic acid-based

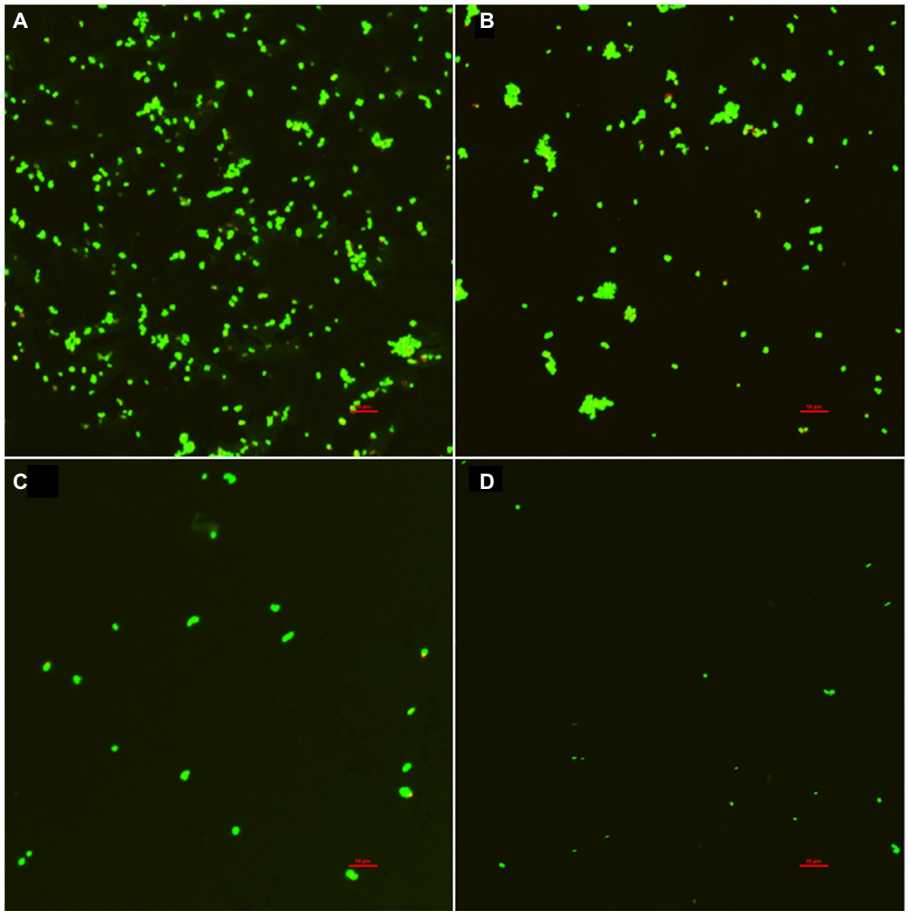

FIGURE 6
Confocal laser scanning microscopic images of *S. aureus* biofilm in the presence of punicalagin at concentrations of 0 **(A)**, 1/64 MIC **(B)**, 1/32 MIC **(C)** and 1/16 MIC **(D)**. Scale bar =10μm.

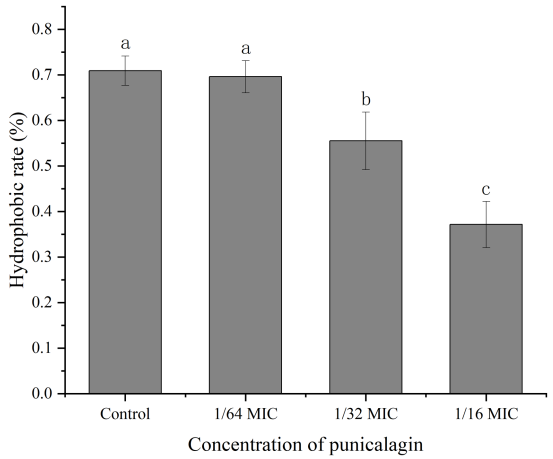

FIGURE 7
The effect of punicalagin on cell surface hydrophobicity of *S. aureus*. Error bars represent standard deviations from triplicate analyzes of each sample. Different letters represent a significant difference in comparison with the control ($p<0.05$).

packaging film to extend the shelf life of beef meat. More studies about its activity in the food system are necessitated before application.

Conclusion

In conclusion, our study demonstrated that punicalagin exhibited good antibiofilm capacity against *S. aureus in vitro*. It reduced the biomass, metabolic activity and the number of microcolonies in the biofilm and impaired biofilm structure at SICs in a dose-dependent manner. Antibiofilm effect of punicalagin could be partly explained by the change of bacteria surface hydrophobicity. Based on these findings, punicalagin may have the potential to be developed as an antibiofilm agent against *S. aureus*.

Data availability statement

The original contributions presented in the study are included in the article/supplementary material, further inquiries can be directed to the corresponding authors.

Author contributions

XX conceived and designed the experiments. YX and WG performed the experiments. JC and QX analyzed the data. DL, PL, and JX contributed to reagents, materials, and analysis tools. YX wrote the

manuscript. All authors contributed to the article and approved the submitted version.

Funding

This work was supported by the Doctor Scientific Research Start-up Fund of Henan University of Science and Technology (13480067).

Conflict of interest

QX was employed by Heilongjiang Feihe Dairy Co. Ltd.

The remaining authors declare that the research was conducted in the absence of any commercial or financial relationships that could be construed as a potential conflict of interest.

Publisher's note

All claims expressed in this article are solely those of the authors and do not necessarily represent those of their affiliated organizations, or those of the publisher, the editors and the reviewers. Any product that may be evaluated in this article, or claim that may be made by its manufacturer, is not guaranteed or endorsed by the publisher.

References

Amalaradjou, M. A. R., and Venkitanarayanan, K. (2011). Effect of trans-cinnamaldehyde on inhibition and inactivation of *Cronobacter sakazakii* biofilm on abiotic surfaces. *J. Food Prot.* 74, 200–208. doi: 10.4315/0362-028x.Jfp-10-296

Andrade, M. A., Rodrigues, P. V., Barros, C., Cruz, V., Machado, A. V., Barbosa, C. H., et al. (2023). Extending high fatty foods shelf-life protecting from lipid oxidation and microbiological contamination: an approach using active packaging with pomegranate extract. *Coatings* 13:93. doi: 10.3390/coatings13010093

Aqil, F., Munagala, R., Vadhanam, M. V., Kausar, N., Jeyabalan, J., Schultz, D. J., et al. (2012). Anti-proliferative activity and protection against oxidative DNA damage by punicalagin isolated from pomegranate husk. *Food Res. Int.* 49, 345–353. doi: 10.1016/j.foodres.2012.07.059

Bai, J., Zhong, K., Wu, Y., Elena, G., and Gao, H. (2019). Antibiofilm activity of shikimic acid against *Staphylococcus aureus*. *Food Control* 95, 327–333. doi: 10.1016/j.foodcont.2018.08.020

Benchagra, L., Berrougui, H., Islam, M. O., Ramchoun, M., Boulbaroud, S., Hajjaji, A., et al. (2021). Antioxidant effect of Moroccan pomegranate (*Punica granatum* L. Sefri variety) extracts rich in punicalagin against the oxidative stress process. *Foods* 10:2219. doi: 10.3390/foods10092219

Berdowska, I., Matusiewicz, M., and Fecka, I. (2021). Punicalagin in cancer prevention-via signaling pathways targeting. *Nutrients* 13:2733. doi: 10.3390/nu13082733

Bouarab Chibane, L., Degraeve, P., Ferhout, H., Bouajila, J., and Oulahal, N. (2019). Plant antimicrobial polyphenols as potential natural food preservatives. *J. Sci. Food Agric.* 99, 1457–1474. doi: 10.1002/jsfa.9357

Čolić, M., Mihajlović, D., Bekić, M., Marković, M., Dragišić, B., Tomić, S., et al. (2022). Immunomodulatory activity of punicalagin, punicalin, and ellagic acid differs from the effect of pomegranate peel extract. *Molecules* 27:7871. doi: 10.3390/molecules27227871

Fan, Q., He, Q., Zhang, T., Song, W., Sheng, Q., Yuan, Y., et al. (2022a). Antibiofilm potential of lactobionic acid against salmonella Typhimurium. *LWT* 162:113461. doi: 10.1016/j.lwt.2022.113461

Fan, Q., Yuan, Y., Zhang, T., Song, W., Sheng, Q., and Yue, T. (2022b). Inhibitory effects of lactobionic acid on *Vibrio parahaemolyticus* planktonic cells and biofilms. *Food Microbiol.* 103:103963. doi: 10.1016/j.fm.2021.103963

Gu, K., Ouyang, P., Hong, Y., Dai, Y., Tang, T., He, C., et al. (2022). Geraniol inhibits biofilm formation of methicillin-resistant *Staphylococcus aureus* and increase the therapeutic effect of vancomycin *in vivo*. *Front. Microbiol.* 13, 1–12. doi: 10.3389/fmicb.2022.960728

Jadhav, S., Shah, R., Bhave, M., and Palombo, E. A. (2013). Inhibitory activity of yarrow essential oil on listeria planktonic cells and biofilms. *Food Control* 29, 125–130. doi: 10.1016/j.foodcont.2012.05.071

Kannappan, A., Gowrishankar, S., Srinivasan, R., Pandian, S. K., and Ravi, A. V. (2017). Antibiofilm activity of *Vetiveria zizanioides* root extract against methicillin-resistant *Staphylococcus aureus*. *Microb. Pathog.* 110, 313–324. doi: 10.1016/j.micpath.2017.07.016

Li, J., Li, S., Li, H., Guo, X., Guo, D., Yang, Y., et al. (2021). Antibiofilm activity of shikonin against listeria monocytogenes and inhibition of key virulence factors. *Food Control* 120:107558. doi: 10.1016/j.foodcont.2020.107558

Li, G., Yan, C., Xu, Y., Feng, Y., Wu, Q., Lv, X., et al. (2014). Punicalagin inhibits salmonella virulence factors and has anti-quorum-sensing potential. *Appl. Environ. Microbiol.* 80, 6204–6211. doi: 10.1128/aem.01458-14

Liu, H., Zhu, W., Cao, Y., Gao, J., Jin, T., Qin, N., et al. (2022). Punicalagin inhibits biofilm formation and virulence gene expression of *Vibrio parahaemolyticus*. *Food Control* 139:109045. doi: 10.1016/j.foodcont.2022.109045

Ming, D., Wang, D., Cao, F., Xiang, H., Mu, D., Cao, J., et al. (2017). Kaempferol inhibits the primary attachment phase of biofilm formation in *Staphylococcus aureus*. *Front. Microbiol.* 8:2263. doi: 10.3389/fmicb.2017.02263

Mun, S.-H., Kong, R., Seo, Y.-S., Zhou, T., Kang, O.-H., Shin, D.-W., et al. (2016). Subinhibitory concentrations of punicalagin reduces expression of virulence-related exoproteins by *Staphylococcus aureus*. *FEMS Microbiol. Lett.* 363, 1–6. doi: 10.1093/femsle/fnw253

Parai, D., Banerjee, M., Dey, P., and Mukherjee, S. K. (2020). Reserpine attenuates biofilm formation and virulence of *Staphylococcus aureus*. *Microb. Pathog.* 138:103790. doi: 10.1016/j.micpath.2019.103790

Peng, Q., Tang, X., Dong, W., Sun, N., and Yuan, W. (2023). A review of biofilm formation of *Staphylococcus aureus* and its regulation mechanism. *Antibiotics* 12:12. doi: 10.3390/antibiotics12010012

Phuong, N. T. M., van Quang, N., Mai, T. T., Anh, N. V., Kuhakarn, C., Reutrakul, V., et al. (2017). Antibiofilm activity of α-mangostin extracted from *Garcinia mangostana* L. against *Staphylococcus aureus*. *J. Trop. Med.* 10, 1154–1160. doi: 10.1016/j.apjtm.2017.10.022

Selvaraj, A., Jayasree, T., Valliammai, A., and Pandian, S. K. (2019). Myrtenol attenuates MRSA biofilm and virulence by suppressing *sarA* expression dynamism. *Front. Microbiol.* 10:2027. doi: 10.3389/fmicb.2019.02027

Tang, C., Chen, J., Zhang, L., Zhang, R., Zhang, S., Ye, S., et al. (2020). Exploring the antibacterial mechanism of essential oils by membrane permeability, apoptosis and biofilm formation combination with proteomics analysis against methicillin-resistant *Staphylococcus aureus*. *Int. J. Med. Microbiol.* 310:151435. doi: 10.1016/j.ijmm.2020.151435

Tayel, A. A., El-Tras, W. F., Moussa, S. H., and El-Sabbagh, S. M. (2012). Surface decontamination and quality enhancement in meat steaks using plant extracts as natural biopreservatives. *Foodborne Pathog. Dis.* 9, 755–761. doi: 10.1089/fpd.2012.1203

Valliammai, A., Selvaraj, A., Yuvashree, U., Aravindraja, C., and Karutha Pandian, S. (2020). sarA-dependent antibiofilm activity of thymol enhances the antibacterial efficacy of rifampicin against *Staphylococcus aureus*. *Front. Microbiol.* 11:1744. doi: 10.3389/fmicb.2020.01744

Wang, F., Wei, F., Song, C., Jiang, B., Tian, S., Yi, J., et al. (2017). *Dodartia orientalis* L. essential oil exerts antibacterial activity by mechanisms of disrupting cell structure and resisting biofilm. *Ind. Crop. Prod.* 109, 358–366. doi: 10.1016/j.indcrop.2017.08.058

Wen, Q., Wang, R., Zhao, S., Chen, B., and Zeng, X. A. (2021). Inhibition of biofilm formation of foodborne *Staphylococcus aureus* by the citrus flavonoid naringenin. *Foods* 10:2614. doi: 10.3390/foods10112614

Xu, J., Cao, K., Liu, X., Zhao, L., Feng, Z., and Liu, J. (2022). Punicalagin regulates signaling pathways in inflammation-associated chronic diseases. *Antioxidants* 11:29. doi: 10.3390/antiox11010029

Xu, Y., Shi, C., Wu, Q., Zheng, Z., Liu, P., Li, G., et al. (2017). Antimicrobial activity of punicalagin against *Staphylococcus aureus* and its effect on biofilm formation. *Foodborne Pathog. Dis.* 14, 282–287. doi: 10.1089/fpd.2016.2226

Zheng, X., Guo, J., Rao, H., Guo, D., Huang, Y., Xu, Y., et al. (2020). Antibacterial and antibiofilm activity of coenzyme Q0 against *Vibrio parahaemolyticus*. *Food Control* 109:106955. doi: 10.1016/j.foodcont.2019.106955

Zhu, W., Gao, J., Liu, H., Liu, J., Jin, T., Qin, N., et al. (2022). Antibiofilm effect of sodium butyrate against *Vibrio parahaemolyticus*. *Food Control* 131:108422. doi: 10.1016/j.foodcont.2021.108422

frontiers | Frontiers in Microbiology

TYPE Original Research
PUBLISHED 12 June 2023
DOI 10.3389/fmicb.2023.1197473

OPEN ACCESS

EDITED BY
Stephen Forsythe,
Foodmicrobe.com, United Kingdom

REVIEWED BY
Rohan V. Tikekar,
University of Maryland, College Park, United States
Jinru Chen,
University of Georgia, United States

*CORRESPONDENCE
Lynne McLandsborough
✉ lm@foodsci.umass.edu

†PRESENT ADDRESS
Lynne McLandsborough,
Chenoweth Laboratory, Amherst, MA,
United States

RECEIVED 31 March 2023
ACCEPTED 16 May 2023
PUBLISHED 12 June 2023

CITATION
Chuang S, Ghoshal M and McLandsborough L (2023) Efficacy of acidified water-in-oil emulsions against desiccated *Salmonella* as a function of acid carbon chain-length and membrane viscosity.
Front. Microbiol. 14:1197473.
doi: 10.3389/fmicb.2023.1197473

Efficacy of acidified water-in-oil emulsions against desiccated *Salmonella* as a function of acid carbon chain-length and membrane viscosity

Shihyu Chuang[1], Mrinalini Ghoshal[2] and Lynne McLandsborough[1*†]

[1]Department of Food Science, University of Massachusetts, Amherst, MA, United States, [2]Department of Microbiology, University of Massachusetts, Amherst, MA, United States

Sanitizing low-moisture food (LMF) processing equipment is challenging due to the increased heat resistance of *Salmonella* spp. in low-water activity (a_w) environments. Food-grade oils mixed with acetic acid have been shown effective against desiccated *Salmonella*. In this study, different hydrocarbon chain-length (C_n) organic acids were tested against desiccated *Salmonella* by using 1% v/v water-in-oil (W/O) emulsion as the delivery system for 200mM acid. Fluorescence lifetime imaging microscopy (FLIM) was utilized with a BODIPY-based molecular rotor to evaluate membrane viscosity under environmental conditions such as desiccation and temperature elevation. Drying hydrated *Salmonella* cells to 75% equilibrium relative humidity (ERH) increased the membrane viscosity from 1,199 to 1,309mPa·s (cP) at 22°C. Heating to 45°C decreased the membrane viscosity of hydrated cells from 1,199 to 1,082mPa·s, and decreased that of the desiccated cells from 1,309 to 1,245mPa·s. At both 22°C and 45°C, desiccated *Salmonella* was highly susceptible (>6.5 microbial log reduction (MLR) per stainless-steel coupon) to a 30-min treatment with the W/O emulsions formulated with short carbon chain acids ($C_{1\text{-}3}$). By comparison, the emulsion formulations with longer carbon chain acids ($C_{4\text{-}12}$) showed little to no MLR at 22°C, but achieved >6.5 MLR at 45°C. Based upon the decreased *Salmonella* membrane viscosity and the increased antimicrobial efficacy of $C_{4\text{-}12}$ W/O emulsions with increasing temperature, we propose that heating can make the membrane more fluid which may allow the longer carbon chain acids ($C_{4\text{-}12}$) to permeate or disrupt membrane structures.

KEYWORDS

cleaning and sanitation, desiccated *Salmonella*, dry food processing, membrane viscosity, oil-based antimicrobial delivery

1. Introduction

Due to the survival kinetics of *Salmonella* under desiccation, this organism is of particular concern across the manufacturing systems of low-moisture foods (LMFs) such as chocolate, peanut butter, and dry pet foods (Gruzdev et al., 2011; Beuchat et al., 2013; Kępińska-Pacelik and Biel, 2021). Recently, *Salmonella* contamination associated with chocolates has prompted a series of recall and regulatory inspection causing a plant shutdown for months and an economic

loss of millions to the manufacturer (Whitworth, 2022). Traditional wet cleaning approaches are not ideal for LMF processing due to the immiscible nature of water and lipids, and that the water residing on the processing equipment can induce microbial growth (Moerman and Mager, 2016). Commercial peanut butter and chocolate processing lines are usually cleaned by flushing with heated oil. Alcohol-based agents are used for sanitization as these compounds can evaporate completely leaving no residue on the contact surface (Grasso et al., 2015). However, since alcohol is flammable, processing shutdown is required for equipment cooldown before sanitization. For this reason, a dry sanitation system that can be applied with temperature elevation would be advantageous.

Oils mixed with food-grade organic acids have been shown to be an effective means for tackling desiccated *Salmonella* (Ghoshal et al., 2022; Chuang et al., 2023). In these reports, synergistic microbial inactivation was achieved by applying acetic acid-acidified oil combined with heating and water-in-oil (W/O) emulsion. Structure-wise, organic acids are a carboxylic group (polar) attached to an aliphatic chain of varying hydrocarbon chain-lengths (nonpolar), rendering these compounds preferentially soluble within a binary system consisting of an aqueous phase and an organic phase. For instance, since acetic acid has a partition coefficient (log *P*) of −0.17 at 25°C, its location within a W/O emulsion colloid is a dynamic motion where the acid mostly remains in the water phase yet being capable of partitioning into the oil phase (Chuang et al., 2023). Depending on the acid carbon chain-length, this motion can change to where more hydrophobic acids (e.g., with log $P > 0$) would mostly remain in oil yet being able to partition into water. The role of W/O emulsion in accelerating microbial inactivation from acidified oil has been linked to several physiological and physicochemical phenomenon such as membrane disruption (Ghoshal et al., 2022), the diffusion and partitioning of acid due to preferential affinity (Chapman and Ross, 2009; Trček et al., 2015; Bertheussen et al., 2017), and osmotic lysis in the presence of unbalanced vapor pressure at the oil-cell interface (Syamaladevi et al., 2016; Xie et al., 2021; Chuang et al., 2023). The dispersion of water in oil allows the partitioning of acetic acid from the continuous oil phase to the water droplets which subsequently functions as the vehicle for the acid to enter the cytoplasm (Chuang et al., 2023).

Researchers have studied the gene expression of *Salmonella* under low-a_w conditions, reporting several biological processes that were involved in the stress response, such as osmoregulation, heat-shock protein synthesis, and fatty-acid metabolism (Gruzdev et al., 2012; Chen et al., 2013; Fong and Wang, 2016; Chen and Jiang, 2017). However, more evidence in the fundamental physiology of desiccated *Salmonella* is needed to support the development of an effective sanitation method. Bacterial cells can adjust membrane viscosity upon environmental fluctuations allowing adaptation (Stein, 2012; Ernst et al., 2016). Viscosity is defined as the resistance of a fluid to deformation at a given rate, which can be mechanically assessed by shearing with liquids assuming homogeneity within a system large in volume. However, measurements will be prone to variation if mechanically assessed at the scale of a micron, such as bacterial plasma membranes, where systemic homogeneity cannot be assumed. Due to the hydrophobic nature, 4,4-difluoro-5,7-dimethyl-4-Bora-3a,4a-diaza-s-indacene (BODIPY)-based molecular rotors localize in certain biological regions such as the lipid bilayer (Kuimova, 2012). Molecular rotors are synthetic fluorophores that, following energy absorption from a certain wavelength of light, can emit photons *via* fluorescent or nonfluorescent pathways. Nonradioactive decay of the activated fluorophore occurs through intramolecular rotation which is dependent upon environmental viscosity. Thus, the fluorescence signal of a molecular rotor increases with increasing viscosity of where it localizes. Fluorescence lifetime imaging microscopy (FLIM) measures the time it takes an excited fluorophore to return to the ground state (Datta et al., 2020). The lifetime of a fluorophore is independent from the local fluorophore concentration and thus can be used for measuring micro-viscosity (Castellani et al., 2020). Application of BODIPY with FLIM allows an effective means to acquire numerical indications of the viscosity of bacterial plasma membrane.

The objective of this study was to evaluate the membrane viscosity of desiccated *Salmonella* and its sensitivity to treatment with W/O emulsions loaded with different chain-length organic acids, with temperature elevation.

2. Materials and methods

2.1. Bacterial strains and inoculum preparation

Salmonella enterica subsp. *enterica* serovars were obtained from the American Type Culture Collection (ATCC, Manassas, VA). These included *S.* Enteritidis phage type 30 (BAA-1045, an outbreak strain associated with LMF processing), and three other strains recommended for testing produce sanitizers (Harris et al., 2001), i.e., *S.* Michigan (BAA-709), *S.* Montevideo (BAA-710), and *S.* Gaminara (BAA-711). Stock cultures were stored at −80°C in tryptic soy broth (TSB, Difco, Becton Dickinson, Sparks, MD) with 25% glycerol (#G7893, Sigma-Aldrich, St. Louis, MO). Working cultures were prepared by streaking stock cultures on tryptic soy agar (TSA, Difco, Becton Dickinson) with overnight incubation at 37°C, which were maintained at 4°C and replaced monthly. Inoculum was prepared following the procedure by Uesugi et al. (2006). Prior to each experiment, an isolated colony was transferred from the working culture to TSB (20 mL) and incubated at 37°C for 24 h. To produce bacterial lawns, 100 μL of this liquid culture was spread onto TSA supplemented with 0.6% yeast extract (TSAYE, #BP1422, Fisher Scientific, Pittsburgh, PA) with incubation at 37°C for 24 h. The sessile cells were harvested using sterile scrapers (Fisher Scientific) and resuspended in distilled water (18.2 MΩ·cm, Direct-Q Water Purification System, Merck KgaA, Darmstadt, Germany). The optical density at 600 nm (OD_{600}) was adjusted to 1.2 to achieve approximately 10^9 CFU/mL as the inoculum. For cocktail studies, this procedure was repeated with each strain and the inocula were combined as a cocktail.

2.2. Desiccation of bacteria

Aliquots (20 μL) of the inoculum were added to stainless-steel coupons (2B-finish, 12.7 mm diameter × 3.8 mm thickness, Biosurface, Bozeman, MT) and held in a desiccator at room temperature (22°C) for 20 h. A saturated solution of sodium chloride (#S271-1, Fisher Scientific) was used to maintain the

equilibrium relative humidity (ERH) at 75%. This was based upon our previous report that the cells desiccated at 75% ERH were more resistant to treatment with acidified W/O emulsions than those desiccated at 33% ERH (Chuang et al., 2023). The time of desiccation was based on a report by Gruzdev et al. that cellular dehydration reached the maximum level after 20 h of desiccation (Gruzdev et al., 2011). Prior to each experiment, the coupons were washed with soapy water, soaked in acetone overnight, rinsed with distilled water, autoclaved, and dried for use.

2.3. Preparation of acidified W/O emulsion

2.3.1. Formulation and emulsification method

Commercially available vegetable oils (canola oil, corn oil, and peanut oil) were used interchangeably as the carrier oil within the tested systems. The types of carrier oil did not influence the antimicrobial efficacy of acidified oils and W/O emulsions (Ghoshal et al., 2022; Chuang et al., 2023). Polyglycerol polyricinoleate (PGPR 4150, Palsgaard, Juelsminde, Denmark), a food-grade hydrophobic surfactant, was dissolved in the carrier oil at 3% w/w. This oil-surfactant stock solution was mixed with organic acids (≥ 97%, Sigma-Aldrich) using a nutating mixer (Orbitron Rotator II Model 260,250, Boekel Scientific, Feasterville-Trevose, PA) at room temperature for 1 h to make acidified oils at 200 mM as calculated based on the sum of the volumes of the oil, surfactant, and acid. The organic acids were of different hydrocarbon chain-lengths (C_n) including formic/methanoic acid (C_1), acetic/ethanoic acid (C_2), propionic/propanoic acid (C_3), butyric/butanoic acid (C_4), valeric/pentanoic acid (C_5), caproic/hexanoic acid (C_6), enanthic/heptanoic acid (C_7), caprylic/octanoic acid (C_8), pelargonic/nonanoic acid (C_9), capric/decanoic acid (C_{10}), undecylic/undecanoic acid (C_{11}), and lauric/dodecanoic acid (C_{12}). For the acids with a melting point above room temperature (i.e., C_{10}, C_{11}, and C_{12}), the oil-surfactant-acid mixture was heated to 45°C to melt the crystalline, vortexed, and allowed cooldown back to room temperature.

For preparation of W/O emulsions, the oil-surfactant stock solution (without organic acid) was blended with 1% v/v distilled water using a high-shear mixer (M133/1281–0, Biospec Products, Inc., ESGC, Switzerland) at room temperature for 2 min. The obtained coarse W/O emulsions were further homogenized with a microfluidizer (M-110 L, Microfluidics, Newton, MA) at 12 kpsi for 2 passes. The obtained fine W/O emulsions were mixed with organic acids as previously described to make acidified W/O emulsions at 200 mM as calculated based on the sum of the volumes of the water, oil, surfactant, and acid. Analysis of emulsion particle/droplet size was performed with dynamic light scattering (DLS) using the Zetasizer Nano ZS (Malvern Instruments, Worcestershire, United Kingdom), with the results reported as the intensity-weighted mean diameter, Z average. Prior to DLS measurements, the samples were diluted 1:100 with hexadecane (refractive index = 1.434, viscosity = 3.13 mPa·s at 22°C) to prevent multi-scattering (Yi et al., 2014). The 1% water in W/O emulsions was selected based on a previous report determining the required water concentration that achieves antimicrobial enhancement (>6.5 MLR) of the acetic acid-acidified oil (Chuang et al., 2023).

2.3.2. Osmotic pressure assay

Glycerol was used to reduce the water activity (a_w) of W/O emulsions. For preparation, the oil-surfactant stock solution (without acid) was blended with 1% v/v distilled water and 3% v/v glycerol, homogenized by microfluidization, and mixed with organic acids as previously described. This allowed the antimicrobial efficacy of acidified W/O emulsions to be evaluated at a constant 1% water with reduced a_w. A dewpoint a_w meter (AquaLab Series 3, v2.3, METER Group, Pullman, WA) was used in continuous mode at 22°C for a_w measurements. The mean of two consecutive readings within ±0.002 was reported (Decagon Devices, Inc, 2015). The concentration of glycerol was selected based upon different water-glycerol fractions to achieve a certain a_w (Nakagawa and Oyama, 2019).

2.4. Antimicrobial assay

2.4.1. Treatment specification

A treatment solution (100 µL) was pipetted onto the desiccated cells on coupon, which was transferred to an incubator set at 22°C or 45°C to equilibrate for 5 min and remain holding at the prevailing temperature for 30 min. Upon end of treatment, one coupon was transferred to TSB (10 mL) buffered with 0.25 mM HEPES (pH 7.2, #H4034, Sigma-Aldrich) in a conical polypropylene tube with sterile glass beads (diameter: 1 mm). This was vortexed at 3200 rpm for 2 min to ensure the removal of cells from the coupon to the medium. Serial dilutions were made in 0.1% buffered peptone water (pH 7.2, Difco, Becton Dickinson).

2.4.2. Determination of survival cell numbers

Microbial survival was determined with plate counts on TSAYE with incubation at 37°C for 24 h. Longer incubation times did not result in different viable cell numbers. The detection limit with plate counts was 2 log CFU/coupon. When microbial survival was reduced to below this point, the experiments were repeated with Most Probable Number (MPN).

The MPN determination was performed according to the Bacteriological Analytical Manual (BAM) by the U.S. Food and Drug Administration (Blodgett, 2010). In this context, transferring one coupon to TSB (10 mL) upon end of treatment was considered as a 1:10 dilution. From here, inocula of 1, 0.1 and 0.01 mL were grown in TSB (20 mL/tube) with three tubes each. This allowed MPN determination per coupon to match the MPN/mL digits listed on the BAM table reference where inocula of 0.1, 0.01 and 0.001 mL were used. Presumptive growth was indicated by turbidity after incubating the tubes at 37°C for 24 h. Confirmatory tests were made by plating the turbid cultures on Xylose Lysine Deoxycholate (XLD) agar (#R459902, Fisher Scientific) with incubation at 37°C for 24 h. When all three tubes at each dilution were negative (0, 0, 0), the outcome was interpreted as less than the outcome with all negative tubes at the two lowest dilutions and one positive tube at the highest dilution (0, 0, 1). Thus, the detection limit was 3 MPN/coupon (0.48 log MPN/coupon). Microbial log reduction (MLR) was calculated with base 10:

$$\mathrm{MLR} = \log\left(N_0 / N\right) = \log N_0 - \log N \qquad (1)$$

where N_0 is the viable count of desiccated cells recovered from coupon, and N stands for the CFU or MPN survival cell number after treatment. When N_0 equals N, the treatment was interpreted as not antimicrobial (NA).

2.5. Fluorescence lifetime microscopy

2.5.1. Sample preparation

Cell staining was performed in dark following the procedure by Mika et al. with modifications (Mika et al., 2016). For preparation of hydrated cells, an isolated colony was transferred from the working culture to TSB (20 mL) and incubated at 37°C for 18 h. On the day of experiment, this culture was diluted 1:100 with fresh TSB (to 0.02 OD_{600}), supplemented with BODIPY FL C_{12} (4,4-difluoro-5,7-dimethyl-4-Bora-3a,4a-diaza-s-indacene-3-dodecanoic acid, #D3822, Fisher Scientific) from a 2.5 mM stock solution in dimethyl sulfoxide (DMSO, #J66650AE, Fisher Scientific) to 2 μM, and incubated at 37°C without shaking for 2–3 h to allow staining. Upon end of incubation, the stained cells were washed twice with dye-free TSB and resuspended in distilled water. A loopful of cells were spread onto a glass bottom dish with poly-d-lysine coating (#P35GC-1.5-10-C, MatTek, Ashland, MA), briefly dried (15 min) in a biosafety cabinet at room temperature, and observed under a microscope. For preparation of desiccated cells, the cells grown on TSAYE plates as lawns were suspended in TSB (to 0.02 OD_{600}), mixed with BODIPY, and incubated as previously described. The stained cells were washed and resuspended in distilled water, from which droplets (20 μL) were added to glass bottom dishes and held in a desiccator at 75% ERH at room temperature for 20 h. The concentration of DMSO during staining was 0.08% v/v. The growth of *Salmonella* was not influenced by BODIPY and DMSO at the specified concentrations (Supplementary Figure S1).

2.5.2. FLIM measurement

Fluorescence lifetime imaging microscopy (FLIM) was performed using a confocal microscope (A1/Ti-E inverted, Nikon, Japan) to which an A1-FLIM module (Becker & Hickl, Berlin, Germany) was attached. Glass bottom dishes were loaded with bacterial samples and mounted on a microscope stage top chamber (H301-MINI, Okolab, Sewickley, PA) which was connected to a controlled heating system (Okolab) at the Light Microscopy Facility, Institute for Applied Life Sciences, University of Massachusetts-Amherst. For temperature elevation assays, the chamber was heated to 45°C and the samples were equilibrated for 5 min prior to FLIM measurements. A wavelength of 488 nm (50 mHz) was used to excite BODIPY FL C_{12}. Pinhole was 1.0 Airy Unit. Dwell time was 2.2 μs/pixel. Image acquisition was set to a size of 1,024 × 1,024 and measured over 30 s. Emitted photons were detected using a time-correlated single photon counting (TCSPC) module (HPM-100-40 detector, SPC-150 N module card, Becker & Hickl) with a 525/50 bandpass filter (peak of BODIPY FL C_{12} emission spectrum: 511 nm). Each sample was measured for less than 1 h to prevent photobleaching. Single-cell images were obtained by cropping the captured field using the NIS-Elements software (Nikon). Cell-cluster images were shown with the entire captured field.

2.5.3. FLIM data analysis

Analysis of FLIM data was performed using the SPCImage software (v8.6, Becker & Hickl). Regions of interest (ROIs) were drawn around isolated single cells identified in the captured FLIM images. This was followed by binning all the pixels within the respective ROI. The instrument response function (IRF) was automatically defined by the software and approximately 10^4 photons were assessed per decay curve. This level of photon number is required for analyzing double-exponential decays (Warren et al., 2013). Fitting data with a double-exponential function showed Chi^2 values ranging from 0.96 to 1.58, indicating a good fit between the observed values and the model predictions. Below is the general expression of a double-exponential decay:

$$f(t) = a_1 e^{-t/\tau_1} + a_2 e^{-t/\tau_2} \quad (2)$$

where f is fluorescence intensity, t is time, τ is the fluorescence lifetime of the exponential components, and α is the amplitude of the exponential components ($\alpha_1 + \alpha_2 = 1$). The BODIPY-based rotors have two conformations within the cytoplastic membrane, which are accompanied by different sensitivities to viscosity due to the molecular orientation (Dent et al., 2015). The long lifetime component derives from the rotor that localizes in the hydrocarbon tail region of the lipid bilayer, and thus is viscosity-sensitive, providing a better representation of the viscosity of ordered membrane structures (Mika et al., 2016). Thus, τ_1 was used to calculate membrane viscosity.

2.5.4. Calibration of lifetime against viscosity

The measured fluorescence lifetime was used for calculation of membrane viscosity using a lifetime-viscosity calibration funtion:

$$\log \mu = (\log \tau + 0.75614) / 0.4569 \quad (3)$$

where μ is viscosity in mPa·s (cP) and τ is fluorescence lifetime in nanosecond. This equation was developed by Hosny et al. by measuring the fluorescence lifetime of BODIPY C_{10} in methanol-glycerol mixtures (bulk liquids of known viscosity) (Hosny et al., 2016). Despite a difference in the hydrocarbon chain-length, the BODIPY-based C_{10} and C_{12} rotors possess identical photophysical properties, such as the viscosity-dependent fluorescence lifetime (Kuimova et al., 2008; Wu et al., 2013; Polita et al., 2020). Thus, Equation (3) was used for lifetime-viscosity calibration of BODIPY FL C_{12} in *Salmonella* membrane.

2.6. Statistical analysis

Experiments were conducted in triplicate independently. Two-way analysis of variance (ANOVA) was performed with post-hoc Tukey for pairwise comparison using the Prism software (v9.5.1, GraphPad, San Diego, CA). Differences were determined statistically significant at $p < 0.05$.

3. Results and discussion

3.1. Formulation screening with *Salmonella* cocktail

The desiccated cells of a four-strain *Salmonella* cocktail were used for screening the antimicrobial efficacy of oil-based formulations (**F1-6**) with a 30-min treatment time (Figure 1). Acetic acid (C_2) was selected for use in the screening procedure based on our previous report that it was the most effective food-grade acid against desiccated *Salmonella* among different chain-length organic acids (Ghoshal et al., 2022). The use of 1% water in W/O emulsions was based upon another report determining the required water level for acidified W/O emulsions to achieve >6.5 MLR with 200 mM acetic acid (Chuang et al., 2023). Likewise, 3% glycerol was used in **F3** and **F6** to decrease the solution a_w while maintaining a constant 1% water. The results showed that the non-acidified controls, including oil with surfactant (**F1**), oil with a W/O emulsion (**F2**), and oil with a W/O emulsion with glycerol (**F3**) had little to no antimicrobial efficacy. Dissolving 200 mM acetic acid (C_2, **F4**) in oil without water showed low levels of antimicrobial efficacy with 0.51 and 0.88 MLR at 22°C and 45°C, respectively. Dispersing 1% water within the acidified oil as a W/O emulsion (**F5**) increased the solution a_w from 0.33 to 0.92 and the antimicrobial efficacy greatly increased compared to without water (**F4**) with a >6.5 MLR at both 22°C and 45°C. Adding glycerol to the acidified oil with a W/O emulsion (**F6**) reduced the solution a_w from 0.92 to 0.38 and the antimicrobial efficacy decreased compared to the emulsion without glycerol (**F5**). The acidified oil with a W/O emulsion with glycerol (**F6**) showed 1.96 and 3.16 MLR at 22°C and 45°C, respectively. The antimicrobial enhancement from water dispersion may be attributed to the partitioning of acetic acid from the oil phase into the aqueous phase which subsequently functioned as a vehicle for the acid to enter the cytoplasm, as depicted in a proposed partition equilibria of organic acids at the oil–water-cell interface (Supplementary Figure S2). Since the antimicrobial efficacy was greatly reduced with the addition of glycerol, these results indicated that the antimicrobial mechanism may be due to differential osmotic pressure. As all the *Salmonella* strains were susceptible to **F5** showing >6.5 MLR at both the tested temperatures, the strain most relevant to LMF processing (*S.* Enteritidis) was used as the representative strain in all subsequent experiments.

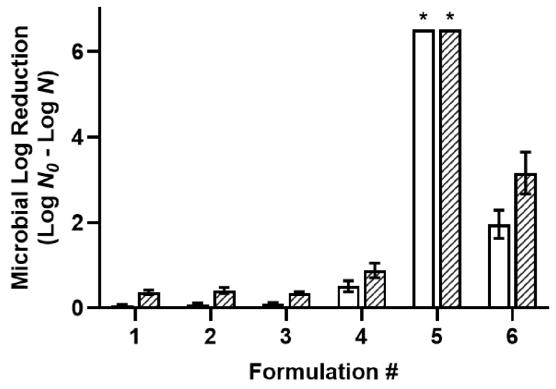

FIGURE 1
Efficacy of oil-based formulations against a five-strain *Salmonella* cocktail desiccated to 75% ERH, with a 30-min treatment at 22°C (white) or 45°C (striped). Formulations: (1) oil with 3% w/w PGPR surfactant, (2) W/O emulsion with 3% w/w PGPR and 1% v/v distilled water, (3) W/O emulsion with 3% w/w PGPR, 1% v/v distilled, and 3% v/v glycerol, (4) acidified oil with 200 mM acetic acid, and 3% w/w PGPR, (5) acidified W/O emulsion with 200 mM acetic acid, 3% w/w PGPR, and 1% v/v distilled water, (6) acidified W/O emulsion with 200 mM acetic acid, 3% w/w PGPR, 1% v/v distilled water, and 3% v/v glycerol. *Microbial survival was reduced to below the detection limit and expressed as >6.5 MLR/coupon.

3.2. Influences of organic acid carbon chain-length, treatment temperature, and solution a_w on the efficacy of acidified W/O emulsions against desiccated *Salmonella*

Formulations comprising different chain-length acids were tested against desiccated *S.* Enteritidis with a 30-min treatment time (Table 1). The measured solution a_w of acidified oil was 0.51 with C_1 and 0.33 with the remaining acids ($C_{2\text{-}12}$), that of acidified W/O emulsion was 0.92 for all the acids, and that of acidified W/O emulsion with glycerol was 0.38 for all the acids (Supplementary Table S1). Acidified oils formulated with the shorter chain-length acids ($C_{1\text{-}3}$) were found more effective than those formulated with the longer chain-length acids ($C_{4\text{-}12}$). The antimicrobial efficacy of C_1 acidified oil was pronounced, showing >6.5 MLR at both 22°C and 45°C. The C_2 acidified oil showed 0.69 MLR at 22°C and 1.42 MLR at 45°C. The C_3 acidified oil showed 0.89 MLR at 22°C and 1.11 MLR at 45°C. By comparison, the $C_{4\text{-}12}$ acidified oils showed little to no MLR at 22°C which slightly increased at 45°C. These increments with temperature elevation were likely due to the sole influence of heating as previously illustrated with the non-acidified controls (F1-3, Figure 1).

Dispersing 1% water within acidified oils as an emulsion enhanced the antimicrobial efficacy depending on the acid carbon chain-length and treatment temperature. Acidified W/O emulsions formulated with $C_{1\text{-}3}$ acids showed >6.5 MLR at both 22°C and 45°C. However, those formulated with $C_{4\text{-}12}$ acids showed little to no MLR at 22°C but were enhanced at 45°C (>6.5 MLR). All the emulsions were stable in terms of droplet size after a 30-min incubation at 45°C (Supplementary Table S2), and thus we do not believe the antimicrobial enhancement by temperature elevation was related to emulsion instability. Glycerol attenuated the antimicrobial efficacy of C_2 and C_3 acidified W/O emulsions at both 22°C and 45°C, and attenuated that of $C_{4\text{-}12}$ acidified W/O emulsions at 45°C, to MLR levels close to the corresponding acidified oils. Such efficacy attenuation aligned with the reduced solution a_w upon glycerol addition. It appeared C_1 was an exception, that the a_w of acidified oil was greater than that of the acidified W/O emulsion with glycerol (Supplementary Table S1), which was in line with the corresponding MLR data (Table 1). However, the difference between the antimicrobial efficacy of C_1 and C_2 acidified oils was pronounced, indicating that the solution a_w measured at 22°C only partially explained the mechanism. Other factors may have been involved, e.g., the a_w of oil is a function of the prevailing temperature (Yang et al., 2020; Xie et al., 2021). Thus, the a_w of acidified oils formulated with different organic acids could exhibit different temperature dependence, thereby showing varying levels of antimicrobial efficacy. In addition, the data with $C_{4\text{-}12}$ acidified

TABLE 1 Influence of organic acid carbon chain-length and treatment temperature on the efficacy of acidified oils and W/O emulsions against desiccated *Salmonella* Enteritidis.

Organic acid[a]	Chain length	Delivery system and treatment temperature (MLR±SD)[b]					
		Oil with PGPR		W/O emulsion		W/O emulsion with glycerol	
		22°C	45°C	22°C	45°C	22°C	45°C
Formic	C_1	$>6.52^{B}$	$>6.52^{B}$	$>6.52^{B}$	$>6.52^{B}$	1.32 ± 0.65^{A}	$>6.52^{B}$
Acetic	C_2	0.69 ± 0.19^{A}	1.42 ± 0.14^{B}	$>6.52^{D}$	$>6.52^{D}$	0.81 ± 0.24^{A}	2.53 ± 0.75^{C}
Propionic	C_3	0.89 ± 0.24^{A}	1.11 ± 0.27^{AB}	$>6.52^{C}$	$>6.52^{C}$	0.73 ± 0.22^{A}	1.41 ± 0.66^{B}
Butyric	C_4	NA	0.52 ± 0.13^{A}	0.55 ± 0.06^{A}	$>6.52^{C}$	0.31 ± 0.16^{A}	1.40 ± 0.31^{B}
Valeric	C_5	NA	0.31 ± 0.02^{A}	0.11 ± 0.05^{A}	$>6.52^{C}$	NA	1.12 ± 0.16^{B}
Caproic	C_6	0.21 ± 0.09^{A}	0.68 ± 0.08^{B}	0.72 ± 0.18^{B}	$>6.52^{C}$	0.10 ± 0.03^{A}	0.74 ± 0.48^{B}
Enanthic	C_7	NA	0.34 ± 0.03^{A}	0.34 ± 0.26^{A}	$>6.52^{C}$	NA	0.79 ± 0.22^{A}
Caprylic	C_8	0.26 ± 0.18^{A}	0.49 ± 0.26^{AB}	0.94 ± 0.26^{B}	$>6.52^{C}$	0.56 ± 0.18^{AB}	0.74 ± 0.11^{B}
Pelargonic	C_9	NA	0.39 ± 0.11^{A}	0.31 ± 0.10^{A}	$>6.52^{B}$	NA	0.30 ± 0.09^{A}
Capric	C_{10}	0.23 ± 0.04^{A}	0.28 ± 0.09^{A}	0.67 ± 0.17^{A}	$>6.52^{B}$	0.37 ± 0.06^{A}	0.57 ± 0.09^{A}
Undecylic	C_{11}	NA	0.31 ± 0.03^{A}	0.38 ± 0.09^{A}	$>6.52^{B}$	NA	0.22 ± 0.18^{A}
Lauric	C_{12}	0.16 ± 0.06^{A}	0.40 ± 0.17^{A}	1.05 ± 0.28^{B}	$>6.52^{C}$	0.49 ± 0.12^{A}	1.02 ± 0.04^{B}

Different uppercase letters indicated significant differences ($p < 0.05$) within each row. Comparison was not drawn where treatment was not antimicrobial (NA).[a]The organic acid concentration was 200 mM based upon the final solution volume.
[b]A 30-min contact time against cells desiccated to 75% ERH.

W/O emulsions suggested there may be a correlation between treatment temperature and the acid carbon chain-length. We hypothesize that heating may result in changes in the ability of the longer chain-length acids to permeate the cells, possibly due to changes in the viscosity of the cellular membrane.

3.3. Membrane viscosity of *Salmonella* upon heating

To test the hypothesis that changing treatment temperature can change the cellular membrane viscosity, FLIM was used to assess the fluorescence lifetime of BODIPY-stained *S.* Enteritidis (Figure 2). The confocal micrograph showed a ring-like fluorescent pattern at the periphery of the stained cells (Figure 2A), indicating rotor localization in the plasma membrane, in agreement with the observation by Nenninger et al. that BODIPY-based rotors stained the plasma membrane of vegetative bacterial cells producing a fluorescent halo (Nenninger et al., 2014). The FLIM images were shown with a single cell (Figures 2B,C) and as a cluster (Figures 2D,E). A decrease in fluorescence lifetime was observed with increasing temperature. The measured fluorescence lifetime values of hydrated cells were 4.46 ns at 22°C and 4.24 ns at 45°C, which were calculated to viscosity values of 1,199 mPa·s at 22°C and 1,082 mPa·s at 45°C. These values are comparable with the existing literature. Oswald et al. measured the protein diffusion coefficients through the membrane of hydrated *Escherichia coli* cells and fitted the values with the Saffman-Delbrück model, reporting a membrane viscosity value of 1,200 mPa·s at 23°C (Oswald et al., 2016). Mika et al. reported that, with the FLIM-BODIPY approach, the membrane viscosity of hydrated *E. coli* cells was 1,160 mPa·s at 23°C which decreased to 950 mPa·s at 37°C (Blodgett, 2010).

After desiccation to 75% ERH, *S.* Enteritidis cells had increased membrane viscosity (Figure 3). At room temperature (22°C), the mean of the calculated membrane viscosity values of hydrated cells was 1,199 mPa·s, while after desiccation to 75% ERH, the mean membrane viscosity increased to 1,309 mPa·s. This was also observed at 45°C, with a mean membrane viscosity of 1,082 mPa·s for hydrated cells and after desiccation to 75% ERH, the mean membrane viscosity increased to 1,245 mPa·s. Temperature elevation to 45°C significantly decreased the membrane viscosity for both cellular hydration levels, and the difference was found more pronounced for the hydrated cells ($p < 0.001$) than the desiccated cells ($p < 0.05$). *Salmonella* exhibits cross-tolerance to multiple environmental stresses following exposure to one stress (Gruzdev et al., 2011; Ye et al., 2019; Datta et al., 2020). In particular, the thermal resistance of desiccated *Salmonella* is pronounced. One proposed mechanism is that the fluidity of cellular membrane can vary upon environmental conditions, thereby affecting thermodynamics (Álvarez-Ordóñez et al., 2008, 2009; Stein, 2012; Ernst et al., 2016; Chen and Jiang, 2017).

Based upon our results, we propose that the increased antimicrobial efficacy of $C_{4\text{-}12}$ acidified W/O emulsions at 45°C (Table 1), may be due to a lower membrane viscosity upon temperature elevation (Figure 3). This decrease in membrane viscosity could allow longer chain-length acids ($C_{4\text{-}12}$) to diffuse into the cellular membrane causing damage. The damaged membrane in combination with the water in the W/O emulsion contributes to cellular hypoosmotic stress resulting in cellular death at the elevated temperature. The addition of glycerol to the emulsions (Table 1) reduces the antimicrobial efficacy, confirming the involvement of water stress in cellular destruction.

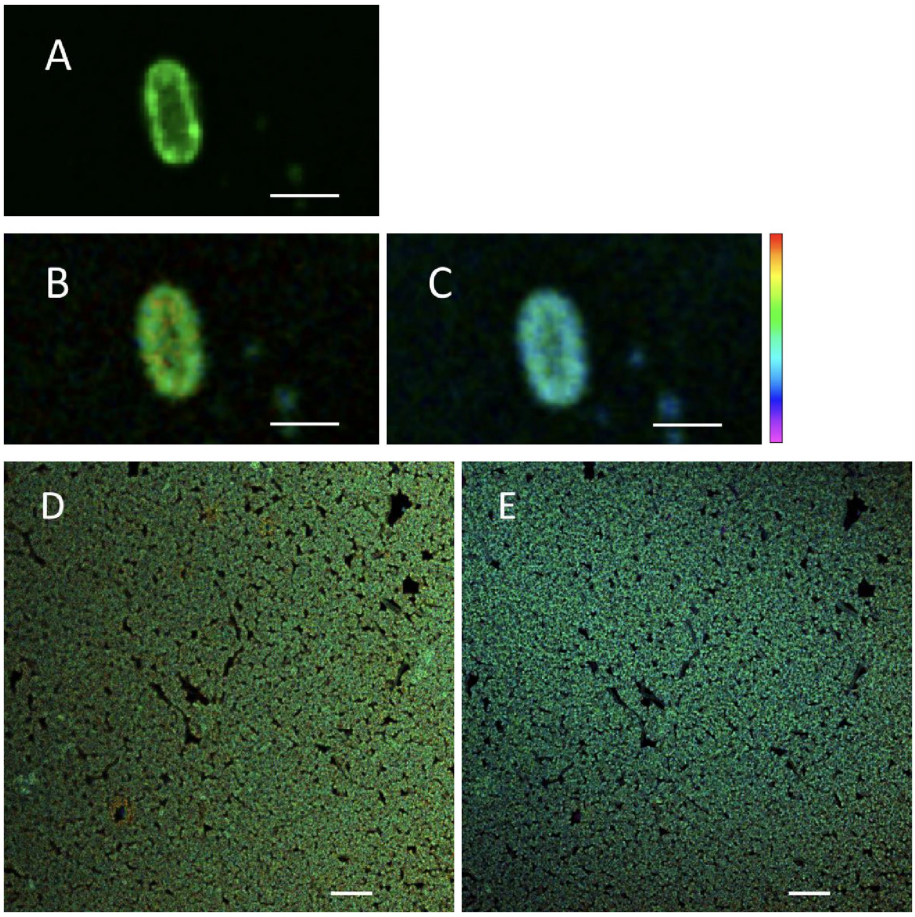

FIGURE 2
Fluorescent micrographs of hydrated *Salmonella* Enteritidis stained with BODIPY FL C_{12}: confocal scanned **(A)**, FLIM measured at 22°C **(B,D)**, and FLIM measured at 45°C **(C,E)**. Scale bar: 2μm [**(A–C)**, single cell]; 10μm [**(D,E)**, cell cluster]. Of the lifetime color scale, the upper (red) and lower (purple) limits were 5.5 and 3ns, respectively.

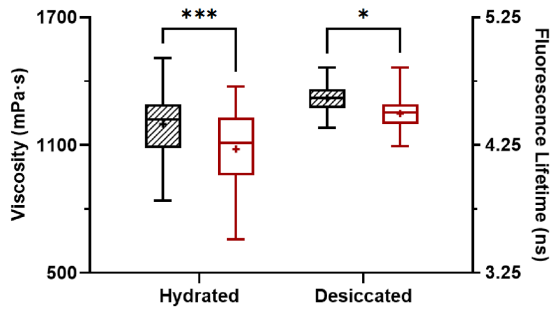

FIGURE 3
Membrane viscosity of hydrated and desiccated *Salmonella* Enteritidis at 22°C (striped) and 45°C (white). The FLIM data was obtained from 37 hydrated cells and 49 desiccated cells. The same cells were used for measurements at 22°C and 45°C. Within each data set, whiskers (error bars) indicated the maximum and minimum values, the box covered the interquartile range (25–75th percentile), the horizontal line in the box was the median, and the plus mark was the mean. Differences were significant at $p<0.05$ (*) and <0.001 (***).

In conclusion, we have found that the antimicrobial efficacy of organic acids within W/O emulsion systems is dependent upon acid chain-length and treatment temperature, with the longer chain acids (C_{4-12}) becoming greatly antimicrobial when combined with elevated temperature. We have shown that the cellular membrane becomes less viscous at elevated temperatures and likely contributes to the increase in antimicrobial efficacy. However, it is of importance to note a caveat that the temperature-viscosity relationship does not fully explain why some fatty acids that are much smaller than the lipids in bacterial membrane, such as butyric acid, did not show antimicrobial efficacy without temperature elevation.

Data availability statement

The original contributions presented in the study are included in the article/Supplementary material, further inquiries can be directed to the corresponding author.

Author contributions

SC: methodology, acquisition, analysis interpretation of data, drafting, and editing. MG: methodology development. LM:

conception of project, data analysis drafting, editing and revising, and approval for publication. All authors contributed to the article and approved the submitted version.

Funding

This work is based upon work supported by the National Institute of Food and Agriculture (NIFA), U.S. Department of Agriculture (USDA), and the Center for Agriculture, Food, and the Environment and the Department of Food Science at the University of Massachusetts—Amherst, under project number MAS00567, with support from the Foundational and Applied Science Program (grant number 2020-67017-30786) of the USDA—NIFA.

Acknowledgments

The mention of trade names or commercial products is solely for the purpose of providing specific information and does not imply recommendation or endorsement by USDA.

Conflict of interest

The authors declare that the research was conducted in the absence of any commercial or financial relationships that could be construed as a potential conflict of interest.

Publisher's note

Supplementary material

The Supplementary material for this article can be found online at: https://www.frontiersin.org/articles/10.3389/fmicb.2023.1197473/full#supplementary-material

References

Álvarez-Ordóñez, A., Fernández, A., López, M., Arenas, R., and Bernardo, A. (2008). Modifications in membrane fatty acid composition of *Salmonella typhimurium* in response to growth conditions and their effect on heat resistance. *Int. J. Food Microbiol.* 123, 212–219. doi: 10.1016/j.ijfoodmicro.2008.01.015

Álvarez-Ordóñez, A., Fernández, A., López, M., and Bernardo, A. (2009). Relationship between membrane fatty acid composition and heat resistance of acid and cold stressed Salmonella Senftenberg CECT 4384. *Food Microbiol.* 26, 347–353. doi: 10.1016/j.fm.2008.11.002

Bertheussen, A., Simon, S., and Sjöblom, J. (2017). Equilibrium partitioning of naphthenic acids and bases and their consequences on interfacial properties. *Colloid Surf. Physicochem Eng. Asp.* 529, 45–56. doi: 10.1016/j.colsurfa.2017.05.068

Beuchat, L. R., Komitopoulou, E., Beckers, H., Betts, R. P., Bourdichon, F., Fanning, S., et al. (2013). Low–water activity foods: increased concern as vehicles of foodborne pathogens. *J. Food Prot.* 76, 150–172. doi: 10.4315/0362-028X.JFP-12-211

Blodgett, R.. (2010). BAM appendix 2: most probable number from serial dilutions. Available at: https://www.fda.gov/food/laboratory-methods-food/bam-appendix-2-most-probable-number-serial-dilutions (accessed 24 February 2023).

Castellani, C. M., Torres-Ocampo, A. P., Breffke, J., White, A. B., Chambers, J. J., Stratton, M. M., et al. (2020). "Live-cell FLIM-FRET using a commercially available system" in *Methods in cell biology*. eds. P. Tran and I. Curie (Cambridge, MA: Academic Press)

Chapman, B., and Ross, T. (2009). Escherichia coli and *Salmonella enterica* are protected against acetic acid, but not hydrochloric acid, by hypertonicity. *Appl. Environ. Microbiol.* 75, 3605–3610. doi: 10.1128/AEM.02462-08

Chen, Z., Diao, J., Dharmasena, M., Ionita, C., Jiang, X., and Rieck, J. (2013). Thermal inactivation of desiccation-adapted Salmonella spp. in aged chicken litter. *Appl. Environ. Microbiol.* 79, 7013–7020. doi: 10.1128/AEM.01969-13

Chen, Z., and Jiang, X. (2017). Thermal resistance and gene expression of both desiccation-adapted and rehydrated *Salmonella enterica* serovar typhimurium cells in aged broiler litter. *Appl. Environ. Microbiol.* 83, e00367–e00317. doi: 10.1128/AEM.00367-17

Chuang, S., Ghoshal, M., and McLandsborouh, L. (2023). Oil-based sanitization in low-moisture environments: delivery of acetic acid with water-in-oil emulsions. *Microbiol. Spectr.* e05293–e05222. doi: 10.1128/spectrum.05293-22. [E-pub ahead of print].

Datta, R., Heaster, T. M., Sharick, J. T., Gillette, A. A., and Skala, M. C. (2020). Fluorescence lifetime imaging microscopy: fundamentals and advances in instrumentation, analysis, and applications. *J. Biomed. Opt.* 25:071203. doi: 10.1117/1.JBO.25.7.071203

Decagon Devices, Inc. (2015). Measuring the water activity of vegetable oil. Available at: http://manuals.decagon.com/ApplicationNotes/13464_MeasuringtheAwofVegetableOil_Print.pdf (accessed 24 February 2023).

Dent, M. R., López-Duarte, I., Dickson, C. J., Geoghegan, N. D., Cooper, J. M., Gould, I. R., et al. (2015). Imaging phase separation in model lipid membranes through the use of BODIPY based molecular rotors. *Phys. Chem. Chem. Phys.* 17, 18393–18402. doi: 10.1039/C5CP01937K

Ernst, R., Ejsing, C. S., and Antonny, B. (2016). Homeoviscous adaptation and the regulation of membrane lipids. *J. Mol. Biol.* 428, 4776–4791. doi: 10.1016/j.jmb.2016.08.013

Fong, K., and Wang, S. (2016). Heat resistance of *Salmonella enterica* is increased by pre-adaptation to peanut oil or sub-lethal heat exposure. *Food Microbiol.* 58, 139–147. doi: 10.1016/j.fm.2016.04.004

Ghoshal, M., Chuang, S., Zhang, Y., and McLandsborough, L. (2022). Efficacy of acidified oils against Salmonella in low-moisture environments. *Appl. Environ. Microbiol.* 88, e00935–e00922. doi: 10.1128/aem.00935-22

Grasso, E. M., Grove, S. F., Halik, L. A., Arritt, F., and Keller, S. E. (2015). Cleaning and sanitation of Salmonella-contaminated peanut butter processing equipment. *Food Microbiol.* 46, 100–106. doi: 10.1016/j.fm.2014.03.003

Gruzdev, N., McClelland, M., Porwollik, S., Ofaim, S., Pinto, R., and Saldinger-Sela, S. (2012). Global transcriptional analysis of dehydrated *Salmonella enterica* serovar typhimurium. *Appl. Environ. Microbiol.* 78, 7866–7875. doi: 10.1128/AEM.01822-12

Gruzdev, N., Pinto, R., and Sela, S. (2011). Effect of desiccation on tolerance of *Salmonella enterica* to multiple stresses. *Appl. Environ. Microbiol.* 77, 1667–1673. doi: 10.1128/AEM.02156-10

Harris, L. J., Beuchat, L. R., Kajs, T. M., Ward, T. E., and Taylor, C. H. (2001). Efficacy and reproducibility of a produce wash in killing Salmonella on the surface of tomatoes assessed with a proposed standard method for produce sanitizers. *J. Food Prot.* 64, 1477–1482. doi: 10.4315/0362-028X-64.10.1477

Hosny, N. A., Fitzgerald, C., Vyšniauskas, A., Athanasiadis, A., Berkemeier, T., Uygur, N., et al. (2016). Direct imaging of changes in aerosol particle viscosity upon hydration and chemical aging. *Chem. Sci.* 7, 1357–1367. doi: 10.1039/C5SC02959G

Kępińska-Pacelik, J., and Biel, W. (2021). Microbiological hazards in dry dog chews and feeds. *Anim* 11:631. doi: 10.3390/ani11030631

Kuimova, M. K. (2012). Mapping viscosity in cells using molecular rotors. *Phys. Chem. Chem. Phys.* 14, 12671–12686. doi: 10.1039/c2cp41674c

Kuimova, M. K., Yahioglu, G., Levitt, J. A., and Suhling, K. (2008). Molecular rotor measures viscosity of live cells via fluorescence lifetime imaging. *J. Am. Chem. Soc.* 130, 6672–6673. doi: 10.1021/ja800570d

Mika, J. T., Thompson, A. J., Dent, M. R., Brooks, N. J., Michiels, J., Hofkens, J., et al. (2016). Measuring the viscosity of the *Escherichia coli* plasma membrane using molecular rotors. *Biophys. J.* 111, 1528–1540. doi: 10.1016/j.bpj.2016.08.020

Moerman, F., and Mager, K. (2016). "Cleaning and disinfection in dry food processing facilities" in *Handbook of hygiene control in the food industry*. eds. H. Lelieveld, J. Holah and D. Gabrić (Sawston, United Kingdom: Woodhead Publishing)

Nakagawa, H., and Oyama, T. (2019). Molecular basis of water activity in glycerol–water mixtures. *Front. Chem.* 7:731. doi: 10.3389/fchem.2019.00731

Nenninger, A., Mastroianni, G., Robson, A., Lenn, T., Xue, Q., Leake, M. C., et al. (2014). Independent mobility of proteins and lipids in the plasma membrane of *Escherichia coli*. *Mol. Microbiol.* 92, 1142–1153. doi: 10.1111/mmi.12619

Oswald, F., Varadarajan, A., Lill, H., Peterman, E. J., and Bollen, Y. J. (2016). MreB-dependent organization of the *E. coli* cytoplasmic membrane controls membrane protein diffusion. *Biophys. J.* 110, 1139–1149. doi: 10.1016/j.bpj.2016.01.010

Polita, A., Toliautas, S., Žvirblis, R., and Vyšniauskas, A. (2020). The effect of solvent polarity and macromolecular crowding on the viscosity sensitivity of a molecular rotor BODIPY-C 10. *Phys. Chem. Chem. Phys.* 22, 8296–8303. doi: 10.1039/C9CP06865A

Stein, W. (2012). *Transport and diffusion across cell membranes*. Amsterdam: Elsevier.

Syamaladevi, R. M., Tang, J., and Zhong, Q. (2016). Water diffusion from a bacterial cell in low-moisture foods. *J. Food Sci.* 81, R2129–R2134. doi: 10.1111/1750-3841.13412

Trček, J., Mira, N. P., and Jarboe, L. R. (2015). Adaptation and tolerance of bacteria against acetic acid. *Appl. Microbiol. Biotechnol.* 99, 6215–6229. doi: 10.1007/s00253-015-6762-3

Uesugi, A. R., Danyluk, M. D., and Harris, L. J. (2006). Survival of *Salmonella* Enteritidis phage type 30 on inoculated almonds stored at −20, 4, 23, and 35 C. *J. Food Prot.* 69, 1851–1857. doi: 10.4315/0362-028X-69.8.1851

Warren, S. C., Margineanu, A., Alibhai, D., Kelly, D. J., Talbot, C., Alexandrov, Y., et al. (2013). Rapid global fitting of large fluorescence lifetime imaging microscopy datasets. *PLoS One* 8:e70687. doi: 10.1371/journal.pone.0070687

Whitworth, J. (2022). Strauss feels the impact of Salmonella related to chocolate recall and site shutdown. Available at: https://www.foodsafetynews.com/2022/08/strauss-feels-impact-of-salmonella-related-to-chocolate-recall-and-site-shutdown/ (accessed February 24, 2023).

Wu, Y., Štefl, M., Olzyńska, A., Hof, M., Yahioglu, G., Yip, P., et al. (2013). Molecular rheometry: direct determination of viscosity in L_o and L_d lipid phases via fluorescence lifetime imaging. *Phys. Chem. Chem. Phys.* 15, 14986–14993. doi: 10.1039/c3cp51953h

Xie, Y., Xu, J., Yang, R., Alshammari, J., Zhu, M. J., Sablani, S., et al. (2021). Moisture content of bacterial cells determines thermal resistance of *Salmonella enterica* serotype Enteritidis PT 30. *Appl. Environ. Microbiol.* 87, e02194–e02120. doi: 10.1128/AEM.02194-20

Yang, R., Guan, J., Sun, S., Sablani, S. S., and Tang, J. (2020). Understanding water activity change in oil with temperature. *Curr. Res. Food Sci.* 3, 158–165. doi: 10.1016/j.crfs.2020.04.001

Ye, B., He, S., Zhou, X., Cui, Y., Zhou, M., and Shi, X. (2019). Response to acid adaptation in *Salmonella enterica* serovar Enteritidis. *J. Food Sci.* 84, 599–605. doi: 10.1111/1750-3841.14465

Yi, J., Zhu, Z., McClements, D. J., and Decker, E. A. (2014). Influence of aqueous phase emulsifiers on lipid oxidation in water-in-walnut oil emulsions. *J. Agric. Food Chem.* 62, 2104–2111. doi: 10.1021/jf404593f

frontiers | Frontiers in Microbiology

TYPE Original Research
PUBLISHED 03 July 2023
DOI 10.3389/fmicb.2023.1193810

OPEN ACCESS

EDITED BY
Chao Shi,
Northwest A&F University, China

REVIEWED BY
Hossein Mahmoudvand,
Lorestan University of Medical Sciences, Iran
Evdokia Vassalou,
University of West Attica, Greece
Reghaissia Nassiba,
University of Souk Ahras, Algeria

*CORRESPONDENCE
Shahira A. Ahmed
✉ shahira_ahmed@med.suez.edu.eg
Panagiotis Karanis
✉ karanis.p@unic.ac.cy

†These authors have contributed equally to this work

RECEIVED 25 March 2023
ACCEPTED 06 June 2023
PUBLISHED 03 July 2023

CITATION
Ahmed SA, Eltamany EE, Nafie MS, Elhady SS, Karanis P and Mokhtar AB (2023) Anti-*Cryptosporidium parvum* activity of *Artemisia judaica* L. and its fractions: *in vitro* and *in vivo* assays.
Front. Microbiol. 14:1193810.
doi: 10.3389/fmicb.2023.1193810

Anti-*Cryptosporidium parvum* activity of *Artemisia judaica* L. and its fractions: *in vitro* and *in vivo* assays

Shahira A. Ahmed[1*†], Enas E. Eltamany[2], Mohamed S. Nafie[3], Sameh S. Elhady[4,5], Panagiotis Karanis[6,7*] and Amira B. Mokhtar[1†]

[1]Department of Medical Parasitology, Faculty of Medicine, Suez Canal University, Ismailia, Egypt, [2]Department of Pharmacognosy, Faculty of Pharmacy, Suez Canal University, Ismailia, Egypt, [3]Department of Chemistry (Biochemistry Program), Faculty of Science, Suez Canal University, Ismailia, Egypt, [4]Department of Natural Products, Faculty of Pharmacy, King Abdulaziz University, Jeddah, Saudi Arabia, [5]Center for Artificial Intelligence in Precision Medicines, King Abdulaziz University, Jeddah, Saudi Arabia, [6]University of Cologne, Medical Faculty and University Hospital, Cologne, Germany, [7]Department of Basic and Clinical SciencesUniversity of Nicosia Medical School, Nicosia, Cyprus

Background: This study investigates the toxic activity of *Artemisia judaica* ethanolic extract (ArEx) as well as its phenolic fraction (ArPh), and terpenoid fraction (ArT) against *Cryptosporidium parvum* (*C. parvum*) oocysts.

Methods: Over a 4 months period, estimation of the total phenolic (TPC), total flavonoids (TFC), and total terpenoids contents (TTC) in ArEx; investigation of the *in vitro* antioxidant activity of ArEx, ArPh, and ArT; evaluation of ArEx, ArPh, and ArT toxic activity against *C. parvum* oocysts using MTT assay; parasitological analysis on ArPh-treated *C. parvum* oocysts and comet assay were performed both *in vitro* and *in vivo* (infectivity).

Results: The ArEx TPC, TFC, and TTC was 52.6±3.1 mgGAE/g, 64.5±3.1mg QE/g, and 9.5±1.1mg Linol/g, respectively. Regarding the phytochemical *in vitro* antioxidant activity, the ArPh exhibited the highest antioxidant activity compared to the ArEx and ArT. The ArPh showed promising free radical scavenging activity of DPPH and $ABTS^{\bullet+}$ with IC_{50} values of 47.27±1.86μg/mL and 66.89±1.94μg/mL, respectively. Moreover, the FRAP of ArPh was 2.97±0.65 mMol Fe^{+2}/g while its TAC was 46.23±3.15mg GAE/g. The ArPh demonstrated toxic activity against *C. parvum* oocysts with a potent IC_{50} value of 31.6μg/mL compared to ArT (promising) and ArEx (non-effective). ArPh parasitological analysis demonstrated MIC_{90} at 1000μg/ml and effective oocysts destruction on count and morphology. ArPh fragmented oocysts nuclear DNA in comet assay. Beginning at 200μg/mL, ArPh-treated oocysts did not infect mice.

Conclusion: To combat *C. parvum* infection, the phenolic fraction of *A. judaica* L. shows promise as an adjuvant therapy or as a source of potentially useful lead structures for drug discovery.

KEYWORDS

Cryptosporidium* sp., *Artemisia judaica* L., drug discovery and public health, MTT assay, comet assay, *in vivo*, *in vitro

1. Introduction

The waterborne pathogen *Cryptosporidium* sp. is widely recognized as having medical importance for both immunocompetent and immunocompromised patients. Around 905 waterborne and 25 foodborne outbreaks are reported by *Cryptosporidium* sp. worldwide (Baldursson and Karanis, 2011; Efstratiou et al., 2017; Ahmed and Karanis, 2018b).

The most common transmission routes are contaminated food or water consumption, zoonotic transmission, person-to-person contact, and the underestimated but critical route of airborne transmission (Ahmed et al., 2018; Ahmed and Karanis, 2020). At least 47 species (Ježková et al., 2021; Zahedi et al., 2021) and more than 120 genotypes of *Cryptosporidium* sp. have been identified (Ryan et al., 2021). Almost 20 species of them have been observed in humans, with *Cryptosporidium hominis* (*C. hominis*) and *Cryptosporidium parvum* (*C. parvum*) being the two most notable species (Innes et al., 2020).

In the first 2 years of life, *Cryptosporidium* sp. is the second most prevalent cause of diarrhea in developing countries (Kotloff et al., 2012). In seven areas of Sub-Saharan Africa and Asia, it is considered the fourth leading cause of diarrhea (Checkley et al., 2015).

With the highest estimated prevalence range of 21–50%, *Cryptosporidium* sp. is the third most often reported pathogenic protist in African nations. In Egypt, the prevalence of *Cryptosporidium* sp. in humans is between 11 and 20% (Ahmed et al., 2022). Egypt led the way in reporting more than one-third (36/122) of waterborne protozoa reports in Africa, with *Cryptosporidium* sp. likely being common in numerous Egyptian water supplies (Ahmed et al., 2018). Despite the availability of several diagnostic procedures for detecting *Cryptosporidium* sp. in feces, food, and water (Ahmed et al., 2018; Ahmed and Karanis, 2018a,b), diagnosis for *Cryptosporidium* sp. is not controlled in Egyptian laboratories (Ahmed et al., 2022) indicating that the prevalence above is greatly underestimated.

Nitazoxanide is the only drug that has been FDA-approved for treating *Cryptosporidium* sp. infection in people with healthy immune systems. However, the efficacy of nitazoxanide in immunocompromised patients is unclear (CDC, 2021; Schneider et al., 2021). The lack of continuous culturing, cumbersome screening procedures for chemotherapeutic treatments, and a scarcity of genetic manipulation tools limits drug and vaccine research against *Cryptosporidium* sp. (Karanis, 2018; Gururajan et al., 2021).

Severe cases frequently necessitate hospitalization in immunocompetent individuals and are more common in youngsters and the elderly (Shaposhnik et al., 2019; Collier et al., 2021). Immuno-compromised people, including transplant patients, HIV and cancer patients receiving chemotherapy, frequently have to temporarily halt their treatment regimens when they contract *Cryptosporidium* sp. infection (Sparks et al., 2015; Schneider et al., 2021; Ahmed et al., 2023). Significant economic losses and zoonotic relevance are associated with cryptosporidiosis, specifically *C. parvum*. Due to the disease's harmfulness and the ease with which newborn calves might develop it, it is difficult to control (Zhang et al., 2018). Anti-cryptosporidials would undoubtedly benefit patients at high risk of *Cryptosporidium* infection and the veterinary industry.

Herbal formulations with anti-*Cryptosporidium* sp. activity have been identified in recent years. They proposed effective treatment against *C. parvum in vitro* (Jin et al., 2019; Mendonça et al., 2021). The biodiversity of plants makes them a commonly explored source of novel bioactive compounds, providing molecules with distinct structures, complex or simple, with colossal chemical variety (Morais et al., 2020). Natural products, particularly crude forms, have been used traditionally to treat various parasitic diseases, such as babesiosis, leishmaniasis, malaria, and trypanosomiasis (Ismail et al., 2020; Kingston and Cassera, 2022). Moreover, natural products have afforded the pharmaceutical industry potential antiparasitic drugs, such as the antimalarial drugs artemisinin from *Artemisia annua* and quinine from *Cinchona succirubra* (Kayser et al., 2002) in addition to licochalcone A, amphotericin B, and ivermectin (Kayser et al., 2003).

Asteraceae (Compositae) is considered one of the most prominent and widely distributed plant families (Panda and Luyten, 2018). In Egypt, this plant family comprises 14 genera, including the genus *Artemisia* (Mokhtar et al., 2019) which is represented by five species; *A. monosperma* Delile, *A. vulgaris, A. verlotiorum, A. scoparia* Waldst and *A. judaica* L. (Badr et al., 2012). Plants of this genus were reported to possess antioxidant, antimicrobial, and cytotoxic activities (Bora and Sharma, 2011; Pandey and Singh, 2017). These biological activities are linked to their phytoconstituents, of which terpenoids and phenolics predominate (Bora and Sharma, 2011; Pandey and Singh, 2017; Goda et al., 2021).

A. judaica (Asteraceae) is a perennial aromatic shrub, wildly distributed in Egypt, particularly in Sinai, Gabal Elba, Mediterranean, and Red Sea regions (Ahmed et al., 2017) and has been extensively employed in traditional medicine practices. Therefore, it is almost ubiquitous in Egyptian households. *A. judaica* has demonstrated potent wound healing, antiviral, antibacterial, antihelminth, and antiprotozoal properties in previous research (Mokhtar et al., 2019; Kshirsagar and Rao, 2021; EDA, 2022; Marakhova and Emam, 2022; Mohammed et al., 2022; Qanash et al., 2023). Due to its availability, affordability, and anti-protozoal activity, *A. judaica* is a prime candidate for testing against *Cryptosporidium* oocysts. This study, therefore, aims to investigate the cytotoxic activity of *A. judaica* L. ethanolic extract and its fractions against *C. parvum* using (a) *in vitro* experiments, (b) acting mechanism, (c) *in vivo* bioassay to demonstrate the infectivity of the treated oocysts.

2. Materials and methods

2.1. Oocysts source and staining

Fecal samples containing *Cryptosporidium* sp. oocysts were collected from a farm with a known history of cryptosporidiosis in its newborn calves (Ahmed et al., 2019). The feces of 15 neonatal calves were collected in plastic bags and labeled with the number of calves and their section. The samples were promptly transferred to the Medical Parasitology laboratory. Each sample was smeared directly and allowed to dry at ambient temperature. The samples were fixed and stained using the modified technique of Ziehl-Neelsen procedure (mZN) (Henriksen and Pohlenz, 1981) to determine the infection status and oocysts load. Four samples with significant cryptosporidial infection (≥ 10–20 oocysts/field) were chosen for additional processing in the experiment.

Approximately 2 mL of the watery fecal specimens were immediately transferred into 2-mL Eppendorf tubes and stored at

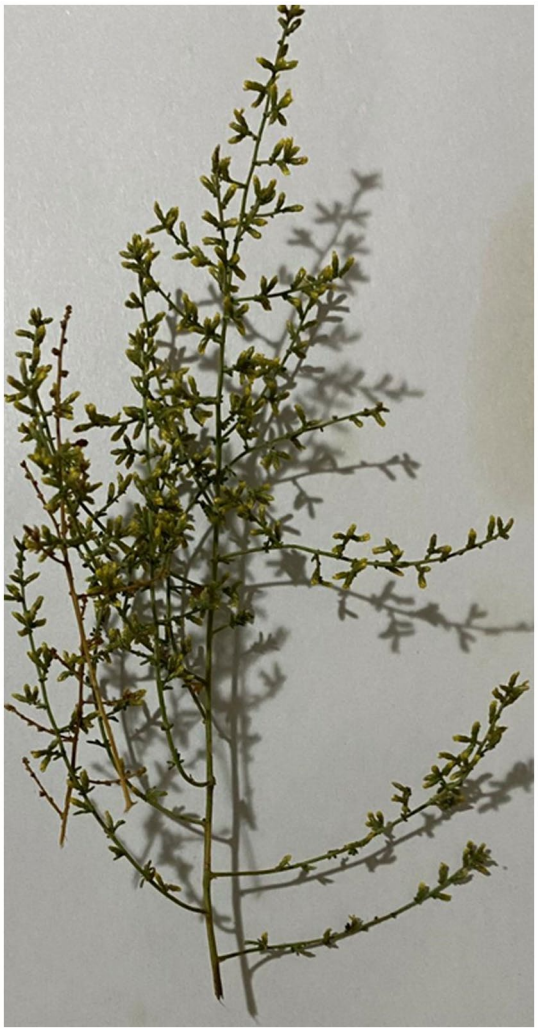

FIGURE 1
The aerial parts of *Artemisia judaica* L.

minus 20°C for further molecular identification and confirmation. The remaining part of fecal samples containing oocysts were filtered through four layers of gauze and stored in potassium dichromate ($K_2Cr_2O_7$) (1:4, *v/v*) for subsequent oocysts processing at 4°C.

Before purification, the suspension of preserved oocysts and potassium dichromate was concentrated using the formalin-ethyl acetate technique, but potassium dichromate was used in place of formalin. Briefly, after thorough mixing, the potassium dichromate fecal suspension was split into 15 mL Falcon tubes. The top three milliliters of each tube were produced by adding ethyl acetate to the fecal - potassium dichromate suspension. Before centrifuging for 10 min at 2100 g, the tubes were tightly sealed and shook for 20 s. Using a wooden stick, the top lipid layer was discarded after being loosened. After decanting the supernatant, the residual sediment was washed three times with phosphate-buffered saline (PBS) (0.324 g KH_2PO_4, 1.368 g Na_2HPO_4, 7.014 g NaCl, 0.651 g KCl, and 1,000 mL H_2O; pH 7.4) (Arrowood and Sterling, 1987).

Each sample's 3 mL final volume of concentrated sediment was mixed in potassium dichromate at 4°C until the purification process commenced.

2.1.1. Purification of *Cryptosporidium* oocysts

To purify oocysts from previously concentrated fecal samples, discontinuous gradient sucrose flotation was applied (Castro-Hermida et al., 2004; Kourenti and Karanis, 2006). On a discontinuous gradient of sucrose, potassium dichromate-preserved sediments were layered.

Solution A (1:2 v/v, specific gravity 1.11) and solution B (1:4 v/v, specific gravity 1.07) were prepared by diluting a stock solution of modified Sheather's sugar (El-Nasr Co. for Intermediate Chemicals, Egypt) (500 g sucrose, 320 mL water, and 6.5 g phenol) with PBS. In a 15-mL conical tube, 5 mL of solution A was poured first, followed by 5 mL of solution B.

Oocysts were previously condensed into a suspension (3 mL), which was then carefully poured over the gradients. For 30 min, the gradient tubes were centrifuged at 1200 g (Universal Centrifuge, PLC-012E). After the second layer from the top had been separated, it was washed in saline and finally PBS. Decanting the supernatant allowed the sediments (about 1 mL/tube) to be examined in wet mount (WM) and mZN stain for oocysts of *Cryptosporidium* sp. Purified oocysts were stored in a solution of 2.5% potassium dichromate 1:4 v/v at 4°C for use in subsequent research within 4 months period.

2.1.2. Molecular identification of *Cryptosporidium* species

The species/genotypes of *Cryptosporidium* used were determined using molecular identification. Frozen fecal samples were thawed in cold PBS and filtered through two layers of gauze. PBS washed and centrifuged at least three times. The Qiagen DNA stool-mini kit were used to extract DNA from 200 µL of collected silt, per manufacturer directions (50, manufactured in Germany). The Qiagen method was modified by raising the water bath temperature to 90°C and storing a 100 µL DNA aliquot at – 20°C for PCR amplification.

Nested PCR primers CPr I (5'-AAACCCCTTTACAAGTA TCAATTGGA-3′) and CPr II (5'-TTCCTATGTCTGGACCTGG TGAGTT-3′), CPr III (5'-TGCTTAAAGCAGGCATATGCCTTG AA-3′) and CPr IV (5'-AACCTCCAATCTCTAGTTGGCATAGT-3′) were employed to amplify the small subunit ribosomal RNA gene of the four calves' fecal samples (Bialek et al., 2002). With previously mentioned modification (Ahmed et al., 2019), initial amplification was conducted at 94°C for 5 min, followed by 35 cycles of 94°C for 30 s, 55°C for 30 s, and 72°C for 45 s, with the final extension at 72°C for 5 min. After electrophoresis on a 1% agarose gel stained with ethidium bromide, the amplified products were visualized using a UV transilluminator.

2.2. Phytochemical investigations of *Artemisia judaica* L.

2.2.1. Plant collection and preparation of its crude extract

A. judaica aerial parts (Figure 1) were bought from the Egyptian market in September 2018. Plant authentication was carried out by Prof. Dr. Elsayeda M. Gamal El-Din (Department of Botany, Faculty of Science, Suez Canal University). A voucher sample of the plant (#Aj-2018-1) was placed in the herbarium of Pharmacognosy Department, faculty of Pharmacy, Suez Canal University.

Aerial parts of *A. judaica* were air-dried at room temperature in shade for 1 week prior to grinding. As previously mentioned, (Mokhtar et al., 2019), the crude ethanolic extract of *A. judaica*

(ArEx) was prepared by macerating 0.2 Kg of the plant twice with 95% ethyl alcohol (300 mL, 48 h) at 25°C. The combined extracts were vacuum - concentrated to obtain *A. judaica* crude extract (17 g), which was then kept at 4°C.

2.2.2. Preparation of terpenoids and phenolic fractions of *Artemisia judaica* L.

The terpenoid fraction of *A. judaica* was prepared according to a previously described method (Leyva-López et al., 2016) with few modifications. The crude *A. judaica* extract (5 g) was extracted with chloroform (3 × 25 mL). The chloroform extracts were filtered, combined then concentrated under reduced pressure to afford 0.45 g of the terpenoid fraction of *A. judaica* (ArT).

The phenolic fraction of *A. judaica* was prepared according to a previously mentioned method (Eltamany et al., 2022). An amount of 10 g of *A. judaica* crude extract was suspended in aqueous solution of 5% Na_2CO_3 before being extracted chloroform (3 × 50 mL). The aqueous extract lift was then acidified with HCl and fractionated successively with chloroform, ethyl acetate, and *n*-butanol. These obtained extracts were combined and vacuum dried to yield approximately 8.5 g of the phenolic fraction of *A. judaica* (ArPh).

2.2.3. Estimation of total phenolic and total flavonoids contents in ArEx

Total phenolics content (TPC) in ArEx was quantified spectrophotometrically by the Folin–Ciocalteu assay as previously described (Eltamany et al., 2020, 2022) where gallic acid was served as a standard. At λ 630 nm, the UV absorbances against blank were recorded in triplicate by Milton Roy Spectronic 1,201 UV/Vis Spectrophotometer (Houston, TX, United States). The result was obtained in terms of gallic acid equivalents (mg·GAE/g dry extract).

The total flavonoid content (TFC) was quantified by $AlCl_3$ method, as previously stated (Eltamany et al., 2020). Quercetin was employed as a standard. The UV absorbances against blank at λ 510 nm were measured in triplicate using Milton Roy Spectronic 1,201 UV/Vis Spectrophotometer (Houston, TX, United States). The result was expressed as quercetin equivalent per gram of dry extract (mg QE/g).

2.2.4. Estimation of total terpenoids content in ArEx

The total terpenoids content (TTC) in ArEx was analyzed quantitatively using Salkowski test described by Kim et al. (2018). Linalool (a monoterpene compound) was employed as a standard. The absorbance at λ538 nm against blank was recorded in triplicate by Milton Roy Spectronic 1,201 UV/Vis Spectrophotometer (Houston, TX, United States). TTC of *A. judaica* was determined as linalool equivalents per gram of dry extract (mg Linol/g).

2.3. *In vitro* studies of antioxidant activity and cytotoxic assays of *Artemisia judaica* L against *Cryptosporidium* oocysts

2.3.1. Evaluation of the *in vitro* antioxidant activity of *Artemisia judaica* L.

2.3.1.1. DPPH free radical scavenging activity of *Artemisia judaica*

The ArEx as well as its ArPh and ArT fractions were investigated for their scavenging activity of 2,2-diphenyl-1-picrylhydrazyl (DPPH) radical using the procedure previously detailed (Eltamany et al., 2020, 2022). Ascorbic acid served as a standard.

In triplicate, the absorbances at λ 515 nm were recorded against blank by Milton Roy Spectronic 1,201 UV/Vis Spectrophotometer (Houston, TX, United States). The DPPH radical quenching the sample of was calculated applying this equation: PI = [{(AC − AT)/AC} × 100].

Where PI = percent inhibition, AC = control absorbance and AT = absorbance of DPPH + sample mixture. The IC_{50} of DPPH was estimated from the dose/response curve created by Graphpad Prism software (San Diego, CA, United States).

2.3.1.2. ABT assay of *Artemisia judaica*

The ability of ArEx, ArT, and ArPh to capture and neutralize $ABTS^{\bullet+}$ radical cation [2, 2′-azino-bis (3-ethylbenzothiazoline-6-sulfonic acid)] was assayed using the procedure described in detail by Abouseadaa et al. (2020). Butylhydroxytoluene (BHT) was used as a positive control. The absorbances at λ 734 nm were recorded in triplicate against blank by Milton Roy Spectronic 1,201 UV/Vis Spectrophotometer (Houston, TX, USA).

The $ABTS^{\bullet+}$ neutralizing activity of a sample was estimated using the following equation: PI = 100 [(Control – Sample)/Control].

The IC_{50} was obtained from the dose/response curve obtained by Graphpad Prism software (San Diego, CA, United States).

2.3.1.3. Ferric reducing antioxidant power assay for *Artemisia judaica*

The reducing power of ArEx, ArPh, and ArT was estimated spectrophotometrically by FRAP assay mentioned before (Eltamany et al., 2020, 2022). This assay is based on the reduction of ferricyanide ions in to ferrocyanide by an antioxidant substance.

At λ700 nm, the absorbances were measured against a blank (in triplicate) by Milton Roy Spectronic 1,201 UV/Vis Spectrophotometer (Houston, TX, USA). Ascorbic acid and BHT were utilized as standards. Results were represented in terms of m Mol Fe^{+2} equivalents per gram of dry sample (mMol Fe^{+2}/g).

2.3.1.4. Total antioxidant capacity assay for *Artemisia judaica*

TAC of ArEx, ArT, and ArPh were estimated using the phosphomolybdenum spectrophotometric assay according to the method previously described (Eltamany et al., 2020, 2022). This test is based on the conversion of Mo^{+6} to Mo^{+5} in an acidic media by an antioxidant substance, resulting in a green phosphate/Mo^{+5} complex.

The absorbances were recorded in triplicate at λ 695 nm against blank by Milton Roy Spectronic 1,201 UV/Vis Spectrophotometer (Houston, TX, USA). The standards were ascorbic acid and BHT. Data were obtained as mg equivalents of gallic per gram of dry extract (mg GAE/g).

2.3.2. Cytotoxic assay of *Artemisia judaica* against *Cryptosporidium* oocysts using MTT assay

The MTT assay was performed to primarily determine the most potent herbal treatment of *A. judaica* L (ArEx, ArPh, and ArT) against *C. parvum* oocysts. In a 96-well plate, *C. parvum* oocysts-PBS suspension were plated in triplicate at a density of 1×10^4 oocysts. The oocysts were treated with ArEx, ArPh, and ArT at concentrations of

(100, 200, 500, 1,000, and 2000 μg/mL). These concentrations were produced in a double-fold manner. Oocysts viability was assessed after 48 h using the MTT assay kit "Promega, New York, NY, USA" (Mosmann, 1983). Three hours after adding MTT dye (3-(4,5-dimethylthiazol-2-yl)-2,5-diphenyl-2H-tetrazolium bromide) to the wells of a microtiter plate, the plate was incubated at 37°C.

Using an ELISA microplate reader, the absorbance was determined to be 570 nm (BIO-RAD, model iMark, Tokyo, Japan). Half-maximal inhibitory concentration (IC_{50}) values were computed from the relative viability using GraphPad prism 7. A blank treatment of PBS and ethanol was applied to three wells, and untreated *C. parvum* oocysts were utilized as a control in another three wells. Based on the results of MTT assay, ArPh was used in the subsequent experiments.

2.3.3. Parasitological toxic activity of ArPh against *Cryptosporidium parvum* oocysts

2.3.3.1. *In vitro* exposure of *Cryptosporidium parvum* oocysts to ArPh

Within 2 weeks of preparation of the previously prepared suspension (section 2.1.1), the concentration of cryptosporidial oocysts was determined using a Neubauer hemocytometer. After multiple washing with PBS (to remove potassium dichromate), the stock suspension was diluted by a factor determined by the mean of four hemocytometer counts (Finch et al., 1993; Karanis and Schoenen, 2001).

Between the hemocytometer cover slide and counting chambers, oocyst suspension in a 10-μL aliquot was pipetted. Counting oocysts were performed under a 400x dry microscopic objective. A final concentration of oocysts/PBS suspension (1×10^5/mL) was stored. An antibiotic suspension was added at room temperature (10,000 U Pen/ml, 10,000 g Strep/ml, and 25 g Amphotericin B/mL).

To generate a total volume of 1 mL, various quantities of ArPh (100, 200, 500, 1000, 2000 μg/mL) were added to the estimated oocysts solution. A control of untreated oocysts (*C. parvum* oocysts, PBS, antibiotic) was used for comparison with ArPh-treated oocysts (ArPh-TO). Assessments of the cytotoxic effects of ArPh on oocysts' number, viability, and shape were made after 2, 24, and 48 h of incubation. For each time period, the findings were compared to a control group, and the differences between the two groups were computed.

With the aid of a viability dye [0.4% Trypan Blue (TB)], the number of oocysts/μL was calculated after measuring the oocysts distress in count on a Neubauer hemocytometer of Kao and Ungar (1994).

The lethal dose was calculated by applying the destruction rate equation (A-B/A) and multiplying it by 100. In this equation, A represents the mean number of intact oocysts found in the control tube, and B represents the mean number of intact oocysts found in the ArPh-TO tube (Ahmed et al., 2019).

Alterations in morphological size were captured on camera with the use of an Olympus bright field 1,000x oil immersion lens and an ocular micrometer. The *in vitro* exposure experiment was carried out with three separate replicates for each different concentration of ArPh. Based on preliminary trials, the different ArPh concentrations were chosen (Ahmed and Mokhtar, unpublished data).

2.3.3.2. *In vitro* evaluation of the effect of ArPh on *Cryptosporidium parvum* oocysts using the comet assay

The neutral comet assay was applied to *C. parvum* oocysts exposed to varying doses of ArPh based on Ostling and Johanson (1984). ArPh-TO was mixed with molten low-melting-point agarose at a ratio of 1:10 (*v/v*), and 75 μL of this mixture was immediately imbedded in a CometSlide (frosted slide) placed flat at 4°C in the dark for 10 min.

The slides were then placed in lysis buffer (2.5 M NaCl, 100 mM NaEDTA, 10 mM Tris pH 10, 1% Triton X, and 10% dimethylsulphoxide (DMSO; Sigma) at pH 10) with the coverslips removed. To remove the lysis solution from the slide, it was placed twice for 5 min at room temperature in electrophoresis buffer (90 mM Tris base, 90 mM boric acid, and 2 mM ethylenediaminetetraacetic acid). The slide was then placed in a horizontal electrophoresis tank, and 20 min of electrophoresis at 28 V (1 V/cm, 400 mA) was conducted. After removing the excess electrophoresis buffer from the slide, it was gently rinsed in distilled water. The gel was then fixed by immersion in 70% ethanol for 5 min and air-dried for 15 min at room temperature. The slide was stained with 50 μL of 20 μg/mL ethidium bromide for 1 h. The migrating DNA (comet) was spotted at 400x magnification using an Epifluorescence optika microscope.

Using an automatic image analysis system (Comet score V software), DNA damage was determined by measuring the tail moment, which is defined as the product of the amount of DNA in the tail and the displacement between the center of mass of the comet head and the center of mass of the tail (tail length) (Olive and Banáth, 2006). The olive tail moment was defined as tail DNA% multiplied by tail moment (Cell Biolab, 2013). Each experimental group received triplicate samples, from which 100 oocysts were randomly selected and analyzed. As a control, the same previous technique was used to handle DNA damage of *C. parvum* untreated oocysts in PBS.

2.4. *In vivo* experiment (infectivity assay)

2.4.1. Animals

Nine-week-old male SPF Swiss Albino mice weighing an average of 24–32 g were purchased from The Egyptian Organization for Biological Products and Vaccines (Vacsera, Cairo, Egypt), and maintained under a regular day/night cycle and sanitary conditions. The animals were pathogen-free, as evidenced by a sanitary certificate. Before the experiment, the mice were acclimatized to the experimental environment for 10 days and basal diet and water were administered *ad libitum*. Even though the mice were guaranteed to be free of pathogens when they were acquired, WM and mZN were used to check their feces for three successive days (Ma and Soave, 1983; Ungar et al., 1990).

2.4.2. Study design

The mice were randomly divided into seven groups of three mice each to conduct a biological test to determine the infectivity of treated *C. parvum* oocysts (Karanis and Schoenen, 2001).

Group 1: Negative control (non-infected animals, untreated).

Group 2: Positive control (infected and untreated animals).

Groups 3–7: Infected animals with the five concentrations of ArPh-TO.

In the animal house of the Faculty of Medicine at Suez Canal University, every mouse was kept individually and in accordance with the established protocols for animal care.

2.4.3. Infectivity investigation

Using a hemocytometer/TB, 500 µL of suspension inoculums were administered to the mice 48 h after treatment (section 2.3.3.1) (Karanis and Schoenen, 2001). All the mice were administered the estimated inoculums via gavage at the same time. Each mouse's fresh feces were collected by exerting moderate pressure to their abdomens. Purified fecal samples from mice were examined post-inoculation for oocysts shedding at third, fifth, six, seventh and 10 days using mZN stain. On the tenth day after inoculation, all the animals were killed by dislocating the cervix. The infection status of each group was determined based on microscopic observations of *Cryptosporidium* oocysts and was graded as positive or negative (Korich et al., 2000).

2.5. Statistical analysis

Three independent experiments with three replicates per test sample were used to conduct the MTT assay. The mean absorbance values were represented as a percentage of the values of the untreated control oocysts standard error of the mean. The IC_{50} was expressed with a non-linear regression curve fit using Microsoft Excel software. The statistical significance was calculated using an unpaired t-test. One-way analysis of variance (ANOVA) test was used to determine the statistical significance of differences between treatments and the control group in the hemocytometer and comet assays. The p values of ≤ 0.05 were considered significant. IBM SPSS Statistics V26.0 was used for all statistical analyzes (IBM Corp., Armonk, NY, United States). The charts were made with GraphPad Prism 7. (Dotmatics, San Diego, CA, United States).

3. Results

3.1. Genetic identification of *Cryptosporidium* oocysts by nested PCR assay

The *Cryptosporidium* species in the examined samples was determined using a *C. parvum*-specific nested PCR technique. *C. parvum* was present in all the calves' fecal samples. The four employed samples' amplified products of 285 bp were successfully electrophoresed (Figure 2).

3.2. Phytochemical investigations of *Artemisia judaica* L.

3.2.1. Total phenolic, flavonoids, and terpenoids contents

Using the Folin–Ciocalteu colorimetric technique, the TPC of ArEx was quantified to be 52.6 ± 3.1 mg GAE/g extract. While the TFC of ArEx was estimated to be 64.5 ± 3.1 mgQE/g of plant extract using $AlCl_3$ spectrophotometric method (Table 1).

The TTC of ArEx was quantified spectrophotometrically at λ538 nm based on the intensity of the reddish-brown color produced by them. As depicted in Table 1, the TTC of ArEx was found to be 9.5 ± 1.1 mg Linol/g.

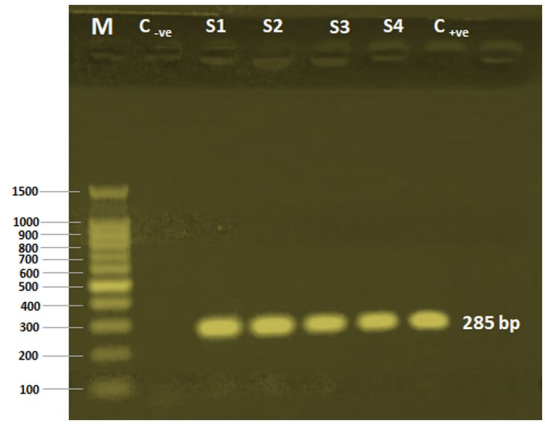

FIGURE 2
PCR-nested analysis of four calves' fecal samples. M, 100 bp DNA ladder (Applied Biotechnology Co. Ltd., Egypt); C-ve, Control negative; S1-S4: *Cryptosporidium* oocysts sample sources; C+ve, Control positive.

TABLE 1 TPC, TFC and TTC of *A. judaica* crude extract.

Sample	TPC (mg GAE/g)	TFC (mgQE/g)	TTC (mg Linol/g)
ArEx	52.6 ± 3.1	64.5 ± 3.1	9.5 ± 1.1

Data are expressed as mean ± SD of three independent values. TPC, Total phenolic content; TFC, total flavonoids content; TTC, Total terpenoids content; GAE, Gallic acid equivalents; ArEx, *A. judaica* ethanolic extract.

3.2.2. Evaluation of antioxidant activity of ArEx, ArT, ArPh

As shown in Table 2, among ArEx, ArT, and ArPh, the ArPh exhibited a distinctive radical scavenging ability on DPPH and ABT with IC_{50} = 47.27 ± 1.86 µg/mL and 66.89 ± 1.94 µg/mL compared to ascorbic acid and BHT (IC_{50} = 10.64 ± 0.82 µg/mL and 141.98 ± 3.46 µg/mL), respectively.

The ferric ion reducing power of ArEx, ArT, and ArPh expressed in terms of mMol Fe^{+2} /g were demonstrated in Table 2. The ArPh possessed the highest reducing power 2.97 ± 0.65 mMol Fe^{+2} /g, compared with ArEx (2.34 ± 0.42 mMol Fe^{+2} /g) and the ArT (1.38 ± 0.26 mMol Fe^{+2} /g). Ascorbic acid (7.41 ± 0.57 mMol Fe^{+2} /g) and BHT (2.86 ± 0.38 mMol Fe^{+2} /g) served as positive controls.

The obtained results (Table 2) revealed that the ArPh exhibited the highest TAC (46.23 ± 3.15 mg GAE/g) in comparison with the ArEx (40.91 ± 2.63 mg GAE/g) and the ArT (23.54 ± 1.98 mg GAE/g). The TAC of the positive controls, ascorbic acid and BHT, were 72.68 ± 3.74 mg GAE/g and 79.31 ± 3.95 mg GAE/g, respectively.

3.3. *In vitro* oocysts-toxic activity of *Artemisia judaica* L.

3.3.1. Cytotoxicity of ArEx, ArPh, and ArT against *Cryptosporidium* oocysts

Table 3 summarizes the IC_{50} values of the ArEx, ArPh, and ArT. The ArPh displayed significant toxicity against *C. parvum* oocysts, with an IC_{50} value of 31.6 µg/mL (Table 3) and a cell viability percentage of 0.87% at the highest concentration. In the meantime,

TABLE 2 Antioxidant activities of ArEx, ArPh, and ArT by DPPH, ABT, FRAP and TAC assays.

Sample	DPPH (IC_{50} in µg/mL)	ABT (IC_{50} in µg/mL)	FRAP (mMol Fe^{+2}/g)	TAC (mg GAE/g)
ArEx	123.83 ± 2.71	154.15 ± 4.92	2.34 ± 0.42	40.91 ± 2.63
ArT	233.24 ± 5.17	481.92 ± 8.76	1.38 ± 0.26	23.54 ± 1.98
ArPh	47.27 ± 1.86	66.89 ± 1.94	2.97 ± 0.65	46.23 ± 3.15
Ascorbic acid	10.64 ± 0.82	NT	7.41 ± 0.57	72.68 ± 3.74
BHT	NT	141.98 ± 3.46	2.86 ± 0.38	79.31 ± 3.95

Data expressed as mean ± SD of three independent values. NT, Not tested. ArEx, *A. judaica* ethanolic extract; ArPh, *A. judaica* phenolic fraction; ArT, *A. judaica* terpenoid fraction; DPPH, 2,2-diphenyl-1-picrylhydrazyl; FRAP, Ferric reducing antioxidant power; TAC, Total antioxidant capacity; Fe^{+2}, Iron; GAE, Gallic acid equivalents; BHT, Butylated hydroxytoluene.

TABLE 3 IC_{50} values of ArEx, ArPh and ArT using MTT assay against *Cryptosporidium* oocysts.

Sample	Working concentration	*IC_{50} [µg/mL]
ArEx	100, 200, 500, 1,000, 2000 µg/mL	213 ± 4.26
ArPh		31.6 ± 1.98
ArT		64.56 ± 2.42

*IC_{50} were expressed as Mean ± SD of three independent trials and calculated by non-linear regression curve fit using EXCEl. ArEx, *A. judaica* ethanolic extract; ArPh, *A. judaica* phenolic fraction; ArT, *A. judaica* terpenoid fraction.

ArT displayed promising cytotoxicity with an IC_{50} value of 64.5 µg/mL, and the greatest concentration achieved 6.4% cell viability. With an IC_{50} value of 213 µg/mL and a cell survival rate of 9.44%, the ArEx displayed poor cytotoxicity. The most potent oocysts-toxic compound is ArPh, according to the dose–response curves of ArEx, ArPh, and ArT (Figure 3). Due to its potential oocysts-killing properties, ArPh was selected to be used in subsequent studies.

3.3.2. Parasitological *in vitro* exposure of *Cryptosporidium* oocysts to ArPh

3.3.2.1. Activity of ArPh on the number of oocysts

Figure 4; Table 4 depict a summary of differences in ArPh dose-dependent inhibition of *C. parvum* oocysts *in vitro*. Different concentrations of ArPh (100, 200, 500, 1,000, 2000 µg/mL) caused "visible stress" on the total number of *C. parvum* oocysts compared to control ($p < 0.05$; Figure 4). The equation for the rate of destruction was used to calculate the proportion of oocysts that were reduced. The minimal lethal concentration at which 90% of oocysts are killed (MLC_{90}) was determined to be 1,000 µg/mL. The highest rate of oocysts destruction (100%) was recorded 48 h later at a concentration of 2000 µg/mL. The data revealed a statistically significant difference ($p < 0.05$) in the concentrations of ArPh measured at various time intervals throughout the experiment.

3.3.2.2. Activity of ArPh and Its impact on the oocyst's morphology.

Oocysts of *Cryptosporidium* are typically brightly colored, range in size from 4 to 6 micrometers, and consist of a center globule, one to four sporozoites, and eccentric black granules. TB and mZN stain were used to track the morphological changes of oocysts. When ArPh was applied to oocysts at varying concentrations and exposure times, the oocysts exhibited cascades of death beginning with inflating, filling with single/multiple vacuoles, granulation of content, cracking, expulsion of content, and shrinkage (Figure 5). These alterations were first noticed at a concentration of 200 µg/mL and peaked after 48 h with variation among different concentrations.

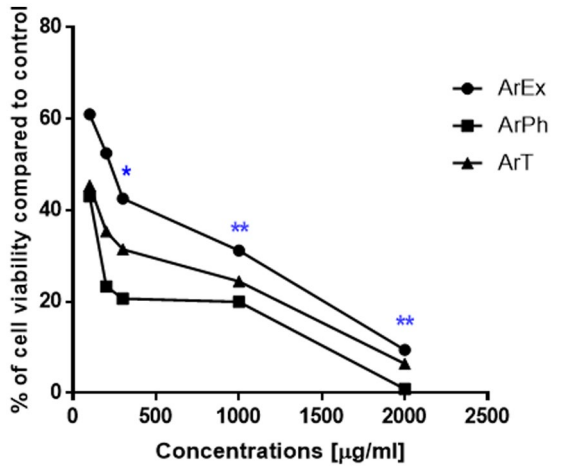

FIGURE 3
Dose-response curve for the viability at different working concentrations of ArEx, ArPh, ArT using MTT assay. *($p \leq 0.05$) and **($p \leq 0.001$) significantly different using unpaired *t*-test of treated oocysts and control using GraphPad prism software. ArEx, *A. judaica* ethanolic extract; ArPh, *A. judaica* phenolic fraction; ArT, *A. judaica* terpenoid fraction.

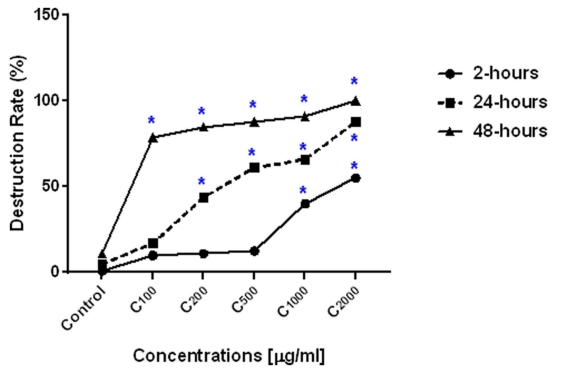

FIGURE 4
ArPh activity on the number of oocysts. Count distress of oocysts by destruction rate (%) = (A-B/A) x100 in varied periods of exposure with various concentrations of ArPh. The values are presented as the means of three separate experiments. ArPh, *A. judaica* phenolic fraction. *Significant difference between concentrations using one way ANOVA test.

3.3.2.3. Results of comet assay for ArPh-To.

The nuclear DNA of untreated control *C. parvum* oocysts stained with ethidium bromide was spherical and had a well-defined nucleoid margin (Figure 6A). However, the nuclear DNA of ArPh-TO appeared to be damaged. The nuclear DNA of treated oocysts stained with ethidium bromide looked more prominent and had a longer migratory tail at the different concentrations of ArPh (Figures 6B–F).

In the neutral comet assay, the comet tail moment increased significantly between the control and the different concentrations used with ArPh-TO, in which the tail length and tail DNA (%) increased considerably ($p \leq 0.05$; Table 5).

3.3.3. *In vivo* infectivity biological assay of treated oocysts using the mice model

Although the *in vitro* assay demonstrated that at 200 µg/mL oocysts count and morphological changes had begun and at 1000 and 2000 µg/mL ArPh was sufficient to destroy >90% of the visible endogenous components of *C. parvum* oocysts, it is unknown whether the remaining intact oocysts are viable and able to cause infection. Table 6 presents the details and outcomes of the *in vivo* experiment. Infectivity was observed in 2 groups out of 7 (control positive group 2 and treated group 3 with 100 µL ArPh). The rest of the treated groups exhibited no infectiousness (Table 6). Group 1, which served as the experiment's negative control demonstrated being negative along the duration of the experiment.

4. Discussion

Herbals have selective actions against parasites without reduction of host cell viability (Haynes and Krishna, 2004). *Artemisia* was reported worldwide as an effective treatment against several protozoa parasites, including *Giardia duodenalis*, *Blastocystis* sp., *Leishmania*

TABLE 4 Count distress of ArPh-TO according to different concentrations and different times.

ArPh-concentrations	Time					
	2h		24h		48h	
	*Mean±SD	DR (%)	Mean±SD	DR (%)	Mean±SD	DR (%)h
$C_{100\ \mu g/mL}$	9 ± 1.4	10.0 ^{c}	8.5 ± 0.7	17.0 ^{e}	1.75 ± 0.35	78.8 ^{e}
$C_{200\ \mu g/mL}$	9.5 ± 0.7	11.0 ^{c}	5.75 ± 1.1	43.9 ^{d}	1.25 ± 0.35	84.8 ^{d}
$C_{500\ \mu g/mL}$	8.75 ± 0.35	12.5 ^{c}	4 ± 0.7	61.0 ^{c}	1 ± 0	87.9 ^{c}
$C_{1000\ \mu g/mL}$	6 ± 0	40.0 ^{b}	3 ± 0.7	65.9 ^{b}	0.75 ± 0.35	90.9 ^{b}
$C_{2000\ \mu g/mL}$	4 ± 1.4	55.0 ^{a}	0.5 ± 1.06	87.8 ^{a}	0 ± 0	100.0 ^{a}

*All mean values are multiplied by 10^4. Different super script letters in a column mean significant difference between concentrations using one way ANOVA test. DR, Destruction rate; ArPh, *A. judaica* phenolic fraction.

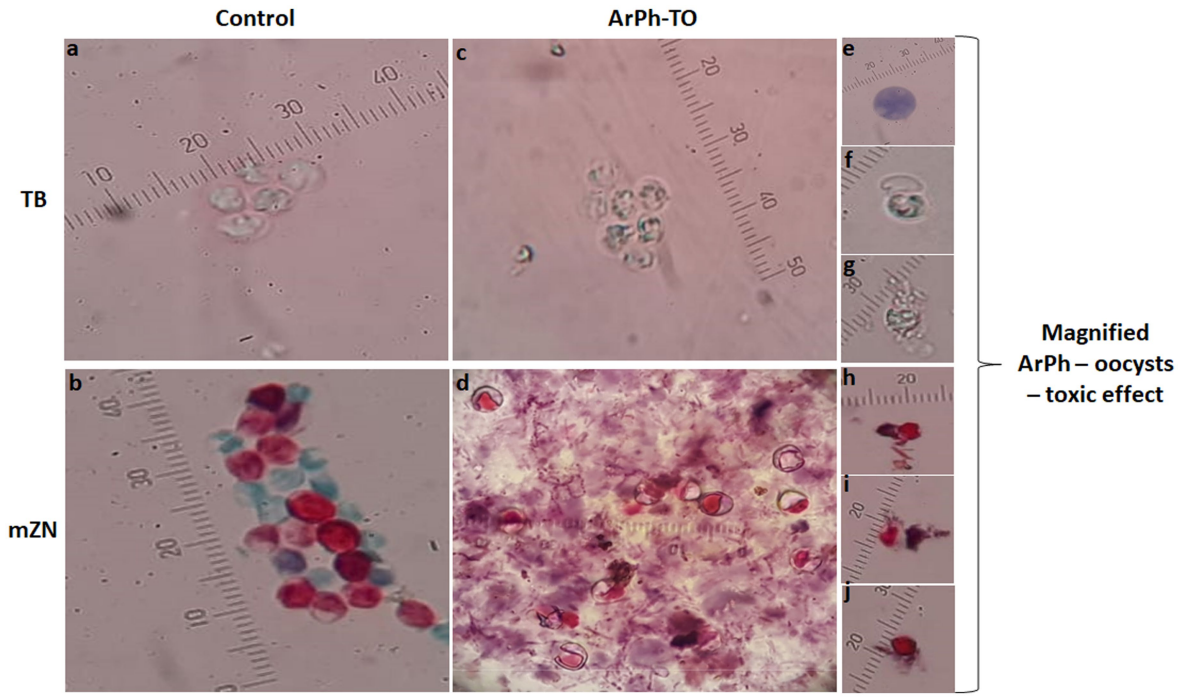

FIGURE 5
Morphological alterations of ArPh-TO using TB and mZN stains. In the control (vertical arrangement of TB and mZN), the usual architecture of oocysts was displayed photos **(A,B)**. In the ArPh-TO morphological alterations in a group of oocysts were displayed photos **(C,D)**. Cascades of ArPh-TO deaths were magnified and exhibited in single images for TB photos **(E–G)** and mZN photos **(H–J)**. Observable programed oocysts death includes vacuolation, granulation, cracking, content expulsion, and shrinking photos **(E–J)**. A micrometer was added to each photograph to compensate for the varying zoom levels of each shot. ArPh-TO, *A. judaica* phenolic fraction treated oocysts; TB, Trypan blue; mZN, modified Ziehl Neelsen.

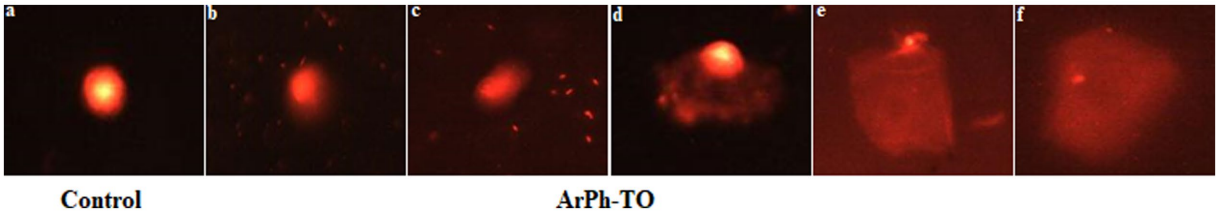

FIGURE 6
Comet assay indicating changes in nuclear morphology and nuclear DNA fragmentation of *C. parvum* sporozoites when treated with different concentrations of ArPh at the incubation time of 48 hours photos **(B–F)**. The nuclear DNA fragmentation appeared in the DNA tailing, which steadily increased as the fragmentation increased. All stages of nuclear DNA fragmentation photographs **(B–F)** were observed beginning with the concentration of 200 μg/mL. DNA was stained with ethidium bromide and observed by epifluorescence microscopy. Untreated *C. parvum* oocysts was used as a control photo **(A)**.

TABLE 5 Parameters of the comet assay of *C. parvum* oocysts after exposure to different doses of ArPh.

Samples	% Tailed Mean±SD	Tail length (PX) Mean±SD	% DNA in tail Mean±SD	Tail moment Mean±SD	Olive tail moment
Control	9.46 ± 0.24 ^{f}	8.91 ± 0.08 ^{a}	4.97 ± 0.97 ^{b}	0.409 ± 0.015 ^{b}	8.48 ± 0.01 ^{d}
C_{100}	15.13 ± 0.40 ^{e}	8.06 ± 0.35 ^{a}	7.27 ± 0.31 ^{a}	0.640 ± 0.03 ^{ab}	1.28 ± 0.09 ^{ab}
C_{200}	17.5 ± 0.28 ^{d}	7.09 ± 0.69 ^{a}	9.74 ± 0.51 ^{a**}	0.705 ± 0.025 ^{a*}	1.33 ± 0.06 ^{ab}
C_{500}	20.4 ± 0.30 ^{c}	7.53 ± 1.08 ^{a}	8.66 ± 0.45 ^{a}	0.783 ± 0.038 ^{b}	1.04 ± 0.002 ^{c}
C_{1000}	24.4 ± 0.48 ^{b}	8.36 ± 0.72 ^{a}	8.33 ± 0.70 ^{a}	0.753 ± 0.13 ^{ab}	1.48 ± 0.051^{a***}
C_{2000}	37.5 ± 0.28 ****	8.44 ± 0.91 ^{a}	7.93 ± 0.60 ^{a}	0.688 ± 0.11 ^{ab}	1.21 ± 0.13 ^{bc}

Nuclear DNA damage was determined using an image analysis system. Data are mean ± SD values ($n = 100$). Values with different superscripts in the same column differ significantly at $p \leq 0.05$. ***High significance; **Moderate significance; *Mild significance. Untreated *C. parvum* oocysts were used as a control.

major, and *Plasmodium falciparum* (Mokhtar et al., 2019; Abd-Elhamid et al., 2021; Gruessner and Weathers, 2021; Najm et al., 2021). Since ancient times in Egypt, natural products have been favored and widely used to cure parasitic infections and other diseases (Aboelsoud, 2010). The cost-effectiveness and absence of adverse effects of natural products made them favorable (Ahmed et al., 2019).

Artemisia judaica L. is indigenous to Sinai Peninsula (Bakr, 2014). *A. judaica* infusion treats many diseases in folk medicine. Moreover, its diverse pharmacological effects were evidenced (Goda et al., 2021). These bioactivities could be attributed to the plant's phytochemicals. *A. judaica* accumulates volatile oil, sesquiterpene lactones, and phenolic compounds (Galal et al., 1974; Abdelgaleil et al., 2008; Janaćković et al., 2015). Recent phytochemical research by LC/MS/MS showed that *A. judaica* possessed a plethora of flavonoids, phenolic acids, and terpenoids (Goda et al., 2021).

Plant phenolics are a diverse, widely distributed group of phytochemicals. They comprise stilbenes, tannins, coumarins, phenolic acids and flavonoids (Abotaleb et al., 2019). Polyphenols are natural antioxidants in fruits and vegetables (Abotaleb et al., 2019; Zhang et al., 2022). The most predominant polyphenolic compounds in the plant kingdom are phenolic acids and flavonoids (Chen et al., 2022). In recent years, plant polyphenols have received increasing attention and drawn much interest due to their diverse biological activities (Zhang et al., 2022), including antiprotozoal activities (Phillipson and Wright, 1991). Therefore, In the current study, the total phenolics, flavonoids contents in *A. judaica* were quantified. The obtained results revealed that the plant was a rich source of phenolic and flavonoids (52.6 ± 3.1 mgGAE/g, 64.5 ± 3.1 mg QE/g, respectively).

On the other hand, terpenes and terpenoids are a large, chemically, and functionally diverse group of secondary metabolites, among which several members exhibited cytotoxic, antimicrobial, and antiparasitic effects (Ajikumar et al., 2008). Thus, in this study, the amount of such compounds in *A. judaica* was estimated spectrophotometrically, where linalool was employed as a standard. Our findings demonstrated that *A. judaica* contained a considerable amount of terpenoids (9.5 ± 1.1 mg Linol/g).

Plant antioxidants, among them polyphenolics (phenolic acids and flavonoids) and terpenoids exert their effect through various processes, including metal reduction, chelation, hydrogen transfer, electron transfer, and singlet oxygen quenching (Graßmann, 2005; Eltamany et al., 2020). In the current study, reactive oxygen species (ROS) scavenging mechanisms, the antioxidant potential of the ArEx, as well as ArT and ArPh, was evaluated simultaneously using four indicative assays (DPPH, ABT, FRAP and TAC). The current study findings demonstrated that ArPh exhibited the highest DPPH and $ABTS^{\bullet+}$ radical quenching effects (IC_{50} values of 47.27 ± 1.86 μg/mL and 66.89 ± 1.94 μg/mL, respectively) as well as the FRAP and TAC (2.97 ± 0.65 mMol Fe^{+2}/g and 46.23 ± 3.15 mg GAE/g, respectively). The ArEx showed noticeable anti-free radical effects against DPPH and $ABTS^{\bullet+}$ (IC_{50} = 123.83 ± 2.71 μg/mL and 154.15 ± 4.92 μg/mL, respectively), FRAP (2.34 ± 0.42 mMol Fe^{+2}/g) and TAC (40.91 ± 2.63 mg GAE/g) compared to ArT (233.24 ± 5.17 μg/mL, 481.92 ± 8.76 μg/mL, 1.38 ± 0.26 mMol Fe^{+2}/g and 23.54 ± 1.98 mg GAE/g, respectively).

ROS boost infection as they regulate growth, proliferation, pathogenesis, and virulence of bacteria, viruses, and parasites at physiological levels as cellular signaling molecules (Goes et al., 2016; Szewczyk-Golec et al., 2021). Excessive generation of ROS can generate oxidative stress, resulting in cell damage and death. Consequently, cells include antioxidant networks to scavenge excess

TABLE 6 The infectivity assay design and outcomes after the *in vitro* assay of *Cryptosporidium* treated with ArPh.

Code of the group	Mean inoculum per mouse	*Inoculation schedule	Ratio of infected mice/ total inoculated mice	Starting day of shedding
Group 1	There is no inoculation	500 µL PBS	Zero/Three	None shed oocysts
Group 2	0.925×10^5	500 µL untreated oocysts per animal	Three/Three	d.p.i 3
Group 3	0.175×10^5	500 µL of 100 µg/mL ArPh treated oocysts per animal	One/Three	d.p.i 5
Group 4	0.125×10^5	500 µL of 200 µg/mL ArPh treated oocysts per animal	Zero/Three	None shed oocysts
Group 5	0.1×10^5	500 µL of 500 µg/mL ArPh treated oocysts per animal	Zero/Three	None shed oocysts
Group 6	0.75×10^4	500 µL of 1,000 µg/mL ArPh treated oocysts per animal	Zero/Three	None shed oocysts
Group 7	0×10^5	500 µL of 2000 µg/mL ArPh treated oocysts per animal	Zero/Three	None shed oocysts

*Infectivity experiment began on day zero and concluded on day 10 following inoculation. After 48 h of the *in vitro* treatment, mice were given 500 µL of ArPh-TO solution by gastric gavage. Experiments were designed according to Karanis and Schoenen (2001), ArPh-TO, *A. judaica* phenolic fraction treated oocysts; d.p.i., days post inoculation.

ROS (Poljsak et al., 2013). For instance, iron-dependent ROS signaling triggers the differentiation of virulent *Leishmania amazonensis* amastigotes (Mittra and Andrews, 2013). *Blastocystis hominis* virulence and infectivity were increased by oxidant-antioxidant homeostasis changes. Oxidative stress was also crucial to *C. parvum* infection in mice (Bhagat et al., 2017). Antioxidants slow infectious illnesses (Kaur et al., 2018). *In vivo* anti-*Cryptosporidium* actions were reported in olive and fig extracts, which increased glutathione reduced form, superoxide dismutase and catalase plasma levels compared to the infected control group (Abd El-Hamed et al., 2021).

The oocysts of *Cryptosporidium* sp. are known to be small (4–6 µm) and have a low infectious dose (1–10 oocysts); it is reported that they can survive in water for 6–12 months or longer and can produce epidemics even with the drinking of a treated water (Karanis, 2018; Omarova et al., 2018). The adverse effects and growing resistance to the available antiparasitic medicines used to treat *C. parvum* make it difficult for researchers to identify a natural herbal alternative that is nontoxic and easily accessible in sufficient numbers to replace the market-standard drugs (Abdelmaksoud et al., 2020). Therefore, *Cryptosporidium* sp. would be a parasite of particular interest in terms of its interaction with *A. judaica*.

Based on the preceding considerations and the demonstrated antioxidant activity of *A. judaica* crude extracts and fractions; specifically, the phenolic one, the ArEx and its fractions; ArPh and ArT were tested for their toxicity to *C. parvum* oocysts using the MTT assay. This colorimetric test estimates cellular metabolic activity as an indicator of cell viability and cytotoxicity. The ArPh demonstrated a potent toxic effect against *C. parvum* oocysts with an IC_{50} value of (IC_{50} = 31.6 µg / mL). MTT assay is the gold standard for cytotoxicity testing and promptly determines the viability of microorganisms following drug treatment (Iqbal and Keshavarz, 2017; Holzhausen et al., 2019). The potency of phenolic fraction in the present study is aligned with earlier studies that revealed the high concentration of phenolics was highly efficient in the treatment of quinine-resistant malaria (Ferreira et al., 2010; Fordjour and Adjimani, 2020; Mamede et al., 2020).

Since the phenolic fraction of *A. judaica* was the most effective treatment based on the MTT assay, it was chosen to evaluate the effect of ArPh on *C. parvum* oocysts using parasitological experiments. The current investigation indicated that the harmful activity of ArPh against *C. parvum* oocysts is dose-dependent (Table 4). The influence significantly affected the count and the oocysts's morphological characteristics. Another study proved that six polyphenolic compounds displayed anti - *C. parvum* and anti - *Encephalitozoon intestinalis* action, indicating that these compounds may be employed alone or in conjunction with other moderately active drugs to enhance efficacy (Mead and McNair, 2006). Against *Trypanosoma brucei* and *Toxoplasma gondii* cultures, phenolic compounds displayed strong action (Sun et al., 2016; Jafari et al., 2021). Extracts of the *Artemisia herba-alba* plant included a variety of phenolic compounds, which had antibacterial and antioxidant effects, and hence slowed the growth of both gram-positive and gram-negative bacteria (Mohammed et al., 2021).

In the current study, oocysts stained with TB and mZN exhibited microscopically observable morphological alterations produced by ArPh. The ArPh-TO were lysed, resulting in the loss of oocysts membrane and the expulsion of their contents (Figure 5). ArPh induced morphological alterations in *C. parvum* oocysts due to a cascade of programmed cell death, during which the oocysts membrane became deformed and created pores inside the cell membrane, resulting in cell lysis and death of the parasite. In another study that examined the effect of chitosan nanoparticles, a similar cascade to that of chitosan-treated *C. parvum* oocysts was seen, wherein the authors demonstrated that recorded changes altered the oocysts' size, shape, interior content, and degree of staining (Ahmed et al., 2019). Additional research on other parasites confirmed the same fact. *A. annua* seeds and leaves have been observed to induce cell death in *Leishmania donovani* promastigotes (Islamuddin et al., 2014; Antwi et al., 2019). Infusions of *A. afra* at low concentrations had strong inhibitory effects on all *Plasmodium* species and stages examined (Gruessner and Weathers, 2021; Ashraf et al., 2022). *Artemisinin* was also observed to induce ultrastructural activity and damage the mitochondria of *Toxoplasma gondii* (Rosenberg et al., 2019).

In the current study, the exhibited ArPh activity against *C. parvum* could be linked to the previously reported flavonoids and phenolic acids in *A. judaica* (Goda et al., 2021). Quercetin and apigenin displayed an antiparasitic effect against *Enterocytozoon intestinalis* while naringenin and genistein were effective against *C. pavum* (Mead and McNair, 2006). Different phenolic components of *A. judaica* displayed substantial antileishmanial action via distinct pathways against diverse strains of *Leishmania*. Quercetin, fisitin, and luteolin inhibited darginase, a key enzyme in *Leishmania* (Manjolin et al., 2013). On the other hand, caffeic acid promoted

amastigote apoptosis by TNF-α/ROS/NO production and reduced iron availability (Bortoleti et al., 2019). Apigenin was leishmanicidal against *L. amazonensis*-infected macrophages via the generation of ROS (Fonseca-Silva et al., 2016). It was demonstrated that *p*-hydroxybenzoic acid had an antiparasitic impact on *Entamoeba histolytica* trophozoites (Degerli and Tepe, 2015). The exact mechanism adopted by the ArPh in the damage of *C. parvum* remains of utmost interest.

The comet assay analyzed several types of DNA damage and repair in individual cells, including invertebrate and plant cells (Olive, 1999). This approach has the advantages of requiring a small number of cells, being highly sensitive to the detection of nuclear DNA damage and applying it to all eukaryotic cell types (Olive, 1999). Consequently, it was utilized to examine the apoptotic mechanism in ArPh-TO. In the present study, the comet tail moment indicated nuclear DNA of *C. parvum* produced by ArPh exposure increased in comparison to control. The tail length reflected the distance the DNA traveled from the oocyst cell and moved to its most distant location (Figure 6). This finding strongly implies that as the ArPh dose is increased, nuclear DNA fragmentation of oocysts increases.

The nuclear DNA fragmentation of ArPh-TO might be related to both parasite-specific and ArPh-specific mechanisms. While *C. parvum* lacks genes for typical molecular therapeutic targets seen in other protozoan parasites, it has numerous genes encoding unique plant-like and bacterial-like enzymes that catalyze potentially critical biosynthetic and metabolic pathways (Abrahamsen et al., 2004). *C. parvum* lacks both the tricarboxylic acid cycle and the oxidative phosphorylation steps necessary for generating metabolic energy (ATP). As a result, the parasite solely depends on anaerobic respiration (the glycolytic pathway) to generate ATP, which is essential for the parasite's survival and the pathogenesis it causes in the host (Abrahamsen et al., 2004). Previous research has demonstrated the significance of glycolytic enzymes (pyruvate kinase) as possible therapeutic targets for the treatment of cryptosporidiosis (Eltahan et al., 2018, 2019; Khan et al., 2022). An earlier study has reported that luteolin possessed anti-leishmanial activity exerted by the induction of apoptosis through the activation of topoisomerase II-mediated kinetoplast DNA cleavage (Mittra et al., 2000). Bioflavonoids induced apoptosis and DNA damage to *Leishmania donovani* amastigotes and promastigotes (Mehwish et al., 2021). Ferulic acid-induced cellular disturbances in adult worms characterized by *in situ* DNA fragmentation, nucleosomal DNA laddering, and chromatin condensation (Saini et al., 2012).

Through the previous results we can infer that apoptosis is the mechanism of action of ArPh-oocysts toxicity as indicated by the following: i. Trypan blue staining, which was used as a basic protocol to indicate early and late apoptosis (Zhivotosky and Orrenius, 2001); ii. Comet assay, which demonstrated DNA fragmentation of oocysts, an important biochemical hallmark of apoptosis (Zhang and Xu, 2000); and iii. High ROS–mediated DNA fragmentation apoptotic properties of ArPh (Higuchi, 2003).

The animal model remains the gold standard for assessing the infectivity of oocysts (Robertson and Gjerde, 2007). Mice were fed ArPh-TO after 48 h to evaluate whether the *in vitro* impact of ArPh could reach infectivity *in vivo*. In the current study, when compared to mice that were fed with an untreated *C. parvum* oocyst infection, ArPh-TO did not induce infection in mice at 200 μg/mL (the minimum fatal dose) of ArPh *in vitro*. Similar reported data were obtained from *in vivo* experiments with *Cryptosporidium* sp. at 20 mg/mL, *A. spicigera* possessed significant anti-*Cryptosporidium* efficacy in mice (Shahbazi et al., 2021). The methanol extract of Asafoetida reduced *Cryptosporidium* sp. infection in experimentally infected mice and improved the histological alterations of small intestinal villi (Abdelmaksoud et al., 2020). The ethanolic extract of olive (*Olea europaea*) pomace, after oil pressing and phenol recovery, reduced *C. parvum* development in a reproducible manner. *Curcuma longa* L. extract significantly impacted *Cryptosporidium* oocyst shedding in *in vivo* research (Khater et al., 2017). In contrast, neither water nor ethanol extracts of propolis could eliminate the infection, but they did lower oocysts shedding (Soufy et al., 2017). The promising antioxidant activity of phenolic fraction of *A. judaica* demonstrated in the current investigation may be the responsible for the negative results of the infectivity assay, since the *C. parvum* infection is ROS-dependent (Bhagat et al., 2017). However, the role of plant extracts and phytochemicals against *Cryptosporidium* oocysts is still debatable (Almoradie et al., 2018; Ullah et al., 2020). Further clinical trials would also be encouraging in future studies.

5. Conclusion

This study demonstrates that the phenolic fraction of *A. judaica* L. can be a potentially medication effective against *C. parvum* oocysts by activating nuclear DNA fragmentation and destroying its morphological characteristics and the number of viable oocysts.

The benefits of using ArPh are its simple application method and its high level of safety as a herb. *A. judaica* phenolic part can be utilized to treat water systems and evident *Cryptosporidium* sp. contamination and thereby avert multiple waterborne epidemics. It can also be added to food sources to avert foodborne cryptosporidiosis or formulated into a medicine to treat humans and animals, and particularly in farm cows, to prevent cryptosporidiosis-related industrial losses.

Data availability statement

The original contributions presented in the study are included in the article/Supplementary material, further inquiries can be directed to the corresponding authors.

Ethics statement

The animal study was reviewed and approved by Suez Canal University's Research and Ethics Review Committee (Approval number: 5603, October 2022).

Author contributions

SA and PK contributed to conception and design of the study. SA, EE, SE, MN, and AM organized the database. SA, EE, SE, and MN

performed the statistical analysis. SA wrote the first draft of the manuscript. EE, SE, and MN wrote sections of the manuscript. SA, EE, MN, and AM funded resources of the experiment. SE funding of publication. All authors contributed to manuscript revision, read, and approved the submitted version.

Funding

This research work was funded by Institutional Fund Projects under grant no. (IFPIP:1929-166-1443). The authors gratefully acknowledge technical and financial support provided by the Ministry of Education and King Abdulaziz University, DSR, Jeddah, Saudi Arabia.

Conflict of interest

The authors declare that the research was conducted in the absence of any commercial or financial relationships that could be construed as a potential conflict of interest.

Publisher's note

All claims expressed in this article are solely those of the authors and do not necessarily represent those of their affiliated organizations, or those of the publisher, the editors and the reviewers. Any product that may be evaluated in this article, or claim that may be made by its manufacturer, is not guaranteed or endorsed by the publisher.

References

Abd El-Hamed, W. F., Yousef, N. S., Mazrou, Y. S. A., Elkholy, W. A. E. S., El-Refaiy, A. I., Elfeky, F. A., et al. (2021). Anti-*Cryptosporidium* efficacy of *Olea europaea* and *Ficus carica* leaves extract in immunocompromised mice associated with biochemical characters and antioxidative system. *Cells* 10:2419. doi: 10.3390/CELLS10092419

Abdelgaleil, S. A. M., Abbassy, M. A., Belal, A. S. H., and Abdel Rasoul, M. A. A. (2008). Bioactivity of two major constituents isolated from the essential oil of *Artemisia judaica* L. *Bioresour. Technol.* 99, 5947–5950. doi: 10.1016/J.BIORTECH.2007.10.043

Abd-Elhamid, T. H., Abdel-Rahman, I. A. M., Mahmoud, A. R., Allemailem, K. S., Almatroudi, A., Fouad, S. S., et al. (2021). A complementary herbal product for controlling giardiasis. *Antibiotics* 10:477. doi: 10.3390/antibiotics10050477

Abdelmaksoud, H. F., El-Ashkar, A. M., Elgohary, S. A., and El-Wakil, E. S. (2020). Potential therapeutic and prophylactic effects of asafoetida in murine cryptosporidiosis. *J. Parasit. Dis.* 44, 646–653. doi: 10.1007/S12639-020-01241-5

Aboelsoud, N. H. (2010). Herbal medicine in ancient Egypt. *J. Med. Plants Res.* 4, 82–86.

Abotaleb, M., Samuel, S. M., Varghese, E., Varghese, S., Kubatka, P., Liskova, A., et al. (2019). Flavonoids in cancer and apoptosis. *Cancers (Basel)* 11:28. doi: 10.3390/cancers11010028

Abouseadaa, H. H., Atia, M. A. M., Younis, I. Y., Issa, M. Y., Ashour, H. A., Saleh, I., et al. (2020). Gene-targeted molecular phylogeny, phytochemical profiling, and antioxidant activity of nine species belonging to family Cactaceae. *Saudi J. Biol. Sci.* 27, 1649–1658. doi: 10.1016/j.sjbs.2020.03.007

Abrahamsen, M. S., Templeton, T. J., Enomoto, S., Abrahante, J. E., Zhu, G., Lancto, C. A., et al. (2004). Complete genome sequence of the apicomplexan, *Cryptosporidium parvum*. *Science* 304, 441–445. doi: 10.1126/science.1094786

Ahmed, S. A., El-Mahallawy, H. S., and Karanis, P. (2019). Inhibitory activity of chitosan nanoparticles against *Cryptosporidium parvum* oocysts. *Parasitol. Res.* 118, 2053–2063. doi: 10.1007/S00436-019-06364-0

Ahmed, S. A., Guerrero Flórez, M., and Karanis, P. (2018). The impact of water crises and climate changes on the transmission of protozoan parasites in Africa. *Pathog. Glob. Health* 112, 281–293. doi: 10.1080/20477724.2018.1523778

Ahmed, S. A., and Karanis, P. (2018a). An overview of methods/techniques for the detection of *Cryptosporidium* in food samples. *Parasitol. Res.* 117, 629–653. doi: 10.1007/S00436-017-5735-0

Ahmed, S. A., and Karanis, P. (2018b). Comparison of current methods used to detect *Cryptosporidium* oocysts in stools. *Int. J. Hyg. Environ. Health* 221, 743–763. doi: 10.1016/j.ijheh.2018.04.006

Ahmed, S. A., and Karanis, P. (2020). *Cryptosporidium* and cryptosporidiosis: the perspective from the gulf countries. *Int. J. Environ. Res. Public Health* 17, 1–34. doi: 10.3390/ijerph17186824

Ahmed, S. A., Kotepui, M., Masangkay, F. R., Milanez, G. D., and Karanis, P. (2022). Gastrointestinal parasites in Africa: a review. *Adv. Parasitol.* 119, 1–64. doi: 10.1016/bs.apar.2022.10.001

Ahmed, E. S., Mabrouk, D. M., Hassanane, M. M., and Khalil, W. K. B. (2017). Protective effect of *Artemisia judaica* against doxorubicin-induced toxicity in mice. *Annu. Res. Rev. Biol.* 18, 1–10. doi: 10.9734/ARRB/2017/35990

Ahmed, S. A. A., Mohamed, S. F., Fouad, A. M., and Karanis, P. (2022). Gastrointestinal parasites diagnoses at the primary health care units: a comparative analysis of diagnostic abilities of parasitology staff technicians versus medical parasitologists in Ismailia, Egypt. *Trans. R. Soc. Trop. Med. Hyg.* 116, 1191–1201. doi: 10.1093/trstmh/trac072

Ahmed, S., Quattrocchi, A., and Karanis, P. (2023). *Cryptosporidium* sp. infection in solid organ transplant recipients: a systematic review and meta-analysis. *Pathog. Glob. Health.*

Ajikumar, P. K., Tyo, K., Carlsen, S., Mucha, O., Phon, T. H., and Stephanopoulos, G. (2008). Terpenoids: opportunities for biosynthesis of natural product drugs using engineered microorganisms. *Mol. Pharm.* 5, 167–190. doi: 10.1021/mp700151b

Almoradie, A. M., Angeles, R. J., Beltran, E. V., Ugali, M., Valles, N. S., Los Banos, Z. D., et al. (2018). Cryptosporicidal activity of plant extracts against *Cryptosporidium parvum* and *Cryptosporidium hominis*. *Asian J. Pharmacogn.* 2, 22–31.

Antwi, C. A., Amisigo, C. M., Adjimani, J. P., and Gwira, T. M. (2019). In vitro activity and mode of action of phenolic compounds on *Leishmania donovani*. *PLoS Negl. Trop. Dis.* 13:e0007206. doi: 10.1371/journal.pntd.0007206

Arrowood, M. J., and Sterling, C. R. (1987). Isolation of *Cryptosporidium* oocysts and sporozoites using discontinuous sucrose and isopycnic percoll gradients. *J. Parasitol.* 73, 314–319. doi: 10.2307/3282084

Ashraf, K., Tajeri, S., Arnold, C. S., Amanzougaghene, N., Franetich, J. F., Vantaux, A., et al. (2022). Artemisinin-independent inhibitory activity of *Artemisia* sp. infusions against different *Plasmodium* stages including relapse-causing hypnozoites. *Life Sci. Alliance* 5:e202101237. doi: 10.26508/lsa.202101237

Badr, A., Morsy, W., Abdelfattah, S., Shams, S., and Shehab, A. (2012). Genetic diversity in *Artemisia monosperma* and *Artemisia judaica* populations in Egypt based on morphological, karyological and molecular variations. *J. Med. Plants Res* 6, 66–78. doi: 10.5897/JMPR11.975

Bakr, R. O. (2014). Microscopical and phytochemical investigation of Egyptian *Artemisia judaica* L. Var. *sinaitica tackholm* and its free radical scavenging activity. *Int. J. Pharmacogn. Phytochem. Res.* 6, 698–709.

Baldursson, S., and Karanis, P. (2011). Waterborne transmission of protozoan parasites: review of worldwide outbreaks–an update 2004-2010. *Water Res.* 45, 6603–6614. doi: 10.1016/j.watres.2011.10.013

Bhagat, M., Sood, S., Yadav, A., Verma, P., Manzoor, N., Chakraborty, D., et al. (2017). Alterations in oxidative stress parameters and its associated correlation with clinical disease on experimental *Cryptosporidium parvum* infection in Swiss albino mice. *J. Parasit. Dis.* 41, 707–712. doi: 10.1007/S12639-016-0871-5

Bialek, R., Binder, N., Dietz, K., Joachim, A., Knobloch, J., and Zelck, U. E. (2002). Comparison of fluorescence, antigen and PCR assays to detect *Cryptosporidium parvum* in fecal specimens. *Diagn. Microbiol. Infect. Dis.* 43, 283–288. doi: 10.1016/S0732-8893(02)00408-X

Bora, K. S., and Sharma, A. (2011). The genus *Artemisia*: a comprehensive review. *Pharm. Biol.* 49, 101–109. doi: 10.3109/13880209.2010.497815

Bortoleti, B. T. D., Tomiotto-Pellissier, F., Gonçalves, M. D., Miranda-Sapla, M. M., Assolini, J. P., Carloto, A. C., et al. (2019). Caffeic acid has antipromastigote activity by apoptosis-like process; and anti-amastigote by TNF-α/ROS/NO production and decreased of iron availability. *Phytomedicine* 57, 262–270. doi: 10.1016/j.phymed.2018.12.035

Castro-Hermida, J., Porsi, I., Ares-Mazas, E., and Chartier, C. (2004). In vitro activity on *Cryptosporidium parvum* oocyst of different drugs with recognized anticryptosporidial efficacy. *Rev. Med. Vet. (Toulouse)* 155, 453–456. doi: 10.3115/1697236.1697278

CDC. (2021). *Parasites–Cryptosporidium–Treatment*. Available at: https://www.cdc.gov/parasites/crypto/treatment.html#two (Accessed August 22, 2022).

Cell Biolab. (2013). *OxiSelect ™ comet assay control cells*. Cell Biolabs Prod. Datasheet, pp. 2–5.

Checkley, W., White, A. C., Jaganath, D., Arrowood, M. J., Chalmers, R. M., Chen, X. M., et al. (2015). A review of the global burden, novel diagnostics, therapeutics, and vaccine targets for *Cryptosporidium*. *Lancet Infect. Dis.* 15, 85–94. doi: 10.1016/S1473-3099(14)70772-8

Chen, X., He, X., Sun, J., and Wang, Z. (2022). Phytochemical composition, antioxidant activity, α-glucosidase and acetylcholinesterase inhibitory activity of quinoa extract and its fractions. *Molecules* 27:2420. doi: 10.3390/molecules27082420

Collier, S. A., Deng, L., Adam, E. A., Benedict, K. M., Beshearse, E. M., Blackstock, A. J., et al. (2021). Estimate of burden and direct healthcare cost of infectious waterborne disease in the United States. *Emerg. Infect. Dis.* 27, 140–149. doi: 10.3201/EID2701.190676

Degerli, S., and Tepe, B. (2015). Phenolic acid composition and anti-parasitic effects of four *Peucedanum* species on *Entamoeba histolytica* trophozoites. *Iran. J. Parasitol.* 10, 420–431.

EDA. (2022). *Egyptian herbal monograph volume 1 traditional wild medicinal plants*. Cairo: Egyptian Drug Authority.

Efstratiou, A., Ongerth, J. E., and Karanis, P. (2017). Waterborne transmission of protozoan parasites: review of worldwide outbreaks - an update 2011-2016. *Water Res.* 114, 14–22. doi: 10.1016/j.watres.2017.01.036

Eltahan, R., Guo, F., Zhang, H., Xiang, L., and Zhu, G. (2018). Discovery of ebselen as an inhibitor of *Cryptosporidium parvum* glucose-6-phosphate isomerase (CpGPI) by high-throughput screening of existing drugs. *Int. J. Parasitol. Drugs Drug Resist.* 8, 43–49. doi: 10.1016/j.ijpddr.2018.01.003

Eltahan, R., Guo, F., Zhang, H., and Zhu, G. (2019). The action of the hexokinase inhibitor 2-deoxy-d-glucose on *Cryptosporidium parvum* and the discovery of activities against the parasite hexokinase from marketed drugs. *J. Eukaryot. Microbiol.* 66, 460–468. doi: 10.1111/jeu.12690

Eltamany, E. E., Elhady, S. S., Ahmed, H. A., Badr, J. M., Noor, A. O., Ahmed, S. A., et al. (2020). Chemical profiling, antioxidant, cytotoxic activities and molecular docking simulation of *Carrichtera annua* DC. (Cruciferae). *Antioxidants.* 9:1286. doi: 10.3390/antiox9121286

Eltamany, E. E., Goda, M. S., Nafie, M. S., Abu-Elsaoud, A. M., Hareeri, R. H., Aldurdunji, M. M., et al. (2022). Comparative assessment of the antioxidant and anticancer activities of *Plicosepalus acacia* and *Plicosepalus curviflorus*: metabolomic profiling and in silico studies. *Antioxidants (Basel, Switzerland)* 11:1249. doi: 10.3390/antiox11071249

Ferreira, J. F. S., Luthria, D. L., Sasaki, T., and Heyerick, A. (2010). Flavonoids from *Artemisia annua* L. as antioxidants and their potential synergism with artemisinin against malaria and cancer. *Molecules* 15, 3135–3170. doi: 10.3390/molecules15053135

Finch, G. R., Daniels, C. W., and Black, E. K.., Schaefer, F. W., and Belosevic, M.. (1993). *Dose response of Cryptosporidium parvum in outbred neonatal CD-1 mice*. Available at: https://www.ncbi.nlm.nih.gov/pmc/articles/PMC182513/pdf/aem00040-0157.pdf (Accessed December 3, 2018).

Fonseca-Silva, F., Inacio, J. D. F., Canto-Cavalheiro, M. M., Menna-Barreto, R. F. S., and Almeida-Amaral, E. E. (2016). Oral efficacy of Apigenin against cutaneous leishmaniasis: involvement of reactive oxygen species and autophagy as a mechanism of action. *PLoS Negl. Trop. Dis.* 10:e0004442. doi: 10.1371/journal.pntd.0004442

Fordjour, P. A., and Adjimani, J. P.. (2020). *Anti-malarial activity of phenolic acids is structurally related*. Research square.

Galal, E. E., Kandil, A., Abdel-Latif, M., Khedr, T., and Khafagy, S. M. (1974). Cardiac pharmaco-toxicological studies of judaicin, isolated from *Artemisia judaica*. *Planta Med.* 25, 88–91. doi: 10.1055/S-0028-1097918

Goda, M. S., Nafie, M. S., Awad, B. M., Abdel-Kader, M. S., Ibrahim, A. K., Badr, J. M., et al. (2021). In vitro and in vivo studies of anti-lung cancer activity of *Artemesia judaica* L. crude extract combined with LC-MS/MS metabolic profiling, docking simulation and HPLC-DAD quantification. *Antioxidants (Basel, Switzerland)* 11:11. doi: 10.3390/antiox11010017

Goes, G. R., Rocha, P. S., Diniz, A. R. S., Aguiar, P. H. N., Machado, C. R., and Vieira, L. Q. (2016). *Trypanosoma cruzi* needs a signal provided by reactive oxygen species to infect macrophages. *PLoS Negl. Trop. Dis.* 10:e0004555. doi: 10.1371/journal.pntd.0004555

Graßmann, J. (2005). Terpenoids as plant antioxidants. *Vitam. Horm.* 72, 505–535. doi: 10.1016/S0083-6729(05)72015-X

Gruessner, B. M., and Weathers, P. J. (2021). In vitro analyses of *Artemisia* extracts on *Plasmodium falciparum* suggest a complex antimalarial effect. *PLoS One* 16:e0240874. doi: 10.1371/journal.pone.0240874

Gururajan, A., Rajkumari, N., Devi, U., and Borah, P. (2021). *Cryptosporidium* and waterborne outbreaks–a mini review. *Trop. Parasitol.* 11, 11–15. doi: 10.4103/TP.TP_68_20

Haynes, R. K., and Krishna, S. (2004). Artemisinins: activities and actions. *Microbes Infect.* 6, 1339–1346. doi: 10.1016/j.micinf.2004.09.002

Henriksen, S. A., and Pohlenz, J. F. (1981). Staining of cryptosporidia by a modified Ziehl-Neelsen technique. *Acta Vet. Scand.* 22, 594–296. doi: 10.1186/BF03548684

Higuchi, Y. (2003). Chromosomal DNA fragmentation in apoptosis and necrosis induced by oxidative stress. *Biochem. Pharmacol.* 66, 1527–1535. doi: 10.1016/S0006-2952(03)00508-2

Holzhausen, I., Lendner, M., and Daugschies, A. (2019). Bovine *Cryptosporidium parvum* field isolates differ in cytopathogenicity in HCT-8 monolayers. *Vet. Parasitol.* 273, 67–70. doi: 10.1016/j.vetpar.2019.08.006

Innes, E. A., Chalmers, R. M., Wells, B., and Pawlowic, M. C. (2020). A one health approach to tackle cryptosporidiosis. *Trends Parasitol.* 36, 290–303. doi: 10.1016/J.PT.2019.12.016

Iqbal, H. M. N., and Keshavarz, T. (2017). "The challenge of biocompatibility evaluation of biocomposites" in *Biomedical Composites*. ed. L. Ambrosio (Amsterdam, Netherlands: Elsevier), 303–334.

Islamuddin, M., Sahal, D., and Afrin, F. (2014). Apoptosis-like death in *Leishmania donovani* promastigotes induced by eugenol-rich oil of *Syzygium aromaticum*. *J. Med. Microbiol.* 63, 74–85. doi: 10.1099/JMM.0.064709-0

Ismail, F. M. D., Nahar, L., Zhang, K. Y., and Sarker, S. D. (2020). Antiparasitic natural products. *Annu. Rep. Med. Chem.* 55, 115–151. doi: 10.1016/BS.ARMC.2020.03.001

Jafari, M., Lorigooini, Z., Kheiri, S., and Naeini, K. M. (2021). Anti-toxoplasma effect of hydroalchohlic extract of *Terminalia chebula* retz in cell culture and murine model. *Iran. J. Parasitol.* 16, 631–640. doi: 10.18502/ijpa.v16i4.7876

Janaćković, P., Novaković, J., Soković, M., Vujisić, L., Giweli, A. A., Stevanović, Z. D., et al. (2015). Composition and antimicrobial activity of essential oils of *Artemisia judaica*, *A. herba-alba* and *A. arborescens* from Libya. *Arch. Biol. Sci.* 67, 455–466. doi: 10.2298/ABS141203010J

Ježková, J., Limpouchová, Z., Prediger, J., Holubová, N., Sak, B., Konečný, R., et al. (2021). *Cryptosporidium myocastoris* n. sp. (Apicomplexa: Cryptosporidiidae), the species adapted to the nutria (*Myocastor coypus*). *Microorganisms* 9:813. doi: 10.3390/microorganisms9040813

Jin, Z., Ma, J., Zhu, G., and Zhang, H. (2019). Discovery of novel anti-cryptosporidial activities from natural products by in vitro high-throughput phenotypic screening. *Front. Microbiol.* 10:1999. doi: 10.3389/fmicb.2019.01999/bibtex

Kao, T. C., and Ungar, B. L. P. (1994). Comparison of sequential, random, and hemacytometer methods for counting *Cryptosporidium* oocysts. *J. Parasitol.* 80, 816–819. doi: 10.2307/3283263

Karanis, P. (2018). The truth about *in vitro* culture of *Cryptosporidium* species. *Parasitology* 145: 855864. doi: 10.1017/S0031182017001937

Karanis, P., and Schoenen, D. (2001). *Biological test for the detection of low concentrations of infectious Cryptosporidium parvum oocysts in water*. Available at: https://onlinelibrary.wiley.com/doi/pdf/10.1002/1521-401X%28200111%2929%3A4%3C242%3A%3AAID-AHEH242%3E3.0.CO%3B2-2 (Accessed December 6, 2018).

Kaur, J., Kaur, R., and Kaur, A. (2018). "Dietary antioxidants and infectious diseases" in *Infectious Diseases and Your Health*. ed. P. Singh, 307–316.

Kayser, O., Kiderlen, A. F., and Croft, S. L. (2002). Natural products as potential antiparasitic drugs. *Stud. Nat. Prod. Chem.* 26, 779–848. doi: 10.1016/S1572-5995(02)80019-9

Kayser, O., Kiderlen, A. F., and Croft, S. L. (2003). Natural products as antiparasitic drugs. *Parasitol. Res.* 90, S55–S62. doi: 10.1007/S00436-002-0768-3

Khan, S. M., Zhang, X., and Witola, W. H. (2022). *Cryptosporidium parvum* pyruvate kinase inhibitors with in vivo anti-cryptosporidial efficacy. *Front. Microbiol.* 12, 1–14. doi: 10.3389/fmicb.2021.800293

Khater, M. M., El-Sayed, S. H., Yousof, H.-A. S., Mahmoud, S. S., El-Dib, N., and El-Badry, A. A. (2017). Anti-*Cryptosporidium* efficacy of Olea europaea and *Actinidia deliciosa* in a neonatal mouse model. *Kasr Al Ainy Med. J.* 23:32. doi: 10.4103/1687-4625.207190

Kim, S., Oh, S., Noh, H. B., Ji, S., Lee, S. H., Koo, J. M., et al. (2018). In vitro antioxidant and anti- propionibacterium acnes activities of cold water, hot water, and methanol extracts, and their respective ethyl acetate fractions, from *Sanguisorba officinalis* L. *Roots. Molecules* 23:3001. doi: 10.3390/molecules23113001

Kingston, D. G. I., and Cassera, M. B. (2022). Antimalarial natural products. *Prog. Chem. Org. Nat. Prod.* 117, 1–106. doi: 10.1007/978-3-030-89873-1_1

Korich, D. G., Marshall, M. M., Smith, H. V., O'Grady, J., Bukhari, Z., Fricker, C. R., et al. (2000). Inter-laboratory comparison of the CD-1 neonatal mouse logistic dose-response model for *Cryptosporidium parvum* oocysts. *J. Eukaryot. Microbiol.* 47, 294–298. doi: 10.1111/j.1550-7408.2000.tb00050.x

Kotloff, K. L., Blackwelder, W. C., Nasrin, D., Nataro, J. P., Farag, T. H., Van Eijk, A., et al. (2012). The global enteric multicenter study (GEMS) of diarrheal disease in infants and young children in developing countries: epidemiologic and clinical methods of the case/control study. *Clin. Infect. Dis.* 55, S232–S245. doi: 10.1093/cid/cis753

Kourenti, C., and Karanis, P. (2006). Evaluation and applicability of a purification method coupled with nested PCR for the detection of toxoplasma oocysts in water. *Lett. Appl. Microbiol.* 43, 475–481. doi: 10.1111/j.1472-765X.2006.02008.x

Kshirsagar, S. G., and Rao, R. V. (2021). Antiviral and immunomodulation effects of *Artemisia*. *Medicina (B. Aires).* 57:217. doi: 10.3390/medicina57030217

Leyva-López, N., Nair, V., Bang, W. Y., Cisneros-Zevallos, L., and Heredia, J. B. (2016). Protective role of terpenes and polyphenols from three species of oregano (*Lippia graveolens*, *Lippia palmeri* and *Hedeoma patens*) on the suppression of lipopolysaccharide-induced inflammation in RAW 264.7 macrophage cells. *J. Ethnopharmacol.* 187, 302–312. doi: 10.1016/j.jep.2016.04.051

Ma, P., and Soave, R. (1983). Three-step stool examination for cryptosporidiosis in 10 homosexual men with protracted watery diarrhea. *J. Infect. Dis.* 147, 824–828. doi: 10.1093/infdis/147.5.824

Mamede, L., Ledoux, A., Jansen, O., and Frédérich, M. (2020). Natural phenolic compounds and derivatives as potential antimalarial agents. *Planta Med.* 86, 585–618. doi: 10.1055/A-1148-9000

Manjolin, L. C., Dos Reis, M. B. G., Maquiaveli, D. C., Santos-Filho, O. A., and Da Silva, E. R. (2013). Dietary flavonoids fisetin, luteolin and their derived compounds inhibit arginase, a central enzyme in *Leishmania* (Leishmania) *amazonensis* infection. *Food Chem.* 141, 2253–2262. doi: 10.1016/j.foodchem.2013.05.025

Marakhova, A. I., and Emam, E. M. (2022). A study of active medicinal plant (*Artemisia judaica*) against *Staphylococcus aureus*. *Clin. Res. Clin. Trials* 5, 1–7. doi: 10.31579/2693-4779/092

Mead, J. R., and McNair, N. (2006). Antiparasitic activity of flavonoids and isoflavones against *Cryptosporidium parvum* and *Encephalitozoon intestinalis*. *FEMS Microbiol. Lett.* 259, 153–157. doi: 10.1111/J.1574-6968.2006.00263.X

Mehwish, S., Varikuti, S., Khan, M. A., Khan, T., Khan, I. U., Satoskar, A., et al. (2021). Bioflavonoid-induced apoptosis and DNA damage in amastigotes and promastigotes of *Leishmania donovani*: deciphering the mode of action. *Molecules* 26:5843. doi: 10.3390/molecules26195843

Mendonça, F. L. M., Carvalho, J. G., Silva, R. J., Ferreira, L. C. A., Cerqueira, D. M., Rogge, H. I., et al. (2021). Use of a natural herbal-based feed additive containing isoquinoline alkaloids in newborn calves with cryptosporidiosis. *Vet. Parasitol.* 300:109615. doi: 10.1016/j.vetpar.2021.109615

Mittra, B., and Andrews, N. W. (2013). IRONy OF FATE: role of iron-mediated ROS in *Leishmania* differentiation. *Trends Parasitol.* 29, 489–496. doi: 10.1016/J.PT.2013.07.007

Mittra, B., Saha, A., Chowdhury, A. R., Pal, C., Mandal, S., Mukhopadhyay, S., et al. (2000). Luteolin, an abundant dietary component is a potent anti-leishmanial agent that acts by inducing topoisomerase II-mediated kinetoplast DNA cleavage leading to apoptosis. *Mol. Med.* 6, 527–541. doi: 10.1007/BF03401792/FIGURES/8

Mohammed, M. J., Anand, U., Altemimi, A. B., Tripathi, V., Guo, Y., and Pratap-Singh, A. (2021). Phenolic composition, antioxidant capacity and antibacterial activity of white wormwood (*Artemisia herba-alba*). *Plants (Basel, Switzerland)* 10, 1–14. doi: 10.3390/plants10010164

Mohammed, H. A., Qureshi, K. A., Ali, H. M., Al-omar, M. S., Khan, O., and Mohammed, S. A. A. (2022). Bio-evaluation of the wound healing activity of *Artemisia judaica* L. as part of the plant's use in traditional medicine; phytochemical, antioxidant, anti-inflammatory, and antibiofilm properties of the plant's essential oils. *Antioxidants* 11:332. doi: 10.3390/antiox11020332/s1

Mokhtar, A. B., Ahmed, S. A., Eltamany, E. E., and Karanis, P. (2019). Anti-*Blastocystis* activity in vitro of Egyptian herbal extracts (family: Asteraceae) with emphasis on *Artemisia judaica*. *Int. J. Environ. Res. Public Health* 16:1555. doi: 10.3390/ijerph16091555

Morais, T. R., Conserva, G. A. A., Varela, M. T., Costa-Silva, T. A., Thevenard, F., Ponci, V., et al. (2020). Improving the drug-likeness of inspiring natural products - evaluation of the antiparasitic activity against *Trypanosoma cruzi* through semi-synthetic and simplified analogues of licarin A. *Sci. Rep.* 10:5467. doi: 10.1038/s41598-020-62352-w

Mosmann, T. (1983). Rapid colorimetric assay for cellular growth and survival: application to proliferation and cytotoxicity assays. *J. Immunol. Methods* 65, 55–63. doi: 10.1016/0022-1759(83)90303-4

Najm, M., Hadighi, R., Heidari-Kharaji, M., Alipour, M., Hajizadeh, M., Rafiei-Sefiddashti, R., et al. (2021). Anti-leishmanial activity of *Artemisia persica*, *A. spicigera*, and *A. fragrance* against *Leishmania* major. *Iran. J. Parasitol.* 16, 464–473. doi: 10.18502/ijpa.v16i3.7100

Olive, P. L. (1999). DNA damage and repair in individual cells: applications of the comet assay in radiobiology. *Int. J. Radiat. Biol.* 75, 395–405. doi: 10.1080/095530099140311

Olive, P. L., and Banáth, J. P. (2006). The comet assay: A method to measure DNA damage in individual cells. *Nat. Protoc.* 11, 23–29. doi: 10.1038/nprot.2006.5

Omarova, A., Tussupova, K., Berndtsson, R., Kalishev, M., and Sharapatova, K. (2018). Protozoan parasites in drinking water: A system approach for improved water, sanitation and hygiene in developing countries. *Int. J. Environ. Res. Public Health* 15:495. doi: 10.3390/ijerph15030495

Ostling, O., and Johanson, K. J. (1984). Microelectrophoretic study of radiation-induced DNA damages in individual mammalian cells. *Biochem. Biophys. Res. Commun.* 123, 291–298. doi: 10.1016/0006-291X(84)90411-X

Panda, S. K., and Luyten, W. (2018). Antiparasitic activity in Asteraceae with special attention to ethnobotanical use by the tribes of Odisha, India. *Parasite* 25:10. doi: 10.1051/parasite/2018008

Pandey, A. K., and Singh, P. (2017). The genus *Artemisia*: A 2012-2017 literature review on chemical composition, antimicrobial, insecticidal and antioxidant activities of essential oils. *Med. (Basel, Switzerland)* 4:68. doi: 10.3390/medicines4030068

Phillipson, J. D., and Wright, C. W. (1991). Antiprotozoal agents from plant sources. *Planta Med.* 57, S53–S59. doi: 10.1055/s-2006-960230

Poljsak, B., Šuput, D., and Milisav, I. (2013). Achieving the balance between ROS and antioxidants: when to use the synthetic antioxidants. *Oxidative Med. Cell. Longev.* 2013:956792. doi: 10.1155/2013/956792

Qanash, H., Bazaid, A. S., Aldarhami, A., Alharbi, B., Almashjary, M. N., Hazzazi, M. S., et al. (2023). Phytochemical characterization and efficacy of *Artemisia judaica* extract loaded chitosan nanoparticles as inhibitors of cancer proliferation and microbial growth. *Polymers (Basel).* 15:391. doi: 10.3390/polym15020391

Robertson, L. J., and Gjerde, B. K. (2007). *Cryptosporidium* oocysts: challenging adversaries? *Trends Parasitol.* 23, 344–347. doi: 10.1016/j.pt.2007.06.002

Rosenberg, A., Luth, M. R., Winzeler, E. A., Behnke, M., and Sibley, L. D. (2019). Evolution of resistance in vitro reveals mechanisms of artemisinin activity in *Toxoplasma gondii*. *Proc. Natl. Acad. Sci. U. S. A.* 116, 26881–26891. doi: 10.1073/pnas.1914732116/

Ryan, U. M., Feng, Y., Fayer, R., and Xiao, L. (2021). Taxonomy and molecular epidemiology of *Cryptosporidium* and *Giardia*–a 50 year perspective (1971–2021). *Int. J. Parasitol.* 51, 1099–1119. doi: 10.1016/j.ijpara.2021.08.007

Saini, P., Gayen, P., Nayak, A., Kumar, D., Mukherjee, N., Pal, B. C., et al. (2012). Effect of ferulic acid from *Hibiscus mutabilis* on filarial parasite *Setaria cervi*: molecular and biochemical approaches. *Parasitol. Int.* 61, 520–531. doi: 10.1016/j.parint.2012.04.002

Schneider, A., Wendt, S., Lübbert, C., and Trawinski, H. (2021). Current pharmacotherapy of cryptosporidiosis: an update of the state-of-the-art. *Expert. Opin. Pharmacother.* 22, 2337–2342. doi: 10.1080/14656566.2021.1957097

Shahbazi, P., Nematollahi, A., Arshadi, S., Farhang, H. H., and Shahbazfar, A. A. (2021). The protective effect of *Artemisia spicigera* ethanolic extract against *Cryptosporidium parvum* infection in immunosuppressed mice. *Iran. J. Parasitol.* 16, 279–288. doi: 10.18502/ijpa.v16i2.6318

Shaposhnik, E. G., Abozaid, S., Grossman, T., Marva, E., On, A., Azrad, M., et al. (2019). The prevalence of *Cryptosporidium* among children hospitalized because of gastrointestinal symptoms and the efficiency of diagnostic methods for *Cryptosporidium*. *Am. J. Trop. Med. Hyg.* 101, 160–163. doi: 10.4269/ajtmh.19-0057

Soufy, H., El-Beih, N. M., Nasr, S. M., Abd El-Aziz, T. H., Khalil, F. A. M., Ahmed, Y. F., et al. (2017). Effect of Egyptian propolis on cryptosporidiosis in immunosuppressed rats with special emphasis on oocysts shedding, leukogram, protein profile and ileum histopathology. *Asian Pac J Trop Med* 10, 253–262. doi: 10.1016/j.apjtm.2017.03.004

Sparks, H., Nair, G., Castellanos-Gonzalez, A., and White, A. C. (2015). Treatment of *Cryptosporidium*: what we know, gaps, and the way forward. *Curr. Trop. Med. Reports* 2, 181–187. doi: 10.1007/S40475-015-0056-9

Sun, Y. N., No, J. H., Lee, G. Y., Li, W., Yang, S. Y., Yang, G., et al. (2016). Phenolic constituents of medicinal plants with activity against *Trypanosoma brucei*. *Molecules* 21:480. doi: 10.3390/molecules21040480

Szewczyk-Golec, K., Pawłowska, M., Wesołowski, R., Wróblewski, M., and Mila-Kierzenkowska, C. (2021). Oxidative stress as a possible target in the treatment of toxoplasmosis: perspectives and ambiguities. *Int. J. Mol. Sci.* 22:5705. doi: 10.3390/ijms22115705

Ullah, F., Ayaz, M., Sadiq, A., Ullah, F., Hussain, I., Shahid, M., et al. (2020). Potential role of plant extracts and phytochemicals against foodborne pathogens. *Appl. Sci.* 10:4597. doi: 10.3390/app10134597

Ungar, B. L., Burris, J. A., Quinn, C. A., and Finkelman, F. D. (1990). New mouse models for chronic *Cryptosporidium* infection in immunodeficient hosts. *Infect. Immun.* 58, 961–969. doi: 10.1128/iai.58.4.961-969.1990

Zahedi, A., Bolland, S. J., Oskam, C. L., and Ryan, U. (2021). *Cryptosporidium abrahamseni* n. sp. (Apicomplexa: Cryptosporidiidae) from red-eye tetra (*Moenkhausia sanctaefilomenae*). *Exp. Parasitol.* 223:108089. doi: 10.1016/j.exppara.2021.108089

Zhang, X., Jian, Y., Li, X., Ma, L., Karanis, G., Qigang, C., et al. (2018). Molecular detection and prevalence of *Cryptosporidium* spp. infections in two types of domestic farm animals in the Qinghai-Tibetan plateau area (QTPA) in China. *Parasitol. Res.* 117, 233–239. doi: 10.1007/S00436-017-5697-2

Zhang, J. H., and Xu, M. (2000). DNA fragmentation in apoptosis. *Cell Res.* 10, 205–211. doi: 10.1038/sj.cr.7290049

Zhang, C., Yu, J., Tu, Q., Yan, F., Hu, Z., Zhang, Y., et al. (2022). Antioxidant capacities and enzymatic inhibitory effects of different solvent fractions and major flavones from celery seeds produced in different geographic areas in China. *Antioxidants (Basel, Switzerland)* 11:1542. doi: 10.3390/antiox11081542

Zhivotosky, B., and Orrenius, S. (2001). Assessment of apoptosis and necrosis by DNA fragmentation and morphological criteria. *Curr. Protoc. Cell Biol. Chapter* Chapter 18, 18.3.1–18.3.23. doi: 10.1002/0471143030.cb1803s12

frontiers | Frontiers in Microbiology

TYPE Original Research
PUBLISHED 18 July 2023
DOI 10.3389/fmicb.2023.1163841

OPEN ACCESS

EDITED BY
Stephen Forsythe,
Foodmicrobe.com, United Kingdom

REVIEWED BY
Arthur William Pightling,
United States Food and Drug Administration, United States
Amit Mathews,
Canadian Food Inspection Agency, Canada

*CORRESPONDENCE
Yohan Yoon
✉ yyoon@sm.ac.kr

†These authors have contributed equally to this work

RECEIVED 11 February 2023
ACCEPTED 12 May 2023
PUBLISHED 18 July 2023

CITATION
Ryu J, Choi Y and Yoon Y (2023) Comparison of genetic variations between high- and low-risk *Listeria monocytogenes* isolates using whole-genome *de novo* sequencing. *Front. Microbiol.* 14:1163841. doi: 10.3389/fmicb.2023.1163841

Comparison of genetic variations between high- and low-risk *Listeria monocytogenes* isolates using whole-genome *de novo* sequencing

Jihye Ryu[1†], Yukyung Choi[2†] and Yohan Yoon[1,2*]

[1]Department of Food and Nutrition, Sookmyung Women's University, Seoul, Republic of Korea, [2]Risk Analysis Research Center, Sookmyung Women's University, Seoul, Republic of Korea

In this study, genetic variations and characteristics of *Listeria monocytogenes* isolates from enoki mushrooms (23), smoked ducks (7), and processed ground meat products (30) were examined with respect to hemolysis, virulence genes, growth patterns, and heat resistance. The isolates that showed the highest pathogenicity and the lowest pathogenicity were analyzed to obtain the whole-genome sequence, and the sequences were further analyzed to identify genetic variations in virulence, low-temperature growth-related, and heat resistance-related factors. All isolates had β-hemolysis and virulence genes (*act*A, *hly*A, *inl*A, *inl*B, and *plc*B). At low temperatures, isolates with high growth (*L. monocytogenes* strains SMFM 201803 SD 1-1, SMFM 201803 SD 4-2, and SMFM 201804 SD 5-3) and low growth (*L. monocytogenes* strains SMFM 2019-FV43, SMFM 2019-FV42, and SMFM 2020-BT30) were selected. Among them, *L. monocytogenes* SMFM 201804 SD 5-3 showed the highest resistance at 60°C and 70°C. The strains SMFM 201804 SD 5-3 (high-risk) and SMFM 2019-FV43 (low-risk) harbored 45 virulence genes; 41 single nucleotide variants (SNVs) were identified between these two isolates. A comparison of 26 genes related to low-temperature growth revealed 18 SNVs between these two isolates; a comparison of the 21 genes related to heat resistance revealed 16 SNVs. These results indicate that the differences in the pathogenicity of *L. monocytogenes* SMFM 201804 SD 5-3 and *L. monocytogenes* SMFM 2019-FV43 are associated with the SNVs identified in virulence genes, low-temperature growth-related genes, and heat resistance-related genes.

KEYWORDS

enoki mushroom, smoked duck, processed ground meat product, next-generation sequencing, genetic variation, *Listeria monocytogenes*

1. Introduction

Listeria monocytogenes contaminates various foods, such as meat, fresh agricultural products, and smoked salmon; thus, foodborne illnesses caused by *L. monocytogenes* are frequent, throughout the year (Sheng et al., 2018). In Korea, recalls of processed meat products due to *L. monocytogenes* contamination occur continuously (Lee and Yoon, 2021). *L. monocytogenes* is a gram-positive facultative anaerobe that causes listeriosis in humans (Chen and Knabel, 2007; Yang and Moon, 2021). The pathogen may also cause severe infectious diseases in pregnant women and the immunocompromised (Shin et al., 2007). The fatality rate

of individuals infected with *L. monocytogenes* is 20–30%; this pathogen may cause infection even when present in low numbers compared to other pathogenic bacteria (Lee, 2010). The minimum infectious dose varies among patients and foods, but it is generally estimated 10^2–10^3 CFU/g (Park et al., 2014). *L. monocytogenes* can grow under anaerobic conditions, and thus, they can grow under vacuum or nitrogen-filled packaging (Duffy et al., 1994). It can grow even at refrigerated temperatures and survive under conditions of high-salt (≥10%), extreme acidity, and carbon-source depletion (Liu et al., 2006). Also, *L. monocytogenes* is one of the most heat-resistant pathogens and poses a notable risk to food safety, particularly when mild heat is treated in food processing and preparation (Pöntinen et al., 2017). These survival and viability characteristics of *L. monocytogenes* raise concerns regarding foodborne illnesses caused by the consumption of foods contaminated with this pathogen.

The advancement of next-generation sequencing (NGS) techniques has allowed the cost- and time-effective sequencing of DNA for microbial genome research. NGS techniques are used in various fields, including verification of the functionality of probiotics and investigation of the causes of foodborne outbreaks. They have also been used to establish a database of genomic information for foodborne pathogenic bacteria and to analyze the safety of microorganisms (Kwon et al., 2019; Cao et al., 2021). Whole-genome sequencing (WGS)-based methods have contributed to the identification of outbreak sources in several listeriosis outbreaks (Lüth et al., 2018). According to Hilliard et al. (2018), WGS analysis is a valuable methodology for classifying *L. monocytogenes* isolates and identifying virulence islands that may influence infectivity. WGS is increasingly used in the United States to facilitate detecting, investigating, and controlling foodborne bacterial outbreaks (Brown et al., 2019). In Ireland, WGS and phenotypic assays were used to explain the virulence of *L. monocytogenes* isolates (Stratakos et al., 2020). WGS provides an opportunity to determine strain characteristics typically obtained through resource-intensive traditional methodologies such as species identification, serotyping, virulence, and antimicrobial resistance profiling, all of which can be consolidated into a single WGS workflow (Ribot et al., 2019). The objective of this study was to identify phenotypes and genetic variations among *L. monocytogenes* isolates using WGS.

2. Materials and methods

2.1. Isolation of *Listeria monocytogenes*

The *L. monocytogenes* isolates from enoki mushrooms and other isolates (7 isolates from smoked ducks and 30 isolates from processed ground meat products) previously studied by Park et al. (2021) were used in the present study.

A total of 127 enoki mushrooms were collected from supermarkets in Korea between August 2019 and March 2020. The samples were transported in a cooler to our laboratory. Briefly, 25 g of each sample was placed in sample bags (3 M™, St. Paul, MN, USA) containing 225 mL of Listeria Enrichment Broth (Becton Dickinson and Company). The sample bags were hand-shaken for 1 min and incubated at 30°C for 48 h to enrich *L. monocytogenes*.

One-milliliter aliquots of the enriched cultures were spread-plated on Chrom agar (CHROM™ agar Listeria; Paris, France), and the plates were incubated at 37°C for 24 h. The isolated colonies were subjected to real-time PCR analysis to investigate the presence of the *iap* gene for the confirmatory test of *L. monocytogenes* [Food and Drug Administration (FDA), 2018] with a 264-bp DNA fragment, using suitable primers (F: 5′-TGG GAT TGC GGT AAC AGC AT-3′ R: 5′-TA TCA ACA CCA GCG CCA CT-3′) (Kim, 2019). A single colony was suspended in 50 μL of 0.25% sodium dodecyl sulfate (Biosesang, Gyeonggi-do, Korea)–0.05 N NaOH solution (Daejung, Gyeonggi-do, Korea) and 100 μL of dH_2O. The suspensions were heated at 99°C for 15 min, left at room temperature (25°C) for 3 min, and centrifuged at 5,989 × *g* at 4°C for 3 min; the supernatants were used as DNA templates. Real-time PCR amplification was performed using a Rotor-Gene SYBR® Green PCR Kit (Qiagen, Hilden, Germany). Briefly, 1 μL DNA template was mixed with 2.5 μL of forward primer, 2.5 μL of reverse primer, 12.5 μL of SYBR green master mix, and 6.5 μL of dH_2O. For *iap* amplification, an initial denaturation step at 95°C for 90 s and 35 cycles of denaturation at 95°C for 5 s, annealing at 56°C for 10 s, and extension at 72°C for 5 s were conducted. Finally, a 5-min extension was performed at 72°C. Amplified PCR products were loaded onto a 1.5% agarose gel and visualized under UV light.

2.2. Analysis of hemolytic property

Isolated colonies of *L. monocytogenes* were inoculated in 10 mL tryptic soy broth with 0.6% yeast extract (TSBYE; Becton Dickinson and Company) and incubated at 30°C overnight. Then, 100-μL aliquots of the cultures were transferred to fresh 10 mL TSBYE and incubated at 30°C for another 24 h. The sub-cultures were streaked onto Columbia agar with 5% sheep blood (bioMérieux, Mercy 1′Etoile, France) and incubated at 30°C for 48 h. Hemolytic properties (α-, β-, or γ-hemolysis) were determined by observing the zones formed around the bacterial colonies. β-hemolysis (complete hemolysis) was confirmed if a clear zone around the bacteria was observed.

2.3. Detection of virulence genes

Isolated colonies of *L. monocytogenes* isolates were suspended in 50 μL of 0.25% sodium dodecyl sulfate–0.05 N NaOH solution. One hundred microliters of sterile dH_2O was added to the suspension, and the mixtures were incubated at 99°C for 15 min. Aliquots (2 μL) of the mixtures were mixed with the components of the Phire Hot Start II DNA Polymerase Kit (Thermo Fisher Scientific, Waltham, MA, US), Taq DNA polymerase mix (20 mM Tris–HCl; pH 7.4 at 25°C, 0.1 mM EDTA, 1 mM DTT, 100 mM KCl, 200 μg/mL BSA, and 50% glycerol), 1X reaction buffer (1.5 mM $MgCl_2$), 200 μM deoxynucleoside triphosphates (dNTPs), and 0.5 μM of each of the virulence gene primers. Five virulence genes (*act*A, *hly*A, *inl*A, *inl*B, and *plc*B) were detected with PCR using the primers listed in Table 1. PCR was performed on a Rotor-Gene Q thermal cycler (Qiagen) at the following conditions: initial denaturation at 98°C for 30 s, followed by 35 cycles of 98°C for 5 s,

TABLE 1 Information of primers used for the detection of virulence genes (*actA*, *hlyA*, *inlA*, *inlB*, and *plcB*) in *Listeria monocytogenes*.

Target gene	Primer sequence (5′ to 3′)		Size (bp)	Reference
*act*A	Forward	GAC GAA AAT CCC GAA GTG AA	268, 385	Gianfranceschi et al. (1998)
	Reverse	CTA GCG AAG GTG CTG TTT CC		
*hly*A	Forward	GCA TCT GCA TTC AAT AAA GA	174	Riedo et al. (1994)
	Reverse	TGT CAC TGC ATC TCC GTC GT		
*inl*A	Forward	CCT AGC AGG TCT AAC CGC AC	255	Khelef et al. (2006)
	Reverse	TCG CTA ATT TGG TTA TGC CC		
*inl*B	Forward	AAA GCA CGA TTT CAT GGG AG	146	Jung et al. (2003)
	Reverse	ACA TAG CCT TCT TTG GTC GGG		
*plc*B	Forward	GGG AAA TTT GAC ACA GCG TT	261	Winters et al. (1999)
	Reverse	ATT TTC GGG TAG TCC GCT TT		

60°C for 5 s, and 72°C for 10 s, with a final extension step at 72°C for 1 min. Amplified PCR products were loaded onto a 1.5% agarose gel and visualized under UV light.

2.4. Comparing the growth patterns of *Listeria monocytogenes* isolates cultured at low temperature

As described in the section "2.2. Analysis of hemolytic property," *L. monocytogenes* isolates were cultured and then sub-cultured in TSBYE at 30°C overnight. The sub-cultures were centrifuged at 1,912 × *g* and 4°C for 15 min. Cell pellets were washed twice with phosphate-buffered saline (PBS), and the suspensions were diluted with PBS and inoculated at 5 Log CFU/mL. The aliquots (0.2 mL) of the inocula of each *L. monocytogenes* isolates were inoculated into tubes containing 20 mL of TSBYE and incubated at 4°C for 288 h. During incubation, the cultures of *L. monocytogenes* were diluted with buffered peptone water (BPW; Bacto, Becton, Dickinson, Sparks, MD, USA), and 0.1-mL aliquots of the diluents were plated on tryptic soy agar with 0.6% yeast extract (TSAYE; Becton Dickinson and Company). The plates were incubated at 30°C for 48 h, and the colonies on the plates were manually counted. The six for each strain were repeated for each time point.

2.5. Comparing the growth patterns of *Listeria monocytogenes* isolates after vacuum treatment

Aliquots (0.1 mL) of the inocula were placed on a 10-g beef rump. The inoculated samples were vacuum-packed and stored at 4°C for 20 days. The samples were analyzed every 5 days. The samples were aseptically removed from the vacuum bags and placed in filter bags (3 M™) containing 20 mL BPW. The samples were then pummeled for 1 min in a pummeler (BagMixer; Interscience, St. Nom, France). Aliquots (1 mL) of the homogenates were diluted with BPW, and 0.1 mL of the diluents was spread-plated on Palcam agar (Becton Dickinson and Company). The plates were incubated at 30°C for 48 h, and the colonies on the plates were manually counted. The six for each strain were repeated for each time point.

2.6. Heat resistance

Aliquots (0.1 mL) of the inoculum were inoculated into tubes containing 9.9 mL of TSBYE; the tubes were preheated at 60°C and 70°C in a water bath. After 0, 3, 5, 8, and 10 min at 60°C and 0, 0.17, 3, 5, 8, and 10 min at 70°C, one-milliliter aliquots of the samples were retrieved and diluted with BPW, and 0.1-mL aliquots of the diluents were spread-plated on TSAYE, respectively. The plates were incubated at 30°C for 48 h, and the colonies on the plates were manually counted. The cell counts were then used to calculate *D*-values (decimal reduction time) as follows:

$$D_T = t / (\text{Log } N_0 - \text{Log } Nt),$$

Where *T* is temperature, *t* is time, Log N_0 is the initial number of bacteria, and Log Nt is the number of bacteria remaining at time. The six for each strain were repeated for each time point.

2.7. Whole-genome sequencing

2.7.1. DNA extraction and library preparation

After sub-culturing as described in the section "2.2. Analysis of hemolytic property" 3-mL aliquots of the sub-cultures were precipitated at 5,264 × *g* for 30 s. The cell pellets were used for extraction of DNA with the DNeasy Blood and Tissue Kit (Qiagen), according to the manufacturer's protocol. Briefly, 5 μg of each extracted DNA sample was used to construct a library using the SMRTbell™ Template Prep Kit 1.0 (PN 100-259-100) (Pacific Biosciences, Menlo Park, CA, USA) following the manufacturer's

instructions. Fragments smaller than 20 kb of the SMRTbell template were removed using the BluePippin size selection system (Sage Science, Beverly, MA, USA) to construct large-insert libraries. The constructed library was validated using the 2100 Bioanalyzer (Agilent, Santa Clara, CA, USA) for quality control.

2.7.2. Sequencing and *de novo* assembly

The SMRTbell libraries were annealed to sequencing primers, and DNA polymerase was bound to the complex using the DNA/Polymerase Binding Kit P6 (Pacific Biosciences). This polymerase-SMRTbell-adaptor complex was loaded into SMRT cells (Pacific Biosciences) and sequenced using the PacBio RS II sequencing platform (Pacific Biosciences) which produce continuous long read (CLR). Long contigs were generated via *de novo* assembly (DNA LinkInc., Seoul, South Korea), and gene annotation and prediction were performed to analyze their genetic properties.

2.7.3. Analysis of genetic factors and genetic variations

Genetic characteristics of two high-risk and low-risk *L. monocytogenes* isolates were analyzed for 45 virulence factors, 26 low-temperature growth-related factors, and 21 heat resistance-related factors using CLC Genomics Workbench ver. 12.0 (Qiagen) (Table 2). The sequences of these factors were obtained from the NCBI GenBank database. The presence of genetic factors in the two *L. monocytogenes* isolates was determined using a Basic Local Alignment Search Tool (BLAST), and genetic variations were assessed by comparing the sequences of each gene.

2.8. Statistical analysis

Statistical analysis was performed using SAS® version 9.4 (SAS Institute Inc., Cary, NC, USA). Significant differences among strains were determined using analysis of covariance and a general linear model at $\alpha = 0.05$.

3. Results and discussion

3.1. Isolation and identification of *Listeria monocytogenes*

In this study, 23 *L. monocytogenes* isolates from 127 enoki mushrooms (Table 3), and 37 *L. monocytogenes* isolates (7 isolates from smoked ducks and 30 isolates from processed ground meat products) previously isolated (Table 4) were obtained. The *iap* gene for the confirmatory test of *L. monocytogenes* was detected in all 23 *L. monocytogenes* isolates from 127 enoki mushrooms (data not shown).

3.2. Hemolytic property

Listeria spp. which causes β-hemolysis is mostly pathogenic, and most of the isolated *L. monocytogenes* cause β-hemolysis (Farber and Peterkin, 1991). Examinations showed that all *L. monocytogenes* isolates caused β-hemolysis with narrow zone (Figure 1).

3.3. Virulence genes

Five virulence genes (*act*A, *hly*A, *inl*A, *inl*B, and *plc*B) were detected in all *L. monocytogenes* isolates (Figure 2). In another study, most *L. monocytogenes* isolates harbored these virulence genes, and polymorphisms in the *act*A gene have been found between carcass and human isolates (Oh et al., 2018). *Act*A in *L. monocytogenes* encodes the surface protein *act*A, which is responsible for actin-based motility and cell-to-cell spread (Vàzquez-Boland et al., 2001). Rezaei et al. (2019) showed that the presence of *hly*A and *iap* in *L. monocytogenes* is effective in increasing its aggressiveness and pathogenicity. Cellular invasion requires the presence of bacterial surface proteins internalin A (*inl*A) and/or *inl*B and their interaction with the cellular receptors E-cadherin and/or Met, respectively (Kühbacher et al., 2018). Virulence-associated genes *plc*A and *plc*B encode phosphatidylinositol phospholipase C (PI-PLC) and phosphatidyl-choline phospholipase (PC-PLC), respectively. Both

TABLE 2 The list of genetic factors of *Listeria monocytogenes*.

Genetic factor	Function	Gene
Virulence factor	Adherence	*dlt*A, *fbp*A, *ami*, *inl*F, *inl*J, *lap*, *lap*B
	Enzyme	*mpl*, *plc*B, *plc*A, *stp*
	Immune modulator	*inl*C, *inl*K, *lnt*A
	Intracellular survival	*lpl*A1, *opp*A, *prs*A2, *hpt*
	Invasion	*aut*, *iap*/*cwh*A, *gtc*A, *inl*A, *inl*B, *inl*P, *lpe*A, *vip*
	Iron uptake	*hbp*2
	Nucleation-promoting factor	*act*A
	Bile resistance	*bsh*
	Peptidoglycan modification	*oat*A, *pdg*A
	Regulation	*agr*A, *agr*C, *che*A, *che*Y, *lis*R, *lis*K, *prf*A, *vir*R, *vir*S
	Surface protein anchoring	*lgt*, *lsp*A, *srt*A, *srt*B
	Toxin	*hly*
Low-temperature growth-related factor	Cell-membrane-associated protein genes	*opp*A, *gbu*A, *gbu*B, *gbu*C, *fla*A, *bet*L, *fbp*, *mot*A, *flh*A
	Cold stress adaptive regulatory protein genes	*htp*, *deg*U, *yycJ*, *lhk*A
	Cold shock phase protein genes	*csp*LA, *fri*, *csp*D, *csp*B
	Other cold stress protein genes	*trx*B, trpG, *ltr*A, *ltr*B, *ltr*C
	General stress response protein genes	*gro*EL, *clp*P, *sig*B, *rsb*U
Heat resistance-related factor	Heat shock protein genes	*dna*J, *dna*K, *grp*E, *hrc*A, *gro*EL, *gro*ES, *lmo*0229, *lmo*2030, *lmo*0231, *lmo*1138, *lmo*1279, *clp*C, *clp*E, *clp*B, *clp*P, *hsl*O, *lmo*0942, *lmo*0963, *lmo*0056, *lmo*0222, *lmo*0292

TABLE 3 Information regarding *Listeria monocytogenes* isolates from enoki mushrooms purchased from a market in Korea.

No.	*L. monocytogenes* isolate	Date of purchase
1	SMFM 2019-FV41	August 2019
2	SMFM 2019-FV42	August 2019
3	SMFM 2019-FV43	August 2019
4	SMFM 2019-FV44	August 2019
5	SMFM 2019-FV45	August 2019
6	SMFM 2019-FV46	August 2019
7	SMFM 2019-FV47	August 2019
8	SMFM 2019-FV48	September 2019
9	SMFM 2019-FV49	September 2019
10	SMFM 2019-FV50	September 2019
11	SMFM 2019-FV51	September 2019
12	SMFM 2019-FV52	September 2019
13	SMFM 2019-FV53	September 2019
14	SMFM 2019-FV54	September 2019
15	SMFM 2019-FV55	September 2019
16	SMFM 2019-FV56	September 2019
17	SMFM 2019-FV57	October 2019
18	SMFM 2020-FV1	March 2020
19	SMFM 2020-FV2	March 2020
20	SMFM 2020-FV3	March 2020
21	SMFM 2020-FV4	March 2020
22	SMFM 2020-FV5	March 2020
23	SMFM 2020-FV6	March 2020

phospholipases are related to effective escape from the phagocytic vacuole into the cytoplasm (Gründling et al., 2003; Hadjilouka et al., 2016). These results indicate that the isolates examined in this study are pathogenic to humans.

3.4. Growth of *Listeria monocytogenes* isolates at 4°C

According to Kim et al. (1995), *L. monocytogenes* isolates from humans do not grow at 4°C; however, Seeliger and Jones (1986) reported that most *L. monocytogenes* could grow at 4°C. In this study, all the *L. monocytogenes* isolates showed growth at 4°C (Figure 3). Considering growth rates based on statistical difference over all time points (0, 48, 96, 144, 192, 240, and 288 h), high and low growth group were divided. *L. monocytogenes* SMFM 201803 SD 1-1 was in high growth group at all time points (48, 96, 144, 192, 240, and 288 h), and *L. monocytogenes* SMFM 201803 SD 4-2 was in high growth group at five time points (48, 144, 192, 240, and 288 h). *L. monocytogenes* SMFM 201804 SD 5-3 was in the high growth group at four points (48, 144, 240, and 288 h). *L. monocytogenes* SMFM 2019-FV43 was in the low growth group at all time points (48, 96, 144, 192, 240, and 288 h).

TABLE 4 Information regarding *Listeria monocytogenes* isolates from smoked ducks and processed ground meat products.

Food	*L. monocytogenes* isolate	Date of purchase	Place of purchase
Smoked duck	SMFM 201803 SD 1-1	March 2018	Market
	SMFM 201803 SD 4-1		
	SMFM 201803 SD 4-2		
	SMFM 201804 SD 5-2	April 2018	
	SMFM 201804 SD 5-3		
	SMFM 201804 SD 6-2		
	SMFM 201804 SD 7-1		
Processed ground meat product	SMFM 2020-BT1	January 2020	Online market
	SMFM 2020-BT2		
	SMFM 2020-BT3		
	SMFM 2020-BT4		
	SMFM 2020-BT5		
	SMFM 2020-BT6		
	SMFM 2020-BT8		
	SMFM 2020-BT9		
	SMFM 2020-BT10		
	SMFM 2020-BT11		
	SMFM 2020-BT12		
	SMFM 2020-BT13		
	SMFM 2020-BT14		
	SMFM 2020-BT15		
	SMFM 2020-BT16		
	SMFM 2020-BT17		
	SMFM 2020-BT18		
	SMFM 2020-BT19		
	SMFM 2020-BT20		
	SMFM 2020-BT21		
	SMFM 2020-BT22		
	SMFM 2020-BT23		
	SMFM 2020-BT24		
	SMFM 2020-BT25		
	SMFM 2020-BT26	February 2020	
	SMFM 2020-BT27		
	SMFM 2020-BT28		
	SMFM 2020-BT29		
	SMFM 2020-BT30	April 2020	
	SMFM 2020-BT31		

L. monocytogenes SMFM 2020-BT30 was in low growth group at four time points (144, 192, 240, and 288 h), and *L. monocytogenes* SMFM 2019-FV42 was in low growth group at three time points (48, 96, and 240 h). Three (*L. monocytogenes* SMFM 201803 SD 1-1, *L. monocytogenes* SMFM 201803 SD 4-2, and

L. monocytogenes SMFM 201804 SD 5-3) with high growth and three (*L. monocytogenes* SMFM 2019-FV42, *L. monocytogenes* SMFM 2019-FV43, and *L. monocytogenes* SMFM 2020-BT30) with low growth at 4°C were selected (Figure 3). The average cell counts (288 h – 0 h) of the high and low growth group were 5.3 and 4.6 Log CFU/mL, respectively. The three high-growth isolates were from smoked ducks; two low-growth isolates were from enoki mushrooms, while one low-growth isolate was from to the processed ground meat product.

FIGURE 1
β-hemolytic property of *Listeria monocytogenes* SMFM 201803 SD 4-2, *Listeria monocytogenes* SMFM 201804 SD 5-2, and *Listeria monocytogenes* SMFM 201804 SD 6-2.

3.5. Growth of *Listeria monocytogenes* isolates in vacuum

Isolates with high and low growth (three each) at 4°C were further analyzed to compare their growth under vacuum conditions at 4°C. Duffy et al. (1994) showed that *L. monocytogenes* can grow in vacuum-packed foods stored in a refrigerator. However, in our study, the *L. monocytogenes* isolates showed high mortality rates (Figure 4). Isolates with high growth at 4°C (*L. monocytogenes* SMFM 201803 SD 1-1, *L. monocytogenes* SMFM 201803 SD 4-2, and *L. monocytogenes* SMFM 201804 SD 5-3) had better survival under vacuum conditions than those with low growth (*L. monocytogenes* SMFM 2019-FV42, *L. monocytogenes* SMFM 2019-FV43, and *L. monocytogenes* SMFM 2020-BT30) (Figure 4). These results showed that high-growth *L. monocytogenes* isolates in low temperature survive long in vacuum conditions.

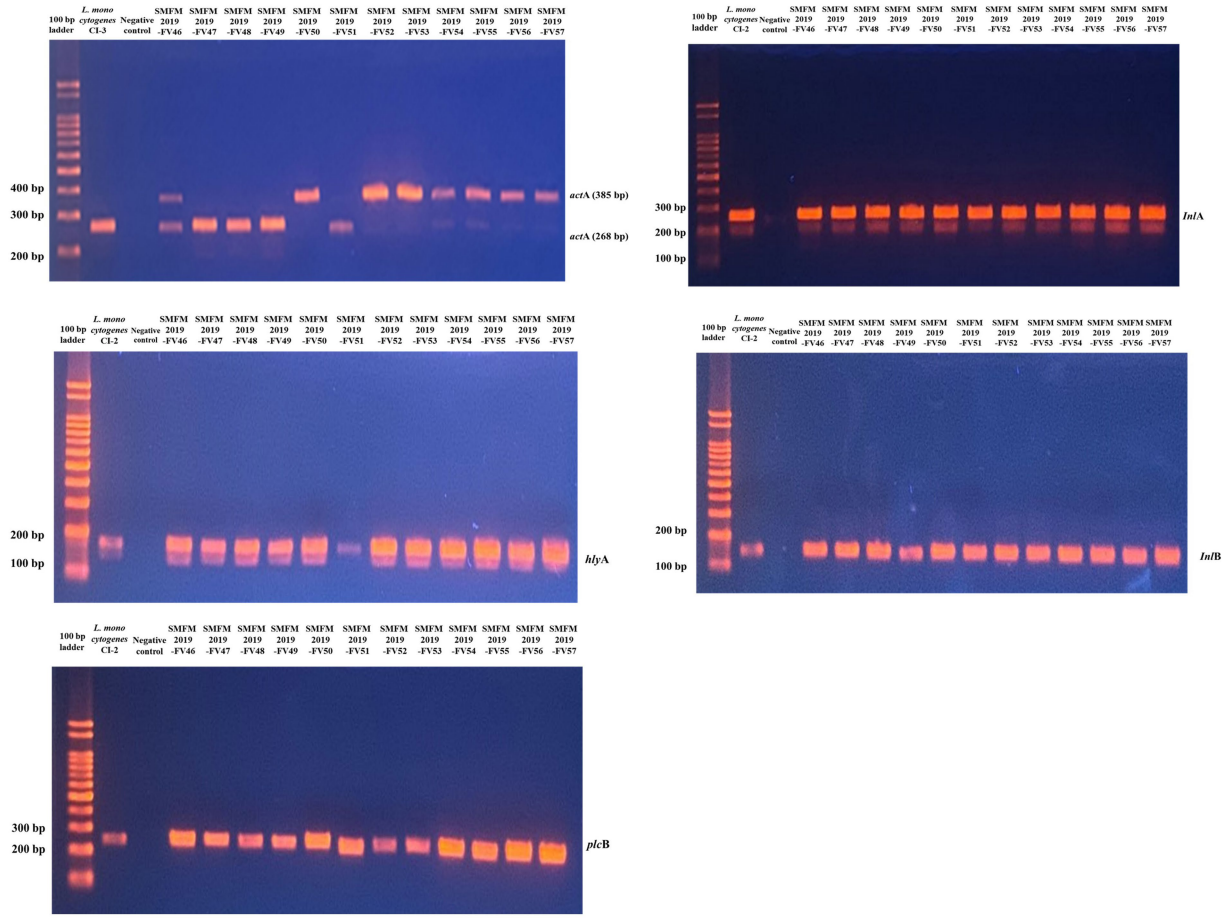

FIGURE 2
Gel image of PCR results for 12 *Listeria monocytogenes* isolates targeting *actA*, *hlyA*, *inlA*, *inlB*, and *plcB* genes.

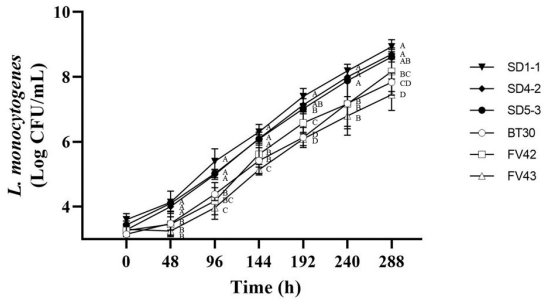

FIGURE 3
Cell counts of *Listeria monocytogenes* isolates in tryptic soy broth with 0.6% yeast extract during storage at 4°C. Error bars in the figure mean standard error. $^{A–D}$ means in the figure with different letters are significantly different (p<0.05).

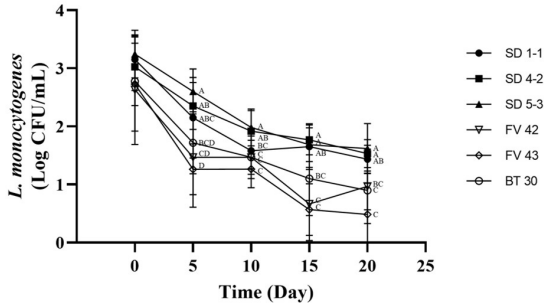

FIGURE 4
Cell counts of *Listeria monocytogenes* isolates inoculated in beef during storage under vacuum at 4°C. Error bars in the figure mean standard error. $^{A–D}$ means in the figure with different letters are significantly different (p<0.05).

3.6. Heat resistance

The D_{60} and D_{70} values of the *L. monocytogenes* isolates, which describe heat resistance at 60°C and 70°C, ranged 2.37–3.55 min and 1.83–2.20 min, respectively (Table 5). According to Tangwatcharin et al. (2019), *D*-values of *L. monocytogenes* in inoculated restructured goat steaks ranged from 7.27 min at 60°C to 0.46 min at 70°C. In our study, at 60°C, *L. monocytogenes* SMFM 201804 SD 5-3 (3.55 min) had higher D_{60} value than the others followed by *L. monocytogenes* SMFM 2019-FV42 (3.17 min), and the D_{70} value (2.20 min) of *L. monocytogenes* SMFM 201804 SD 5-3 was also higher than that of the other isolates (Table 5). This indicated that *L. monocytogenes* SMFM 201804 SD 5-3 had the highest heat resistance.

There was association between cold and heat resistance. The growth of *L. monocytogenes* SMFM 201804 SD 5-3 at 4°C was significantly higher than that of *L. monocytogenes* SMFM 2020-BT30 and *L. monocytogenes* SMFM 2019-FV43 (p < 0.05, Figure 3). The D_{60} and D_{70} of *L. monocytogenes* SMFM 201804 SD 5-3 were significantly higher than those of *L. monocytogenes* SMFM 2019-FV43 (p < 0.05, Table 5). These results show a correlation between *L. monocytogenes* SMFM 201804 SD 5-3 (high cold- and heat-resistance) and *L. monocytogenes* SMFM 2019-FV43 (low cold- and heat-resistance) for growth at low temperature and survival in heat resistance. In the case of *L. monocytogenes* SMFM 201803 SD 1-1, the growth of the isolate was significantly higher than *L. monocytogenes* SMFM 2020-BT30, *L. monocytogenes* SMFM 2019-FV42, and *L. monocytogenes* SMFM 2019-FV43 at 4°C (p < 0.05, Figure 3), and there was no significant difference in D_{60}. However, D_{70} of *L. monocytogenes* SMFM 201803 SD 1-1 was higher than that of *L. monocytogenes* SMFM 2019-FV42 and *L. monocytogenes* SMFM 2020-BT30 (p < 0.05, Table 5). *L. monocytogenes* SMFM 201803 SD 4-2 grew significantly higher than *L. monocytogenes* SMFM 2020-BT30, *L. monocytogenes* SMFM 2019-FV42, and *L. monocytogenes* SMFM 2019-FV43 at 4°C (p < 0.05, Figure 3), however, there was no significant difference in both D_{60} and D_{70}.

TABLE 5 *D*-values of *Listeria monocytogenes* isolates at 60°C and 70°C.

L. monocytogenes isolate	D_{60}°C (min)	D_{70}°C (min)
ATCC13932	2.37^{C}	1.90^{BC}
SMFM 201803 SD 1-1	2.80^{BC}	2.07^{AB}
SMFM 201803 SD 4-2	2.47^{C}	1.83^{BC}
SMFM 201804 SD 5-3	3.55^{A}	2.20^{A}
SMFM 2019-FV42	3.17^{AB}	1.85^{C}
SMFM 2019-FV43	2.60^{C}	1.97^{BC}
SMFM 2020-BT30	2.65^{C}	1.83^{C}

$^{A–C}$means in the same column with different letters are significantly different (p < 0.05).

3.7. Selection of high- and low-risk *Listeria monocytogenes* isolates

Analyses for hemolytic property, virulence genes, growth patterns, and the heat resistance test showed that *L. monocytogenes* SMFM 201804 SD 5-3 had the highest risk, while *L. monocytogenes* SMFM 2019-FV43 had the lowest risk. Thus, *L. monocytogenes* SMFM 201804 SD 5-3 and *L. monocytogenes* SMFM 2019-FV43 were defined as a high- and low-risk isolates, respectively. *L. monocytogenes* SMFM 201804 SD 5-3, isolated from smoked duck, showed relatively high growth at 4°C, the highest heat resistance, and relatively slow reduction in vacuum condition. *L. monocytogenes* SMFM 2019-FV43, isolated from the enoki mushrooms, had the lowest growth at 4°C, fast reduction under vacuum conditions, and low heat resistance compared with *L. monocytogenes* SMFM 201804 SD 5-3. For tracing the causes of these different characteristics between high- and low-risk *L. monocytogenes*, WGS was performed.

3.8. *De novo* assembly results

The *de novo* assembly results showed that *L. monocytogenes* SMFM 2019-FV43 and *L. monocytogenes* SMFM 201804 SD 5-3

TABLE 6 Single nucleotide variants in virulence genes of *Listeria monocytogenes* SMFM 2019-FV43 and *Listeria monocytogenes* SMFM 201804 SD 5-3.

Virulence genes	SNV frequency % (no.)	Virulence genes	SNV frequency % (no.)
lntA	9.78% (62/634)	*virR*	0.30% (2/677)
inlK	1.70% (31/1820)	*lgt*	0.24% (2/832)
actA	1.27% (13/1022)	*lapB*	0.23% (12/5138)
plcB	1.16% (10/865)	*OatA*	0.21% (4/1884)
cheY	0.84% (3/359)	*iap/cwhA*	0.21% (3/1440)
bsh	0.72% (7/978)	*pdgA*	0.21% (3/1399)
prfA	0.70% (5/714)	*plcA*	0.21% (2/954)
inlJ	0.65% (12/1859)	*inlA*	0.17% (4/2402)
lap	0.62% (16/2599)	*inlP*	0.17% (2/1167)
lisR	0.59% (4/681)	*virS*	0.17% (1/582)
hly	0.57% (9/1584)	*agrC*	0.15% (2/1296)
inlF	0.53% (13/2470)	*lisK*	0.14% (2/1452)
ami	0.47% (13/2751)	*stp*	0.13% (1/758)
mpl	0.46% (7/1530)	*srtB*	0.13% (1/741)
lpeA	0.43% (4/933)	*aut*	0.12% (2/1718)
agrA	0.41% (3/726)	*hbp2*	0.12% (2/1710)
dltA	0.39% (6/1533)	*oppA*	0.12% (2/1677)
hpt	0.36% (5/1384)	*inlB*	0.11% (2/1890)
fbpA	0.35% (6/1712)	*prsA2*	0.11% (1/881)
cheA	0.32% (6/1857)	*lplA1*	0.10% (1/966)
vip	0.32% (4/1255)		

had three contigs. The genome sizes of contigs 1, 2, and 3 for *L. monocytogenes* SMFM 2019-FV43 were 3,071,014, 60,439, and 6,273 bp, respectively, with GC contents of 37.92, 36.69, and 50.39%, respectively. The genome sizes of contigs 1, 2, and 3 for *L. monocytogenes* SMFM 201804 SD 5-3 were 3,038,302, 57,472, and 6,011 bp, with GC contents of 38.05, 36.04, and 50.39%, respectively.

3.9. Genetic variations for virulence factors

Single nucleotide variants (SNVs) are variations reflecting differences between a single base [Ministry of Food and Drug Safety (MFDS), 2019]. The gene sequences of the virulence factors of *L. monocytogenes* SMFM 201804 SD 5-3 and *L. monocytogenes* SMFM 2019-FV43 were mapped to identify genetic variations. We identified 45 virulence genes in the two isolates. For these 45 virulence genes, 41 SNVs were found between the isolates (Table 6). The SNVs were found in 91% (41/45) of virulence genes. Among the genes, the four pathogenic genes (*lnt*A, *plc*B, *inl*K, and *act*A), in which the frequency of SNVs was high, were focused (Figure 5). *lnt*A in *L. monocytogenes* encodes a secretory protein that controls the expression of IFN-stimulated genes. This allows the bacterium to govern both the induction and repression of the host cell immune response to optimize conditions for specific stages of infection or colonization (Camejo et al., 2011). *plc*B encodes PC-PLC, which is involved in effective escape from the phagocytic vacuole to the cytoplasm (Gründling et al., 2003; Hadjilouka et al., 2016). Dortet et al. (2011) confirmed *inl*K as a gene highly activated during infection and that it may play a role in the infection process. *actA* is responsible for actin-based motility and the spread of *L. monocytogenes* to neighboring cells (Vàzquez-Boland et al., 2001).

Therefore, these variations of virulence genes may affect the high risk of *L. monocytogenes* SMFM 201804 SD 5-3. In particular, pathogenic genes (*lnt*A, *plc*B, *inl*K, and *act*A) of the strain could improve attachment and invasion of host cells and affect the host cell immune response.

3.10. Genetic variations related to growth at 4°C

We identified genes related to growth at 4°C for *L. monocytogenes* SMFM 2019-FV43 and *L. monocytogenes* SMFM 201804 SD 5-3 and also found genetic variations in these genes. In all, 26 genes were identified in the two isolates. Among these 26 genes, 18 SNVs were identified (Table 7). The SNVs were found in 69% (18/26) of cold resistance genes. Among the genes, the four pathogenic genes (*motA*, *ltrC*, *betL*, and *gbuB*), in which the frequency of SNVs was high, were focused (Figure 6). Reportedly, *gbu* (*gbu*A, *gbu*B, and *gbu*C) and *bet*L encode proteins involved in the betaine uptake system, and *L. monocytogenes* accumulates betaine when grown at low temperature, which functions as a cryoprotectant and osmoprotectant (Ko et al., 1994; Wemekamp-Kamphuis, 2003). Single and multiple deletions of these genes significantly reduce the viability of *L. monocytogenes* when exposed to low temperatures (Ko and Smith, 1999; Wemekamp-Kamphuis, 2003). *ltr*C is a stress-response gene essential for the growth of *L. monocytogenes* at cold temperatures (e.g., 4°C) (Zheng and Kathariou, 1995; Chan et al., 2007); *flh*A and *mot*A also play a role in the cold tolerance of *L. monocytogenes* (Mattila et al., 2011). In this study, *L. monocytogenes* SMFM 201804 SD 5-3 had a high growth rate at 4°C than *L. monocytogenes* SMFM 2019-FV43 did, with a difference of 1.1 Log CFU/mL after storage for 288 h (Figure 3). Thus, it is reasonable to consider that *L. monocytogenes* SMFM 201804 SD 5-3 can sustain and grow at low temperatures, compared with *L. monocytogenes* SMFM 2019-FV43, given the genetic variations *gbu*B, *bet*L, *mot*A, and *ltr*C (which are related to cold stress) in the former.

3.11. Genetic variations related to heat resistance

We analyzed heat resistance-related genes and genetic variations in *L. monocytogenes* SMFM 2019-FV43 and

FIGURE 5
Single nucleotide variants in virulence factors (*lnt*A, *plc*B, *inl*K, and *act*A) of *Listeria monocytogenes* SMFM 2019-FV43 and *Listeria monocytogenes* SMFM 201804 SD 5-3. contig.1.cir: *Listeria monocytogenes* SMFM 2019-FV43 contig 1; blue line: nucleotide sequence boundary. All dissimilar nucleotides are indicated in red.

TABLE 7 Single nucleotide variants in low-temperature growth-related genes of *Listeria monocytogenes* SMFM 2019-FV43 and *Listeria monocytogenes* SMFM 201804 SD 5-3.

Low-temperature growth-related genes	SNV frequency % (no.)
*bet*L	1.97% (33/1671)
*mot*A	1.30% (11/851)
*ltr*C	1.20% (6/499)
*gbu*B	1.06% (9/849)
*trx*B	0.83% (8/959)
*sig*B	0.77% (6/778)
*gro*EL	0.55% (9/1625)
*csp*B	0.50% (1/201)
*rsb*U	0.50% (1/201)
*ltr*A	0.45% (5/1113)
*ltr*B	0.44% (7/1590)
fbp	0.35% (6/1712)
*flh*A	0.24% (5/2074)
*yyc*J	0.24% (2/831)
*clp*P	0.17% (1/596)
*opp*A	0.12% (2/1677)
*gbu*C	0.11% (1/903)
*gbu*A	0.08% (1/1194)

L. monocytogenes SMFM 201804 SD 5-3. We identified 21 genes related to heat resistance. For these 21 genes, 16 SNVs were identified (Table 8). The SNVs were found in 76% (16/21) of heat resistance-related genes. The *cts*R involved in regulating stress and heat shock, may coordinate the expression of stress genes (*clp*C, *clp*P, and *clp*E) in *L. monocytogenes* under stress conditions and in infected hosts. Stress-induced *clp*C, *clp*P, and *clp*E proteins are crucial for virulence (Nair et al., 2000). Regulation of gene expression in response to environmental stress is essential for bacterial survival (Akbar et al., 1997). Stress proteins play an important role in virulence, and therefore, variations in the heat resistance-related genes may be the plausible reasons underlying the heat resistance of *L. monocytogenes* SMFM 201804 SD 5-3.

4. Conclusion

Listeria monocytogenes isolates have different risks, with different survival responses and pathogenicity under stressful conditions. These differences are caused by SNVs in virulence genes, low-temperature-related genes, and heat resistance-related genes. Our results support the position that *L. monocytogenes* SMFM 201804 SD 5-3 is a

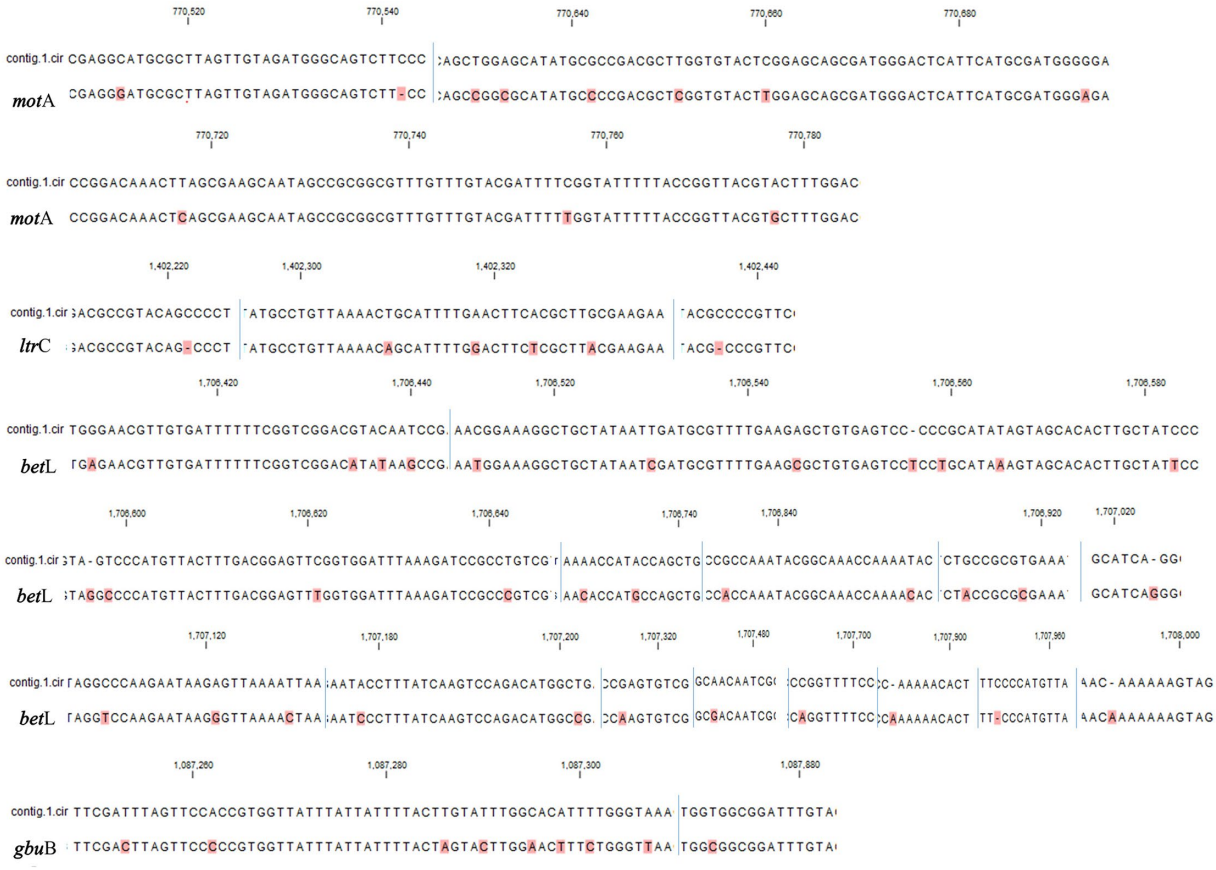

FIGURE 6
Single nucleotide variants in low-temperature growth related factors of *Listeria monocytogenes* SMFM 2019-FV43 and *Listeria monocytogenes* SMFM 201804 SD 5-3 (*motA*, *ltrC*, *betL*, and *gbuB*). contig.1.cir: *Listeria monocytogenes* SMFM 2019-FV43 contig 1; blue line: nucleotide sequence boundary. All dissimilar nucleotides are indicated in red.

TABLE 8 Single nucleotide variants in heat resistance-related genes of *Listeria monocytogenes* SMFM 2019-FV43 and *Listeria monocytogenes* SMFM 201804 SD 5-3.

Heat resistance-related gene	SNV frequency % (no.)
*clp*E	0.51% (11/2169)
*lmo*0942	0.37% (3/806)
*gro*EL	0.35% (1/285)
*gro*ES	0.35% (1/285)
*lmo*0963	0.33% (3/914)
*lmo*0231	0.29% (3/1023)
*dna*J	0.27% (3/1131)
*dna*K	0.22% (4/1841)
*lmo*1279	0.21% (3/1410)
*lmo*0292	0.20% (3/1502)
*clp*P	0.17% (1/596)
*grp*E	0.17% (1/576)
*lmo*0038	0.17% (1/572)
*lmo*1138	0.17% (1/572)
*clp*B	0.12% (3/2600)
*hrc*A	0.10% (1/1038)

high-risk isolate whereas *L. monocytogenes* SMFM 2019-FV43 is a low-risk one.

Data availability statement

The datasets presented in this study can be found in the NCBI database. The Bioproject IDs are PRJNA958457 and PRJNA958458.

Author contributions

JR, YC, and YY made significant contributions to the manuscript and agree to its publication. YY and YC conceived and designed the study. JR performed laboratory experiments. All authors analyzed the data, draft the manuscript, and approved the final manuscript.

Conflict of interest

The authors declare that the research was conducted in the absence of any commercial or financial relationships that could be construed as a potential conflict of interest.

Publisher's note

References

Akbar, S., Kang, C. M., Gaidenko, T. A., and Price, C. W. (1997). Modulator protein *Rsb*R regulates environmental signalling in the general stress pathway of *Bacillus subtilis*. *Mol. Microbiol.* 24, 567–578. doi: 10.1046/j.1365-2958.1997.3631732.x

Brown, E., Dessai, U., McGarry, S., and Gerner-Smidt, P. (2019). Use of whole-genome sequencing for food safety and public health in the United States. *Foodborne Pathog. Dis.* 16, 441–450. doi: 10.1089/fpd.2019.2662

Camejo, A., Carvalho, F., Reis, O., Leitão, E., Sousa, S., and Cabanes, D. (2011). The arsenal of virulence factors deployed by *Listeria monocytogenes* to promote its cell infection cycle. *Virulence* 2, 379–394. doi: 10.4161/viru.2.5.17703

Cao, H., Yan, Y., Wang, L., Dong, L., Pang, X., Tang, S., et al. (2021). High-throughput sequencing reveals bacterial diversity in raw milk production environment and production chain in Tangshan city of China. *Food Sci. Anim. Resour.* 41, 452–467. doi: 10.5851/kosfa.2021.e10

Chan, Y. C., Raengpradub, S., Boor, K. J., and Wiedmann, M. (2007). Microarray-based characterization of the *Listeria monocytogenes* cold regulon in log-and stationary-phase cells. *Appl. Environ. Microbiol.* 73, 6484–6498. doi: 10.1128/AEM.00897-07

Chen, Y., and Knabel, S. J. (2007). Multiplex PCR for simultaneous detection of bacteria of the genus *Listeria, Listeria monocytogenes*, and major serotypes and epidemic clones of *L. monocytogenes*. *Appl. Environ. Microbiol.* 73, 6299–6304. doi: 10.1128/AEM.00961-07

Dortet, L., Mostowy, S., Louaka, A. S., Gouin, E., Nahori, M. A., Wiemer, E. A., et al. (2011). Recruitment of the major vault protein by *Inl*K: a *Listeria monocytogenes* strategy to avoid autophagy. *PLoS Pathog.* 7:e1002168. doi: 10.1371/journal.ppat.1002168

Duffy, L. L., Vanderlinde, P. B., and Grau, F. H. (1994). Growth of *Listeria monocytogenes* on vacuum-packed cooked meats: effects of pH, aw, nitrite and ascorbate. *Int. J. Food Microbiol.* 23, 377–390. doi: 10.1016/0168-1605(94)90164-3

Farber, J. M., and Peterkin, P. I. (1991). *Listeria monocytogenes*, a food-borne pathogen. *Microbiol. Rev.* 55, 476–511. doi: 10.1128/mr.55.3.476-511.1991

Food and Drug Administration (FDA). (2018) BAM protocol: simultaneous confirmation of Listeria species and *L. monocytogenes* isolates by real-time PCR. Available at: https://www.fda.gov/food/laboratory-methods-food/bam-protocol-simultaneous-confirmation-listeria-species-and-l-monocytogenes-isolates-real-time-pcr (Accessed April 2, 2023).

Gianfranceschi, M., Fransiosa, G., Gattuso, A., and Aureli, P. (1998). Detection of two phospholipases C by means of plate tests for the rapid identification of pathogenic *Listeria monocytogenes*. *Archiv. fuer Lebensmittelhygiene (Germany)* 49, 54–57.

Gründling, A., Gonzalez, M. D., and Higgins, D. E. (2003). Requirement of the *Listeria monocytogenes* broad-range phospholipase PC-PLC during infection of human epithelial cells. *J. Bacteriol.* 185, 6295–6307. doi: 10.1128/JB.185.21.6295-6307.2003

Hadjilouka, A., Molfeta, C., Panagiotopoulou, O., Paramithiotis, S., Mataragas, M., and Drosinos, E. H. (2016). Expression of *Listeria monocytogenes* key virulence genes during growth in liquid medium, on rocket and melon at 4, 10 and 30°C. *Food Microbiol.* 55, 7–15. doi: 10.1016/j.fm.2015.11.008

Hilliard, A., Leong, D., O'Callaghan, A., Culligan, E. P., Morgan, C. A., DeLappe, N., et al. (2018). Genomic characterization of *Listeria monocytogenes* isolates associated with clinical listeriosis and the food production environment in Ireland. *Genes* 9:171. doi: 10.3390/genes9030171

Jung, Y. S., Frank, J. F., Brackett, R. E., and Chen, J. (2003). Polymerase chain reaction detection of *Listeria monocytogenes* on frankfurters using oligonucleotide primers targeting the genes encoding internalin AB. *J. Food Prot.* 66, 237–241. doi: 10.4315/0362-028x-66.2.237

Khelef, N., Lecuit, M., Bierne, H., and Cossart, P. (2006). Species specificity of the *Listeria monocytogenes Inl*B protein. *Cell. Microbiol.* 8, 457–470. doi: 10.1111/j.1462-5822.2005.00634.x

Kim, W. R. (2019) *Development of Listeria monocytogenes detection technology in mushroom based on real-time PCR through development of enrichment medium and primer*. Thesis for the Master's degree. Sookmyung Women's University.

Kim, Y. M., Park, U. Y., Mok, J. S., and Chang, D. S. (1995). Physiological characteristics of *Listeria monocytogenes* YM-7. *Korean J. Fish Aquat. Sci.* 28, 443–450.

Ko, R., and Smith, L. T. (1999). Identification of an ATP-driven, osmoregulated glycine betaine transport system in *Listeria monocytogenes*. *Appl. Environ. Microbiol.* 65, 4040–4048. doi: 10.1128/aem.65.9.4040-4048.1999

Ko, R., Smith, L. T., and Smith, G. M. (1994). Glycine betaine confers enhanced osmotolerance and cryotolerance on *Listeria monocytogenes*. *J. Bacteriol.* 176, 426–431. doi: 10.1128/jb.176.2.426-431.1994

Kühbacher, A., Novy, K., Quereda, J. J., Sachse, M., Moya-Nilges, M., Wollscheid, B., et al. (2018). Listeriolysin O-dependent host surfaceome remodeling modulates *Listeria monocytogenes* invasion. *Pathog. Dis.* 76, 1–12. doi: 10.1093/femspd/fty082

Kwon, J. G., Kim, S. K., and Lee, J. H. (2019). Recent next-generation sequencing and bioinformatic analysis methods for food microbiome research. *Food Sci.* 52, 220–228. doi: 10.23093/FSI.2019.52.3.220

Lee, J. Y. (2010) *Molecular typing and antimicrobial susceptibility of Listeria monocytogenes in meats*. Thesis for the degree of Philosophiae Doctor. Konkuk University. Seoul.

Lee, H., and Yoon, Y. (2021). Etiological agents implicated in foodborne illness world wide. *Food Sci. Anim. Resour.* 41, 1–7. doi: 10.5851/kosfa.2020.e75

Liu, D., Lawrence, M. L., Gorski, L., Mandrell, R. E., Ainsworth, A. J., and Austin, F. W. (2006). *Listeria monocytogenes* serotype 4b strains belonging to lineages I and III possess distinct molecular features. *J. Clin. Microbiol.* 44, 214–217. doi: 10.1128/JCM.44.1.214-217.2006

Lüth, S., Kleta, S., and Al Dahouk, S. (2018). Whole genome sequencing as a typing tool for foodborne pathogens like *Listeria monocytogenes*–the way towards global harmonisation and data exchange. *Trends Food Sci. Technol.* 73, 67–75. doi: 10.1016/j.tifs.2018.01.008

Mattila, M., Lindstrom, M., Somervuo, P., Markkula, A., and Korkeala, H. (2011). Role of *flh*A and *mot*A in growth of *Listeria monocytogenes* at low temperatures. *Int. J. Food Microbiol.* 148, 177–183. doi: 10.1016/j.ijfoodmicro.2011.05.022

Ministry of Food and Drug Safety (MFDS) (2019) Guideline of next generation sequencing (NGS). Available at: http://www.kmdia.or.kr/board/board_10V.asp?mode=VIEW&bid=notice&bidsrl=2&bidssrl=5&intseq=10141 (Accessed May 18, 2023).

Nair, S., Derré, I., Msadek, T., Gaillot, O., and Berche, P. (2000). *Cts*R controls class III heat shock gene expression in the human pathogen *Listeria monocytogenes*. *Mol. Microbiol.* 35, 800–811. doi: 10.1046/j.1365-2958.2000.01752.x

Oh, H., Kim, S., Lee, S., Lee, H., Ha, J., Lee, J., et al. (2018). Prevalence, serotype diversity, genotype and antibiotic resistance of *Listeria monocytogenes* isolated from carcasses and human in Korea. *Food Sci. Anim. Resour.* 38, 851–865. doi: 10.5851/kosfa.2018.e5

Park, M. S., Cho, J. I., Lee, S. H., and Bahk, G. J. (2014). The analysis for minimum infective dose of foodborne disease pathogens by meta-analysis. *J. Food Hyg. Saf.* 29, 305–311. doi: 10.13103/JFHS.2014.29.4.305

Park, E., Ha, J., Oh, H., Kim, S., Choi, Y., Lee, Y., et al. (2021). High prevalence of *Listeria monocytogenes* in smoked duck: antibiotic and heat resistance, virulence, and genetics of the isolates. *Food Sci. Anim. Resour.* 41, 324–334. doi: 10.5851/kosfa.2021.e2

Pöntinen, A., Aalto-Araneda, M., Lindström, M., and Korkeala, H. (2017). Heat resistance mediated by pLM58 plasmid-borne *Clp*L in *Listeria monocytogenes*. *mSphere* 2, e00364–e00317. doi: 10.1128/mSphere.00364-17

Rezaei, M., Kazemipour, N., Vand Yousefi, J., Rokhbakhsh Zamin, F., and Irajian, G. (2019). Determination of dominant serovars and molecular analysis of hly and iap genes related to *Listeria monocytogenes* strains isolated from spontaneous human abortions in Tehran. *Iran. J. Microbiol.* 13, 102–113. doi: 10.30699/ijmm.13.2.102

Ribot, E. M., Freeman, M., Hise, K. B., and Gerner-Smidt, P. (2019). PulseNet: entering the age of next-generation sequencing. *Foodborne Pathog. Dis.* 16, 451–456. doi: 10.1089/fpd.2019.2634

Riedo, F. X., Pinner, R. W., Tosca, M. L., Cartter, M. L., Graves, L. M., Reeves, M. W., et al. (1994). A point-source foodborne listeriosis outbreak: documented incubation period and possible mild illness. *J. Infect. Dis.* 170, 693–696. doi: 10.1093/infdis/170.3.693

Seeliger, H., and Jones, D. (1986). "Listeria" in *Bergey's Manual of Systematic Bacteriology*. ed. H. Sneath (Baltimore, MD: Williams and Wilkins), 1235–1245.

Sheng, J., Tao, T., Zhu, X., Bie, X., Lv, F., Zhao, H., et al. (2018). A multiplex PCR detection method for milk based on novel primers specific for *Listeria monocytogenes* 1/2a serotype. *Food Control* 86, 183–190. doi: 10.1016/j.foodcont.2017.11.028

Shin, D. H., Song, D. E., and Kim, K. R. (2007). Placental findings of *Listeria monocytogenes* infection in twin pregnancy. A Case Report. *Korean J. Pathol.* 41, 119–122. Available at: https://www.jpatholtm.org/journal/view.php?number=2550

Stratakos, A. C., Ijaz, U. Z., Ward, P., Linton, M., Kelly, C., Pinkerton, L., et al. (2020). *In vitro* and *in vivo* characterisation of *Listeria monocytogenes* outbreak isolates. *Food Control* 107:106784. doi: 10.1016/j.foodcont.2019.106784

Tangwatcharin, P., Sorapukdee, S., and Kongsrirat, K. (2019). Sous-vided restructured goat steaks: process optimized by thermal inactivation of *Listeria monocytogenes* and their quality characteristics. *Food Sci. Anim. Resour.* 39, 863–876. doi: 10.5851/kosfa.2019.e64

Vàzquez-Boland, J. A., Kuhn, M., Berche, P., Chakraborty, T., Dominguez-Bernal, G., Goebe, W., et al. (2001). *Listeria* pathogenesis and molecular virulence determinants. *Clin. Microbiol. Rev.* 14, 584–640. doi: 10.1128/CMR.14.3.584-640.2001

Wemekamp-Kamphuis, H. H. (2003) *Survival strategies of Listeria monocytogenes: Roles of regulators and transporters*. Wageningen: Wageningen University and Research.

Winters, D. K., Johnson, M. G., and Maloney, T. P. (1999). Rapid detection of *Listeria monocytogenes* by a PCR assay specific for an amino peptidase. *Mol. Cell. Probes* 13, 127–131. doi: 10.1006/mcpr.1999.0224

Yang, J. M., and Moon, G. S. (2021). Partial characterization of an anti-Listerial bacteriocin from *Enterococcus faecium* CJNU 2524. *Food Sci. Anim. Resour.* 41, 164–171. doi: 10.5851/kosfa.2020.e98

Zheng, W., and Kathariou, S. (1995). Differentiation of epidemic-associated strains of *Listeria monocytogenes* by restriction fragment length polymorphism in a gene region essential for growth at low temperatures (4 degrees C). *Appl. Environ. Microbiol.* 61, 4310–4314. doi: 10.1128/aem.61.12.4310-4314.1995

Frontiers in Microbiology

Explores the habitable world and the potential of microbial life

The largest and most cited microbiology journal which advances our understanding of the role microbes play in addressing global challenges such as healthcare, food security, and climate change.

Discover the latest Research Topics

See more →

Frontiers

Avenue du Tribunal-Fédéral 34
1005 Lausanne, Switzerland
frontiersin.org

Contact us

+41 (0)21 510 17 00
frontiersin.org/about/contact